

Cell wall architecture and the role of wall teichoic acid in *Staphylococcus aureus*

By

Victoria L. Kent BSc (Hons)
(University of Sheffield)

A thesis submitted for the degree of Doctor of Philosophy
April 2013

Department of Molecular Biology and Biotechnology, University of Sheffield,
Firth Court, Western Bank, Sheffield, S10 2TN

Abstract

The bacterium *Staphylococcus aureus* only synthesises peptidoglycan during cell division at the septum using a complex protein biosynthetic apparatus called the divisome. It divides sequentially in three orthogonal planes, using heritable features within the peptidoglycan architecture to maintain this process over generations. The 'rib' features that form this 'memory' are remnants of a large belt of peptidoglycan called the 'piecrust' that is formed at the initiation of septation and before the septal plate. After division, the ribs remain as orthogonal features, which are bisected by further 'piecrust' features from ensuing division cycles. This results in a characteristic pattern of different age peptidoglycan sectors, delineated by ribs of a different architecture.

As well as maintaining cellular viability and shape the peptidoglycan layer also acts as a scaffold for many other polymers, including wall teichoic acid (WTA). WTA is known to direct and modulate cell wall hydrolase activity. There has been recent debate as to its subcellular localisation. In this study, using the bacterial two-hybrid assay, four putative WTA biosynthesis enzymes were found to interact with numerous members of the divisome. Microscopy techniques localised WTA across the entire cell surface except on the piecrust and rib features. It was hypothesised that WTA blocks the rest of the peptidoglycan thereby directing the localisation of hydrolases and other proteins.

The localisation of peptidoglycan hydrolases was studied. Those found to localise to the rib and piecrust features (Atl(glucosaminidase), Atl(amidase), SagB and ScaH) showed a distinct pattern which was completely disrupted in a strain missing WTA. Conversely those (SceD) not associated with rib/piecrust showed no difference to localisation with loss of WTA. The processed forms of Atl (glucosaminidase and amidase) demonstrated different binding properties during the cell cycle and a model to illustrate the cell cycle dependent binding is proposed.

Acknowledgements

I would like to thank the MRC and Prof. Simon Foster for giving me the opportunity to carry out this PhD. Furthermore, I would like to thank Simon for his support, guidance and humour throughout my studies. Thanks to all past and present members of the Foster lab; particularly Azhar, Amy and Alex for technical help, Emma for the AFM help and Bob for all things STORM, and all other members for laughter, gossip and cake.

I'm also incredibly grateful to all my fantastic Sheffield friends; Julie, Anna, Claudia, Denny and Rick thank you for empathising with my PhD woes; Holly, Jess, Tara and the whole Sheffield Uni Waterpolo team thank you for helping me vent my frustrations. To all my other friends, thank you for your patience when I couldn't see you or answer the phone! Finally, I would like to say a big thank you to my parents and brothers for their support and encouragement throughout my three year (and a bit) stint.

Abbreviations

| | |
|-------------------|--|
| α | Antibody |
| 3D | Three dimensional |
| A _x | Absorbance at indicated wavelength x (nm) |
| AFM | Atomic force microscopy |
| Ami | Amidase |
| Amp | Ampicillin |
| APS | Ammonium Persulphate |
| bp | Base pair |
| C6 | Carbon six |
| cfu | Colony forming unit |
| CHAP | Cysteine, histidine-dependent amidohydrolases/peptidases |
| ChBD | Choline-binding domain |
| Chl | Chloramphenicol |
| cpm | Counts per minute |
| D-Ala | D-alanine |
| <i>m</i> -DAP | <i>Meso</i> -diaminopimelic acid |
| DAPI | 4', 6-diamidino-2-phenylindole |
| D-Glu | D-glutamic acid |
| dH ₂ O | Distilled water |
| DMSO | Dimethyl sulphoxide |
| DNA | Deoxyribonucleic acid |
| DPX | Distyrene-plasticizer-xylene |
| DV | DeltaVision |
| ECM | Extracellular matrix |
| EDTA | Ethylenediamine tetra-acetic acid |
| EM | Electron microscopy |
| Ery | Erythromycin |
| FITC | Flourescein isothiocyanate |
| FL | Fluorescent |
| FPLC | Fast protein liquid chromatography |
| g | Grams |
| GlcNAc | <i>N</i> -acetyl glucosamine |
| Glu | Glucosaminidase |
| Gly | Glycine |
| h | Hour |
| H | Height image |
| HF | Hydrofluoric acid |
| HMW | High molecular weight |
| HPLC | High performance liquid chromatography |
| IPTG | Isopropyl beta-D-1-thiogalactopyranoside |
| Kan | Kanamycin |
| kb | Kilobase pairs |
| kDa | Kilodaltons |
| l | Litre |
| L-Ala | L-alanine |

| | |
|--------------------|---|
| LB | Luria-Bertani medium |
| Lin | Lincomycin |
| LPS | Lipopolysaccharide |
| LTA | Lipoteichoic acid |
| M | Molar |
| mA | Milliamps |
| Mb | Megabase |
| MCS | Multiple cloning site |
| MDa | Megadalton |
| mg | Milligram |
| min | Minutes |
| ml | Millilitres |
| mM | Millimolar |
| mRFP | Monomeric red fluorescent protein |
| MurNAc | <i>N</i> -acetyl muramic acid |
| Neo | Neomycin |
| nm | Nanometre |
| nM | Nanomolar |
| NMR | Nuclear magnetic resonance |
| OD _x | Optical density at indicated wavelength x (nm) |
| OMX | Optical microscopy experimental |
| P | Phase image |
| PALM | Photoactivated localisation microscopy |
| PBP | Pencillin-binding protein |
| PBS | Phosphate buffered saline |
| PCR | Polymerase chain reaction |
| pfu | Plaque forming unit |
| psi | Pounds per square inch |
| P _{spac} | Spac promoter |
| RP-HPLC | Reverse-phase high performance liquid chromatography |
| rpm | Revolutions per min |
| RT | Room temperature |
| sdH ₂ O | Streilised distilled water |
| SDS | Sodium dodecyl sulphate |
| SDS-PAGE | Sodium dodecyl sulphate polyacrylamide gel electrophoresis |
| s | Seconds |
| SEC | Size exclusion chromatography |
| SIM | Structured illumination microscopy |
| <i>Spp.</i> | Species |
| STORM | Stochastic optical reconstruction microscopy |
| t | Time |
| TA | Teichoic acid |
| TAE | Tris-acetate EDTA (buffer) |
| Taq | Thermostable DNA polymerase derived from <i>Thermus aquaticus</i> |
| TBS | Tris buffered saline |
| TEMED | <i>N,N,N',N'</i> -tetramethyl-ethylenediamine |
| Tet | Tetracycline |

| | |
|-------|--|
| Tris | Tris (hydroxymethyl) aminomethane |
| TSA | Tryptone soya agar |
| TSB | Tryptone soya buffer |
| μg | Microgram |
| μl | Microlitre |
| μm | Micrometre |
| μM | Micromolar |
| UDP | Undecaprenylphosphate |
| UV | Ultra violet |
| V | Volts |
| Van | Vancomycin |
| v/v | Volume for volume |
| WGA | Wheat germ agglutinin |
| WT | Wild-type |
| WTA | Wall teichoic acid |
| w/v | Weight for volume |
| x | Times |
| X-Gal | 5-bromo-4-chloro-3-indolyl-β-D-galactoside |
| YFP | Yellow fluorescent protein |
| σ | Sigma |
| φ | Phage |
| Ω | Ohms |
| ~ | Approximately |
| % | Percentage |

Table of contents

| | Page Number |
|---|--------------|
| Title page | i |
| Abstract | ii |
| Acknowledgements | iii |
| Abbreviations | iv |
| Table of contents | vii |
| List of Figures | xiii |
| List of Tables | xv |
| | |
| CHAPTER 1: Introduction | 1-39 |
| | |
| 1.1 <i>Staphylococcus aureus</i> | 1 |
| 1.2 Pathogenesis of <i>staphylococcus aureus</i> | 2 |
| 1.2.1 Treatment and antibiotic resistance | 3 |
| 1.3 Bacterial cell division | 5 |
| 1.4 The divisome | 6 |
| 1.4.1 FtsZ | 10 |
| 1.4.2 FtsZ interacting partners | 11 |
| 1.4.3 Septal biosynthesis machinery | 13 |
| 1.4.4 Penicillin binding proteins | 16 |
| 1.5 <i>S.aureus</i> cell wall | 17 |
| 1.6 Peptidoglycan synthesis | 22 |
| 1.7 Peptidoglycan hydrolysis | 24 |
| 1.8 Peptidoglycan hydrolases | 26 |
| 1.8.1 Regulation of peptidoglycan hydrolases | 30 |
| 1.9 Cell surface glycopolymers | 32 |
| 1.9.1 Teichoic acids | 33 |
| 1.10 Surface proteins | 38 |
| 1.11 Project aims | 39 |
| | |
| CHAPTER 2: Materials and methods | 40-76 |
| | |
| 2.1 Media | 40 |
| 2.1.1 Tryptone Soya Broth (TSB) | 40 |
| 2.1.2 Luria- Bertani (LB) | 40 |
| 2.1.3 Buffered Luria- Bertani | 40 |
| 2.1.4 LK | 40 |
| 2.1.5 Nutrient Broth (NB) | 41 |
| 2.1.6 Minimal media | 41 |
| 2.1.7 Phage agar | 41 |
| 2.1.8 Nutrient agar (NA) | 41 |
| 2.2 Antibiotics | 42 |
| 2.3 Enzymes and chemicals | 42 |
| 2.4 Buffers and solutions | 43 |
| 2.4.1 Phosphate buffered saline (PBS) | 43 |
| 2.4.2 Tris buffered saline (TBS) | 43 |

| | |
|---|----|
| 2.4.3 TAE (50x) | 43 |
| 2.4.4 Phage buffer | 43 |
| 2.4.5 DNA loading buffer (6x) | 44 |
| 2.4.6 Qiagen buffers | 44 |
| 2.4.6.1 P1 | 44 |
| 2.4.6.2 P2 | 44 |
| 2.4.6.3 P3 | 44 |
| 2.4.6.4 EB | 44 |
| 2.4.6.5 N3, PB and PE. | 44 |
| 2.4.7 β -galactosidase liquid assay solutions | 44 |
| 2.4.7.1 ABT | 44 |
| 2.4.7.2 Stopping solution | 44 |
| 2.4.7.3 ABTN | 45 |
| 2.4.8 SDS PAGE solutions | 45 |
| 2.4.8.1 SDS PAGE loading buffer (2x) | 45 |
| 2.4.8.2 SDS PAGE reservoir buffer (10x) | 45 |
| 2.4.8.3 Coomassie Brilliant Blue stain | 45 |
| 2.4.8.4 Coomassie destain | 45 |
| 2.4.8.5 Transfer buffer | 45 |
| 2.4.9 Western blotting buffers | 46 |
| 2.4.9.1 Blotting buffer | 46 |
| 2.4.9.2 TSBT (20x) | 46 |
| 2.4.9.3 Blocking solution | 46 |
| 2.4.10 Zymogram solutions | 46 |
| 2.4.10.1 Renaturing solution | 46 |
| 2.4.10.2 Renaturing gel stain (10x) | 46 |
| 2.4.11 Nickel affinity purification buffers | 46 |
| 2.4.11.1 Buffer A (START buffer) | 46 |
| 2.4.11.2 Buffer B (elution buffer) | 47 |
| 2.5 Bacterial strains and growth conditions used | 47 |
| 2.6 Plasmids used | 48 |
| 2.7 Centrifugation | 51 |
| 2.8 Determining bacterial cell density | 52 |
| 2.8.1 Spectrophotometry measurement (OD_{600}) | 52 |
| 2.8.2 Direct cell count ($cfu\ ml^{-1}$) | 52 |
| 2.9 DNA purification techniques | 52 |
| 2.9.1 Genomic DNA extraction | 52 |
| 2.9.2 Small scale plasmid purification from <i>E.coli</i> | 52 |
| 2.9.3 Gel extraction of DNA using QIAquick spin column | 53 |
| 2.9.4 Purification of PCR products using QIAquick spin column | 53 |
| 2.10 <i>In vitro</i> DNA manipulation techniques | 54 |
| 2.10.1 Primers | 54 |
| 2.10.2 PCR amplification | 55 |
| 2.10.3 Colony PCR screening of <i>E.coli</i> | 56 |
| 2.10.4 Colony PCR screening of <i>S.aureus</i> | 56 |
| 2.10.5 Restriction endonuclease digestion | 56 |
| 2.10.6 Phosphotase treatment of vector DNA | 56 |

| | |
|---|----|
| 2.10.7 DNA ligation and ethanol precipitation | 57 |
| 2.10.8 Agarose gel electrophoresis | 57 |
| 2.10.9 Plasmid sequencing | 58 |
| 2.11 Transformation techniques | 58 |
| 2.11.1 Transformation of <i>E.coli</i> | 58 |
| 2.11.1.1 Preparation of electrocompetent <i>E.coli</i> BTH101 cells | 58 |
| 2.11.1.2 Electroporation into <i>E.coli</i> | 59 |
| 2.11.2 Transformation of <i>S.aureus</i> | 59 |
| 2.11.2.1 Preparation of electrocompetent <i>S.aureus</i> RN4220 cells | 59 |
| 2.11.2.2 Electroporation into <i>S.aureus</i> | 60 |
| 2.12 Phage transformation techniques | 60 |
| 2.12.1 Bacteriophage | 60 |
| 2.12.2 Preparation of phage lysate | 60 |
| 2.12.3 Determination of phage titre | 60 |
| 2.12.4 Phage transduction | 61 |
| 2.13 Protein analysis | 61 |
| 2.13.1 SDS PAGE | 61 |
| 2.13.2 Coomassie staining | 63 |
| 2.13.3 Western blot | 63 |
| 2.13.4 Zymogram | 63 |
| 2.13.5 Mini scale protein extraction of <i>S.aureus</i> | 64 |
| 2.13.6 Whole cell lysate | 64 |
| 2.13.7 Bradford estimation of protein concentration | 64 |
| 2.14 Production of recombinant protein | 65 |
| 2.14.1 Expression in <i>E.coli</i> BL21 | 65 |
| 2.14.2 Analysis of recombinant protein stability | 65 |
| 2.14.3 Separation of insoluble and soluble proteins | 66 |
| 2.14.4 HiTrap purification | 66 |
| 2.14.5 Protein dialysis | 67 |
| 2.14.5.1 Preparation of dialysis membrane | 67 |
| 2.14.5.2 Dialysis of recombinant protein | 67 |
| 2.15 Generation of antibodies | 67 |
| 2.16 Bacterial two-hybrid assay (BACTH) | 67 |
| 2.16.1 BACTH solid assay | 68 |
| 2.16.2 BACTH liquid culture assay | 68 |
| 2.16.3 β -galactosidase liquid assay calibration curve | 69 |
| 2.17 Preparation of samples for fluorescence microscopy | 70 |
| 2.17.1 Attachment of cells | 70 |
| 2.17.2 Live cell treatment | 70 |
| 2.17.3 Fixing cells | 71 |
| 2.17.4 Removal of Lipoteichoic acid (LTA) | 71 |
| 2.17.5 Removal of surface proteins | 71 |
| 2.17.6 Removal of Wall teichoic acids (WTA) | 71 |
| 2.17.7 Cell breakage | 72 |
| 2.17.8 Trypsination | 72 |
| 2.17.9 <i>In vitro</i> staining | 72 |
| 2.17.10 Lectin labelling | 72 |

| | |
|--|----------------|
| 2.17.11 Vancomycin labelling | 73 |
| 2.17.12 Immunofluorescence | 73 |
| 2.18 Fluorescence microscopy | 74 |
| 2.19 Preparation of samples for AFM | 74 |
| 2.19.1 Extraction of cell walls for AFM | 74 |
| 2.19.2 Preparation of cell walls | 74 |
| 2.20 AFM microscopy | 75 |
| 2.21 Preparation of samples for STORM | 75 |
| 2.22 STORM microscopy | 75 |
| | |
| CHAPTER 3: Identification of interaction between cell division proteins and cell wall polymer synthetic machinery | 77-107 |
| | |
| 3.1 Introduction | 77 |
| 3.1.1 Aims of this investigation | 82 |
| 3.2 Results | 83 |
| 3.2.1 Genes chosen for investigation | 83 |
| 3.2.2 Construction of BACTH plasmids | 84 |
| 3.2.3 <i>E.coli</i> BTH101 as a reporter strain for the detection of protein-protein interactions | 86 |
| 3.2.4 Investigating physical interactions with <i>S.aureus</i> WTA biosynthesis proteins of interest | 86 |
| 3.2.4.1 Solid assay | 86 |
| 3.2.4.2 Liquid assay | 90 |
| 3.2.5 Investigating physical interactions with <i>S.aureus</i> PBP4 | 99 |
| 3.2.5.1 Solid assay | 99 |
| 3.2.5.2 Liquid assay | 99 |
| 3.3 Discussion | 100 |
| | |
| CHAPTER 4: The localisation of wall teichoic acids in <i>S.aureus</i> | 108-142 |
| | |
| 4.1 Introduction | 108 |
| 4.1.1 Aims of this investigation | 111 |
| 4.2 Results | 115 |
| 4.2.1 Identification of the localisation of WTA using AFM | 115 |
| 4.2.2 Analysis of the binding of ConA | 118 |
| 4.2.2.1 Lectin labelling of <i>S.aureus</i> in SH1000 | 118 |
| 4.2.2.2 Lectin labelling of <i>S.aureus</i> $\Delta tarO$ | 119 |
| 4.2.2.3 Lectin labelling of <i>S.aureus</i> $\Delta srtA$ | 119 |
| 4.2.3 Is WTA present at the septum? | 126 |
| 4.2.4 Analysis of ConA binding patterns | 126 |
| 4.2.4.1 Investigation into the surface binding of ConA | 126 |
| 4.2.4.2 Lectin labelling in <i>S.aureus</i> $\Delta clfA2$ | 130 |
| 4.2.4.3 Lectin labelling in <i>S.aureus</i> $\Delta gtfAB$ | 130 |
| 4.2.4.4 lectin labelling in <i>S.aureus</i> $\Delta gtfAB \Delta clfA2$ | 131 |
| 4.3 Discussion | 138 |

| | |
|---|--------------------|
| CHAPTER 5: Investigation into the localisation of autolysins and their relationship to WTA | 143-205 |
| 5.1 Introduction | 143 |
| 5.1.1 Atl | 143 |
| 5.1.2 Amidase (Sle1/Aaa (ScaA) and SA1687) | 147 |
| 5.1.3 The CHAP family | 148 |
| 5.1.4 Glucosaminidases (SagA, SagB and ScaH) | 148 |
| 5.1.5 Lytic transglycosylases (IsaA and SceD) | 149 |
| 5.1.6 Lysostaphins (LytM, SA0191 and SA2195) | 149 |
| 5.1.8 Aims of this investigation | 151 |
| 5.2 Results | 152 |
| 5.2.1 Atl amidase | 152 |
| 5.2.1.1 Generation of recombinant Atl amidase | 152 |
| 5.2.1.2 Overexpression and purification of Atl amidase | 152 |
| 5.2.1.3 Confirmation of Atl amidase activity | 154 |
| 5.2.1.4 Generation of antibodies | 154 |
| 5.2.1.5 Localisation of Atl amidase in SH1000 <i>spa::kan</i> | 154 |
| 5.2.1.6 Re-emergence of Atl amidase after trypsination | 157 |
| 5.2.1.7 Does Atl amidase localise to cell surface features? | 157 |
| 5.2.1.8 Colocalisation of peptidoglycan features and Immunofluorescence | 164 |
| 5.2.1.9 Atl amidase localisation in SH1000 $\Delta tarO$ | 165 |
| 5.2.1.10 Colocalisation of Atl amidase and ConA | 169 |
| 5.2.2 Atl glucosaminidase | 171 |
| 5.2.2.1 Generation of Atl glucosaminidase antibodies | 171 |
| 5.2.2.2 Localisation of Atl glucosaminidase in SH1000 <i>spa::kan</i> | 171 |
| 5.2.2.3 Re-emergence of Atl glucosaminidase after trypsination | 176 |
| 5.2.2.4 Does Atl glucosaminidase localise to peptidoglycan features? | 176 |
| 5.2.2.5 Atl glucosaminidase localisation in SH1000 $\Delta tarO$ | 180 |
| 5.2.3 Co-localisation of Atl amidase and Atl glucosaminidase | 180 |
| 5.2.3.1 Co-localisation in SH1000 <i>spa::kan</i> | 180 |
| 5.2.3.2 Co-localisation in SH1000 $\Delta tarO$ | 186 |
| 5.2.4 Other hydrolases (SagB, ScaH and SceD) | 186 |
| 5.2.4.1 SagB localisation | 186 |
| 5.2.4.2 ScaH localisation | 187 |
| 5.2.4.3 SceD localisation | 192 |
| 5.3 Discussion | 201 |
| CHAPTER 6: General discussion | 206-214 |
| 6.1 <i>S.aureus</i> peptidoglycan architecture | 206 |
| 6.2 How does a sphere divide faithfully in three planes? | 208 |
| 6.3 How are the 'piecrust' features recognised? | 208 |
| 6.4 Where are WTAs localised? | 209 |
| 6.5 Which cellular processes do WTA influence? | 210 |
| 6.6 How is the active division plane differentiated from others? | 212 |

| | |
|------------------------|----------------|
| 6.7 Future work | 214 |
| References | 216 |
| Appendices | 238-242 |
| Appendix I | 238 |
| Appendix II | 242 |

Enclosed CD-ROM contains an electronic copy of this thesis. Images may be better seen electronically.

List of Figures

| | | |
|--------------------|--|-----|
| Figure 1.1 | Division site selection in rod-shaped bacteria | 7 |
| Figure 1.2 | Divisome of <i>S.aureus</i> | 9 |
| Figure 1.3 | General structure of the Gram-negative and Gram-positive envelopes | 18 |
| Figure 1.4 | Chemical structure of peptidoglycan | 19 |
| Figure 1.5 | Peptidoglycan arrangement models | 20 |
| Figure 1.6 | Peptidoglycan dynamics in cocci and ovococci | 22 |
| Figure 1.7 | Growth of peptidoglycan and structural inheritance of division plane in <i>S.aureus</i> | 25 |
| Figure 1.8 | The specificity of peptidoglycan hydrolases | 27 |
| Figure 1.9 | Schematic diagrams of WTA and LTA | 34 |
| Figure 1.10 | Pathways of <i>S.aureus</i> WTA biosynthesis | 37 |
| Figure 3.1 | Construction of BACTH plasmids carrying C-terminal fusions | 87 |
| Figure 3.2 | Restriction enzyme digests of BACTH plasmids | 88 |
| Figure 3.3 | β -Galactosidase activity of T18 fused proteins of interest with T25 division proteins | 93 |
| Figure 3.4 | β -Galactosidase activity of T25 fused proteins of interest with T18 division proteins | 95 |
| Figure 3.5 | β -Galactosidase activities of T18 and T25 fused <i>S.aureus</i> PBP4 with T25 and T18 division proteins, respectively | 98 |
| Figure 3.6 | Interaction maps of POI's | 101 |
| Figure 3.7 | Interaction maps of PBP4 | 106 |
| Figure 3.8 | Schematic representation of the <i>S.aureus</i> divisome | 107 |
| Figure 4.1 | Super resolution imaging principles | 112 |
| Figure 4.2 | Schematic representative of Atomic Force Microscopy (AFM) | 114 |
| Figure 4.3 | AFM images of purified sacculi from exponentially growing <i>S.aureus</i> SH1000 | 116 |
| Figure 4.4 | AFM images of purified sacculi from exponentially growing <i>S.aureus</i> $\Delta tarO$ | 117 |
| Figure 4.5 | Lectin labelling of <i>S.aureus</i> SH1000 | 120 |
| Figure 4.6 | Lectin labelling of <i>S.aureus</i> $\Delta tarO$ | 121 |
| Figure 4.7 | Lectin labelling of <i>S.aureus</i> $\Delta srtA$ | 124 |
| Figure 4.8 | ConA labelling of <i>S.aureus</i> sacculi | 127 |
| Figure 4.9 | ConA binding pattern to <i>S.aureus</i> WTA | 128 |
| Figure 4.10 | ConA binding pattern to <i>S.aureus</i> surface proteins | 129 |
| Figure 4.11 | Lectin labelling of <i>S.aureus</i> $\Delta clfA$ | 132 |
| Figure 4.12 | Lectin labelling of <i>S.aureus</i> $\Delta gtfAB$ | 134 |
| Figure 4.13 | Lectin labelling of <i>S.aureus</i> $\Delta clfA\Delta gtfAB$ | 136 |
| Figure 4.14 | Peptidoglycan patterning models | 140 |
| Figure 5.1 | Domain structure of Atl | 145 |
| Figure 5.2 | Recombinant Atl amidase protein production | 153 |
| Figure 5.3 | Purification of Atl amidase | 155 |
| Figure 5.4 | Localisation of Atl amidase | 158 |

| | | |
|--------------------|---|-----|
| Figure 5.5 | Expanded images showing SH1000 <i>spa::kan</i> Atl amidase localisation | 159 |
| Figure 5.6 | Analysis of Atl amidase localisation | 160 |
| Figure 5.7 | Schematic model of Atl amidase throughout the cell cycle | 161 |
| Figure 5.8 | Re-emergence of Atl amidase after trypsination of cells | 162 |
| Figure 5.9 | Atl amidase binds piecrust | 166 |
| Figure 5.10 | Atl amidase localisation viewed by STORM microscopy | 167 |
| Figure 5.11 | Localisation of Atl amidase in $\Delta tarO$ | 168 |
| Figure 5.12 | Binding of ConA to antibodies and vancomycin | 170 |
| Figure 5.13 | Purification of Atl glucosaminidase | 172 |
| Figure 5.14 | Localisation of Atl glucosaminidase | 173 |
| Figure 5.15 | Analysis of Atl glucosaminidase localisation | 174 |
| Figure 5.16 | Schematic model of Atl glucosaminidase throughout the cell cycle | 175 |
| Figure 5.17 | Re-emergence of Atl glucosaminidase after trypsination at specific time points | 177 |
| Figure 5.18 | Atl glucosaminidase binds piecrusts | 179 |
| Figure 5.19 | Localisation of Atl glucosaminidase in $\Delta tarO$ | 181 |
| Figure 5.20 | Co-localisation of Atl(ami) and Atl(glu) in SH1000 cells | 183 |
| Figure 5.21 | Schematic model of Atl(ami) and Atl(glu) throughout the cell cycle | 184 |
| Figure 5.22 | Co-localisation of Atl(ami) and Atl(glu) in $\Delta tarO$ | 185 |
| Figure 5.23 | Localisation of SagB | 188 |
| Figure 5.24 | SagB localisation pattern | 189 |
| Figure 5.25 | Re-emergence of SagB after trypsination | 190 |
| Figure 5.26 | Localisation of ScaH | 193 |
| Figure 5.27 | ScaH localisation pattern | 194 |
| Figure 5.28 | Re-emergence of ScaH after trypsination | 195 |
| Figure 5.29 | Localisation of SceD | 197 |
| Figure 5.30 | SceD localisation pattern | 198 |
| Figure 5.31 | Re-emergence of SceD after trypsination | 199 |
| Figure 5.32 | Cell-cell separation model | 202 |
| Figure 6.1 | Division plane growth choice through peptidoglycan ribs and growth by hydrolysis and piecrust | 207 |
| Figure 6.2 | The localisation of WTA and how it directs other proteins | 211 |
| Figure 6.3 | Cells split from one side only | 213 |

List of tables

| | | |
|------------------|--|-----|
| Table 2.1 | Antibiotic stock solutions and concentrations | 42 |
| Table 2.2 | Stock solutions and concentrations | 42 |
| Table 2.3 | Bacterial strains used in this study | 47 |
| Table 2.4 | Plasmids used in this study | 48 |
| Table 2.5 | Primers used in this study | 54 |
| Table 2.6 | DNA markers | 58 |
| Table 2.7 | Protein size standards | 62 |
| Table 2.8 | DeltaVision filter set | 74 |
| Table 3.1 | Results obtained from bioinformatics search of proteins of interest | 85 |
| Table 3.2 | Expected band size of restriction fragments of BACTH plasmids digested with <i>EcoRI</i> and <i>BamHI</i> | 89 |
| Table 3.3 | Summary of β -galactosidase activity of bacterial WTA biosynthesis two hybrid fusions on solid media | 92 |
| Table 3.4 | Summary of β -galactosidase activity of PBP4 two hybrid fusions on solid media | 97 |
| Table 5.1 | A list of putative hydrolases identified by an <i>in silico</i> screen of the <i>S.aureus</i> COL genome | 145 |

CHAPTER 1

Introduction

3.1 *Staphylococcus aureus*

Staphylococcus aureus is a gram-positive spherical bacterium with a diameter between 0.5-1.5µm. Cell division occurs sequentially in three perpendicular planes with the daughter cells not completely separating, resulting in irregular grape like clusters (Tzagoloff and Novick, 1977). It is from this cellular arrangement that the genus gets its name, *staphylo-* describes the clustered arrangement and *-coccus* refers to the sphere-like shape. The species name, '*aureus*' is Latin for golden, referring to the colour of many colonies of this bacterium (Lowy, 1998). This golden colour is due to the production of carotenoids including staphyloxanthin in stationary phase cells (Marshall and Wilmoth, 1981). Of the 32 species and 8 subspecies of *staphylococcus* (Kloos and Bannerman, 1994), *S.aureus* and *S.epidermis* are the best studied. The staphylococci, are non-spore forming, non-motile facultative anaerobe that grow by aerobic respiration or fermentation. Furthermore *S.aureus* can survive outside the body and is resistant to temperatures as high as 50°C and most disinfectants (Novick *et al.*, 1993). Members of this genus are catalase positive and oxidase negative but can be either coagulase positive or negative. *S.aureus* produces coagulase, an enzyme which clots fibrinogen in mammalian blood, it is also the most prominent pathogen of man (Tortora, P.J. *et al.*, 1997). Coagulase negative species are also capable of causing disease however this is often linked to prosthetic devices such as pacemakers and indwelling catheters (Lowy, 1998). *S.aureus* is also deoxyribonuclease positive, which allows it to degrade DNA (Lowy, 1998).

The first *S.aureus* genomes to be sequenced were those of the methicillin resistant strain N315 and vancomycin insensitive strain Mu50, both isolated from Japanese patients (Kuroda *et al.*, 2001). This revealed a low G+C content, 2.8MB genome encoding approximately 2500 genes (Baba *et al.*, 2002; Kuroda *et al.*, 2001). Subsequently a number of strains, such as *S.aureus* COL (The Institute for genomic Research, TIGR database; www.tigr.org/tdb) and *S.aureus* NCTC8325 (Oklahoma university; www.genome.ou.edu/staph.html) have been sequenced and annotated.

1.2. Pathogenesis of *Staphylococcus aureus*.

S.aureus is a commensal, that is carried transiently in up to 60%, and permanently in up to 20%, of the population (Lowy, 1998). It is usually found within the anterior nares or on the skin and transmission is most commonly via hands but can be airborne (Lowy, 1998; Whitt and Salyers, 2001). The presence of *S.aureus* doesn't necessarily indicate infection but does indicate a higher risk of one developing (Peacock *et al.*, 2001). It causes a wide range of diseases which have been separated into three categories; firstly the superficial lesions such as wound infections and skin abscesses, secondly systemic and life threatening conditions such as osteomyelitis, endocarditis and septicaemia and lastly toxin related disease such as toxic shock syndrome or food poisoning (Novick R. P., 2000; Sivaraman *et al.*, 2009). Given that it is a commensal organism, it has a remarkable array of virulence factors which work in concert with its adaptive physiology to cause this wide variety of infections. These virulence factors can be grouped into three categories: firstly, attachment factors involved in attaching the bacteria to cells or extracellular matrices; secondly, evasion of host defence factors that prevent or reduce phagocytosis, that interfere with the function of specific anti-staphylococcal host-defence mechanisms or antibodies, or both; and lastly, tissue penetration factors that specifically attack host cells and factors that specifically degrade components of extracellular matrices (Projan, S. J. and Novick, R. P., 1997). *S.aureus* has the ability to grow well under high osmotic conditions and low moisture, which allows it adapt to three distinct environments: freely outside the host, as an external colonizer, and living within tissues (Novick R. P., 2000). Furthermore, it has been shown that the risk of infection is increased where an individual is immunocompromised, a surgical patient or has an indwelling device such as a catheter (Lowy, 1998). Adding another facet to the infection process, it is possible for local infections to cause specific systemic syndromes, such as scalded skin syndrome or food borne gastroenteritis, even though the bacteria do not invade the bloodstream. The reverse is also true where dissemination from the blood stream can cause particular infections such as septic arthritis or epidural abscess (Archer, 1998). Pathogenicity of *S.aureus* is multifactorial in the majority of the diseases and is still poorly understood.

Though initially an organism associated with hospital acquired infections (nosocomial), in the 1990's community acquired methicillin resistant *S.aureus* began to emerge. The emergence of multidrug resistant strains and the spread of hypervirulence within both hospital and community settings (Sivaraman *et al.*, 2009) has made the study of *S.aureus* important as alternative therapies are required.

3.2.1. Treatment and antibiotic resistance

In recent years *S.aureus* has received much interest from the research community due to its position as one of the most important pathogens of man (Tortora, P.J. *et al.*, 1997). Similarly to other bacteria, *S.aureus* develops its resistance to antibiotics by selection of chromosomal mutations and acquisition of resistance genes on extrachromosomal plasmids, transducing particles, transposons or other types of DNA inserts.

The first, front line, drug to combat *S.aureus* infection was Penicillin G, however within 3 years of its introduction resistance had developed (Schito, 2006). Resistance was due to the production of β -lactamase, a serine protease that hydrolyses β -lactam rings rendering the antibiotic inactive. The enzyme is encoded by the *blaZ* gene, located on a transposable element carried by a plasmid (Lowy, 2003; Richmond, 1966). The first semi-synthetic penicillin, methicillin, was introduced in 1961 to combat this problem but resistance rapidly emerged again (Schito, 2006). Here, resistance is due to the production of an additional penicillin binding protein (PBP2a) which has a low affinity for β -lactams, allowing it to catalyze the otherwise blocked transpeptidation reaction (Berger-Bächi, 1994; Ghuysen, 1994). PBP2a is encoded by *mecA*, part of a chromosomal cassette (Woodford, 2005). This resistance mechanism is crucial as it confers resistance to all available β -lactams (Lowy, 2003).

The glycopeptide vancomycin was introduced in 1958 to combat the emergence of β -lactam resistance. It remained viable until 1996 when a vancomycin intermediate *S.aureus* strain (VISA) was identified (Hiramatsu *et al.*, 1997; Schito, 2006) and a fully resistant (VRSA) strain was reported in 2002 (Chang *et al.*, 2003). Worryingly all VISA strains were noted as being MRSA (Lowy, 2003). The reduced susceptibility seen in VISA isolates is thought to result from changes in peptidoglycan biosynthesis, which

has been seen as irregular shape, thicker cell walls, poorly separated cells, decreased cross-linking in the peptidoglycan, changes in structure and/or metabolism of teichoic acids, reduced rates of cell wall turnover and autolysis (Hiramatsu and Hanaki, 1998; Sieradzki and Tomasz, 2006, 2003). Sieradzki and Tomasz (1999) proposed that a decrease in peptidoglycan cross-linking traps the drug and thus reducing the efficacy. VRSA isolates gain their resistance from the conjugal transfer of the *vanA* operon, originally from vancomycin resistant *E.faecalis* (Noble *et al.*, 1992). This allows the synthesis of a cell wall precursor that ends in D-Ala-D-Lac instead of D-Ala-D-Ala which has a reduced affinity for vancomycin (Murray, 2000). In 2005 a compound which blocked the action of the DltA enzyme (a D-alanyl carrier protein ligase which is involved in the tailoring of Wall Teichoic Acid) was found to enhance the susceptibility of vancomycin against *B.subtilis* (May *et al.*, 2005).

While research into the discovery of a new antimicrobial targets is ongoing focus has been shifted into other defensive methods. There have been a variety of attempts to make a *S.aureus* vaccine. StaphVAX (Nabi pharmaceuticals) is a bivalent polysaccharide and protein conjugated vaccine. Although based on the two most prevalent serotype antigens (CP5 and CP8) which have been shown to successfully raise opsonising antibodies, StaphVAX was found to offer no significant protection in phase III trials (Fattom *et al.*, 1990; García-Lara and Foster, 2009; Jones, 2002). *In vivo* actively replicating *S.aureus* are capsular whilst lab strains do not have a capsule, which offers an explanation for the failure of StaphVAX (Poehlmann-Dietze *et al.*, 2000; O’Riordan *et al.*, 2004). Similarly, a vaccine based on iron-regulated surface determinant B (IsdB), being developed by Merck and Intercell, was halted due to safety concerns and the suggestion that significant protection would not be obtained (Harro *et al.*, 2012). Furthermore, passive immunisation strategies, such as Aurexis (Inhibitex) a humanised monoclonal antibody targeting the surface protein clumping factor A (ClfA), failed to obtain significant protection in phase II trials (Spellberg *et al.*, 2010).

Clearly it is essential that other ways of combating *S.aureus* and other antibiotic resistant microbes need to be developed, and to do this an understanding of the complex nature of *S.aureus* virulence, its life cycle and structure are required.

3.3 Bacterial cell division

In prokaryotes cell division is performed by a process known as binary fission. This is a type of asexual reproduction that results in the formation of two daughter cells from a parent cell without the formation of spindles. The single chromosomal DNA molecule is replicated and separated. Membrane invagination, growth of a cell cross wall and cytokinesis complete replication (Errington *et al.*, 2003) (Figure 1.6 shows cell division in rod, ovicocci and cocci). The whole process is performed with high fidelity, both spatially and temporally regulated so that complete copies of genetic information can be passed over to the next generation. It is worth noting that some species use alternative methods of cell division either as its normal propagation or conditionally e.g. under stress. Examples of this are; multiple offspring formation as seen for *Metabacterium polyspora* which forms multiple endospores routinely (Angert and Losick, 1998); the hyphal growth shown by Streptomycetes which contains many nucleoids but few septa (Xu *et al.*, 2008); or budding seen in *Hyphomonas* and other α -proteobacteria where swarmer cells differentiate to stalked cells, which produce budded progeny (Angert, 2005).

Cell division and growth need to be coordinated so that cells are the appropriate size before division occurs. It appears that either a constant cell volume, as shown in *Streptococcus faecium* (Gibson *et al.*, 1983), or a critical cell length, as shown in *E.coli* and *B.subtilis* (Donachie and Begg, 1989; Sharpe *et al.*, 1998), needs to be achieved before chromosome segregation. Cell growth rate regulates the timing of division (Den Blaauwen *et al.*, 1999; Weart and Levin, 2003) and in at least *B.subtilis*, the metabolic sensor coordinating cell size and growth rate with division has been identified as the glucolipid pathway (Weart *et al.*, 2007). The pathway transduces nutritional information directly to the divisome through an effector (UgtP), which inhibits *in vitro* and regulates *in vivo* septum formation. Although the direct mechanism of inhibition is still unknown, division is delayed until the critical mass is achieved and cytokinesis can be initiated. Interestingly, the glucolipid pathway synthesises uridine -5'-diphosphoglucose (UDP-Glc), which is in turn involved in the production of teichoic acids (Lu and Kleckner, 1994).

The first stage in bacterial cell division is represented by the formation of the Z ring. All other division proteins require FtsZ for correct localisation, and thus Z ring formation must be spatially controlled. For the localisation to occur at the high accuracy it does, the standard deviation for central Z ring position is 2.2% in *B.subtilis* and 2.6% in *E.coli*, two systems are employed. In *E.coli*, the Min system is composed of 3 components, MinC, MinD and MinE, which prevent cell division at the cell poles by oscillating between them (outlined in Figure 1.1A). In *B.subtilis* homologues of MinCD are present but not MinE; DivIVA fulfils this role (Figure 1.1B). Interestingly the Min system is not employed by gram positive cocci and when present does not have set members, indeed certain *Clostridia* possess both MinE and DivIVA (Errington *et al.*, 2003; Hu *et al.*, 2003; Margolin, 2001). In the nucleoid occlusion model, division is inhibited in the vicinity of nucleoids, providing temporal and spacial regulation of cell division (Figure 1.1C). In *B.subtilis*, Noc, a DNA-binding protein, co-localises with the nucleoid by binding consensus Noc-binding DNA sequences thus preventing assembly of the division machinery in the vicinity of the nucleoid (Wu *et al.*, 2009). SlmA has been identified as the division inhibitor in *E.coli* and although functionally analogous, they share no sequence similarity (Bernhardt and Boer, 2005). Division site selection within cocci is more complex because they have the potential to divide in an infinite number of planes. Nevertheless, *S.aureus* deleted of nucleoid occlusion factor (Noc) have been shown to form multiple Z rings which are no longer placed in perpendicular planes, indicating nucleoid occlusion may play a role in determining the plane of septum placement (Veiga *et al.*, 2011). It has been suggested that the epigenetic information encoded within the cell wall, potentially in combination with nucleoid occlusion, is used to select the division plane (Turner *et al.*, 2010). This will be discussed further in section 1.5.

3.4 The divisome

Components of the divisome have been identified within model organisms, however, not all are conserved across species, have been shown to be essential or have even been assigned functions. *B.subtilis*, *E.coli* and *Caulobacter crescentus* each have ten genes which have been shown to be essential (Figure 1.2 A and B show schematic representations of *B.subtilis* and *E.coli*)

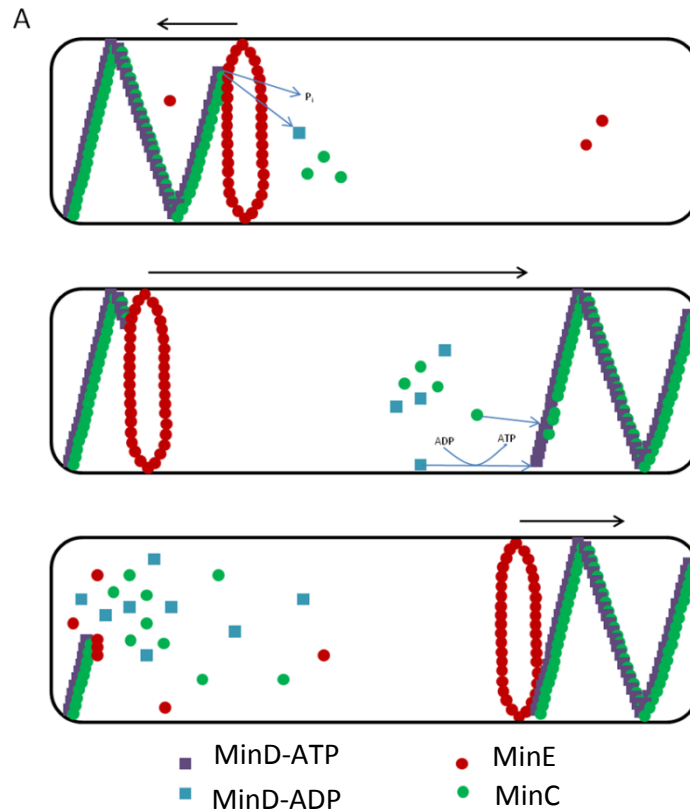
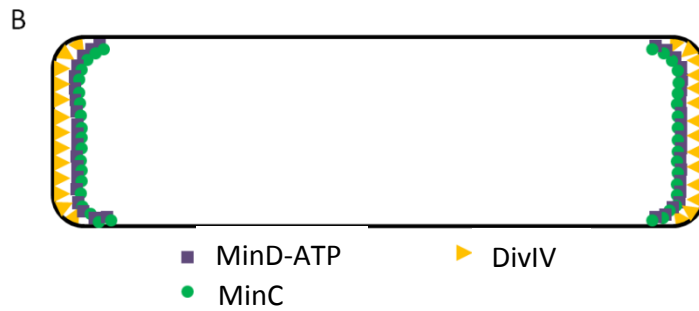
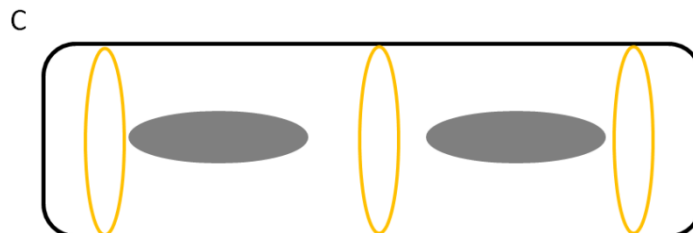


Figure 1.1 Division site selection in rod-shaped bacteria.

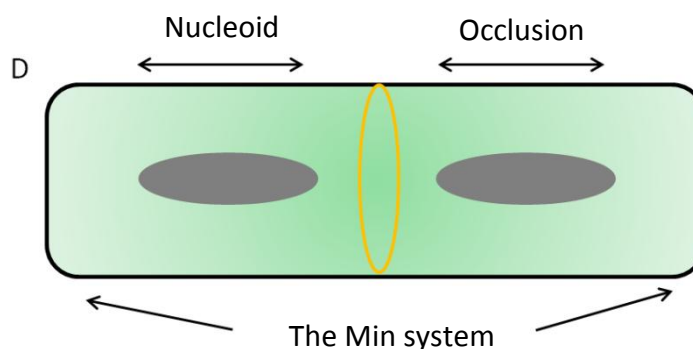
A) In *E. coli*; MinD dimerises and binds the lipid bilayer in an ATP-dependent manner. MinD recruits MinC to the bilayer; activating MinC. Together the MinCD acts as a regulator of FtsZ ring formation and polymerises in a helical pattern. MinD-ATP recruits MinE displacing MinC from the MinCD-bilayer complex in an ATP-independent reaction; inactivating MinC. MinE stimulates MinD ATPase resulting in release of MinD and MinE from the membrane (P. A. de Boer et al., 1992; de Boer et al., 1991; Hu and Lutkenhaus, 2000).



B) In *B.subtilis*; DivIVA is recruited permanently to the division site at a late stage of septation and is retained at the newly formed cell poles. DivIVA has an affinity for phospholipids and preferably binds strongly curved membranes. The MinCD complexes forms static filaments restricted to the cell pole due to denucleation by DivIVA (Cha and Stewart, 1997; Marston *et al.*, 1998).



C) The divisome is prevented from forming through a nucleoid by the binding of a nucleoid occlusion effector to binding sites on the chromosome and direct or indirect interaction with FtsZ. It does not set the septum localisation by positioning the nucleoid. In rod-cells there remain three available places for Z ring formation where DNA is absent; midcell and at either pole



D) Division at the cell poles is prevented by the Min system leaving the midcell as the only DNA-free site for Z ring formation.

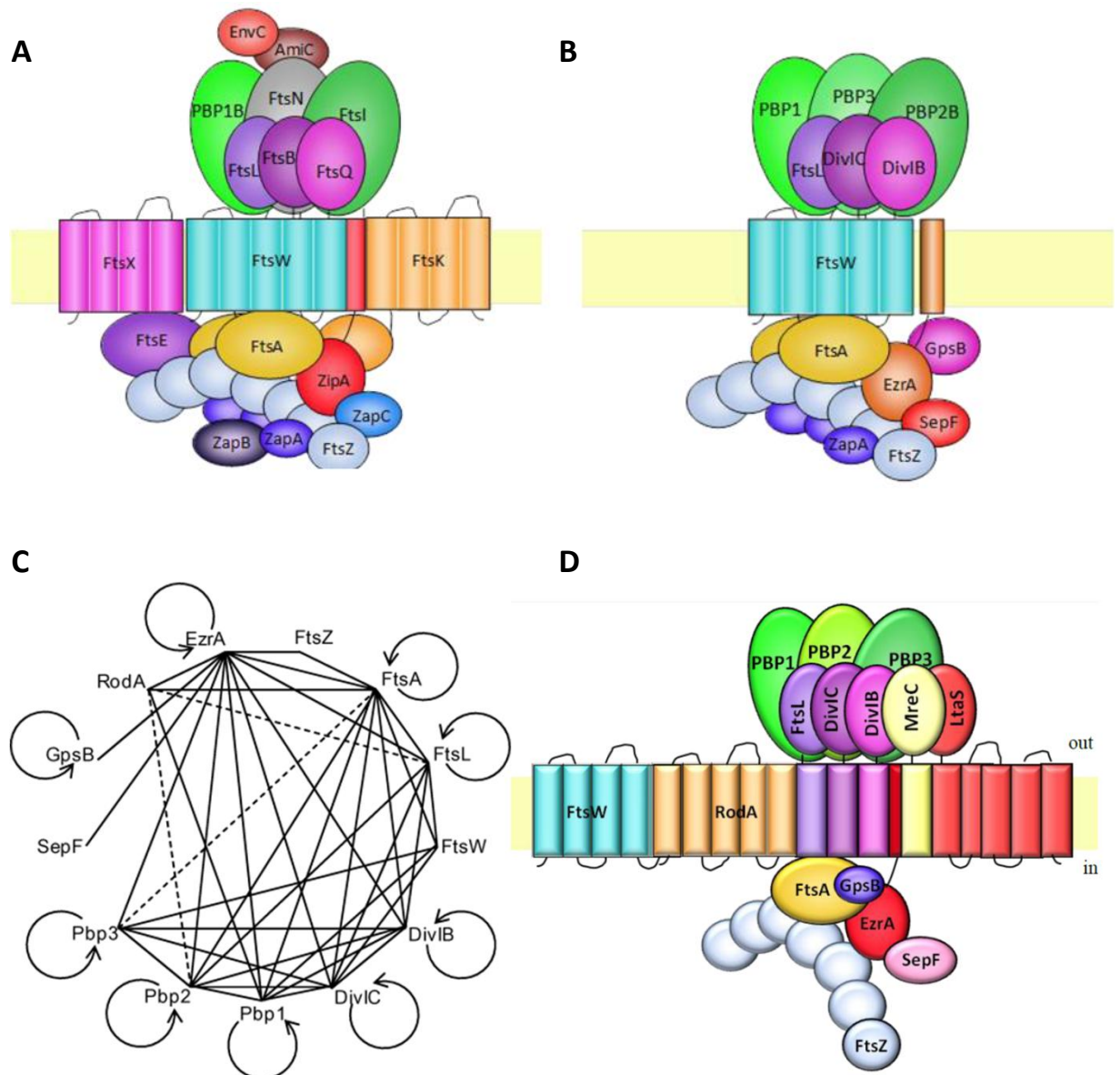


Figure 1.2 Divisome of *E.coli*, *B.Subtilis* and *S.aureus*.

A) Schematic representation of the *E.coli* divisome (reproduced from (Bottomley, 2011).

B) Schematic representation of the *B.subtilis* divisome (reproduced from Bottomley, 2011).

C) Interaction map of the *S.aureus* cell division proteins as determined by two-hybrid analysis. Positive interactions are shown by a solid line and putative interactions with a dashed line. Homodimerisation is indicated by a curved circular arrow (reproduced from Steele *et al.*, 2011).

D) Schematic representation of the *S.aureus* divisome (reproduced from Bottomley, 2011).

(Buddelmeijer and Beckwith, 2004; Goley *et al.*, 2011; Kobayashi *et al.*, 2003) whilst six are essential in *Streptococcus pneumoniae* for cell division. However, many other nonessential proteins with divisome roles have been characterised. The most comprehensive map of the *S.aureus* divisome was built on the basis of homology with cell division components of *B.subtilis*. This study revealed a complex web of sixty-two interactions between thirteen proteins, with nearly all proteins interacting with multiple partners (Steele *et al.*, 2011) (Figure 1.2 C and D). While 29 interactions were novel to *S.aureus*, most of the interactions had been previously characterised in *B.subtilis*, *E.coli* and/or *S.pneumoniae* further suggesting a conserved core of division proteins (Bottomley, 2011). The key components of the cell divisome, such as FtsZ, are faithfully conserved throughout bacterial species, whilst others have diverged significantly (Angert, 2005).

1.4.1 FtsZ

FtsZ is a GTPase which forms a ring found on the leading edge of cell constriction (de Boer *et al.*, 1992a). In *E.coli*, single molecule-based super-resolution microscopy showed that the Z 'ring' is composed of randomly overlapping bundles of FtsZ protofilaments (Anderson *et al.*, 2004; Fu *et al.*, 2010). Time lapse microscopy showed that when not involved in cell division FtsZ forms dynamic membrane bound spots throughout the cell (Thanedar and Margolin, 2004; Peters *et al.*, 2007). In fact quantitative fluorescence imaging showed in *E.coli* and *B.subtilis* the proportion of FtsZ that formed a ring structure was 30% whilst the remaining 70% was diffuse (Anderson *et al.*, 2004). FtsZ is a GTPase that utilises GTP to vertically assemble into protofilaments which, *in vitro*, are one subunit thick and 30-50 subunits long (Chen and Erickson, 2005; Huecas *et al.*, 2008, 2007). Binding of GTP activates FtsZ, which then acts as its own GTPase-activating protein (Scheffers and Driessen, 2001; Scheffers *et al.*, 2002). However, using GTP analogues and FtsZ mutants it was shown that GTP is not required for binding but rather facilitates the constant recycling of FtsZ subunits by destabilizing FtsZ polymers (Huecas and Andreu, 2004; Mateos-Gil *et al.*, 2012). Bramhill (1997) reviewed the three most favoured models of Z ring constriction: short protofilaments of FtsZ, aided by an unknown motor, slide relative to one another causing a reduction in Z ring circumference; secondly, depolymerisation of the Z ring at

membrane anchor points causes constriction; or lastly, protofilaments may bend. Although no model has been definitively proven, straight filaments favour bound GTP and curved filaments favour GDP supporting the last model and suggesting GTP hydrolysis as a motor (Lu *et al.*, 2000). However, the second model also received support by the observation that the Z ring disassembles during constriction (Den Blaauwen *et al.*, 1999; Monahan *et al.*, 2009; Sun and Margolin, 1998).

EM studies, immunofluorescence and GFP fusions have all shown that FtsZ is the first protein to localise to the midcell (Addinall *et al.*, 1996; Bi and Lutkenhaus, 1991; Errington *et al.*, 2003; Ma *et al.*, 1996) with all other division proteins requiring interaction with FtsZ, usually via the conserved C terminus (Din *et al.*, 1998), for correct localisation. It is therefore unsurprising that FtsZ is strongly conserved across prokaryotes, most archaea and the organelles of eukaryotes (Beech *et al.*, 2000; Erickson *et al.*, 2010; Osteryoung *et al.*, 1998). Indeed temperature sensitive and conditional mutants in *E.coli* and *B.subtilis* undergo normal cell elongation, DNA replication and chromosome segregation but fail to divide (Beall and Lutkenhaus, 1989; Dai and Lutkenhaus, 1991). Thus, it is thought that FtsZ is a prokaryotic cytoskeleton element, essential for cell division (Dai and Lutkenhaus, 1991) and critical for septum formation in *S.aureus* (Pinho and Errington, 2003).

1.4.2 FtsZ interacting partners

Apart from FtsZ, FtsA is the only other essential cytoplasmic cell division protein, although it is thought to associate with the membrane. FtsA is a member of the actin/Hsp70/sugar kinase ATPase superfamily and directly interacts with FtsZ, indicating the early localisation later confirmed by yeast two hybrid analysis (Bork *et al.*, 1992; Erickson, 2001; Ma and Margolin, 1999; Wang *et al.*, 1997; Yan *et al.*, 2000). The cellular ratio of FtsA to FtsZ appears to be important for correct division; in *E.coli* the cellular ratio of FtsA:FtsZ is 1:100 (Dai and Lutkenhaus, 1991) whilst in *B.subtilis* the ratio is 1:5 (Feucht *et al.*, 2001). Despite this evidence, the exact mechanism of how FtsA helps FtsZ in cell division is unclear. However FtsA does directly interact with a number of other proteins and together they may tether FtsZ to the membrane (Di Lallo *et al.*, 2003; Karimova *et al.*, 2005; Maggi *et al.*, 2008). Furthermore, FtsA may utilise

energy from ATP hydrolysis to either drive assembly or help control cell constriction (Errington *et al.*, 2003). It is well conserved in most bacteria, although is not found in mycobacteria, cyanobacteria and mycoplasma (Margolin, 2000).

ZipA was found in *E.coli* by affinity blotting for FtsZ-interacting proteins (Hale and de Boer, 1997). It is recruited early to the Z-ring in an FtsZ-dependent FtsA-independent manner (Hale and de Boer, 1999). The Z ring is formed in the presence of either FtsA or ZipA but not in the absence of both proteins, however both are required for septal constriction (Pichoff and Lutkenhaus, 2002). As with FtsA, ZipA binds to the C terminus of FtsZ and it is thought to enhance and stabilise the formation of FtsZ bundles (RayChaudhuri, 1999). It is predicted to be an integral membrane protein and is essential in *E.coli*, with the only other obvious homologue in *Haemophilus influenzae* (RayChaudhuri, 1999). ZapA (FtsZ-associated protein) is thought to have a similar role in cell division to ZipA, interacting directly with FtsZ to promote bundle formation (Gueiros-Filho and Losick, 2002). It is predicted to be cytoplasmic (like FtsZ and FtsA); however it is not essential for septum formation (Gueiros-Filho and Losick, 2002). ZipA is present in *B.subtilis*, and is widely conserved in other bacteria, including *S.aureus*.

EzrA, has a similar membrane topology to ZipA but no significant sequence homology (Errington *et al.*, 2003). Indeed, evidence indicates the opposite role to ZipA as a negative regulator in *B.subtilis* by destabilising FtsZ filaments (Levin *et al.*, 1999). EzrA also binds to the C terminus of FtsZ, and so may compete with the positive regulators FtsA and ZipA (Singh *et al.*, 2007). In contrast, EzrA has also been shown to be required for efficient division in *B.subtilis* and mutants have a reduced diameter, suggesting involvement in elongation. Within *S.aureus*, EzrA is essential for cell growth and the absence results in delocalisation of cell division machinery and a block in peptidoglycan synthesis (Steele *et al.*, 2011). Furthermore, in *B.subtilis* EzrA and GpsB may help with the localisation of PBP1, with the former ensuring midcell localisation and the latter promoting removal from the completed cell pole. It is conserved amongst the low G+C Gram positive bacteria, but is not essential in *B.subtilis* (Levin *et al.*, 1999).

In *B.subtilis* SepF has also been shown to interact directly with FtsZ, by affinity chromatography and yeast two hybrid, at an early stage (Hamoen *et al.*, 2006;

Ishikawa *et al.*, 2006). EM has shown that SepF forms large ring structures, approximately 50nm in diameter, which cause bundling of the FtsZ protofilaments into long tubular structures presumably by co-polymerisation (Gündoğdu *et al.*, 2011). SepF is well conserved throughout gram positive bacteria but is often non essential, with deletion mutants exhibiting aberrant septum formation or altered cell morphology (Fadda *et al.*, 2003; Hamoen *et al.*, 2006; Ishikawa *et al.*, 2006).

ZapB localises to the midcell in an FtsZ- and ZapA- dependent, FtsA-, ZipA- and FtsI (PBP3)- independent, manner polymerising into large filaments that have been shown to constrict slightly ahead of the Z ring (Ebersbach *et al.*, 2008; Galli and Gerdes, 2010). It is thought that ZapB mediates stabilisation of the lateral interactions between FtsZ protofilaments, by cross-linking ZapA molecules bound to the FtsZ polymers (Galli and Gerdes, 2010). Indeed deletion in *E.coli* results in filamentous cells, suggesting the involvement of ZapB in cell division (Ebersbach *et al.*, 2008).

A further FtsZ regulator in *E.coli* has been found in ZapC, which suppresses FtsZ GTPase activity and increases FtsZ protofilament bundling (Durand-Heredia *et al.*, 2011; Hale *et al.*, 2011). ZapC localisation to the midcell was FtsZ dependent but independent of FtsA, ZipA, ZapA and ZapB (Durand-Heredia *et al.*, 2011; Hale *et al.*, 2011).

1.4.3 Septal biosynthesis machinery

The remaining identified divisome proteins are all membrane-bound proteins with roles in synthesis, remodelling and degradation of peptidoglycan. FtsK is a large protein highly conserved in most bacteria. The N-terminal membrane domain is poorly conserved but responsible for midcell targeting (Draper *et al.*, 1998; Yu *et al.*, 1998). The C-terminal domain is required for ATP-dependent chromosome segregation (Yu *et al.*, 1998). Therefore it is thought that FtsK is involved in actively transporting DNA away from the closing septum to prevent chromosome cleavage (Yu *et al.*, 1998; Pease *et al.*, 2005).

FtsW is a division specific lipid II flippase and as a member of the shape, elongation, division and sporulation (SEDS) family has a strong association with class B penicillin-binding proteins (PBP's) (Boyle *et al.*, 1997; Gérard *et al.*, 2002; Lara and Ayala, 2002).

Indeed in *E.coli* there is a perfect presence-absence correlation between FtsI (PBP3) and FtsW (Henriques *et al.*, 1998) and direct interaction has been shown using numerous techniques (Datta *et al.*, 2006; Di Lallo *et al.*, 2003; Fraipont *et al.*, 2011; Karimova *et al.*, 2005). Furthermore FtsW is essential for FtsI recruitment to the division site (Mercer and Weiss, 2002) and both have been shown to interact with the monofunctional glycosyltransferase, MtgA (Derouaux *et al.*, 2008). *E.coli*, *B.subtilis* and also curiously *S.aureus*, encode a SEDS protein apparently involved in cell wall elongation (RodA). It is thought that the staphylococcal RodA has a minor role and functions with the non-essential class B PBP3 (Zapun *et al.*, 2008b).

The formation of a trimeric complex of FtsQ/DivIB, FtsB/DivIC and FtsL is conserved in all species for which division protein interactions have been investigated (Buddelmeijer and Beckwith, 2004; D'Ulisse *et al.*, 2007; Daniel *et al.*, 2006; Noirclerc-Savoye *et al.*, 2005). FtsQ in *E.coli*, and its homologue DivIB in *B.subtilis*, have similar membrane topology to FtsL, FtsN and FtsI and appears to be essential for cell division (Carson *et al.*, 1991). It is thought that this trimer acts as a scaffold for other division proteins, which is stabilised and regulated by FtsQ/DivIB (Daniel and Errington, 2000). Nevertheless the observation that FtsQ/DivIB is often found in operons with genes involved in peptidoglycan precursor synthesis and the abnormal cell wall phenotypes of mutants, has implied a further role in cell wall mechanics (Bottomley, 2011; Le Gouëllec *et al.*, 2008; Thompson *et al.*, 2006; Zapun *et al.*, 2008b). FtsL is a small transmembrane protein that has been shown to interact with many division proteins (Daniel *et al.*, 2006; Di Lallo *et al.*, 2003; Karimova *et al.*, 2005; Maggi *et al.*, 2008) and is required for the assembly of DivIB, DivIC and FtsI at midcell (Weiss *et al.*, 1999). FtsL is very unstable and unfolded and degraded in the absence of other divisome proteins. Overexpression has the ability to recover *ezaA* mutant phenotypes, indicating that FtsL has a regulatory role and acts synergistically with EzrA to regulate Z ring constriction. FtsB, and its *B.subtilis* homologue DivIC (Errington *et al.*, 2003), are small essential transmembrane protein that like FtsL are intrinsically unstable (Buddelmeijer and Beckwith, 2004; Buddelmeijer *et al.*, 2002). DivIC/FtsB and FtsL are dependent on one another for correct septal localisation and stability in both *B.subtilis* and *E.coli* (Buddelmeijer *et al.*, 2002; Gonzalez and Beckwith, 2009). Work within this lab has

shown that all three are peptidoglycan binding proteins, FtsL showing the lowest affinity, and although cell division proteins they apparently localise away from the septum (Bottomley, 2011)

FtsN is an essential division protein, first thought to be conserved only in enteric bacteria but since shown to be present throughout proteobacteria in varying amounts of sequence similarity (Dai *et al.*, 1993; Möll and Thanbichler, 2009). It has been suggested to have a number of functions; stabilising the divisome through direct interaction with peptidoglycan (Arends *et al.*, 2010; Möll and Thanbichler, 2009; Müller *et al.*, 2007; Ursinus *et al.*, 2004); regulating activity of enzymes involved in peptidoglycan turnover or cell separation (Derouaux *et al.*, 2008; Gerding *et al.*, 2009; Karimova *et al.*, 2005; Müller *et al.*, 2007); and globally influencing the cell division machinery (Dai *et al.*, 1993). FtsEX, is an ABC transporter; with FtsX being the integral membrane anchor protein and FtsE the associated cytoplasmic ATPase (de Leeuw *et al.*, 1999; Yang *et al.*, 2011). In *E.coli*, FtsEX localises to the division site, with FtsX localisation requiring FtsZ, FtsA and ZipA (Schmidt *et al.*, 2004). FtsE has shown direct interactions with FtsA and FtsQ, through BATCH (Karimova *et al.*, 2005), and FtsZ, through co-immunoprecipitation (Corbin *et al.*, 2007). FtsE improves assembly or stability of the septal ring (Schmidt *et al.*, 2004) and mutations of FtsE ATP-binding have implied that FtsEX utilises ATP to facilitate Z ring constriction (Arends *et al.*, 2009).

GpsB (also known as YpsA) is a paralogue of the *B.subtilis* DivIVA, with homologues present in several gram positive bacteria (Tavares *et al.*, 2008). Midcell localisation of GpsB is dependent upon FtsZ, FtsA, DivIC and PBP2b; and, unlike DivIVA, GpsB is not retained at newly formed cell poles, indicating a different function. Direct interactions have been seen with PBP1, MreC and EzrA (Tavares *et al.*, 2008). GpsB, in concert with EzrA, is thought to co-ordinate division and elongation in *B.subtilis* (Claessen *et al.*, 2008).

1.4.4 Penicillin binding proteins

Peptidoglycan synthesis requires the family of PBPs for cell wall synthesis through the glycerol transferase, transpeptidase, endopeptidases and carboxypeptidase activity

catalysed by these acyl serine transferases (Ghuysen, 1991). PBP's are classed as high molecular weight (HMW) and low molecular weight (LMW) PBPs, with each class being further subdivided. HMW-PBPs have a cytoplasmic tail with a hydrophobic transmembrane region and two domains located on the outer surface of the cytoplasmic membrane where peptidoglycan synthesis occurs (Sauvage *et al.*, 2008). This class is then subcategorised depending on the catalytic activity of their N-terminal domain. Class A HMW-PBP's are bifunctional enzymes; the N-terminal domain has transglycosylase activity, while the C-terminal domain has transpeptidase activity (Sauvage *et al.*, 2008). Class B HMW-PBPs are monofunctional enzymes with C-terminal transpeptidase activity and an apparently inactive N-terminal, although it has been suggested that it may function as an intramolecular chaperone for folding of the catalytic domain or play a role in cell morphogenesis (Goffin *et al.*, 1996; Höltje, 1998; Sauvage *et al.*, 2008). It follows that, Class A PBPs are capable of elongation of glycan strands and formation of cross-links within peptidoglycan (the two enzymatic activities required for peptidoglycan polymerisation), whilst Class B PBPs only perform the latter. Monofunctional transglycosylases lack a penicillin binding domain but may also carry out transglycosylation.

LMW-PBP's typically have a cleavable amino-terminal signal peptide and are typically anchored to the membrane via the C-terminus, although they can be loosely associated with the membrane via hydrophobic or electrostatic interactions or be soluble (Fonzé *et al.*, 1999; Harris *et al.*, 1998; Pratt, 2008). This class again can be subcategorised into three classes, labelled from A-C and separated primarily by amino acid sequence. All three classes are DD-carboxypeptidases but class C occasionally possess DD-endopeptidase activity (Sauvage *et al.*, 2008).

PBPs can be associated with a specific mode of cell wall synthesis; elongation (in rod shaped organisms) or septal (indicating potential divisome interaction). However the precise role of specific PBPs is often difficult to identify due to the variable number and redundancy shown in many organisms. The number of PBP's within bacteria varies greatly; *E.coli* has 12, *B.subtilis* has 16 while cocci have between 4-7 (Zapun *et al.*, 2008a) and the deletion of different combinations of these PBPs results in many different mutant phenotypes which reflects their participation in multienzyme

complexes (Pratt, 2008). *S.aureus* has four PBP's; one HMW-PBP Class A (PBP2), two HMW-PBP Class B (PBP1 and PBP3) and one LMW-PBP (PBP4) (Sauvage *et al.*, 2008). As a coccus, it does not undergo elongation and PBP2, which we would expect to perform elongation, localises at the septum. Unusually there is only one LMW-PBP which exhibits activity sufficient enough to achieve the high degree of cross-linking seen in *S.aureus* peptidoglycan (Atilano *et al.*, 2010; Wyke *et al.*, 1981). A monofunctional transglycosylase can also be found on the genome and in β -lactam resistant strains an additional PBP, PBP2a, is expressed (Sauvage *et al.*, 2008; Zapun *et al.*, 2008a).

1.5 *S.aureus* cell wall.

The cell wall serves as the interface between the bacterium and its environment, and thus is essential to a cell's survival from both internal and external conditions. The cell wall has an extensive list of functions including, withstanding the internal turgor pressure, preserving cell integrity, maintaining cell shape, acting as a physical barrier and protein scaffold (Osborn and Rothfield, 2007; Pichoff and Lutkenhaus, 2002; Scott and Barnett, 2006). Peptidoglycan is the major component of the cell wall and unique to the bacterial kingdom, its biosynthesis is therefore the site of action of some of the most clinically important antibiotics (e.g. penicillin and vancomycin) (Park and Strongminger, 1957; Courvalin, 2006). As a gram- positive, *S.aureus* is surrounded by a characteristic thick layer of peptidoglycan without an outer lipid membrane (descriptions of gram positive and gram negative cell walls are shown in Figure 1.3) (Höltje, 1998; Scott and Barnett, 2006). This layer is approximately 20 to 35 nm thick, in gram positives, forming up to 90% of the cell dry weight (Vollmer, 2008).

Peptidoglycan is made of a polysaccharide backbone consisting of alternating N-acetylglucosamine and N-acetylmuramic acid residues joined via a β 1,4 glycoside linkage (Cabeen and Jacobs-Wagner, 2005; Hiramatsu, 2001; Lugtenberg and Van Alphen, 1983). Each muramic acid has a covalently attached short amino acid chain consisting of alternating L- and D-isoform amino acids. D- amino acids are a defining characteristic of peptidoglycan because, apart from in a low abundance in teichoic acids (section 1.9.1), and they are not present in any other biomolecule. These peptide stems become highly crosslinked, in *S.aureus* via a pentaglycine interbridge, resulting in a strong 3D mesh-like layer (Wiedel *et al.*, 1960). Almost 85-90% of *S.aureus*

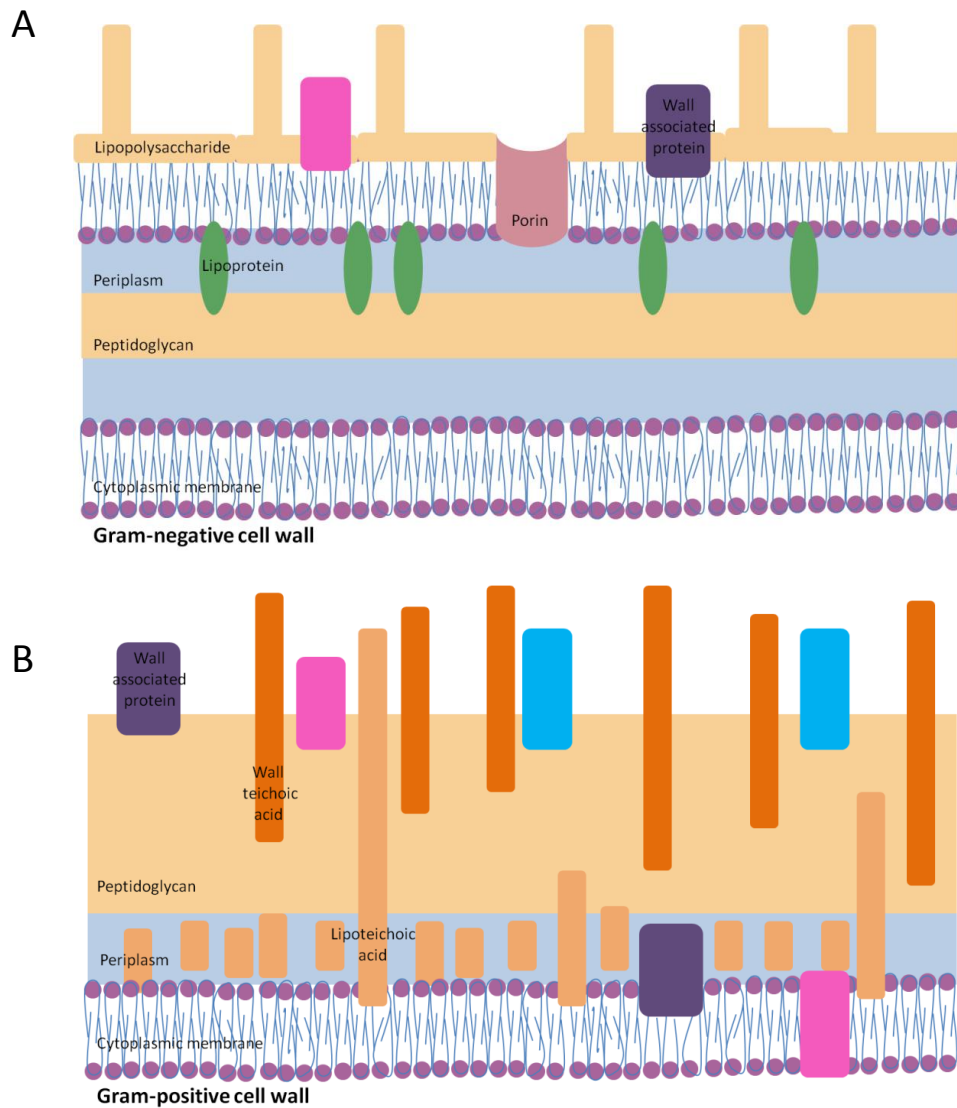


Figure 1.3 General structure of the Gram-negative and Gram-positive cell walls.

A) Gram negative; The cytoplasmic membrane is the inner most layer and acts as the major hydrophobic barrier between cytoplasm and external environment. The outer membrane is mainly Lipopolysaccharide (LPS), and interspersed with trimeric porin proteins which allow the passage of low molecular solutes. The periplasm is protein rich and contains a thin layer, 2-6nm, of peptidoglycan (Matias and Beveridge, 2008; Scott and Barnett, 2006; Silhavy *et al.*, 2010; Vollmer and Seligman, 2010).

B) Gram positive; There is no outer membrane but a much thicker, 20-35nm, layer of peptidoglycan surrounds the cell. Anionic polymers and proteins dot the surface and lipoteichoic acids are the major component of a narrow periplasm-like region (Matias and Beveridge, 2008, 2007, 2006, 2005).

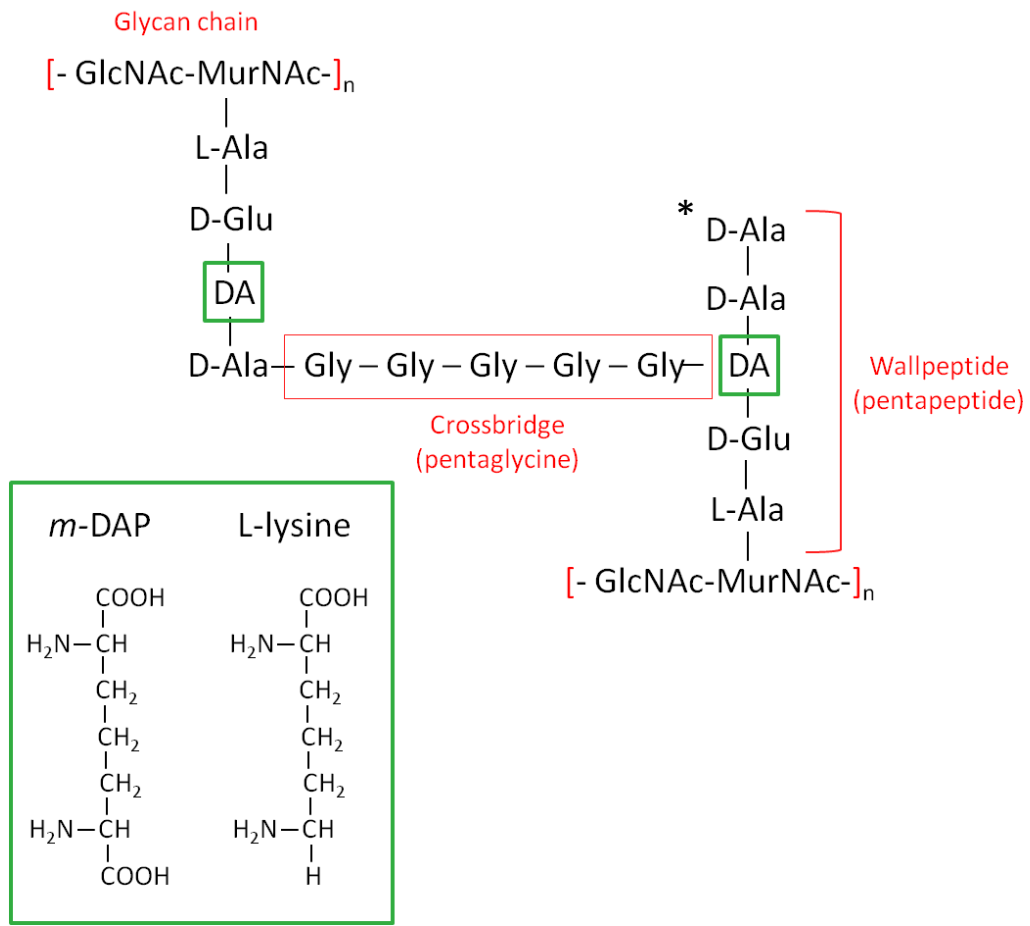


Figure 1.4 Chemical structure of Peptidoglycan (adapted from (Madigan M.T *et al.*, 2002))

The backbone of peptidoglycan is made up of alternating sugar residues. Short peptide arms are attached to MurNAC residues. The presence of a diamino acid (DA) at position 3 is necessary for cross-linking and the structures of two diamino acids, *meso*-diaminopimelic acid (*m*-DAP) and L-lysine are shown. During cross-linking via a pentabridge the second D-Ala is removed (*).

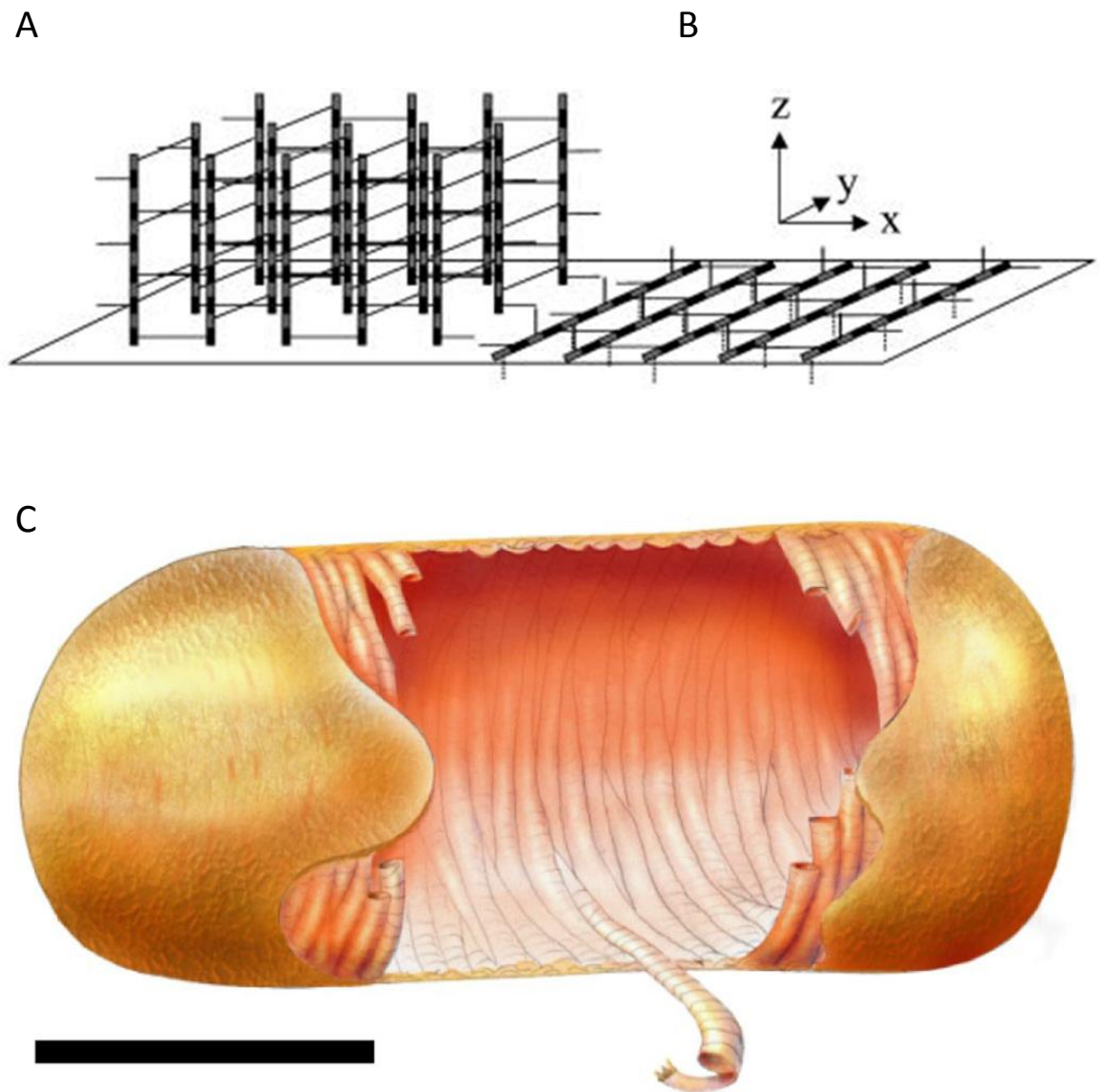


Figure 1.5 Peptidoglycan arrangement models

A) Scaffold model; The glycan chains are orientated perpendicular to the plasma membrane. The peptidoglycan would be maximally cross-linked close to the cytoplasmic membrane (Vollmer and Höltje, 2004).

B) Planar model; The glycan chains are orientated parallel to the lipid membrane. The thick wall of Gram-positive organisms would comprise multiple planar layers. In a rod shaped organism, the glycan strands would be arranged circumferentially providing the mechanical strength (the lateral force acting on a cylinder is twice that of the longitudinal direction) to maintain a rod shape under turgor pressure (Vollmer and Höltje, 2004).

C) *B. subtilis* model; Bundles of glycan strands form a 'rope' of approximately 25nm wide which is coiled into a ~50nm wide cable which is then attached to the existing cell wall (Hayhurst *et al.*, 2008).

peptidoglycan is crosslinked (Wilkinson, 1997). Cross-linking between adjacent stems occurs via linkage of the ϵ -amino group of the dibasic amino acid to the α -carboxyl group of the terminal D-alanine of tetrapeptides. Although rarely, a 3-3 cross-linkage can occur between two dibasic amino acids. The chemical structure of peptidoglycan is outlined in Figure 1.4.

The glycan chain length varies between organisms, *S.aureus* have relatively short chains at approximately 6 disaccharides long (Boneca *et al.*, 2000). The C6 group of the MurNAc may be modified by *O*-acetylation, *N*-glycosylation or de-*N*-acetylation (Vollmer, 2008) in varying degrees and combinations depending on species. These modifications have been shown to provide resistance to lysozyme and other autolysins, and in the case of *O*-acetylation is associated with pathogenesis and modulation of the host immune response. The arrangement of the glycan strands has undergone much debate and two possible models exist; the glycan strands are arranged in the plane of the cytoplasmic membrane (de Pedro *et al.*, 1997; Koch, 1998), or the glycan strands are arranged perpendicular to the cytoplasmic membrane (Dmitriev *et al.*, 2004, 2003) (both models are addressed in figure 1.5). The glycan chain lengths of *S.aureus* are short enough to permit either configuration (disaccharide length ~ 6 at 1.03nm per disaccharide (Carlstrom, 1957); Peptidoglycan layer width 20-35nm). However, recent publications have suggested a poorly ordered planar orientation is adopted by the Gram-negative organisms *E.coli* and *C.crescentus*, as shown by electron microscopy, neutron scattering and atomic force microscopy (Gan *et al.*, 2008; Vollmer and Höltje, 2004; Wang *et al.*, 2012). Furthermore, the rod-shaped Gram-positive *B.subtilis* exhibits a more complicated architecture of peptidoglycan cables wrapping around the cell cylinder (Figure 1.5C) (Hayhurst *et al.*, 2008).

1.6 Peptidoglycan synthesis.

Peptidoglycan is synthesised in three key stages: synthesis in the cytoplasm of a monosaccharide pentapeptide; assembly of the disaccharide-pentapeptide monomer unit on the inner surface of the cytoplasmic membrane and translocation of the monomer to the periplasm; and finally transglycosylation of the monomer unit into a

glycan polymer, and transpeptidation into the sacculus (Typas *et al.*, 2012). Rod-shaped organisms alternate between two modes of cell wall synthesis; elongation, where peptidoglycan occurs in a potential helical pattern along the lateral cell wall (Daniel and Errington, 2003); and septal growth, where synthesis occurs at the septum leading to the formation of the septal disc (Pinho and Errington, 2003). Cocci offer a simpler model of cell wall synthesis, because the FtsZ-dependent cell wall synthesis is predominant and can account for the synthesis of the entire new hemisphere of each daughter cell. It is important to note the difference between the two types of cocci: true cocci, such as *staphylococci*, which are truly round; and ovococci, such as enterococci, which are elongated ellipsoids. Ovococci and true cocci do not have the same mechanisms of cell wall synthesis during the cell cycle (discussed in Figure 1.6, alongside rod-shaped organisms).

The enlargement of the multilayered sacculus has been proposed to occur via a three-for-one mechanism of 'inside-to-outside' growth (Höltje and Heidrich, 2001; Höltje, 1998). An inside-to-outside model for the flux of cell wall material suggests that the cell wall inner layer contains newly synthesized peptidoglycan. This peptidoglycan is introduced in a 'three-for-one' manner, where one glycan strand in the sacculus is replaced by a nascent triplet of cross-linked glycan strands and pulled into plane of the sacculus under turgor pressure. As the cells grow, the new cell wall passes outwards and stretches, becoming the middle stress bearing zone. The outer zone consists of old, partially hydrolyzed peptidoglycan awaiting solubilisation (Höltje and Heidrich, 2001; Höltje, 1998; Pooley *et al.*, 1978). As *S.aureus* grows exclusively by division, they have a single peptidoglycan synthesis machinery, which is coordinated by FtsZ during division (Atilano *et al.*, 2010; Pereira *et al.*, 2007; Pinho and Errington, 2005, 2003). AFM has identified that *S.aureus* forms a thick band of material, which exhibits a corrugated 'piecrust' texture, around the cell in the plane of division (described through the cell cycle in Figure 1.7A) (Turner *et al.*, 2010). This 'piecrust' rib forms before the centripetal synthesis of the septal disc. Once the septal disc is complete the cell splits and produces two pseudo-hemispherical cells. The thick 'piecrust' splits into two ribs which serve to brace the cell, preventing collapse to a smaller energetically

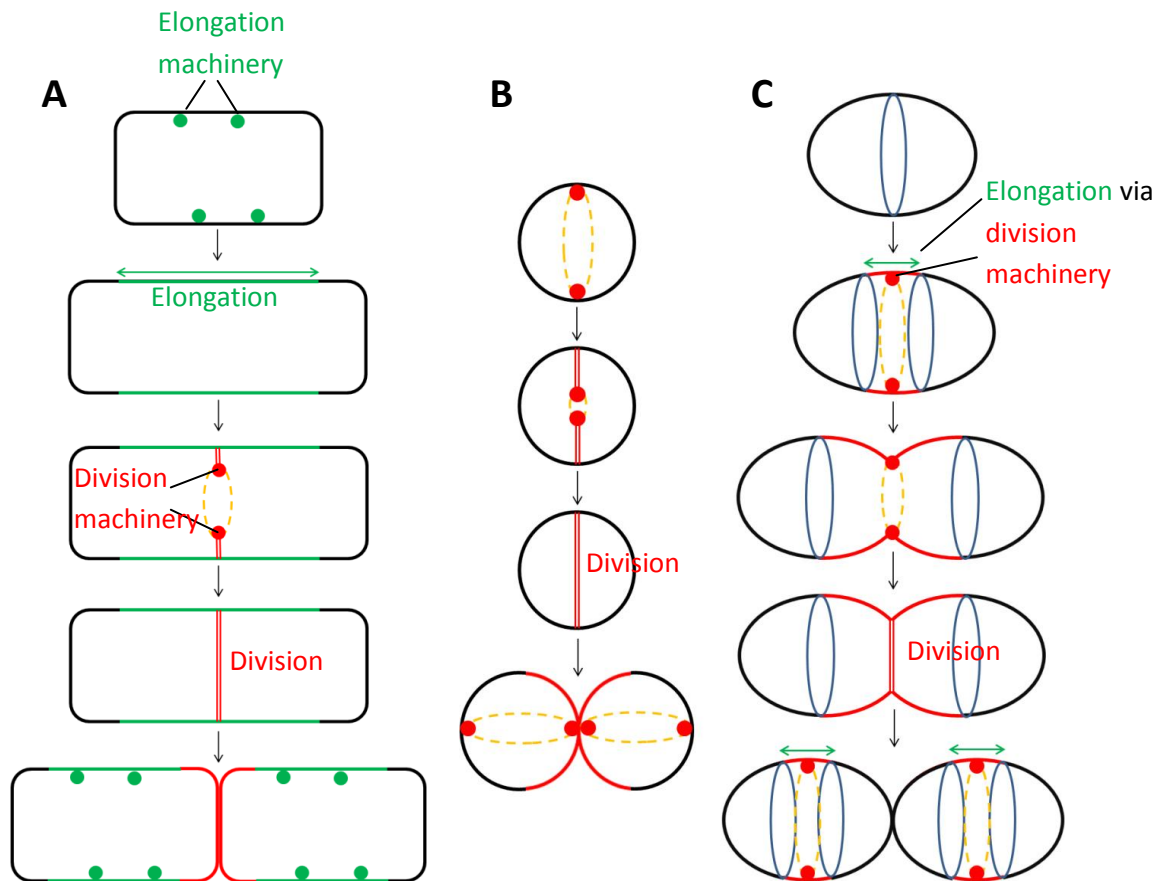


Figure 1.6 Peptidoglycan dynamics in cocci and ovococci

A Rod-shaped. Most rod-shaped organisms elongate by dispersed helical insertion of peptidoglycan (MreB-directed in *E.coli* and Mbl-directed in *B.subtilis*). A short phase of FtsZ driven elongation precedes division. Division occurs rapidly by constriction or septum formation. Daughter cells separate and initiate elongation again.

B True cocci. Peptidoglycan synthesis occurs at septation. The division ring is initiated. The septum then closes centripetally, like the iris of a camera. A complete cross-wall forms, dividing the cell into two hemispherical daughter cell compartments. Daughter cells separate, the septal cross-wall becomes the new cell wall hemisphere and division is initiated on the next orthogonal plane.

C Ovococci. An annular outgrowth of the cell wall termed an equatorial ring, demarks the initiation site of the new cell wall. Synthesis of an invaginating cross-wall is initiated and the equatorial ring is split in two and the rings are driven apart by peripheral wall synthesis. The equatorial rings approach the mid-cell of the forming daughter cells. Peripheral extension switches to constriction. The annular cross-wall closes forming a new cell pole. Peripheral growth initiates in the daughter cells.

favourable shape, and forcing the new cell wall to stretch as the cell grows in size. To allow this growth the peptidoglycan is remodelled by irreversible autolysis of covalent bonds (observed by AFM as a transition from centric ring architecture to a knobbly architecture) within long glycan strands. This makes the cell wall more elastic by sharing the stress bearing function between the glycan strands and more flexible peptide stems and allowing the expansion from hemisphere to spherical (Figure 1.7B) (Wheeler R., 2012). The 'piecrust' ribs are retained after division and have been proposed to encode enough information for the cell to 'remember' previous division planes (Figure 1.7A). The most recent division plane will be seen as a whole rib, the division before as a half rib and the third most recent division as a quarter rib. This rib is uniquely bounded by two T junctions which may allow the cell to mark this plane for the next division (Turner *et al.*, 2010). The question of how the division machinery are recruited to this nascent septal ring is still not understood but has been hypothesised as a function of membrane distortion due to the 'piecrust' ribs (Wheeler R., 2012) which may be recognised by DivIB (Bottomley, 2011).

1.7 Peptidoglycan hydrolysis

For a cell to continue growing and dividing peptidoglycan must be remodelled and hydrolysed at specific times and specific sites. This hydrolysis of either the glycan or peptide chain is carried out by a group of enzymes known as peptidoglycan hydrolases (Vollmer *et al.*, 2008). Some of the physiological roles of peptidoglycan hydrolysis include cell growth, cell-wall turnover, peptidoglycan maturation, cell division, separation and pathogenicity (Foster, 1995; Stapleton *et al.*, 2007; Vollmer *et al.*, 2008). It is also involved in more specialised functions; differentiation to endospores (Errington, 2003), assembly of macromolecular *trans*-envelope complexes (Hirano *et al.*, 2001; Koraimann, 2003), cross-species and inter-species competition (Ellermeier *et al.*, 2006; Russell *et al.*, 2011), competence (Ahn and Burne, 2006; Eldholm *et al.*, 2010) and biofilm formation (Vollmer *et al.*, 2008). In addition, peptidoglycan hydrolysis releases turnover products which serve as signalling molecules for recognition of bacteria by other organisms and, in some bacteria, for the induction of β -lactamase (Jacobs *et al.*, 1997; Vollmer *et al.*, 2008).

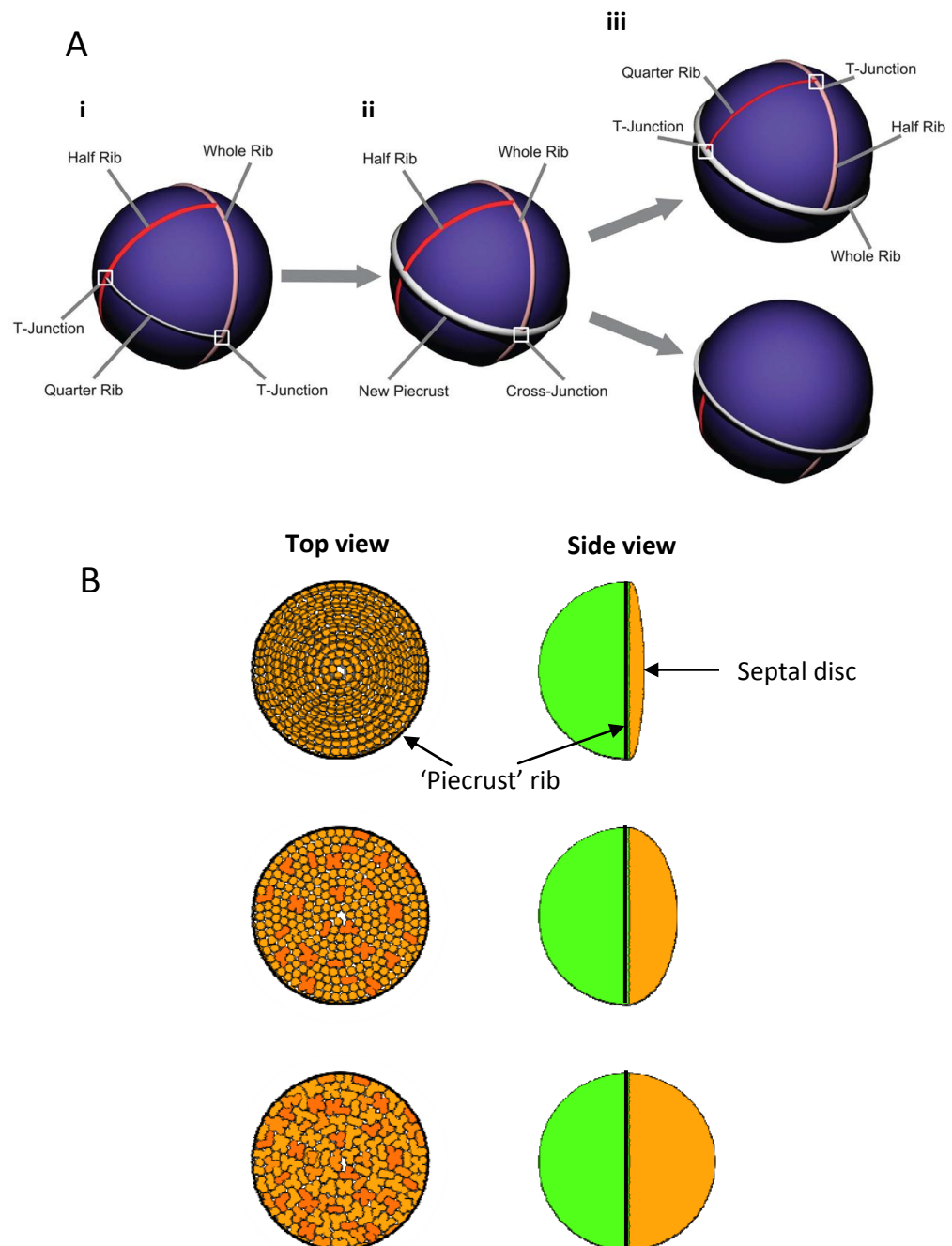


Figure 1.7 Growth of peptidoglycan and structural inheritance of division planes in *S.aureus*

A) Location and remodelling of piecrust and rib features through the division cycle, resulting in T junctions and cross sections. The quarter rib is a distinctive feature (i) and a new piecrust is formed in this plane (ii), it is then split in two as the cell divides (iii). This leads to a revised rib pattern that specifies the next round of division (Taken from Turner *et al.*, 2010).

B) The thick piecrust braces the hemisphere and long, glycan strands predominate in the new cross-wall, preventing expansion or collapse. Hydrolysis of the ring architecture reduces the chain length and increases the elasticity of the wall permitting increase to a spherical shape (Wheeler R., 2012).

1.8 Peptidoglycan hydrolases

A bacterial species may have a variety of peptidoglycan hydrolases which often have more than one physical function and exhibit redundancy, thus the specific roles of a hydrolase are difficult to assign (Heidrich *et al.*, 2002, 2001; Höltje and Tuomanen, 1991; Smith *et al.*, 2000; Vollmer *et al.*, 2008). Indeed, *E. coli* has a complement of 21 known hydrolases and remains viable despite inactivation of apparently whole families of enzymes (Heidrich *et al.*, 2002). Recently, Singh *et al.*, (2012) showed redundant essentiality of three hydrolases (Spr, YdhO and YebA) where a conditional mutant of all three was unable to incorporate new murein and underwent rapid lysis at restrictive conditions. Despite their obvious roles in cell separation hydrolases can participate in host-pathogen interactions and be involved in immune evasion through alteration of the cell wall (Amieva and El-Omar, 2008; Dziarski and Gupta, 2010, 2005; Girardin and Philpott, 2004). Furthermore, hydrolases are also found in higher organisms as a defence against bacterial pathogens, and in phage for infiltration and escape from the bacterial host (Vollmer *et al.*, 2008).

There are peptidoglycan hydrolases to act upon each of the four bond classes, which results in the disruption of the cross linked structure of peptidoglycan. The cleavage sites of the different hydrolase classes are shown in Fig 1.8. *N*-Acetylmuramyl-L-alanine amidases hydrolyse the amide bond between MurNAc and L-alanine, separating the glycan strand from the peptide. They carry signal peptides in their N-termini and a non-catalytic region (cell wall-binding domain), which is responsible for the binding of the protein to the cell wall. The cleavage of the amide bond between amino acids is carried out by peptidases. Endopeptidases cleave all bonds within the peptide stem, while carboxypeptidases specifically cleave the bond required to release the C-terminal amino acid. They can both be prefixed with DD-, LD- or DL- depending on the isoforms of amino acids involved (Shockman G. D. and Holtje J.-V., 1994; Smith *et al.*, 2000; Vollmer *et al.*, 2008). *N*-acetyl muramidases (muramidases) cleave the β -1-4 chain that links *N*-acetylmuramic acid and *N*-acetylglucosamine. This bond can be cleaved in two different ways; lysozymes produce a terminal reducing MurNAc residue and lytic transglycosylases result in the formation of a 1,6-anhydro ring at the MurNAc

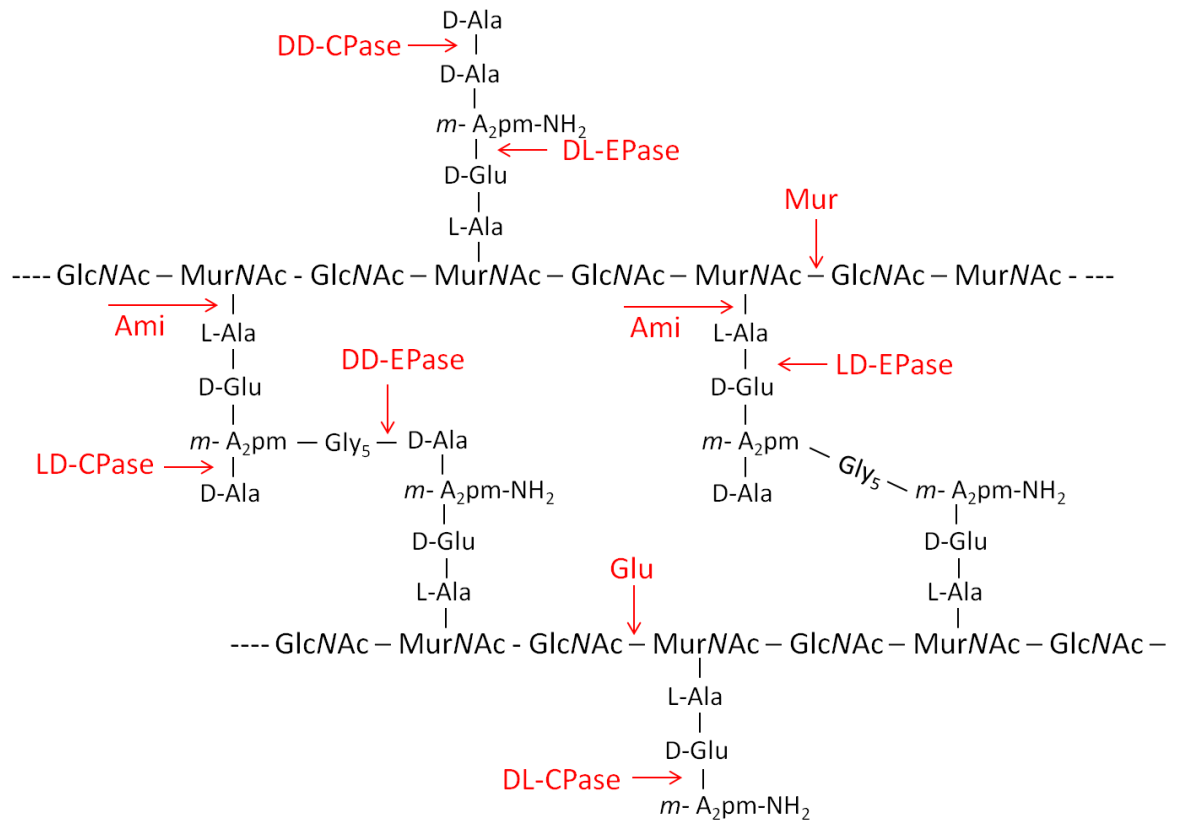


Figure 1.8 The specificity of peptidoglycan hydrolases

Structure of peptidoglycan showing major chemical bonds targeted by peptidoglycan hydrolases. Three classes of hydrolases. Ami, *N*-acetylmuramyl-L-alanine amidase; DD-CPase, DL-CPase, LD-CPase, Carboxypeptidases; DD-EPase, DL-EPase, LD-EPase, Endopeptidase.

(Adapted from (Vollmer *et al.*, 2008))

residue. N-acetylglucosaminidases (glucosaminidases) hydrolyse the bond between N-acetyl- β -D-glucosamine residues and adjacent monosaccharides (Karamanos, 1997).

Several classes of enzyme have been assigned specific functions. For instance, the tightly crosslinked peptidoglycan of *S.aureus* is a product of the relatively low activity of DD-carboxypeptidase. DD-carboxypeptidases trim pentapeptide stems to tetrapeptides, which can only accept bonds during transpeptidation, their low activity leaves many donor/acceptor stems and thus increases the extent of cross-linking (Atrih *et al.*, 1999; Markiewicz *et al.*, 1983; Vollmer *et al.*, 2008). In fact, hydrolases have been suggested as having a role in coordinating Z-ring placement; disruption of certain hydrolases in *S.pneumoniae* (PBP3) and *L.monocytogenes* (PBP5-homologue) results in aberrant septum placement (Guinane *et al.*, 2006; Schuster *et al.*, 1990) and mutants in *E.coli* PBP5, along with other LMW PBPs, display perturbed shape and branched morphology (Nelson and Young, 2001; Potluri *et al.*, 2010). It is well established that hydrolases are responsible for the splitting of the septum, with positive correlation having been reported between a lack of PG hydrolase activity and a failure in cell separation. In *S.aureus* the enzymes involved have been identified as Atl, Sle1, IsaA, ScaD and SA1825 (Foster, 1995; Kajimura *et al.*, 2005; Stapleton *et al.*, 2007). A list of all known and putative *S.aureus* hydrolases is shown in Chapter 6.

Hydrolases aid peptidoglycan maturation and wall turnover (needed for the inside-to-outside model of sacculi enlargement). Glucosaminidase produces an N-acetyl muramic acid at the non-reducing terminus of peptidoglycan. Atrih *et al.*, (1999) demonstrated its presence in *B.subtilis* after peptidoglycan was modified to its mature form, LytD and LytG were identified as the two glucosaminidases responsible (Margot *et al.*, 1994; Rashid *et al.*, 1995). Furthermore, in *B.subtilis* inactivation of *lytC* (encoding the major amidase) results in cell wall and septal thickening and a significant decrease in the rate of turnover, (Blackman *et al.*, 1998) and turnover retardation was enhanced in a *lytClytD* background (Smith *et al.*, 2000). Boneca *et al.*, (2000) saw minor satellite peaks when using Reverse Phase High performance Liquid Chromatography (RP-HPLC) to analyse *S.aureus* glycan strands, again suggesting the role of glucosaminidases in peptidoglycan maturation. Wheeler (2012) worked to confirm this suggestion and was able to suggest a hypothesis where the hydrolysis of peptidoglycan

through the action of glucosaminidases (SagA, SagB, ScaH and Atl(glu)) allows cell growth, which has implications for both *S.aureus* peptidoglycan architecture and cell physiology. Additionally, Δatl and $\Delta sle1$ exhibit altered wall turnover in *S.aureus*, shown by electron microscopy as rougher outer surfaces when compared to those of the parent (Foster, 1995; Kajimura *et al.*, 2005).

Hydrolases are also thought to play a role in competence, the ability of bacteria to take up DNA from its extracellular environment, and competition. AtIA-deficient *Streptococcus mutans* fail to develop competence, whilst liberation of DNA is almost completely abolished in a *S.pneumoniae* *lytA lytC* mutant (Ahn and Burne, 2006; Moscoso and Claverys, 2004). This is due to fratricidal lysis; a subset of cells develop competence and lyse non-competent sister cells or closely related species leaving a rich pool of genetic material, which enhances the uptake of genetic material by competent cells (Eldholm *et al.*, 2010). Similarly, bacteria can secrete hydrolases to cannibalise competitors for nutrients (Singh, 1947; Vollmer *et al.*, 2008). *P. aeruginosa* directly deliver an amidase, Tse1, and lysozyme, Tse3, into the periplasm of competing cells (Russell *et al.*, 2011) and *Myxococcus xanthus* produce several peptidoglycan hydrolases that can participate in this type of predatory lysis (Sudo and Dworkin, 1972). In *B.subtilis*, lysis of vegetative cells by the hydrolytic killing factor SpdC provides a pool of nutrients, preceding sporulation (Ellermeier *et al.*, 2006; González-Pastor *et al.*, 2003). Indeed, Staphylococcal Atl endo- β -N-acetylglucosaminidase inhibits mitogen-induced DNA synthesis of human leukocytes as well as the formation of cytoplasmic immunoglobulin-containing cells by β lymphocytes *in vitro* (Valisena *et al.*, 1991). However *atl* null mutants did not cause an alteration in acute infection in a mouse sepsis model (Takahashi *et al.*, 2002) even though a *sle1* mutant showed less pathogenesis in the same model (Kajimura *et al.*, 2005).

1.8.1 Regulation of peptidoglycan hydrolases

Most cell wall growth models predict a system where cell growth ceases when the activity of peptidoglycan hydrolases is inhibited. Multienzyme complexes consisting of both hydrolases and synthesis machinery help to suggest this prediction (Nelson and Young, 2001; Takahashi *et al.*, 2002). Peptidoglycan hydrolases can be potentially

lethal to a cell if activity is incorrectly timed and thus regulation must be tightly controlled. It is therefore unsurprising that regulation has been seen at the transcription level, post-transcriptionally, by proteolytic cleavage, via secondary wall polymers and substrate modification.

Most of the hydrolytic enzymes involved in sporulation and germination are controlled by the sporulation-specific cascade of sigma factors at the transcriptional level (Vollmer *et al.*, 2008). *B.subtilis* coregulates autolysins and motility to allow dechaining of cells and thus effective chemotaxis. The alternate flagellar chemotaxis and motility sigma factor, *sigD*, the major housekeeping factor, *sigA*, and the late mother-cell specific sigma factor, *sigK*, regulate up to 8 hydrolases (LytD, LytC, LytF, LytG, LytH, CwIC, CwIH and LytE) allowing expression to be coordinated with life cycle stage (Blackman *et al.*, 1998; Horsburgh *et al.*, 2003; Lazarevic *et al.*, 1992; Margot *et al.*, 1994). Furthermore, dual regulation allows for differential coordination of a single enzyme and another level of regulation. *B.subtilis* endopeptidase lytE is regulated by SigA but upregulated as an emergency response by SigI (Tseng *et al.*, 2011; Zuber *et al.*, 2001).

Peptidoglycan hydrolase activity can be regulated in response to environmental signals via a two component signal transduction system. The WalKR (also called YycFG, VicRK and MicAB) is an example of this and thought to be essential in *B.subtilis*, *E.faecalis*, *L.monocytogenes*, *S.aureus*, *S.pneumoniae* and *S.mutans* (Dubrac *et al.*, 2007; Hancock and Perego, 2004; Kallipolitis and Ingmer, 2001; Martin *et al.*, 1999; Ng *et al.*, 2003). In *B.subtilis* the regulon includes four peptidoglycan hydrolases and has been shown to localise to the septum, suggesting that it acts as a sensor for initiation of cell division (Fukushima *et al.*, 2008). *S.aureus* also has a WalKR regulon, which includes nine hydrolases. *S.aureus* contains a second two component signal transduction system, the LytSR system which regulates autolysin expression. Zymogram analysis showed increased expression of HMW peptidoglycan hydrolases and decreased expression of LMW peptidoglycan hydrolases, indicating both positive and negative regulation. Also *lytS* mutants form cell aggregates with a rough wall phenotype and increased rate of autolysis (Brunskill and Bayles, 1996).

Direct protein-protein interaction has been shown to coordinate the activity of hydrolases as well as their localisation. *Mycobacteria* have been shown to have a delicate model in which PBP1B inhibits the activity of the endopeptidase, RipA, until the septum has completely formed when RipA interacts synergistically with RpfB, a putative lytic transglycosylase, to efficiently separate daughter cells (Hett *et al.*, 2007, 2008, 2010). Protein-Protein interaction can be used to colocalise peptidoglycan hydrolysis and synthesis. Yeast two-hybrid analysis in *B.subtilis* showed LytE interaction with, the cytoskeletal elements, MreBH and in *S.pneumoniae*, putative peptidoglycan hydrolase PcsB interacts with FtsX, an FtsZ-dependent division component (Sham *et al.*, 2011). In *E.coli* the lytic transglycosylase MltA, was used as bait in affinity chromatography revealing interactions with five PBPs and SPR revealed a trimeric complex with PBP1B and a scaffold protein, MipA (MltA interacting protein) (Vollmer *et al.*, 1999).

Proteolytic processing is required for activation and stabilisation of peptidoglycan hydrolase activity. The best studied example of proteolytic processing on peptidoglycan hydrolases is the major bifunctional *S.aureus* autolysin Atl. It is synthesised as a 138kDa proenzyme which undergoes multiple rounds of proteolytic cleaving to remove the propeptide and targeting sequences, yielding two mature hydrolases 62kDa amidase and 51kDa glucosaminidases (discussed further in Chapter 6) (Foster, 1995; Oshida *et al.*, 1995). Similarly, in *E.coli* MltB is degraded to release a soluble lytic transglycosylase, Slt35 (Engel *et al.*, 1992; Ehlert *et al.*, 1995). Bublitz *et al.*, (2009) have shown that proteolytic cleaving of *L.monocytogenes* Auto releases a self-inhibitory N-terminal α -helix from the catalytic domain. Furthermore, the unilateral localisation of *B.subtilis* LytF has been shown by mutant studies to be due to the action of the extracellular proteases WprA and Epr (Yamamoto *et al.*, 2003). Recently, the protease/chaperone HtrA in *S.pneumoniae* has been suggested to regulate the balance of secreted peptidoglycan hydrolases via the SecA transport, to which it is associated (Tsui *et al.*, 2011).

Extracellular components, for example teichoic acids (TAs) have also been shown to have a role in the localisation and action of peptidoglycan hydrolases. Teichoic acids are discussed in detail in 1.9.1, and have been shown to target hydrolase activity either

by acting as a scaffold or through an avoidance mechanism. In *L.monocytogenes* the autolysins Auto and EnIA, along with other virulence factors like InIB, localise to the inner periplasmic surface via binding modular repeats to LTAs (Dramsi *et al.*, 1995). The phosphorylcholines within TAs in *S.pneumoniae* are used as a scaffold for the targeting of many gram-positive proteins via their choline binding domains (ChBD)(Fernández-Tornero *et al.*, 2001). *S.pneumoniae* offers several examples of this localisation with its autolysins LytA, LytB, LytC, CbpD and Pce (Lopez and Garcia., 2004; Eldholm *et al.*, 2010) and in the case of LytA choline binding serves a dual function by converting the low activity monomer to the highly active homodimer C-form (Romero *et al.*, 2007) at the appropriate subcellular localisation. Repeat regions have been identified in the major autolysins of *S.aureus* and *S.epidermidis*, Alt and AtlE respectively, which are required for septal binding, potentially through a WTA avoidance mechanism (section 1.9.1) (Baba and Schneewind, 1998; Schlag *et al.*, 2010). Similarly, *S.aureus* Sle1 and LytN could not bind peptidoglycan in the presence of WTA but bound uniformly across the cell wall in the absence of WTAs (Frankel and Schneewind, 2012).

Glycan strands themselves can be sufficient for accurate targeting. LysM domains have been identified as the binding domain in the peptidoglycan hydrolases of several species. The LysM of *L.lactis* AcmA bound TA extracted cells but did not bind regions containing LTAs (Steen *et al.*, 2003). Vollmer has suggested that 'smart autolysins' are directed to sites where peptidoglycan bonds are stretched, like the long glycan within the *S.aureus* septal disc (Vollmer *et al.*, 2008). Although modifications of the glycan strands often confer resistance to autolytic action, the activity of *L.plantarum* LytH is enhanced by the O-acetylation of MurNAc. The covalent modifications of peptidoglycan also allows bacterial cells to differentiate into endospores, by permitting germination specific cortex-lytic enzymes to specifically hydrolyse the spore cortex (Atrih *et al.*, 1996; Popham *et al.* 1996; Smith *et al.*, 2000).

1.9 Cell surface glycopolymers

As discussed the gram-positive cell wall is thicker than that of the gram-negative and lacks an outer membrane. This wider layer of peptidoglycan is studded with

carbohydrate-based anionic polymers that are believed to play an important part in maintaining the cell. They help perform a number of functions similar to the outer membrane in gram negative bacteria; influencing membrane permeability, mediating extracellular interactions, providing additional stability to the plasma membrane. Most importantly for the purposes of this study they act as scaffolds for extracytoplasmic enzymes required for cell-wall growth and degradation, touched upon in section 1.8.1.

1.9.1 Teichoic acids

A major class of the cell surface glycopolymers are the teichoic acids (TAs), which are phosphate rich molecules found in a wide variety of Gram-positive bacteria. There are two types of TAs, wall teichoic acids (WTA) and lipoteichoic acids (LTA) shown in figure 1.9. In *S.aureus* LTAs have a backbone of glycerol phosphate which is anchored to the plasma membrane via a glycolipid anchor of a diglucosyl diacylglycerol and extends from the cell surface into the peptidoglycan layer (Figure 1.9B) (Xia *et al.*, 2010a). More complex LTAs are present in *Lactococcus garviae*, *Clostridium innocum* and *Streptococcus pneumonia* (Reichmann and Gründling, 2011). WTA are much more abundant than LTA accounting for 70-90% of the TA content in *B.subtilis*, and collectively they make up to 60% of the dry mass of the cell wall (Dramsi *et al.*, 1995; Silhavy *et al.*, 2010; Swoboda *et al.*, 2010). The composition of WTA varies within and between species. In the case of *S.aureus* the main backbone is most commonly ribitol phosphate and ~40 residues long. This glycopolymer chain is linked to two glycerol phosphates and connected to the peptidoglycan via a phosphodiester linker of N-acetylglucosamine-1-P and N-acetylmannosamine (Figure 1.9B) (Xia *et al.*, 2010a). The hydroxyls on the ribitol phosphate repeats are tailored with D-alanyl esters and monosaccharides, such as glucose or N-acetylglucosamine (Mirelman *et al.*, 1970; Xia *et al.*, 2010b; Yokoyama *et al.*, 1989). The extent to which these modifications occur is again strain dependent and can be environment dependent (Swoboda *et al.*, 2010). Within *S.aureus*, and conserved across several Gram-positive bacteria, the WTA GlcNAc-transferase activity has been shown to be mediated by TarM (Xia *et al.*, 2010b). These modifications have profound impact on the physiology of the organism, from antibiotic susceptibility to survival within a host, indeed glycosylation of WTA is required for methicillin resistance in *S.aureus* (Brown *et al.*, 2012).

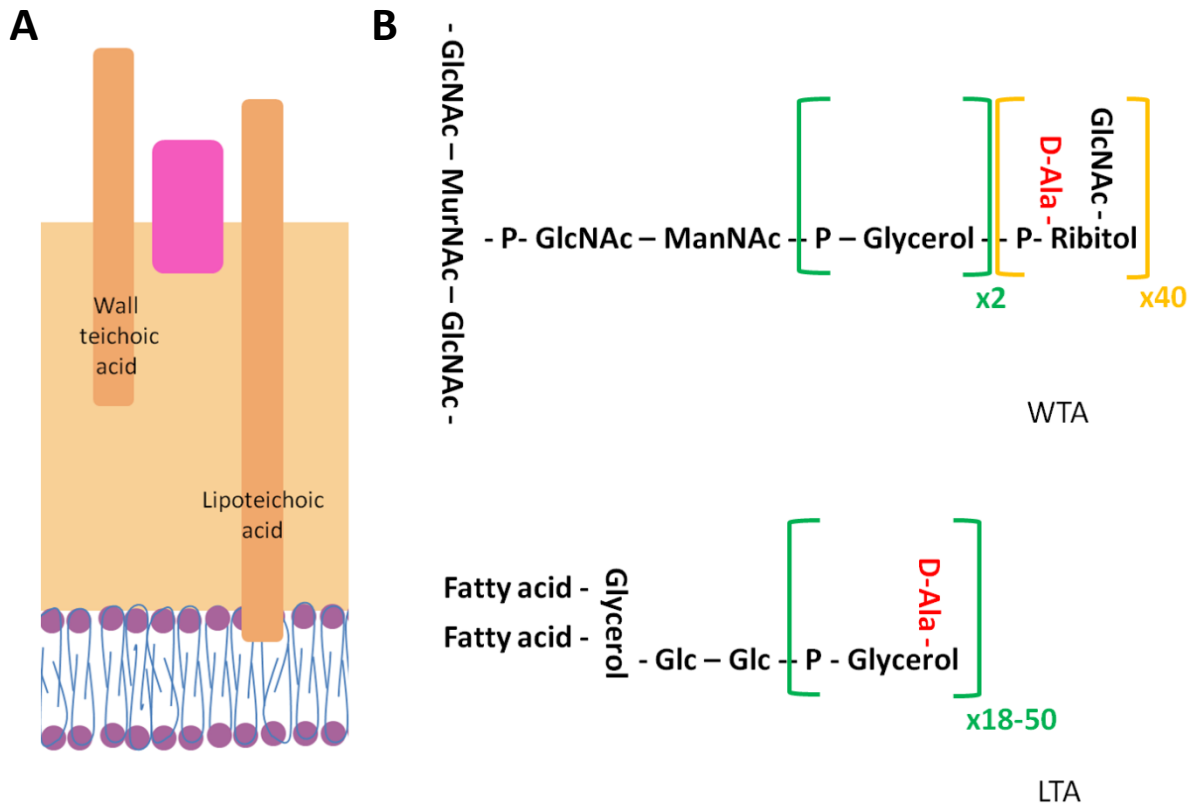


Figure 1.9 Schematic diagrams of WTA and LTA (adapted from (Xia *et al.*, 2010a))

P, phosphate; D-ala, D-alanine; GlcNAc, N-acetylglucosamine; ManNAc, N-acetylmannosamine; Mur-NAc, N-acetylmuramic acid; Glc, Glucose.

A) Schematic localisation in the cell wall and cell envelope of WTA and LTA.

B) Schematic of the chemical structure of WTA and LTA, showing the linking to the cell wall and cell envelope respectively.

D-alanylation, a tailoring modification which introduces positively charged amines of WTAs alters the net charge of the otherwise very negative polymer by adding positively charged amines. This reduces the electrostatic repulsion between TA chains and may allow the stabilising formation of ion-pairs between anionic phosphates and cationic esters (Wickham *et al.*, 2009). The D-alanine modification itself regulates the interaction between the cell envelope and the environment and has been implicated in many scaffold/receptor functions (Gross *et al.*, 2001; Neuhaus and Baddiley, 2003). The absence of D-alanyl esters increases susceptibility to cationic antimicrobial peptides (possibly by increasing the negative charge density on the cell surface (Kristian *et al.*, 2003; Peschel *et al.*, 1999), increases sensitivity to glycopeptide antibiotics and to lytic activity of some host enzymes (Collins *et al.*, 2002; Peschel *et al.*, 2000). Conversely the activity of autolytic enzymes is decreased and the binding of *S.aureus* to surfaces is attenuated (Gross *et al.*, 2001; Peschel *et al.*, 2000). These observations and animal studies have led to the D-alanine modification as a putative target for novel antimicrobials that function by attenuating virulence (Brown *et al.*, 2012; May *et al.*, 2005). The glycosylation modification, which involves the addition of *N*-acetylglucosamine as the carbohydrate in *S.aureus*, is much less understood but known to be ubiquitous (Neuhaus and Baddiley, 2003).

The functions of TA in bacterial physiology are also not fully understood. TAs form a 'continuum of negative charge' which allows the cell to bind cationic groups, further alleviating any repulsive interactions between neighbouring phosphates. Networks of WTA-coordinated cations affect the overall structure of the polymers, and this in turn influences the porosity and rigidity of the cell envelope (Hughes *et al.*, 1973; Lambert *et al.*, 1977; Marquis *et al.*, 1976; Swoboda *et al.*, 2010). Furthermore, WTAs help maintain a pool of ions close to the surface that might be required for enzyme activity or can help ease osmotic pressure (Ellwood and Tempest, 1972). As previously stated D-alanylation modulates this, indeed lack of D-alanyl esters allows cells to bind up to 60% more Mg^{2+} ions, while in *B.subtilis* TA production is unregulated in low Mg^{2+} conditions (Ellwood, 1970; Heptinstall *et al.*, 1970).

Further to binding cations WTAs serve to act as scaffolds or receptors for a wide range of other molecules. They function as receptors that are required for phage infection in

S.aureus (Chatterjee, 1969), anchors for cell surface proteins (Navarre and Schneewind, 1999) and as previously discussed thought to serve as scaffolds for autolysins (Calamita and Doyle, 2002; Peschel *et al.*, 2000; Schlag *et al.*, 2010). WTA have also been shown through localisation studies to associate with the machinery involved in elongation and LTA to associate with septation and cell division machinery (Formstone *et al.*, 2008; Schirner *et al.*, 2009). Indeed *B.subtilis* WTA null mutants produce spherical, severely defective progeny and LTA mutants show defects in septation and cell separation (Pollack and Neuhaus, 1994; Schirner *et al.*, 2009; Soldo *et al.*, 2002). Although preventing WTA production in *S.aureus* leads to less pronounced defects, it has been suggested that they have a role in directing several hydrolases through an avoidance mechanism (as previously described and further addressed in Chapter 6.1). Whilst *S.aureus* strains devoid of LTA show major defects in septal formation, separation and have restrictive growth conditions (Oku *et al.*, 2009). *S.aureus* WTA mutants display reduced adherence to artificial surfaces (Gross *et al.*, 2001) and have also been shown to be impaired in host tissue adhesion (Weidenmaier *et al.*, 2005, 2004). Further still they exhibit an impaired ability to produce biofilms despite no reduction in the production of the major biofilm formation factor (PNAG) (Vergara-Irigaray *et al.*, 2008).

The biosynthetic pathway of *S.aureus* WTA is separate from LTA, requiring at least 12 genes for biosynthesis while LTA biosynthesis requires only 3 (Xia *et al.*, 2010a). It has been identified as very similar to *B.subtilis* W23 WTA pathway and outlined in Figure 1.10 (Swoboda *et al.*, 2010). *S.aureus* synthesise poly-Rbo-P and therefore have been assigned the gene acronym 'tar' within this study, however many of these genes are conserved in poly-Gro-P biosynthesis and can be known as 'tag'. Although previous work had been performed on uncharacterised WTA null mutants, Peschel and co-workers were the first to characterize a WTA mutant as $\Delta tarO$, lacking the first gene in the WTA biosynthetic pathway (Weidenmaier *et al.*, 2004). It has since been reported that *tarA* can also be deleted and produce viable cells however many genes downstream of *tarA* cannot be deleted unless *tarO* is also deleted (D'Elia *et al.*, 2006). This mixed gene dispensability pattern has two possible explanations. Firstly sequestration of the undecaprenyl phosphate-linked peptidoglycan precursor used

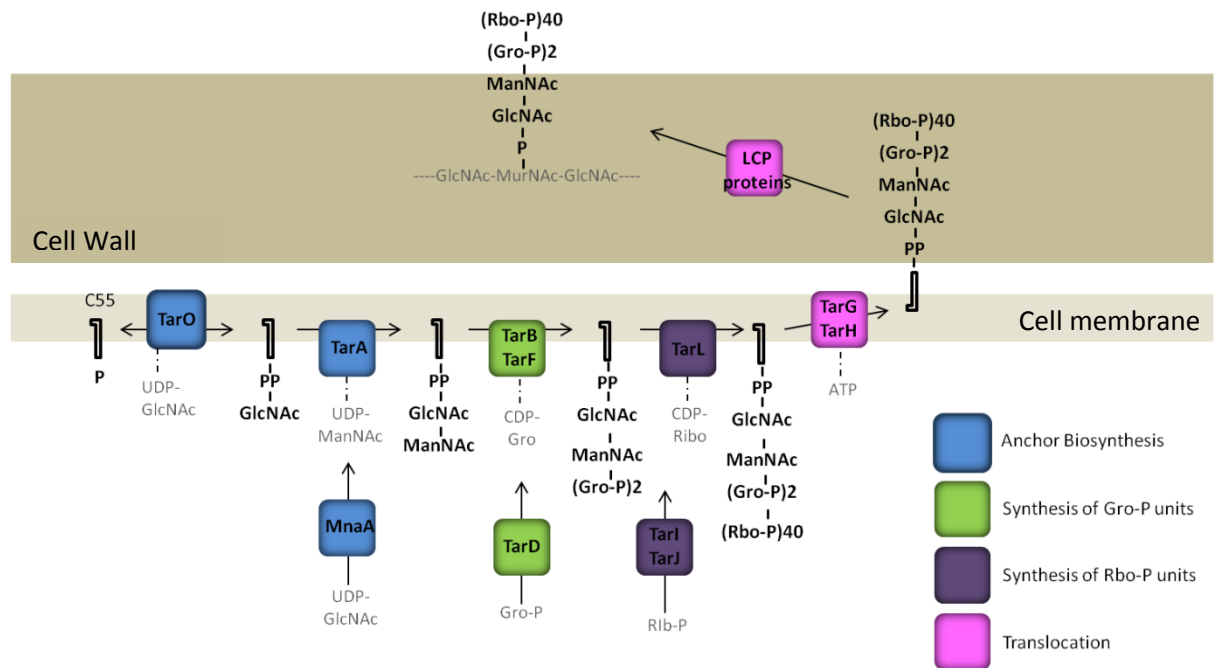


Figure 1.10 Pathway of *S. aureus* WTA biosynthesis. (Adapted from ((Xia *et al.*, 2010a)).

CDP-Gro, cytidyldiphosphate-glycerol; CDP-Rbo, cytidyldiphosphate-ribitol; Glc, Glucose; GlcNAc, N-acetylglucosamine; Gro, glycerol; Gro-P, glycerolphosphate; ManNAc, N-acetylmannosamine; MurNAc, N-acetyl muramic acid; Rbo-P, ribitol phosphate; Rib-P, ribulose-5-phosphate; UDP-Glc, uridine-5-diphosphate-glucose; UDP-GlcNAc, uridine-5-diphosphate-N-acetyl-glucosamine; UDP-ManNAc, uridine-5' diphosphate-N-acetyl-mannosamine.

S. aureus synthesis poly-Rbo-P and therefore have been assigned the gene acronym 'tar' however many of these genes are conserved in poly-Gro-P biosynthesis and can be known as 'tag'. TarO transfers GlcNAc and TarA transfers ManNAc consecutively to the undecaprenylphosphate (C55-P) lipid carrier. TarD synthesizes activated precursor Gro-P molecules. The TarB primase adds the first glycerolphosphate unit and TarF the second. TarIJ synthesize the precursor CDP-ribitol units which are subsequently attached by the polymerase TarL. The completed unit is then translocated via TarG and TarH, an ABC transporter, to the outer membrane leaflet and attached to the 6-OH group of MurNAc in the PG by the LCP proteins, MsrR, SA0908 and SA2103 (discussed in detail in chapter 3.2.1).

from the first step of the pathway, may block the peptidoglycan biosynthetic pathway. In fact this has been proposed as the mechanism for toxicity in *B.subtilis* (D'Elia *et al.*, 2009). Secondly, blocking of nonessential bactoprenol-dependent pathways leads to an accumulation of bactoprenol-linked intermediates that themselves are directly harmful to the cell (Danese *et al.*, 1998). It is important to note that it is not possible to prevent both WTA and LTA expression, suggesting that they have overlapping functions and can potentially partially compensate for one another (Oku *et al.*, 2009). Their roles have not been unequivocally proven but both mutants are temperature sensitive and exhibit growth defects (Oku *et al.*, 2009; Swoboda *et al.*, 2010). Although they have different biosynthetic pathways, D-alanylation of the similar phosphate-linked repeat units is performed by the same machinery (Swoboda *et al.*, 2010).

1.10 Surface Proteins

Further to TAs the surface of *S.aureus* is decorated with a variety of proteins. The first surface protein to be characterised in *S.aureus* was Protein A (Spa), which is a virulence factor and has been shown to bind non-specifically to IgG reducing phagocytosis. This binding can occur via the effector region (Fc γ) halting recognition by the Fc receptor; by interacting with the antigen recognition Fab region of IgG; or through interaction with the heavy chain independent of hypervariable regions (Forsgen *et al.*, 1966; Vidal *et al.*, 1985; Graille *et al.*, 2000). The roles of bacterial surface proteins are varied; protection of bacteria from the environment, including toxic conditions or host immune defence system proteins; nutrient acquisition; bacterial attachment to environmental components; interaction between bacteria, like biofilms; facilitating competition between bacteria; and those required for cell growth, like cell wall maintenance and division. The expressed protein complement is highly influenced by life cycle stage, environment and critical in determining the success of a bacterium, it is therefore unsurprising that they are strongly regulated at a transcriptional level (Scott and Barnett, 2006). The staphylococcal accessory gene regulator locus (*sar*) and the accessory gene regulator locus (*agr*) are the best characterised. The *S.aureus* exoprotein expression locus (*sae*), sigma factors and the ferric uptake repressor have also been identified as controllers. Furthermore, post translational modifications can also play a role in regulation. The most common types of post-translational

modification are; phosphorylation, the reversible addition of a phosphate group to a protein by a kinase, acetylation (Hu *et al.*, 2010) and glycosylation, which forms a glycoprotein.

Surface proteins can again vary, by the methods they are retained to the cell surface. They can contain membrane-spanning helices, be attached to lipid anchors, bind teichoic acids, be ionically or covalently bound. Proteins that bind teichoic acids usually do so through repeats present in the C-terminal domain (Scott and Barnett, 2006). Choline binding repeats bind the choline present in the LTA of some species, and the longer GW repeat modules bind an unknown ligand. In the case of proteins covalently attached to the peptidoglycan, they contain a C-terminal sorting LPXTG signal recognised by the transpeptidase 'sortase' (SrtA) (Schnnewind *et al.*, 1992; Navarre *et al.*, 1994). This enzyme cleaves between the threonine and glycine of the LPXTG motif and lipid II acts as a carrier to link the C terminus of the protein to the free amino group of the peptidoglycan cross bridges. 21 *S.aureus* proteins are covalently anchored via SrtA and one (IsdC) via a different, iron-regulated sortase (SrtB). This sortase recognises and cleaves a NPQTN motif although IsdC is the only known SrtB substrate (Mazmanian *et al.*, 2002).

1.11 Project aims

- To investigate whether the WTA biosynthetic components are associated with the divisome, thereby suggesting the site of WTA production in *S.aureus*.
- To localise mature WTA across the cell wall.
- Characterise the influence WTA have on the localisation of peptidoglycan hydrolases.
- Identify differences in localisation of hydrolases.
- Further develop the model of how *S.aureus* is able to faithfully divide in orthogonal planes.

CHAPTER 2

Materials and methods

2.1 Media

All media was prepared using distilled water and sterilised, in detergent washed and rinsed glassware, by autoclaving for 20 mins at 121°C, 15 lb per square inch. 1.5% (w/v) Oxoid agar was added to liquid media recipes before autoclaving to make solid mediad.

2.1.1 Tryptone Soya Broth (TSB)

Tryptone soya broth (Oxoid) 30g l⁻¹

2.1.2 Luria-Bertani (LB)

Tryptone (Oxoid) 10g l⁻¹

Yeast extract (Oxoid) 5g l⁻¹

NaCl 10g l⁻¹

2.1.3 Buffered Luria-Bertani (LB)

Tryptone (Oxoid) 10g l⁻¹

Yeast extract (Oxoid) 5g l⁻¹

NaCl 10g l⁻¹

KH₂PO₄ 1.5g l⁻¹

Na₂HPO₄ 3.5g l⁻¹

Media was pH-ed to 7.5 with NaOH prior to autoclaving.

2.1.4 LK

Tryptone (Oxoid) 10g l⁻¹

Yeast extract (Oxoid) 5g l⁻¹

KCl 7g l⁻¹

For LK bottom agar 1.5% (w/v) Oxoid agar was added

For LK top agar 0.7% (w/v) Oxoid agar was added.

2.1.5 Nutrient Broth

Nutrient broth 13g l^{-1}

2.1.6 Minimal Media (Daniel et al., 2006)

NH_4Cl 10mM

NH_4NO_3 1.2mM

MgSO_4 1mM

Na_2SO_3 0.75mM

KH_2PO_4 0.5mM

MnCl_2 0.1mM

FeCl_3 $4\mu\text{M}$

The pH was adjusted to 7 with sodium hydroxide and the solution autoclaved. Once the solution was cooled, the following was then added:

Glucose 0.8% (w/v)

Casamino acids 0.4% (w/v)

Thiamine $3\mu\text{M}$

Ampicillin $100\mu\text{g ml}^{-1}$

Kanamycin $50\mu\text{g ml}^{-1}$

IPTG 0.5mM

1% (w/v) Oxoid agar and $150\mu\text{g ml}^{-1}$ X-Gal were added to make minimal medium agar (pre-cooled to 50°C) before pouring plates.

2.1.7 Phage agar

Casamino acids (Oxoid) 3g l^{-1}

Yeast extract (Oxoid) 3g l^{-1}

NaCl 5.9g l^{-1}

For phage bottom agar 1.0% (w/v) Oxoid agar was added.

For phage top agar 0.33% (w/v) Oxoid agar was added.

2.1.8 Nutrient agar

Nutrient agar 28g l^{-1}

2.2 Antibiotics (Table 2.1)

Stock solutions of antibiotics were filter-sterilized, using a 0.2µm pore size and stored at -20°C. For use in agar plates, antibiotics were thawed on ice and added only when media had cooled to below 50°C. For use in liquid media, antibiotics were again thawed on ice and added just before use.

| Antibiotic | Stock concentration (mg ml ⁻¹) | Working concentration (µg ml ⁻¹) | Dissolved in: |
|----------------------|--|--|--------------------|
| Ampicillin (Amp) | 100 | 100 | dH ₂ O |
| Kanamycin (Kan) | 50 | 50 | dH ₂ O |
| Neomycin (Neo) | 50 | 50 | dH ₂ O |
| Tetracycline (Tet) | 5 | 5 | 50% (v/v) ethanol |
| Erythromycin (Ery) | 5 | 5 | 100% (v/v) ethanol |
| Chloramphenicol (Cm) | 10 | 10 | 100% (v/v) ethanol |
| Vancomycin (Vanc) | 0.1 | 1 | dH ₂ O |

Table 2.1 Antibiotic stock solutions and concentrations.

2.3 Enzymes and chemicals (Table 2.2)

All chemicals and enzymes were of analytical grade and purchased from Sigma-Aldrich, Thermo-Fisher Scientific or Roche unless otherwise stated. All restriction enzymes, DNase, T4 ligase and buffers for DNA manipulation were purchased from Promega, New England Biolabs, Fermentas, Thermo-Fisher Scientific or Roche.

| Stock Solution | Stock Solution concentration | Storage conditions |
|--|------------------------------|--|
| Lysostaphin | 5mg ml ⁻¹ | In 20mM sodium acetate, -20°C |
| Formaldehyde | 15% (w/v) | 4°C |
| Glutaraldehyde | 25% (w/v) | -20°C |
| Poly-L-Lysine | 0.01% (w/v) | 4°C |
| GTE | 100mM | R.T. |
| Trypsin | 0.2mg ml ⁻¹ | PBS, 4°C short term storage |
| Phenylmethylsulfonyl flouride (PMSF) | 0.1 M | 100% (v/v) isopropanol, R.T. short term. |
| IPTG (isopropyl-β-D-thiogalactopyranoside) | 0.84M | -20°C |
| MUG (4-methylumbelliferyl-β-D-galactopyranoside) | 4 mg ml ⁻¹ | In DMSO, -20°C, wrapped in foil |
| MU (4-methylumbelliferone) | 1mM | IN DMSO, -20°C |
| X-Gal (5-bromo-4-chloro-3-indolyl-β-D-galactopyranoside) | 20mg ml ⁻¹ | In DMSO, 4°C, wrapped in foil |

Table 2.2 Stock solutions and concentrations.

2.4 Buffers and stock solutions.

Buffers were prepared using dH₂O and stored at room temperature unless otherwise stated. Buffers required for microbiology work and *in vitro* manipulation were sterilised by autoclaving (15min, 121°C, 15 psi).

2.4.1 Phosphate buffered saline (PBS)

| | |
|----------------------------------|----------------------|
| NaCl | 8g l ⁻¹ |
| Na ₂ HPO ₄ | 1.4g l ⁻¹ |
| KCl | 0.2g l ⁻¹ |
| KH ₂ PO ₄ | 0.2g l ⁻¹ |

The pH was adjusted to 7.4, using NaOH

2.4.2 Tris buffered saline (TBS)

| | |
|----------------|-------|
| Tris-HCl pH7.5 | 50mM |
| NaCl | 100mM |

2.4.3 TAE (50x)

| | |
|-----------------------------|----------------------|
| Trisma Base | 242g l ⁻¹ |
| Glacial acetic acid | 0.57% (v/v) |
| Na ₂ EDTA pH 8.0 | 0.05M |

Before use, 50x stock was diluted 1:50 with dH₂O to produce a working TAE concentration.

2.4.4 Phage Buffer

| | |
|-------------------|------------|
| MgSO ₄ | 1mM |
| CaCl ₂ | 4mM |
| Tris-HCl pH 7.8 | 50mM |
| NaCl | 0.6% (w/v) |
| Gelatin | 0.1% (w/v) |

2.4.5 DNA loading buffer (6x)

| | |
|------------------|-------------|
| Bromophenol blue | 0.25% (w/v) |
| Glycerol | 30% (v/v) |

2.4.6 QIAGEN buffers

2.4.6.1 P1

| | |
|----------------|------------------------------|
| Tris-HCL, pH 8 | 50mM |
| EDTA | 10mM |
| RNase A | 100 μ g ml ⁻¹ |

2.4.6.2 P2

| | |
|------|----------|
| NaOH | 200mM |
| SDS | 1% (w/v) |

2.4.6.3 P3

| | |
|---------------------------|------|
| Potassium acetate, pH 5.5 | 3.0M |
|---------------------------|------|

2.4.6.4 EB

| | |
|------------------|------|
| Tris-HCl, pH 8.5 | 10mM |
|------------------|------|

2.4.6.5 N3, PB and PE

Supplied with QIAquick kit, details not provided.

2.4.7 β -galactosidase liquid assay solutions

2.4.7.1 ABT

| | |
|---------------------------------|------------------------|
| NaCl | 5.88g l ⁻¹ |
| K ₂ HPO ₄ | 10.51g l ⁻¹ |
| KH ₂ PO ₄ | 5.44g l ⁻¹ |

2.4.7.2 Stopping Solution

| | |
|---------------------------------|------------------------|
| Na ₂ CO ₃ | 42.39g l ⁻¹ |
|---------------------------------|------------------------|

2.4.7.3 ABTN

| | |
|-------------------|-------|
| ABT | 500ml |
| Stopping Solution | 500ml |

2.4.8 SDS PAGE solutions

2.4.8.1 SDS PAGE loading buffer (2x)

| | |
|------------------|------------|
| Tris HCl pH 6.8 | 0.62M |
| SDS | 10% (w/v) |
| Glycerol | 20% (v/v) |
| Bromophenol blue | 0.1% (w/v) |

10% (v/v) β -mercaptoethanol was added just before use.

2.4.8.2 SDS PAGE reservoir buffer (10x)

| | |
|-----------|-----------------------|
| Glycine | 144g l ⁻¹ |
| Tris base | 30.3g l ⁻¹ |
| SDS | 10g l ⁻¹ |

Before use the 10x solution was diluted 1:10 with dH₂O to a working concentration SDS PAGE reservoir buffer.

2.4.8.3 Coomassie Brilliant Blue stain

| | |
|---------------------|------------|
| Brilliant blue | 0.1% (w/v) |
| Methanol | 5% (v/v) |
| Glacial acetic acid | 10% (v/v) |

2.4.8.4 Coomassie destain

| | |
|---------------------|-----------|
| Methanol | 5% (v/v) |
| Glacial acetic acid | 10% (v/v) |

2.4.8.5 Transfer buffer

| | |
|-----------------|-----------|
| Tris-HCl pH 7.5 | 20mM |
| Glycine | 0.15M |
| Methanol | 20% (v/v) |

2.4.9 Western blotting buffers

2.4.9.1 Blotting buffer

| | |
|-------------|------------------------|
| Trisma base | 2.4g l ⁻¹ |
| Glycine | 11.26g l ⁻¹ |
| Methanol | 20% (v/v) |

2.4.9.2 TBST (20x)

| | |
|-------------|----------------------|
| Trisma base | 48g l ⁻¹ |
| NaCl | 120g l ⁻¹ |
| Tween-20 | 2% (v/v) |

The pH was adjusted to 7.6. Before use the 20x solution was diluted 1:20 with dH₂O to a working TBST concentration.

2.4.9.3 Blocking solution

| | |
|---------------------------|----------|
| Dried skimmed milk powder | 5% (w/v) |
|---------------------------|----------|

In 1xTBST

2.4.10 Zymogram solutions

2.4.10.1 Renaturing solution

| | |
|---|-------------|
| Triton X-100 | 0.1 % (v/v) |
| MgCl ₂ | 10mM |
| Tris HCl (pH 7.5)/ Sodium citrate (pH5) | 25mM |

2.4.10.2 Renaturing gel stain (10x)

| | |
|-------------------|-------------|
| Methylene Blue | 2g |
| KOH (2M) | 1.79ml |
| dH ₂ O | up to 200ml |

For use renaturing gel stain was diluted to 1x with dH₂O

2.4.11 Nickel affinity purification buffers

2.4.11.1 Buffer A (START buffer)

| | |
|----------------------------------|--------|
| NaH ₂ PO ₄ | 0.015M |
|----------------------------------|--------|

Na₂HPO₄ 0.0045M

NaCl 0.5M

The pH was adjusted to 7.4. 8M urea was added when purifying insoluble proteins.

2.4.11.2 Buffer B (elution buffer)

Buffer A containing 0.5M imidazole.

8M urea was added when purifying insoluble proteins

2.5 Bacterial strains and growth conditions used (Table 2.3)

S.aureus strains were taken from glycerol stocks in Microbank storage beads (Pro-lab diagnostics) and streaked for single colonies onto TSB agar plates containing antibiotics, where appropriate. Plates were incubated at 37°C overnight and subsequently stored at 4°C for upto 2 weeks. Long term storage of strains was achieved by adding 1ml of liquid overnight culture to a Microbank tube containing glycerol beads, shaking to mix and removing most of the liquid before storing at -80°C. Liquid cultures were generally inoculated with a single colony into TSB and grown overnight at 37°C with shaking at 250rpm unless otherwise stated.

E.coli strains were grown on LB agar at 37°C overnight and stored the same as *S.aureus* strains. Liquid cultures of LB were inoculated with single colony and grown as *S.aureus* strains.

| Strain (reference) | Genotype | Source | Growth media, Resistances |
|--------------------|--|---------------------------------|--|
| SH1000 (s682) | <i>rsbU+</i> | Horsburgh <i>et al.</i> , 2002 | TSB |
| RN4220 | Restriction deficient transformation recipient | Kreiswirth <i>et al.</i> , 1983 | TSB |
| SH1000 (s2978) | <i>spa::kan</i> | G.Buist | TSB, Kan ^r |
| SA113 (s2206) | <i>tarO::Ery</i> | A.Peschel | TSB, Ery ^r |
| SA113 | <i>tarO::ermB</i> , pRB473- <i>tarO</i> | A.Peschel | TSB, Ery ^r , Cm ^r |
| SA113 | <i>tarO::ermB</i> , <i>spa::kan</i> | This study | TSB, Ery ^r , Kan ^r |
| SRC110 (s2223) | Δ <i>srtA</i> | S. Clarke | TSB |
| SRC110 | <i>\Delta</i> <i>srtA</i> , <i>spa::kan</i> | This study | TSB, Kan ^r |
| ALB1 | SH1000 <i>spa::kan atl::lacZ</i> | A. Bottomley, 2011 | TSB, Ery ^r |
| SHKM06 (s3430) | SH1000 <i>gtfAB::kan clfA2::Tn917</i> | K.McAulay | TSB, Ery ^r , Kan ^r |
| SHRM09 (s2511) | SH1000 <i>gtfAgtfB::kan</i> | R.Mohammed | TSB, Kan ^r |
| SRC018(2) (s2193) | SH1000 <i>clfA2::Tn917</i> | S.Clarke | TSB, Ery ^r |

| | | | |
|------------------------------|--|---------------|--|
| SA18SM (s2117) | <i>sa1825::kan</i> | S.A.S Mohamad | TSB, Kan ^r |
| SA182SM | <i>sa1825::kan, spa::tet</i> | This study | TSB, Kan ^r , Tet ^r |
| SA26SM (s2115) | <i>scaH::tet</i> | S.A.S Mohamad | TSB, Tet ^r |
| SA26SM | <i>scaH::tet, spa::kan</i> | This study | TSB, Kan ^r , Tet ^r |
| MS026 | <i>sceD::tet</i> | R. Hussain | TSB, Tet ^r |
| MS026 | <i>sceD::tet, spa::kan</i> | This study | TSB, Kan ^r , Tet ^r |
| MS001 | <i>IsdA::ery</i> | A. Hurd | TSB, Ery ^r |
| MS001 | <i>IsdA::ery, spa::kan</i> | This study | TSB, Ery ^r , Kan ^r |
| BTH101 <i>E.Coli</i> (s1953) | <i>F-, cya-99, araD139, galE15, galk16, rpsL1 (Str^r), hsdR2, mcrA1, McrB1</i> | L.Cooper | LB |
| Top10 <i>E.coli</i> (s2257) | <i>F-mcr Δ (mrr-hsdRMS-mcrBC) φ 80 lacZ ΔM15 ΔlacX74 recA1 deoR araD139 Δ(ara-leu) 7697 galk rpsL (Str_r) endA1 nupG</i> | Invitrogen | LB |
| BL21 (s2195) <i>E.coli</i> | <i>F- ompT hsdSB (rB- mB-) gal dcm lacY1 (DE3)</i> | Novogen | LB |

Table 2.3 Bacterial strains used in this study.

2.6 Plasmids used (Table 2.4)

Plasmid DNA was isolated using QIAGEN mini plasmid purification kits according to the manufacturer's instructions (Section 2.9.2) and stored EB buffer at -20°C.

| Plasmid | Genotype | Selection | Source |
|------------|---|-----------------------------------|---------------------------------|
| pSRC002 | <i>atl</i> amidase domain in pET21a | 100µg ml ⁻¹ ampicillin | Clarke <i>et al.</i> , 2006 |
| pSRC003 | <i>atl</i> glucosaminidase domain in pET24d | 100µg ml ⁻¹ ampicillin | Clarke <i>et al.</i> , 2006 |
| pKT25 | Encodes the T25 fragment of <i>B.subtilis</i> adenylate cyclase (1-224 amino acids of CyaA). | 50µg ml ⁻¹ kanamycin | Karimova <i>et al.</i> , 1998 |
| pUT18C | Encodes the T18 fragment of <i>B.subtilis</i> adenylate cyclase (225-399 amino acids of CyaA) | 100µg ml ⁻¹ ampicillin | Karimova <i>et al.</i> , 1998 |
| pKT25-zip | A derivative of pKT25 in which the leucine zipper of GCN4 is genetically fused in frame to the T25 fragment | 50µg ml ⁻¹ Kanamycin | Karimova <i>et al.</i> , 1998 |
| pUT18c-zip | A derivative of pUT18c in which the leucine zipper of GCN4 is genetically fused to the T18 fragment | 100µg ml ⁻¹ ampicillin | Karimova <i>et al.</i> , 1998 |
| pGL540 | <i>divIB</i> coding region in PstI/KpnI site of pKT25 | 50µg ml ⁻¹ Kanamycin | J. Kasturiarachchi, unpublished |
| pGL541 | <i>ftsA</i> coding region in PstI/KpnI site of pKT25 | 50µg ml ⁻¹ Kanamycin | J. Kasturiarachchi, unpublished |
| pGL542 | <i>ftsL</i> coding region in PstI/KpnI site of pKT25 | 50µg ml ⁻¹ Kanamycin | J. Kasturiarachchi, unpublished |
| pGL543 | <i>pbp2</i> coding region in PstI/KpnI site of | 50µg ml ⁻¹ | J. Kasturiarachchi, |

| | | | |
|--------|---|--------------------------------------|------------------------------------|
| | pKT25 | Kanamycin | unpublished |
| pGL544 | <i>divB</i> coding region in PstI/KpnI site of pUT18C | 100µg ml ⁻¹ ampicillin | J. Kasturiarachchi, unpublished |
| pGL545 | <i>ftsA</i> coding region in PstI/KpnI site of pUT18C | 100µg ml ⁻¹ ampicillin | J. Kasturiarachchi, unpublished |
| pGL546 | <i>ftsL</i> coding region in PstI/KpnI site of pUT18C | 100µg ml ⁻¹ ampicillin | J. Kasturiarachchi, unpublished |
| pGL547 | <i>pbp2</i> coding region in PstI/KpnI site of pUT18C | 100µg ml ⁻¹ ampicillin | J. Kasturiarachchi, unpublished |
| pGL548 | <i>ftsW</i> coding region in BamHI/EcoRI site of pKT25 | 50µg ml ⁻¹ Kanamycin | J. Kasturiarachchi, unpublished |
| pGL549 | <i>ftsZ</i> coding region in BamHI/EcoRI site of pKT25 | 50µg ml ⁻¹ Kanamycin | J. Kasturiarachchi, unpublished |
| pGL550 | <i>pbpA</i> coding region in BamHI/EcoRI site of pKT25 | 50µg ml ⁻¹ Kanamycin | J. Kasturiarachchi, unpublished |
| pGL551 | <i>divC</i> coding region in BamHI/EcoRI site of pKT25 | 50µg ml ⁻¹ Kanamycin | J. Kasturiarachchi, unpublished |
| pGL552 | <i>ezrA</i> coding region in BamHI/EcoRI site of pKT25 | 50µg ml ⁻¹ Kanamycin | J. Kasturiarachchi, unpublished |
| pGL553 | <i>parC</i> coding region in BamHI/EcoRI site of pKT25 | 50µg ml ⁻¹ Kanamycin | J. Kasturiarachchi, unpublished |
| pGL554 | <i>parE</i> coding region in BamHI/EcoRI site of pKT25 | 50µg ml ⁻¹ Kanamycin | J. Kasturiarachchi, unpublished |
| pGL555 | <i>yneS</i> coding region in BamHI/EcoRI site of pKT25 | 50µg ml ⁻¹ Kanamycin | J. Kasturiarachchi, unpublished |
| pGL556 | <i>pbp3</i> coding region in BamHI/EcoRI site of pKT25 | 50µg ml ⁻¹ Kanamycin | J. Kasturiarachchi, unpublished |
| pGL557 | <i>ypsB</i> coding region in BamHI/EcoRI site of pKT25 | 50µg ml ⁻¹ Kanamycin | J. Kasturiarachchi, unpublished |
| pGL558 | <i>ypsA</i> coding region in BamHI/EcoRI site of pKT25 | 50µg ml ⁻¹ Kanamycin | J. Kasturiarachchi, unpublished |
| pGL559 | <i>ylmF</i> coding region in BamHI/EcoRI site of pKT25 | 50µg ml ⁻¹ Kanamycin | J. Kasturiarachchi, unpublished |
| pGL560 | <i>yyaA</i> coding region in BamHI/EcoRI site of pKT25 | 50µg ml ⁻¹ Kanamycin | J. Kasturiarachchi, unpublished |
| pGL561 | <i>ftsW</i> coding region in BamHI/EcoRI site of pUT18C | 100µg ml ⁻¹ Ampicillin | J. Kasturiarachchi, unpublished |
| pGL562 | <i>ftsZ</i> coding region in BamHI/EcoRI site of pUT18C | 100µg ml ⁻¹ Ampicillin | J. Kasturiarachchi, unpublished |
| pGL564 | <i>divC</i> coding region in BamHI/EcoRI site of pUT18C | 100µg ml ⁻¹ Ampicillin | J. Kasturiarachchi, unpublished |
| pGL565 | <i>ezrA</i> coding region in BamHI/EcoRI site of pUT18C | 100µg ml ⁻¹ Ampicillin | J. Kasturiarachchi, unpublished |
| pGL566 | <i>parC</i> coding region in BamHI/EcoRI site of pUT18C | 100µg ml ⁻¹ Ampicillin | J. Kasturiarachchi, unpublished |
| pGL568 | <i>yneS</i> coding region in BamHI/EcoRI site of pUT18C | 100µg ml ⁻¹ Ampicillin | J. Kasturiarachchi, unpublished |
| pGL570 | <i>ypsB</i> coding region in BamHI/EcoRI site of pUT18C | 100µg ml ⁻¹ Ampicillin | J. Kasturiarachchi, unpublished |
| pGL571 | <i>ypsA</i> coding region in BamHI/EcoRI | 100µg ml ⁻¹ | J. Kasturiarachchi, |

| | | | |
|--------|---|---------------------------------------|------------------------------------|
| | site of pUT18C | Ampicillin | unpublished |
| pGL572 | <i>ylmF</i> coding region in BamHI/EcoRI site of pUT18C | 100µg ml ⁻¹ Ampicillin | J. Kasturiarachchi, unpublished |
| pGL573 | <i>yyaA</i> coding region in BamHI/EcoRI site of pUT18C | 100µg ml ⁻¹ Ampicillin | J. Kasturiarachchi, unpublished |
| pGL574 | <i>zapA</i> coding region in BamHI/EcoRI site of pKT25 | 50µg ml ⁻¹ Kanamycin | J. Kasturiarachchi, unpublished |
| pGL575 | <i>zapA</i> coding region in BamHI/EcoRI site of pUT18C | 100µg ml ⁻¹ Ampicillin | J. Kasturiarachchi, unpublished |
| pALB3 | <i>ftsW</i> coding region in BamHI/EcoRI site of pKT25 | 50µg ml ⁻¹ Kanamycin | A. Bottomley, unpublished |
| pALB4 | <i>mreC</i> coding region in BamHI/EcoRI site of pUT18C | 100µg ml ⁻¹ Ampicillin | A. Bottomley, unpublished |
| pALB5 | <i>mreC</i> coding region in BamHI/EcoRI site of pKT25 | 50µg ml ⁻¹ Kanamycin | A. Bottomley, unpublished |
| pALB6 | <i>ftsW</i> coding region in BamHI/EcoRI site of pUT18C | 100µg ml ⁻¹ Ampicillin | A. Bottomley, unpublished |
| pALB7 | <i>mreD</i> coding region in BamHI/EcoRI site of pKT25 | 50µg ml ⁻¹ Kanamycin | A. Bottomley, unpublished |
| pALB8 | <i>rodA</i> coding region in BamHI/EcoRI site of pKT25 | 50µg ml ⁻¹ Kanamycin | A. Bottomley, unpublished |
| pALB11 | <i>mreD</i> coding region in BamHI/EcoRI site of pUT18C | 100µg ml ⁻¹ Ampicillin | A. Bottomley, unpublished |
| pALB12 | <i>pbp2</i> coding region in BamHI/EcoRI site of pUT18C | 50µg ml ⁻¹ Kanamycin | A. Bottomley, unpublished |
| pALB13 | <i>divIB</i> coding region in BamHI/EcoRI site of pKT25 | 50µg ml ⁻¹ Kanamycin | A. Bottomley, unpublished |
| pALB14 | <i>rodA</i> coding region in BamHI/EcoRI site of pUT18C | 100µg ml ⁻¹ Ampicillin | A. Bottomley, unpublished |
| pALB15 | <i>divIB</i> coding region in BamHI/EcoRI site of pUT18C | 100 µg ml ⁻¹ Ampicillin | A. Bottomley, unpublished |
| pVF29 | <i>ftsZ</i> coding region in BamHI/EcoRI site of pKT25N | 50µg ml ⁻¹ Kanamycin | (Steele <i>et al.</i> , 2011) |
| pVF30 | <i>ezrA</i> coding region in BamHI/EcoRI site of pKT25N | 50µg ml ⁻¹ Kanamycin | (Steele <i>et al.</i> , 2011) |
| pVF31 | <i>ftsZ</i> coding region in BamHI/EcoRI site of pUT18 | 100µg ml ⁻¹ Ampicillin | (Steele <i>et al.</i> , 2011) |
| pVF32 | <i>ezrA</i> coding region in BamHI/EcoRI site of pUT18 | 100µg ml ⁻¹ Ampicillin | (Steele <i>et al.</i> , 2011) |
| pALB50 | <i>divIVA</i> coding region in BamHI/EcoRI site of pKT25N | 50µg ml ⁻¹ Kanamycin | A. Bottomley, unpublished |
| pATL1 | <i>dnaK</i> coding region in BamHI/EcoRI site of pKT25 | 50µg ml ⁻¹ Kanamycin | A. Bottomley, unpublished |
| pALB30 | <i>ItaS</i> coding region in BamHI/EcoRI site of pUT18C | 100µg ml ⁻¹ Ampicillin | Larke, unpublished |
| pALB32 | <i>ItaS</i> coding region in BamHI/EcoRI site of pKT25 | 50µg ml ⁻¹ Kanamycin | Larke, unpublished |
| | <i>ItaA</i> coding region in BamHI/EcoRI site of pUT18 | 100µg ml ⁻¹ Ampicillin | A. Gründling, unpublished |
| | <i>ItaA</i> coding region in BamHI/EcoRI | 100µg ml ⁻¹ | A. Gründling, |

| | | | |
|-------|---|--------------------------------------|------------------------------|
| | site of pUT18C | Ampicillin | unpublished |
| | <i>ltaA</i> coding region in BamHI/EcoRI site of pKNT25 | 50µg ml ⁻¹ Kanamycin | A. Gründling, unpublished |
| | <i>ltaA</i> coding region in BamHI/EcoRI site of pKT25 | 50µg ml ⁻¹ Kanamycin | A. Gründling, unpublished |
| | <i>ypfP</i> coding region in BamHI/EcoRI site of pUT18 | 100µg ml ⁻¹ Ampicillin | A. Gründling, unpublished |
| | <i>ypfP</i> coding region in BamHI/EcoRI site of pUT18C | 100µg ml ⁻¹ Ampicillin | A.Gründling, unpublished |
| | <i>ypfP</i> coding region in BamHI/EcoRI site of pKNT25 | 50µg ml ⁻¹ Kanamycin | A. Gründling, unpublished |
| | <i>ypfP</i> coding region in BamHI/EcoRI site of pKT25 | 50µg ml ⁻¹ Kanamycin | A.Gründling, unpublished |
| pVLK1 | <i>tarO</i> coding region in BamHI/EcoRI site of pUT18C | 100µg ml ⁻¹ Ampicillin | This Study. |
| pVLK2 | <i>tarO</i> coding region in BamHI/EcoRI site of pKT25 | 50µg ml ⁻¹ Kanamycin | This Study. |
| pVLK3 | <i>sa2103</i> coding region in BamHI/EcoRI site of pUT18C | 100µg ml ⁻¹ Ampicillin | This Study. |
| pVLK4 | <i>sa2103</i> coding region in BamHI/EcoRI site of pKT25 | 50µg ml ⁻¹ Kanamycin | This Study. |
| pVLK5 | <i>sa1195</i> coding region in BamHI/EcoRI site of pUT18C | 100µg ml ⁻¹ Ampicillin | This Study. |
| pVLK6 | <i>sa1195</i> coding region in BamHI/EcoRI site of pKT25 | 50µg ml ⁻¹ Kanamycin | This Study. |
| pVLK7 | <i>sa0908</i> coding region in BamHI/EcoRI site of pUT18C | 100µg ml ⁻¹ Ampicillin | This Study. |
| pVLK8 | <i>sa0908</i> coding region in BamHI/EcoRI site of pKT25 | 50µg ml ⁻¹ Kanamycin | This Study. |

Table 2.4 Plasmids used in this study.

Plasmid DNA was purified from overnight cultures using QIAGEN kits according to altered manufacturer's instructions (see section 2.10). All plasmid DNA was stored in dH₂O at -20°C.

2.7 Centrifugation

A number of different centrifuges were used during this study, these were;

- (a) Eppendorf microfuge 5415D (max volume 2ml; max speed 13,200rpm, 10,000xg)
- (b) Sigma centrifuge 4K15C (max volume 50ml; max speed 5,100rpm, 5525xg)
- (c) Jouan centrifuge JAC50.10 (max volume 50ml; max speed 13,000rpm, 10,000xg)

2.8 Determining bacterial cell density

2.8.1 Spectrophotometric measurement (OD₆₀₀)

For quantification of a culture's bacterial yield, spectrophotometric measurements at 600nm (OD₆₀₀) were taken. Where necessary culture samples were diluted 1:10 in the appropriate sterile culture media, this media was also used as the blank. These measurements were taken using a Jenway 6100 spectrophotometer.

2.8.2 Direct cell counts (cfu ml⁻¹)

For quantification of a culture's viable cell number direct cell counts were performed. Bacterial samples were serially diluted 1:10 in PBS in triplicate. 10µl samples of each dilution were spotted onto the appropriate media agar plate containing any necessary antibiotics. After overnight incubation at 37°C, the numbers of colonies were calculated and the number of colony forming units (cfu) determined.

2.9 DNA purification techniques.

2.9.1 Genomic DNA extraction

A 1ml aliquot of a 5ml overnight culture was centrifuged at 1200rpm (300xg) for 10 min. The resulting supernatant was discarded and the pellet resuspended in 180µl sdH₂O. 5µl of 5mg ml⁻¹ Lysostaphin was added and incubated at 37°C until the culture was clear. The DNA was extracted using a Qiagen DNeasy blood and tissue kit following the manufacturer's instructions.

2.9.2 Small scale plasmid purification from *E.coli*

QIAGEN QIAprepTM Spin column kit was used to purify plasmids from *E.coli* on a small scale. The cells from a 5ml overnight culture of *E.coli* were centrifuged at 5100rpm (5525xg) at 4°C for 10min. The resulting pellet was resuspended in 250µl of Buffer P1 with RNase and transferred to a microcentrifuge tube. 250µl of Buffer P2 was added and the tube mixed by inversion 4-6 times. 350µl of Buffer N3 was added and the tube mixed thoroughly by inverting until the precipitation was evenly dispersed. The solution was centrifuged for 10min at 13000rpm (10000xg) and the supernatant applied to a QIAprep spin column. The spin column was centrifuged for 30s and the

flow through discarded. To wash the column, 0.5ml of Buffer PB was added the column centrifuged for 30s and the flow through discarded. This was repeated with 0.75ml Buffer PE and again the flow through discarded. The column was spun for an additional 3min to remove residual buffer and transferred to a clean microcentrifuge tube. To elute DNA, 50µl of Buffer EB was added to the centre of the column and left to stand for 1min and then centrifuged at 13000rpm (10000xg) for 1min. The flow through was reapplied to the column and centrifuged for 1min. The presence of the plasmid DNA in the flow through was checked by separation on a 1% (w/v) agarose gel at 120v for 40min and viewed using a transilluminator.

2.9.3 Gel extraction of DNA using QIAquick spin column

DNA was separated in a 1% (w/v) TAE agarose gel, stained with ethidium bromide, the required band was excised using a sterile scalpel blade. The DNA was extracted from the agarose slice using a QIAGEN QIAquick gel extraction kit. To a universal containing the gel slice 3 times the gel volume (weight) of Buffer QG was added. This was incubated at 50°C, swirling occasionally, until the gel slice had dissolved. To improve purification of smaller DNA molecules, 1 gel volume of isopropanol was added to the sample. To bind the DNA, the solution was added to a QIAquick spin column in 800µl samples with centrifugation for 1min at 13000rpm (10000xg) and discarding the flow through. To remove traces of agarose, 0.5ml of Buffer QG was added to the QIAquick column centrifuged and the flow through was discarded. 0.75ml of Buffer PE was added to the QIAquick spin column, the flow through discarded and the column spun for an additional 3min. The QIAquick spin column was placed in a clean micro centrifuge tube and 50µl Buffer EB applied to the centre of the column and left to stand for 1min. The column was centrifuged at 13000rpm (10000xg) for 1min. The flow through was reapplied to the column and centrifuged again. To confirm presence of DNA in the flow through, 5µl of sample was loaded onto a 1% (w/v) agarose gel, separated at 120v for 40min and viewed using a transilluminator.

2.9.4 Purification of PCR products using QIAquick spin column

To purify products from PCR reactions, 5 times the PCR sample volume of buffer PB was added and mixed. The solution was placed into a QIAquick spin column and

centrifuged at 13000rpm (10000xg) for 1min. The flow through was discarded and the column was washed with 750µl of buffer PE, and then centrifuged. The flow through was again discarded and the column centrifuged for a further 3min before transferring to a fresh microcentrifuge tube. The DNA was eluted by placing 50µl buffer EB into the centre of the column, incubating for 1min and centrifuging at 13000rpm (10000xg) for 1min. The flow through was reapplied to the column and centrifuged again. To confirm the presence of DNA in the flow through, 5µl of sample was loaded onto a 1% (w/v) agarose gel separated at 120v for 40min and viewed using a transilluminator.

2.10 *In vitro* DNA manipulation techniques

2.10.1 Primers (Table 2.5)

Primers were used for PCR amplification, they are short (maximum 30nt) oligonucleotide sequences based on *S.aureus* 8325 genome. Restriction sites were introduced at the 5' or 3' ends of primers to enable cloning and where necessary additional bases were added to allow efficient use. 'Net primer' was used to design the primers; to identify potential secondary structures, dimers or cross-dimers and to predict annealing temperatures. Primers were synthesised by Eurofin and stored in sdH₂O at -20°C as a 100µM stock or a 10µM working solution.

| Primer | Restriction enzyme | Sequence (5' -> 3') | Use |
|---------|--------------------|--|---|
| 5'KT25 | n/a | ATTCGGTGACCGATTACCTG | Amplification of genes inserted into pKT25 plasmid, forward primer |
| 3'KT25 | n/a | AGTCACGACGTTGTAACGACG | Amplification of genes inserted into pKT25 plasmid, reverse primer |
| 5'UT18C | n/a | GAAAAGCCTGTCGACGATG | Amplification of genes inserted into pUT18C plasmid, forward primer |
| 3'UT18C | n/a | ATCAGAGCAGATTGTAAGAGATG | Amplification of genes inserted into pUT18C plasmid, reverse primer |
| vk1 | BamHI | aaaaaaggatccaATGGTTACATTACTAGTTGCAGTA | TagO Forward ligation into pKT25 or pUT18C |
| vk2 | EcoR1 | aaaaaagaattcaaCTATTCCTCTTTATGAGATGACTTAC | Tago Reverse ligation into pKT25 or pUT18C |
| vk3 | BamHI | aaaaaaggatccaATGAGCCTACCGAAAAAATAT | SA2103 Forward Ligation into pKT25 or pUT18C |
| vk4 | EcoR1 | aaaaaagaattcaaCTACTAGATTATCTTTAACTACTTAGTACT | SA2103 Reverse Ligation into pKT25 or pUT18C |

| | | | |
|-------|-------|--|---|
| vk5 | BamHI | aaaaaaggatccaATGGATAAAGAACTAATGA CAACG | SA1195 Forward Ligation into pKT25 of pUT18C |
| vk6 | EcoRI | aaaaaagaattcaaTTAATCTTCATCTAAAAGTCT TTAATAGCT | SA1195 Reverse Ligation into pKT25 or pUT18C |
| vk7 | BamHI | aaaaaaggatccaTCCAATGAATAAATTTTTAAA ATACTTTTTG | SA0908 Forward Ligation into pKT25 or pUT18C |
| vk8 | EcoRI | aaaaaagaattcaaTTATTTACAACAACCTTTGGT TAT | SA0908 Reverse Ligation into pKT25 or pUT18C |
| ALB67 | BamHI | AATTAAGGATCCAATGAAAAATTTAATATCTA TTATCATCA | <i>spa</i> Forward ligation into pKT25 or pUT18C |
| ALB68 | EcoRI | AATTAAGAATTCAATTTTCTTTTCTAAATAAA CGATT | <i>spa</i> Reverse ligation into pKT25 or pUT18C |

Table 2.5 Primers used in this study

2.10.2 PCR amplification

PCR amplification reactions were performed using high-fidelity Extensor PCR ReddyMix™ (ThermoScientific). The working reaction concentration in 25µl of each component is:

| | |
|-------------------|--------|
| DNA polymerase | 1.25 U |
| MgCl ₂ | 2.25mM |
| dNTPs | 0.5mM |

Precipitant and red dye added for electrophoresis

To a sterile 0.5ml PCR tube the following components were added, to give a reaction mixture containing 1x PCR ReddyMix :

| | |
|---------------------------------|--------|
| High-fidelity Extensor ReddyMix | 12.5µl |
| Template DNA | 100ng |
| Forward primer | 200nM |
| Reverse primer | 200nM |
| sdH ₂ O | 9.5µl |

PCR reactions were carried out in a Techgene PCR machine (Techne). The reaction cycle was as follows:

| | | | |
|-----------|----------------------|---------|-------------|
| 1 cycle | Initial denaturation | 94°C | 2min |
| 30 cycles | Denaturation | 94°C | 15s |
| | Annealing | 49-55°C | 30s |
| | Extension | 72°C | 1min per kb |

1 cycle Final extension 72°C 4min

The reaction products were stored at -20°C.

2.10.3 Colony PCR screening of *E.coli*

The reaction mixture was made in a PCR reaction tube as described in Section 2.10.2 without the addition of template DNA. Using a sterile pipette tip, a single colony was patched onto a selective antibiotic agar plate and then introduced into the PCR reaction tube. The PCR reaction was carried out as described above.

2.10.4 Colony PCR screening of *S.aureus*

The reaction mixture was made in a PCR reaction tube as described in Section 2.10.2 without the addition of the template DNA. As described in Section 2.10.3 using a sterile pipette tip, a single colony was patched onto a selective agar plate and then introduced into the PCR reaction tube. To disrupt the cells, the reaction steps were as follows:

37°C 15min

99°C 20min

4°C 1min

99°C 2min

4°C 1min

The PCR reaction was then carried out as described in Section 2.10.2.

2.10.5 Restriction endonuclease digestion

Restriction enzymes were purchased from Promega, New England Biolabs or Sigma. Digestion of DNA was performed according to the manufacturer's instructions, with the buffers supplied. The reaction mixture was incubated for 3hr at 37°C. If digested products are to be used in subsequent reactions they were purified using a QIAquick PCR purification kit as described in section 2.9.4.

2.10.6 Phosphatase treatment of vector DNA.

To decrease self-ligation, digested vector DNA was treated with calf intestinal alkaline phosphatase (CIP) removing the 5'PO₄ from the DNA. Phosphatase was added to the

digested vector along with the provided buffer, according to the manufacturer's instructions, and incubated at 55°C. After 30min a further 1µl CIP was added and incubated for a further 1hr30. The CIP was removed, using the QIAquick PCR purification kit (as described in section 2.9.4). The dephosphorylated vector was stored at -20°C.

2.10.7 DNA ligation and ethanol precipitation.

Plasmid DNA and insert were ligated at different ratios, with 1µl T4 DNA ligase and 1µl T4 DNA ligase buffer added to each and incubated overnight at 15°C. 40µl dH₂O was added to the ligation mixture, mixed and transferred to a clean labelled Eppendorf tube. As a negative control linearised vector was ligated under the same conditions in the absence of insert DNA. To improve efficacy of transformation, 0.1 volumes 3M sodium citrate pH 5.2, 2.5 volumes 100% (v/v) ethanol and 0.05 volumes glycogen were added, the mixture vortexed and incubated overnight at -20°C. The mixture was centrifuged at 13000rpm (10000xg) for 20min at 4°C. The pellet was washed twice with 500µl 70% (v/v) ethanol. The supernatant was discarded and the pellet air dried next to a flame, then resuspended in 10µl dH₂O.

2.10.8 Agarose gel electrophoresis

DNA samples were routinely separated in 1% (w/v) agarose gels in 1X TAE buffer. Horizontally submerged agarose gels were poured and run using various size horizontal electrophoresis tanks (Life Technologies). For the visualisation of DNA, 5-15µl of ethidium bromide (10mg ml⁻¹; BioRad), dependent on the gel size was added to the molten gel before pouring.

DNA samples were mixed with one fifth their volume of DNA loading buffer and loaded into wells of the gel. Gels were resolved for 40min to 1hr30 at 100-120V, at room temperature, before being viewed on an UV transilluminator at 260nm and photographed using the UVi Tec Digital camera and UVi Doc Gel documentation system. The size of DNA fragments was estimated by comparison to a 10µl Quick-Load 1kb DNA ladder

| Marker | DNA fragment size | Mass (ng) |
|--------------------------------------|-------------------|-----------|
| 1Kb DNA Ladder (New England Biolabs) | 10.0 | 42 |
| | 8.0 | 42 |
| | 6.0 | 50 |
| | 5.0 | 42 |
| | 4.0 | 33 |
| | 3.0 | 125 |
| | 2.0 | 48 |
| | 1.5 | 36 |
| | 1.0 | 42 |
| | 0.5 | 42 |
| 500bp DNA markers (gbiosciences) | 5.0 | 40 |
| | 4.5 | 40 |
| | 4.0 | 40 |
| | 3.5 | 40 |
| | 3.0 | 40 |
| | 2.5 | 100 |
| | 2.0 | 40 |
| | 1.5 | 40 |
| | 1.0 | 40 |
| | 0.5 | 40 |
| 50bp DNA markers (Qiagen) | 0.5 | 86 |
| | 0.4 | 86 |
| | 0.35 | 86 |
| | 0.3 | 166 |
| | 0.25 | 86 |
| | 0.2 | 86 |
| | 0.15 | 86 |
| | 0.1 | 86 |
| | 0.05 | 86 |

Table 2.6 DNA markers

2.10.9 Plasmid sequencing

Plasmids were purified using a QIAquick spin column as shown in Section 2.9.2 and sequenced by the Core Genomics Facility, University of Sheffield. Sequencing traces were analysed using FinchTV software (Geospiza).

2.11 Transformation techniques

2.11.1 Transformation of *E.coli*

2.11.1.1 Preparation of electrocompetent *E.coli* BTH101 cells.

An overnight culture was diluted in 400ml LB and grown at 37°C, 250rpm (15xg) until OD_{600nm} between 0.5-0.7. Cultures were kept on ice-slurry for 15min, aliquoted into 4x 50ml falcon tubes and centrifuged at 4°C for 10min at 5500rpm (6000xg). 50ml of culture was added to each pellet and the centrifugation repeated. Pellets were washed with ice-cold sdH₂O three times, with the pellets only being vortexed to resuspend in wash 1. The supernatant was discarded and the pellet resuspended in the remaining liquid. The aliquots were combined and ice-cold glycerol was added to a final concentration of 10% (v/v). The culture was split into 50µl aliquots, snap frozen and stored at -80°C.

2.11.1.2 Electroporation into *E.coli*.

The ethanol precipitated ligation mixture or ~1ng of purified plasmid DNA was added to 50µl of ice- thawed *E.coli* electrocompetent cells and mixed well. The cells were transferred to an ice-cold Bio-Rad 0.1cm cuvette and electroporation was carried out using a Bio-Rad Genepulser at 200Ω, 25µF, 1.75kV. 400µl of LB was added to the cuvette, the mixture transferred to an Eppendorf tube and incubated at 37°C, 250rpm (15xg) for 60min to allow the cells the recover. 100µl samples were spread onto antibiotic LB plates and incubated overnight at 37°C to select transformed colonies.

2.11.2 Transformation of *S.aureus*

2.11.2.1 Preparation of electrocompetent *S.aureus* RN4220 cells.

An overnight culture was set up by inoculating 400ml TSB with a single colony from a fresh RN4220 plate and grown at 37°C at 250rpm. The following day this was used to inoculate 400ml prewarmed TSB to an OD₆₀₀ 0.1 and grown at 37°C, 250rpm until OD₆₀₀ 0.4-0.6. Keeping the culture at room temperature, cells were aliquoted into 4x 50ml Falcon tubes and centrifuged for 10 min at 5000rpm (5525xg). 50ml of culture was added to each pellet and the centrifugation repeated. Pellets were gently washed in 25ml sterile, room temperature sdH₂O three times. After the final wash the pellets were resuspended in 20ml sterile 10% (v/v) glycerol and recovered by centrifugation. The pellets were then resuspended in 10ml sterile, room temperature 10% (v/v) glycerol and incubated for 30min. After centrifugation the supernatant was discarded and the pellet resuspended in the remaining liquid; the cells were aliquoted

into 50µl volume. Competent cells were used immediately or snap frozen and stored at -80°C before use.

2.11.2.2 Electroporation into *S.aureus*.

An appropriate amount of plasmid DNA was added to room temperature thawed competent cells and transferred to a 0.1cm electroporation cuvette. Electroporation was carried out at 100Ω, 2.3kV, 25µF and 1ml pre-warmed was immediately added and the mixture transferred to 25ml universal tubes. Cells were recovered for 3hr at 37°C, 250rpm (15xg) and then 5x 200µl aliquots were spread on reduced concentration selective antibiotic plates.

2.12 Phage transformation techniques

2.12.1 Bacteriophage

In this study, bacteriophage Φ11 (Mani *et al.*, 1993) was used due to its *S.aureus* specific nature. It is a temperature sensitive, transducing phage of serological group B, requiring Ca²⁺ ions for a maintenance of infection and has an approximate genome size of 45kb (Novick, 1991).

2.12.2 Preparation of Phage lysate

The donor strain was grown overnight at 37°C in 5ml BHI containing appropriate antibiotics. Cells were inoculated to an OD₆₀₀ of 0.2 in 5ml TSB in a universal tube. 5ml of phage buffer and 100µl of stock phage lysate (Φ11) were added and the mixture incubated at 30°C for 4-6hr on a rotary shaker at 30rpm. Once cleared, the lysate was filter sterilized (0.2µm pore size) and stored at 4°C.

2.12.3 Determination of phage titre

SH1000 strain was grown in 5ml BHI to OD₆₀₀~0.5. The phage lysate was serially diluted in phage buffer and 100µl of diluted phage added to 400µl of culture with 50µl of 1M CaCl₂. The mixture was allowed to sit at room temperature for 10min before adding 5ml phage top agar and overlaying a phage bottom agar plate. Plates were incubated at 37°C for 48hr, and the number of plaques counted. A successful phage lysate resulted in 10⁻⁷ to 10⁻¹⁰ plaque forming units per ml.

2.12.4 Phage transduction

A culture of the recipient bacteria was grown in 20ml LK overnight, harvested at 5000 rpm for 10min and resuspended in 1ml LK. 500µl of recipient cells were mixed with 500µl of phage lysate and 1ml of LK 10mM CaCl₂. A control mixture containing no phage lysate was also prepared. The mixture was incubated stationary at 37°C for 25min followed by rotary shaking at 250rpm (15xg) for 15min at the same temperature. 1µl of ice-cold 0.02M sodium citrate was added and incubated on ice for 1hr. Aliquots were spread onto LK plates containing 0.05% (w/v) sodium citrate. Plates were incubated at 37°C for 2hr then overlaid with 5ml LK top agar containing 3x concentration of selective antibiotics. Plates were incubated for 36-48hr at 37°C. Colonies were picked and streaked onto LB with appropriate antibiotic plates.

2.13 Protein analysis

2.13.1 SDS PAGE

Resolving gels were prepared using the following recipe, adding the APS and TEMED immediately before pouring;

12% (w/v) Resolving Gel

| | |
|---|--------|
| 30% (w/v) acrylamide/Bis (37.5:1, BioRad) | 4ml |
| 1.5M Tris-HCl (pH8.8) | 2.5ml |
| dH ₂ O | 3.35ml |
| 10% (w/v) SDS | 100µl |
| 10% (w/v) ammonium persulphate (APS) | 100µl |
| TEMED | 15µl |

10% (w/v) Resolving Gel

| | |
|---|-------|
| 30% (w/v) acrylamide/Bis (37.5:1, BioRad) | 3.3ml |
| 1.5M Tris-HCl (pH 8.8) | 2.5ml |
| dH ₂ O | 4ml |
| 10% (w/v) SDS | 100µl |
| 10% ammonium per sulphate (APS) | 100µl |
| TEMED | 15µl |

A layer of isopropanol was applied on top of the gel to exclude bubbles, level out the surface and isolate it from the air until the gel was set when it was removed and the surface dried. A stacking gel was applied on top of this, a comb being placed into the gel immediately to create loading wells. As before the recipe is as follows and the APS and TEMED were added immediately before pouring;

| | |
|---|--------|
| 30% (w/v) acrylamide/Bis (37.5:1, BioRad) | 0.83ml |
| dH ₂ O | 2.5ml |
| 1M Tris-HCl (pH 6.8) | 0.62ml |
| 10% (w/v) SDS | 50µl |
| 10% (w/v) APS | 50µl |
| TEMED | 5µl |

After the stacking gel had solidified, the gel was transferred to a Protean II (BioRad) gel-running tank and submerged in 1x SDS PAGE running buffer reservoir. The comb was removed and the wells washed out with 1X SDS PAGE running buffer. Appropriate volumes of samples (5-20µl) were loaded into the wells and run alongside 10µl of Dalton Mark VII-L (Sigma) or prestained SDS-PAGE Low Range (BioRad) protein size markers (Table 2.8). The gels were run at 150V until the blue dye front of the sample buffer was at the base of the gel plate.

| Marker | Protein | Molecular mass (kDa) |
|--|--|----------------------|
| Dalton Mark VII-L (Sigma) | Bovine serum albumin | 66.0 |
| | Ovalbumin | 45.0 |
| | Glyceraldehyde-3-phosphate dehydrogenase | 36.0 |
| | Carbonic anhydrase | 29.0 |
| | Trypsinogen | 24.0 |
| | Soybean trypsin inhibitor | 20.1 |
| | α-Lactalbumin | 14.2 |
| Prestained SDS-PAGE Low Range (BioRad) | Phosphorylase B | 104.4 |
| | Bovine serum albumin | 81.2 |
| | Ovalbumin | 47.3 |
| | Carbonic anhydrase | 36.2 |
| | Soybean trypsin inhibitor | 26.9 |
| | Lysozyme | 19.1 |

Table 2.7 Protein size standards

2.13.2 Coomassie staining

To visualise proteins, SDS-PAGE gels were placed in Coomassie blue stain for 30min. They were then destained in enough destain to cover overnight until the background was clear. Molecular masses were determined by comparison to the protein standards of known sizes.

2.13.3 Western blot

Immunoblot nitrocellulose membrane (Biorad) was cut to the same size as the SDS PAGE gel. The membrane was wet briefly in 20% (v/v) methanol, washed with dH₂O and then equilibrated in blotting buffer for 10min. Protein was transferred from the gel to the PVDF membrane by electroblotting in cold blotting buffer using a Mini Trans-Blot apparatus (BioRad) at 70 V for 1hr. The nitrocellulose membrane was dried on blotting paper for 5min. The blot was blocked in blocking buffer overnight at 4°C with gentle agitation. The blot was washed every 5-7min for 30min with TBST and then incubated with blocking buffer containing primary antibody at an appropriate dilution for 2hr at room temperature with gentle agitation. The blot was washed every 6x 5min with TBST and then incubated in 10ml blocking solution containing 1:20000 Horseradish peroxidase (HRP) conjugated goat anti-rabbit or anti-mouse secondary antibody (Sigma) for 1hr at room temperature with gentle agitation. The blot was washed as before with TBST for 30min. In the dark room, 1ml of enhanced chemiluminescent (ECL) substrate reagent 1 was combined with 1ml of ECL substrate reagent 2 and the mixture spread over the membrane. It was ensured that at least 0.125ml was used per cm² of membrane. This was incubated for 1min, excess reagent removed with blotting paper and then sealed within clingfilm. Air pockets were gently smoothed out and Kodak Scientific Imaging film was placed on top of the membrane. The film was exposed for 30s, placed in developer until the bands appeared, rinsed with water and placed in fixer and rinsed again. The exposure was repeated, varying the exposure time as needed for optimal detection. Developed films were air dried.

2.13.4 Zymogram

To determine whether a protein is a hydrolase or peptidoglycan binding protein, a zymogram can be performed. An SDS-PAGE gel containing 0.05% (w/v) non HF stripped

peptidoglycan in the separating gel was made. Samples were loaded and the gel run as described above (Section 2.13.1). The gel was washed in dH₂O to remove SDS, the gel was then incubated in renaturing solution gentle shaking at room temperature for 30min. The renaturing solution was exchanged for fresh and the gel incubated overnight at 37⁰C gentle shaking. The gel was rinsed with dH₂O and incubated in 1x renaturing stain for 3hr at RT, gently shaking. The gel was then destained with repeated washes of dH₂O until zones of clearing were seen. The gel was dried using gel drying sheets pre-soaked in 10% (v/v) glycerol.

2.13.5 Mini scale protein extraction of *S.aureus*

A single colony was used to inoculate a 5ml TSB overnight culture, this was used to reinoculate the desired volume at OD₆₀₀ 0.05 +/- IPTG +antibiotics. This was grown to exponential (O.D. ~0.5). The culture was centrifuged at 4⁰C for 10min at 5000rpm (5525xg), the pellet was resuspended in 500µl of PBS per 5ml. 500µl fractions were transferred to FastPrep tubes containing lysing matrix B (MP Biomedicals). Cells were broken using the FastPrep instrument (MP Biomedicals) set at speed 6 for 40s for 5 runs with incubations on ice between each run. The FastPrep beads were allowed to settle before the supernatant was transferred to a clean Eppendorf tube and centrifuged at 4⁰C for 5min at 13000rpm (10000xg). The supernatant was transferred to a clean Eppendorf tube and kept as the soluble fraction. The pellet was resuspended in 1ml PBS kept as the insoluble fraction. A 10µl sample of each was run on an SDS gel.

2.13.6 Whole cell lystae

A single colony was used to inoculate a 5ml TSB overnight culture, this was used to reinoculate 10ml at OD₆₀₀ 0.05 +/- IPTG +antibiotics. This was grown to exponential (OD₆₀₀ ~0.5) and the culture treated with lysostaphin rotating at 37⁰C until clear. The appropriate amount was mixed with sample buffer, boiled for 10min and centrifuged at RT for 3min at 13000rpm (10000xg). A 10µl sample was run on an SDS gel.

2.13.7 Bradford estimation of protein concentration

To determine protein concentration, 10µl of sample was added to 800µl dH₂O in a cuvette. 200µl of BioRad Protean assay dye was added and mixed by inversion. After

incubation for 5min at room temperature the OD₅₉₅ was measured. Protein concentrations were calculated using the following equation;

$$\text{Protein Concentration (mgml}^{-1}\text{)} = \frac{\text{OD} \times 15}{10}$$

2.14 Production of recombinant protein

2.14.1 Expression in *E.coli* BL21

A single colony of freshly streaked *E.coli* BL21 containing pET21d with the desired insert was used to inoculate 5ml LB containing the appropriate antibiotic and incubated overnight at 37°C with shaking at 250rpm (15xg). This culture was used to inoculate 100ml (small scale purification) or 1L (large scale purification) to an absorbance of 0.05 at a reading of OD₆₀₀ and was incubated at 37°C with shaking until the absorbance reached 0.4-0.6. 1mM IPTG was then added and the culture incubated for a further 3hr. Cells were harvested by centrifugation at 5100rpm (5525xg) for 10min at 4°C and the supernatant discarded. The resulting pellet was stored at -20°C.

2.14.2 Analysis of recombinant protein stability

During the preparation of cells in section 2.17.1, 1ml of culture was removed before the addition of IPTG (uninduced sample), and 2 samples of 1ml of culture was removed following the 3hr incubation after the addition of IPTG (induced sample). The cultures were centrifuged at 13000rpm (10000xg) for 5min at room temperature to harvest the cells, and the supernatant was discarded. The uninduced sample was resuspended in 100µl SDS loading buffer and one of the induced samples was resuspended in 250µl SDS loading buffer. The samples were boiled for 5min and then centrifuged at 13000rpm (10000xg) for 3min to sediment any insoluble material. 15µl of each sample were analysed by SDS-PAGE to confirm overexpression of the recombinant protein. To determine the solubility of the recombinant protein, the second induced sample was resuspended in 250µl START buffer and lysozyme was added to a final concentration of 1mg ml⁻¹. The sample was incubated at room temperature for 60min and then sonicated for 3 x 10s using a Sanyo soniprep 150. The sample was then centrifuged at 13000rpm (10000xg) for 10min allowing the separation of soluble and insoluble material. The supernatant, containing soluble proteins, was transferred into a

fresh eppendorf and 250µl SDS loading buffer was added. The pellet, containing insoluble material, was resuspended in 250µl START buffer 8M urea and 250µl SDS loading buffer was added. Both samples were boiled for 5min, centrifuged at 13000rpm (10000xg) for 3min and 15µl of each sample was analysed by SDS-PAGE.

2.14.3 Separation of insoluble and soluble proteins.

Cells from section 2.17.1 were resuspended in 5ml START buffer without urea. The suspension was then freeze-thawed three times by placing the sample at -80°C for 10min and then allowing it to thaw completely on ice. The cells were then broken by sonicating (using a Sanyo soniprep 150) ten times for 10s with 1min rest on ice in between each run. The suspension was centrifuged at 10000rpm (25000xg) for 25min at 4°C. The supernatant containing soluble proteins was removed, filtered using a 0.45µm pore size, and stored at 4°C. If the recombinant protein had been determined to be insoluble (Section 2.12.2), the pellet was resuspended thoroughly in 5ml (small scale purification) or 30 ml (large scale purification) START buffer 8M urea and incubated overnight at 4°C. The sample was then centrifuged (10000rpm (25000xg), 25min, 4°C) to remove any unbroken cells and the resulting supernatant containing the solubilised proteins was filtered using a 0.45µm pore size and stored at 4°C.

2.14.4 HiTrap purification

A 5ml HiTrap column (GE Healthcare) was prepared by washing with 10ml sdH₂O, and then charged with 10ml 50 mM NiSO₄. The column was washed with 10ml sdH₂O to remove excess NiSO₄. The BioRad Econo Gradient pump and Fraction Collector was flushed with START buffer at a flow rate of 1.5ml min⁻¹. When purifying insoluble proteins as determined in Section 2.17.3, 8M urea was added to both the START and elution buffer. The charged HiTrap column was attached to the BioRad Econo Gradient pump and equilibrated by washing with 5ml START buffer. The supernatant containing recombinant protein was applied to the column at a flow rate of 1ml min⁻¹ and any non-specific proteins were removed by washing with 5% elution buffer until the absorbance returned to zero. The his-tagged proteins were eluted from the column using a gradient of 5-100% elution buffer (containing 0.5 M imidazole) at a flow rate of 1ml min⁻¹, with 1ml fractions being collected. Imidazole has a higher affinity for the

nickel than the His-tag displacing recombinant protein. The eluted fractions were then analysed by SDS-PAGE. After elution of the recombinant protein, the HiTrap column was washed with 10ml 50mM EDTA to remove NiSO₄, followed by 10ml sterile water. 10ml 20% (v/v) ethanol was washed through the column before storage at 4°C.

2.14.5 Protein dialysis

2.14.5.1 Preparation of dialysis membrane

Size 2 dialysis membrane tubing (Medicell International) was used, which allows selection of proteins larger than 12kDa. Before use, the dialysis tubing was boiled in 2mM EDTA for 20min and washed thoroughly in sdH₂O. For long term storage, the EDTA-boiled dialysis tubing was placed in 50% (v/v) ethanol and stored at 4°C.

2.14.5.2 Dialysis of recombinant protein

Fractions containing recombinant protein (Section 2.12.4) were placed in dialysis membrane tubing and dialysed in either START buffer, 20mM Tris-HCl pH7.5 plus 0.15M NaCl for 12hr at 4°C. This dialysis step was repeated twice more, replacing the dialysis solution with fresh appropriate buffer each time. If the protein was insoluble, 4 M urea was added to the dialysis solution during the first dialysis. The solution was then replaced by the appropriate buffer containing 2M urea and dialysis carried out for 12hr at 4°C. This was repeated three times using the appropriate buffer containing 1M, 0.5M and 0M urea. After dialysis, the protein fractions were removed from the dialysis tubing and glycerol was added to a final concentration of 10% (v/v). 200µl aliquots of recombinant protein were stored at -70°C.

2.15 Generation of Antibodies

Polyclonal antibodies were raised in rabbits and affinity purified by BioServ (University of Sheffield).

2.16 Bacterial two-hybrid assay (BACTH)

The method was adapted from Karimova *et al.* (1998). Electrocompetent *E.coli* BTH101 which had previously been transformed with one plasmid construct were co-transformed with the opposite plasmid fusion (T25 with T18) following the

electroporation protocol. The successful co-transformations were maintained on LB plates with $100\mu\text{g ml}^{-1}$ ampicillin and $50\mu\text{g ml}^{-1}$ kanamycin. There are two halves of the assay, a solid assay to identify interactions and a liquid assay to quantify the interactions.

2.16.1 BATCH solid assay

To visualise β -galactosidase activity, strains were spotted onto minimal media plates containing the chromogenic substrate X-gal and IPTG to induce expression of the hybrid proteins (protocol optimised by Victoria Fairclough, 2009). Cells were grown overnight in a 5ml LB containing appropriate antibiotics and washed three times by centrifugation (5100rpm (6000xg) at 4°C for 10min) and resuspended in sdH_2O to remove media. After the final wash cells were resuspended in the remaining liquid and diluted 10 fold. $10\mu\text{l}$ aliquots were spotted onto fresh minimal media plates and allowed to dry. The plates were incubated at 30°C for 18hr. A positive control strain carrying plasmids encoding T25 and T18 fused to the leucine zipper domain of GCN4 (pKT25-zip and pUT18C-zip) (Karimova *et al.*, 1998) and a negative control strain carrying unfused T18 and T25 fragments were included. Additional controls were also included: each T18 and T25 fragments were tested against unfused T25 and T18 fragments respectively.

2.16.2 BACTH liquid culture assay

To visualise the strength of protein interactions, liquid cultures were assayed for β -galactosidase activity with MUG (4-methylumbelliferyl- β -D-galactopyranoside). One colony of each *E.coli* co-transformant was inoculated into 5ml minimal medium and incubated at 30°C , 250rpm overnight. Triplicate $100\mu\text{l}$ culture samples were collected and centrifuged at 13000rpm (10000xg) for 5min, the OD_{600} was also recorded. The cell pellets were resuspended in 0.5ml ABT, $50\mu\text{l}$ freshly prepared MUG was added and the tubes were mixed. The reactions were immediately incubated at 25°C for exactly 60mins. During this time MUG is hydrolysed by β -galactosidase to β -D-galactopyranoside and 4-methylumbelliferone (MU). MU is a fluorescent compound and so is a quantifiable measure of β -galactosidase activity. The reaction was stopped by adding 0.5ml stopping solution and vortexing the tubes.

Into the top well of a 96-well microtitre plate, 250µl of each sample was pipetted, and 225µl of ABTN was added to the remaining wells to be used. A 1:10 dilution was made by removing 25µl sample from the top well and mixing it with the 225µl ABTN in the next well. Serial 1:100 and 1:1000 dilutions were also made. 25µl was removed from the final well (1:1000 dilution) to keep a constant well volume of 225µl.

A fluorimeter (Victor²_{TM}, Wallac) was used to measure the fluorescence of each sample (355/460nm,0.1s). The relationship between fluorescence and pmol of MU can be determined using a calibration curve, allowing the amount of MU in 225µl to be calculated. The amount of MU can be related to β-galactosidase activity using the following equation;

$$\text{MUG units} = \frac{(\text{pmoles} \times \frac{A}{B})}{(60 \times \text{OD}_{600} \times 0.1)}$$

Where:

pmoles= p moles MU

A = volume of assay (1.05 = 0.5ml ABT +0.5ml stopping solution + 0.05ml MUG)

B =volume of assay read in plate (0.225ml)

60 = number of minutes incubation

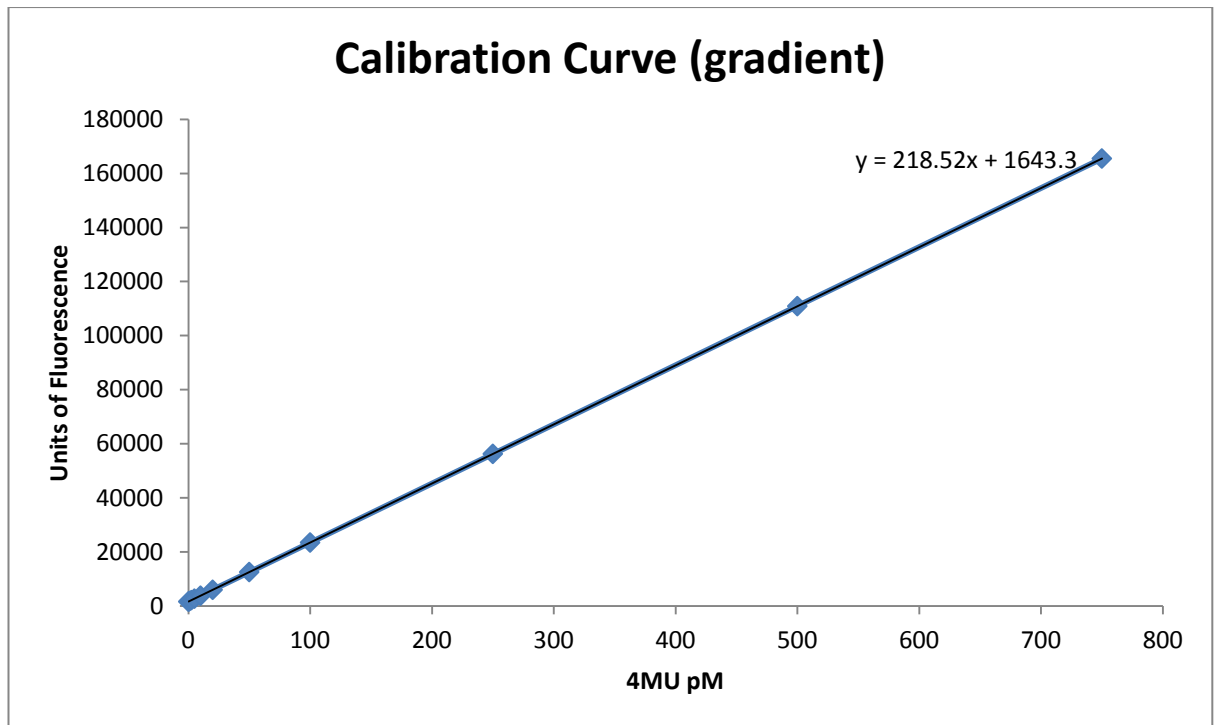
OD₆₀₀ = OD₆₀₀ of culture when cells were harvested

0.1ml = volume of culture sampled

Thus, 1 MUG unit is defined as the amount of β-galactosidase that catalyses the hydrolysis of 1pmol of MUG per min, per ml of culture, per unit of optical density at 600nm.

2.16.3 β-galactosidase liquid assay calibration curve

A calibration curve was prepared using known concentrations of the fluorescent product MU (0, 0.5, 1, 2.5, 5, 10, 20, 50, 100, 250, 500, 750 pM). The gradient of the calibration curve was then used to calculate pmol of MU present in culture samples that had been incubated with MUG.



2.17 Preparation of samples for fluorescence microscopy.

Cells were treated differently depending on what was the subject of study. After any treatment cells were attached to slides as described in 2.15.1.

2.17.1 Attachment of cells.

For all microscopy, cells were attached to labelled Poly-L-Lysine slides. Cell pellets were resuspended in dH₂O or buffer GTE to an appropriate concentration, this was judged by eye. A 10µl drop was spotted onto the slide, spread to a circle roughly 1cm² and allowed to dry. Slides were washed 3 times by deposition of 500µl of dH₂O onto the sample and removal by aspiration. The cover slip was mounted in 5µl of Slow Fade Gold (Invitrogen), gentle pressure applied and sealed with DPX mountant (BDH).

2.17.2 Live cell treatment.

A 5ml overnight of the appropriate strain was used to inoculate a 50ml secondary culture at 0.1 OD₆₀₀ which was grown until 0.5 ± 0.1. Cells were harvested by centrifugation at 5100rpm (5000xg) for 10min at 4°C. They were washed in 30ml of dH₂O three times. Cells were then harvested and attached to slides as described in 2.15.1.

2.17.3 Fixing cells.

For fixation, a pellet of cells (grown as described in 2.15.2) and was resuspended in 0.5ml of PBS. 0.5ml of fresh fixation solution was added and the solution incubated on a rotary wheel for 30min at RT. Fixation solution was made by adding 0.42ml 15% (w/v) formaldehyde and 0.5 μ l of 25% (w/v) glutaraldehyde to 2.08ml PBS. 0.5ml. The cells were washed three times with dH₂O and either viewed immediately or kept as a pellet at -20°C. Only live cells were fixed.

2.17.4 Removal of Lipoteichoic acid (LTA)

The cells were bathed in 30ml of 5% (w/v) SDS at 37°C for 30min. Keeping the cells on ice where possible they were washed 5 times with ice cold dH₂O, recovering cells by centrifugation at 5100rpm (5000xg) for 10min at 4°C between each wash. Cells were immediately viewed or kept as a pellet at -20°C.

2.17.5 Removal of surface proteins

To remove the surface protein cells were treated with pronase. The harvested cells were resuspended in an appropriate amount of 50mM Tris pH 7.5 and 10 μ l of 20mg ml⁻¹ pronase was added per 1ml of suspension. This was incubated for 30min at 37°C; the cells were recovered by centrifugation at 5100rpm (5000xg) for 10min at 4°C. The cells were resuspended in 5% (w/v) SDS and incubated at 50°C for 10min, to inactivate the pronase. The sample was washed 5 times in dH₂O; cells were either immediately viewed or kept as a pellet at -20°C.

2.17.6 Removal of Wall Teichoic Acids (WTA)

Hydrofluoric acid has been shown to remove WTA and was used within this study. The appropriate amounts of cells were resuspended in 250 μ l HF and this was incubated overnight at 4°C. The samples were washed, using disposable Pasteur pipettes, with 0.5ml dH₂O 5 times followed by once with 50mM Tris pH7.5 and then by water another time. Between each wash cells were recovered by centrifugation at 5100rpm (5000xg) for 10min at RT. The pH of the supernatant was checked and if it was still not above 6 further washes were performed. The cells were either viewed immediately or kept as a pellet at -20°C.

2.17.7 Cell breakage

To break *S.aureus* a FastPrep machine was used (MP Biomedicals Fastprep 24 Homogeniser). One ml of cell sample was added to a FastPrep tubes containing lysing matrix B (MP Biomedicals) and run at speed 6 for 40s for 5 runs with incubations on ice in between each run to prevent protein denaturation. The FastPrep beads were allowed to settle before the supernatant was transferred to a clean Eppendorf tube. The FastPrep tube was then centrifuged at 13000rpm (5000xg) for 1min and any extra supernatant removed to another Eppendorf tube.

2.17.8 Trypsination

50ml of exponential culture was harvested and washed twice with 10ml PBS and suspended in 5ml PBS containing 0.2mg ml⁻¹ trypsin. Cells were incubated at 37°C for 1hr, washed twice with 10ml PBS and suspended in 5ml of TSB containing 1mM PMSF. 500µl aliquots were taken and immediately fixed (section 2.15.3) and washed 3 times. The remaining cells were incubated at 37°C and 500µl aliquots removed and fixed after 5, 10, 15, 20, 30 and 60mins.

2.17.9 *In vitro* staining

Cell membrane and DNA were stained *in vitro* with FM4-64 and Hoechst33342, respectively. Following cell fixation and subsequent wash steps, cells were resuspended in 0.5ml dH₂O containing 1.5µl of Hoechst33342 stock solution and 1.2µl FM4-64 stock solution was added. Samples were incubated at room temperature for 15min on a rotary shaker. Cells were harvested by centrifugation at 13000rpm (5000xg) for 1min and washed three times by resuspension in 1ml dH₂O and centrifugation. Cells were mounted onto slides as described in 2.15.1.

2.17.10 Lectin Labelling

Fluorescently labelled lectins are sugar binding proteins that are highly specific for their sugar moieties and used to label cells. Concanavalin A and Wheat germ agglutinin were used to label branched α-mannose structures and N-acetylglucosamine respectively.

Cells were grown and treated as required; an appropriate sample was taken and harvested. For ConA labelling, 25 μ l of 10mM MnCl₂, 25 μ l of 10mM CaCl₂ and 25 μ l of fluorescent ConA were added and the volume made up to 250 μ l with sdH₂O. For WGA labelling, 25 μ l of fluorescent WGA and 25 μ l of 10mM MnCl₂ were added and the volume made up to 250 μ l with sdH₂O. Cells were incubated for 30mins at RT rotating, following incubation they were harvested and washed 3 times in sdH₂O before being fixed (if needed) according to 2.15.3 and mounted as described in 2.15.1.

2.17.11 Vancomycin labelling

Fluorescently labelled vancomycin binds and preferentially labels the nascent peptidoglycan. Vancomycin binds the terminal D-ala D-ala residues present on peptidoglycan pentapeptides not yet cross-linked. Cell pellets were transferred to a micro centrifuge tube containing 10 μ l of 100 μ g ml⁻¹ 1:1 Vancomycin: fluorescently-labelled Vancomycin (at a final concentration of 1 μ g ml⁻¹) and incubated at 37°C, rotating for 5min. Cells were harvested by centrifugation at 13000rpm (5000xg) for 5min and washed 3 times in sdH₂O. Cells were fixed (if needed) according to 2.15.3 and mounted as described in 2.15.1.

2.17.12 Immunofluorescence

Cells were grown, harvested and treated as required. Cells were dried onto a Poly-L-Lysine slide, washed once with PBS, air dried and rehydrated with PBS. They were blocked with 2% BSA in PBS for 15min. Cells were then incubated overnight at 4°C with the primary antibody (concentration stated with each experiment) in 2% (w/v) BSA in PBS. No primary antibody was added to control slides. Cells were washed eight times by addition of 0.5ml of PBS and air aspiration. The secondary antibody (stated with each experiment along with concentration) was diluted in 2% (w/v) BSA in PBS and applied for 2hr at RT. Cells were again washed eight times with PBS and then a cover slip was mounted in 5 μ l Slow fade gold, gentle pressure applied and sealed with DPX mountant (BDH).

2.18 Fluorescence Microscopy

Fluorescence images were acquired using an Olympus IX70 deconvolution microscope and SoftWoRx 3.5.0 software (Applied Precision). Appropriate filters were used for visualisation of each fluorophore (Table 2.8). Samples were prepared in the dark to prevent fluorophore bleaching and mounted in Slow Fade Gold to prolong the life of the fluorophore.

| Filter | Compatible fluorophore | Excitation filter/bandpass (nm) | Excitation filter/bandpass (nm) |
|----------|---------------------------|---------------------------------|---------------------------------|
| DAPI | Alexafluor 350 | 360/40 | 457/50 |
| FITC/YFP | Alexafluor 488, VancFL | 490/20 | 528/38 |
| mRFP | Alexafluor 594 | 580/20 | 630/60 |

Table 2.8 DeltaVision filter set.

2.19 Preparation of samples for AFM.

2.19.1 Extraction of cell walls for AFM.

An exponential phase culture was harvested by centrifugation (5100rpm for 10min at RT) and supernatant discarded. The pellet was immediately resuspended in 20ml boiling dH₂O and boiled in a water bath for 10min to kill the cells and inactivate autolysins. Cells were broken and purified by FastPrep (as described in Section 2.15.7.1). Cells were resuspended in 10ml pre-heated 5% (w/v) SDS and boiled for 25min for removal of non-covalently bound cell wall components. The cell suspension was transferred in 1ml aliquots to Eppendorf tubes, centrifuged (for 10min at RT) and then resuspended in pre-heated 4% (w/v) SDS and boiled for 15min. Material was then washed six times by centrifugation in dH₂O to remove SDS. For hydrolysis of covalently bound proteins, pellets were resuspended in 1ml 50mM Tris-HCl (pH 7.5) containing 2mg ml⁻¹ pronase and incubated at 60°C for 90min. If HF treatment was required, this was performed as described in 2.15.6. The resulting cell walls were harvested by centrifugation and washed once with water.

2.19.2 Preparation of cell walls.

Frozen purified cell walls were thawed and washed by centrifugation (13000rpm (5000xg) for 5min) in LC-MS CHROMASOLV® grade water (Fluka) at room temperature.

Sacculi were prepared at an appropriate working concentration for imaging of the cell walls and sonicated gently with a Sanyo Soniprep 150 for 10-20s to disperse cell wall aggregates. Around 5 μ l was transferred to a freshly cleaved mica sheet attached to a magnetic stub, and dried gently under nitrogen gas.

2.20 AFM microscopy

Sacculi were imaged using a multimode AFM with an Extended Nanoscope IIIa controller (Veeco Instruments). Imaging was carried out in tapping mode using silicon tips (Olympus) under ambient conditions. Post-processing of images was performed using Gwyddeon v2.19 software. All AFM imaging and processing was carried out by Dr Emma Ratcliffe.

2.21 Preparation of samples for STORM

Within this study immunofluorescence was performed with STORM. Cells were grown, harvested and treated as required. A 10 μ l spot of 1:10 gold nano particles was evenly dried onto a poly-L-lysine slide into a 1cm² area using nitrogen gas. A 10 μ l spot of cells was dried into the slide again using nitrogen gas. The slide was blocked in 2% (w/v) BSA in PBS for 15min and then incubated with an appropriate concentration primary antibody overnight at 4°C. The slide was washed 6-8 times in PBS and incubated with anti-rabbit Alexafluor 532, which is compatible with the STORM laser, at 3:1000 for 1-2hr at RT. Cells were washed in PBS 6-8 times, air dried and mounted in 5 μ l 10mM cysteamine in PBS. Slides were completely sealed with DPX.

2.22 STORM microscopy (Turner *et al.*, 2013).

Direct STORM imaging was used (Heilemann *et al.*, 2008). Samples were viewed using a 100-mW, 532-nm diode laser (Laser 2000) which was filtered through a 532-nm longpass dichroic filter (Semrock FF532-DI02) and a 565(24)-nm bandpass emission filter (Semrock Brightline 565/24). Laser power was adjusted by pulse-width modulation to maximise signal without saturating the charge-coupled device. An oil immersion objective mounted in an Olympus IX71 inverted optical microscope and a piezoelectric motor (Physik Instrumente) used to adjust focus. Images were expanded using a 35-nm and a 100-nm lens and captured using a Hamamatsu ImagEM camera.

Focus was maintained by repeatedly localising a gold particle as images were taken. Images of planes where the gold particles were not in focus were obtained by moving the objective to the desired plane, acquiring a series of images and then returning to the original plane to refocus. Image processing was conducted using photoactivation microscopy/STORM methodology as described by others (Betzig et al., 2006; Huang et al., 2008). Data was fitted to a Gaussian functions to individual molecule fluorescence, identified by clear intrinsic blinks, using Matlab. Super-resolution images were rendered by creating an image of desired pixel size and marking each pixel to which a blink event was localised bright. All STORM imaging and processing was carried out by Dr. Robert Turner.

CHAPTER 3

Identification of interactions between cell division proteins and the cell wall polymer synthetic machinery

3.1 Introduction

Most proteins do not exist as separate entities within a cell but instead form dynamic complexes composed of many components that work cooperatively in a wide range of biological processes. There are a wide variety of techniques employed to investigate protein-protein interactions, both biochemical and biophysical; *in vitro* and *in vivo*. Here, a number of the techniques that have helped to build up a map of the division machinery are discussed. Affinity chromatography is arguably one of the most extensively used techniques when investigating protein-protein interactions. It allows the investigation of interacting partners from *in vitro* mixtures, or potential discovery of novel components from *in vivo* samples, using matrix-bound ligands that capture a bait protein engineered with an attached tag (Chepelev *et al.*, 2008; Voet and Voet, 1995). Following removal of non-specifically bound proteins, interacting proteins are retained on the matrix via specific interactions with the bait proteins, they can then be eluted using competitive molecules, such as imidazole or glutathione, and analysed. There are a number of tags that can be attached to the bait protein ranging from genetically made hexa-histidine (his) and glutathione-S-transferase (GST) to commercially available tags or antibodies against the bait protein itself (Chepelev *et al.*, 2008). Of the commercially available tags FLAGTM, myc and GFP are good examples; FLAGTM is an immunogenic, hydrophilic synthetic eight amino acid tag; similarly the 10 amino acid long myc tag is a short artificial peptide, derived from the C-terminal amino acids of the human c-myc protein. Both synthetic tags and GFP can be attached to either C-terminus or N-terminus of a protein and not potentially interfere with its function, although expression yields may be more variable at the C-terminal end (Chepelev *et al.*, 2008; Einhauer and Jungbauer, 2001).

Indeed His-tagged *E.coli* PBP3 was used to show an interaction with PBP1B (Bertsche *et al.*, 2006) and also His-tagged FtsX showed an interaction with FtsE during cobalt

affinity purification (de Leeuw *et al.*, 1999). GST tags have been used to demonstrate that *S.pneumoniae* DivIVB co-purifies with a His-tagged FtsL/DivIC complex using both glutathione and cobalt affinity purification (Noirclerc-Savoie *et al.*, 2005). Both techniques were combined by Datta *et al.* (2006) to show an interaction between FtsW, FtsZ and PBP3 in mycobacteria. FLAG fusion has also been valuable in the investigation of divisome components; in *E.coli* FLAG-FtsE and FtsZ were shown to interact (Corbin *et al.*, 2007) and FtsL, Myc-tagged FtsQ and FLAG-tagged FtsB interact (Buddelmeijer and Beckwith, 2004). Furthermore, again in *E.coli*, ParC, ParE and the FLAG-tagged FtsK were isolated together using anti-FLAG antibodies (Espeli *et al.*, 2003) and Corbin *et al.* (2007) revealing a direct interaction between FtsZ and FtsE and that this interaction was independent of FtsA and ZipA.

The main drawback of affinity chromatography is that it requires the interacting proteins to bind tightly through the washing steps and is therefore unable to identify transient interactions. One way of overcoming this is to 'fix' the protein interactions; DSP (dithiobis[succinimidyl propionate]) and its water soluble counterpart DTSSP (3,3'-dithiobis[sulfosuccinimidyl propionate]) are able to do this by forming a stable bond between primary amines. The presence of a reducible thiol bond allows for the crosslinking to be reversed and the detection of weak and transient protein interactions. This technique was utilised to show an interaction between *B.subtilis* FtsZ with both his-tagged and thioredoxin fused EzrA (Chung *et al.*, 2007; Haeusser *et al.*, 2004) and in *E.coli*, to show an interaction between PBP3 and FtsN (Müller *et al.*, 2007).

Surface Plasmon Resonance and two hybrid systems are often used in conjunction with affinity purification to confirm interactions. All three methodologies were used to confirm the interactions of FtsW and PBP1B (Müller *et al.*, 2007) and PBP3 and PBP1B (Bertsche *et al.*, 2006). Surface plasmon resonance is the most common label-free technique for the measurement of protein interactions; it measures the change in the refractive index of light reflected from a metal biosensor when molecules bind to the surface. One binding partner is immobilized on the biosensor and a solution with potential binding partners is passed over this surface, the change in refractive index is proportional to the mass added to the sensor (Liedberg *et al.*, 1983). Mass

spectrometry can also be used to validate an interaction detected by affinity chromatography and was used to confirm the members of a *B.subtilis* complex consisting of EzrA, FtsZ, ZapA, FtsA and the novel YlmF (SepF), all first identified using his-tagging and nickel affinity purification (Ishikawa *et al.*, 2006). Gel filtration, sometimes known as size exclusion chromatography, has been employed to show an interaction between *B.subtilis* EzrA and FtsA, and the dissociation constant was calculated based on binding studies using fluorescently labelled EzrA (Singh *et al.*, 2007). The same group used the technique to establish SepF as an FtsZ-interacting protein in *B.subtilis* (Singh *et al.*, 2008).

Many other methods are also used to confirm or elucidate protein-protein interactions. Sucrose gradient ultracentrifugation consists of adding the proteins of interest to the top of a sucrose density gradient and centrifuging to separate out the components, and has been used to demonstrate interactions between ZapA and ZapB directly and the formation of a complex with FtsZ (Galli and Gerdes, 2010). Similarly sedimentation assays followed by 90°-angle light scattering analysis have identified ZapA as an FtsZ-interacting protein (Hale *et al.*, 2011). Typically used to validate protein interactions, bimolecular fluorescence complementation has been used to analyse the core cell cycle proteins of *Arabidopsis*, identifying novel active kinase complexes (Boruc *et al.*, 2010). Proteins are fused to complementary fragments of a fluorescent reporter protein and when the two fragments interact a fluorescent signal is emitted. Beneficially the interacting proteins are not required at large or stoichiometric proportions. Phage display is another high-throughput technique that can be used for the screening of protein interactions. The DNA encoding the protein of interest is ligated to the *pIII* or *pVIII* gene, which encodes the minor pIII coat protein or the major pVIII coat protein respectively. The phage and insert DNA hybrid are then inserted into *E.coli*, where mature virions are assembled with the relevant protein fragment as part of their outer coat. The phage particles are washed over wells containing immobilised protein; those that interact remain attached while others are removed by washing (Smith, 1985). This technique was exploited in 2003 to suggest the homodimerisation of FtsA (Carettoni *et al.*, 2003).

Fluorescence can also be used to demonstrate protein-protein interactions; Förster

resonance energy transfer uses the energy transfer between two fluorophores within less than 10nm of one another. A donor fluorophore, initially in its electronic excited state, transfers energy to an acceptor resulting in emission at a different wavelength. It has been used to demonstrate homodimerisation of PBP3 and the formation of an FtsW-PBP3 complex in *E.coli* (Fraipont et al., 2011) and interactions between Cy3-labelled MinC and Cy5-labelled FtsZ (Okuno et al., 2009). Furthermore, a SepF homologue in the cyanobacterium *Synechocystis*, fused with a His-GFP tag, was shown to physically interact with FtsZ polymers *in vitro* using fluorescence microscopy (Marbouty et al., 2009). Fluorescence recovering after photobleaching (FRAP) describes a technique capable of quantifying the two dimensional lateral diffusion of fluorescently labelled molecules and was used to demonstrate that the Z ring short overlapping filaments have a rapid turnover (Erickson et al., 2010).

Immunoblotting involves binding a protein onto a nitrocellulose membrane and visualising interactions by probing either directly with antibody or with antibodies against the fusion tag of a fused protein. This technique has been used to corroborate the interaction between ParC and FtsK in *E.coli* (Espeli et al., 2003). Non-denaturing PAGE and Western blotting are common place lab techniques that can be used to detect protein-protein interactions as done by Sievers and Errington (2000) to detect the formation of an FtsL and DivIC complex. Premature targeting manipulates the linear protein recruitment seen in *E.coli* to identify the individual contributions of upstream proteins to specific recruitment steps. The proteins of interest can be fused to ZapA, which binds to FtsZ early within the division process. FtsA also binds early in the division process and is required for the recruitment and therefore localisation of downstream proteins. When the fusion protein is expressed within an *ftsA* mutant, proteins downstream of the protein of interest will have their localisation restored to midcell. Goerhring et al. (2005) fused FtsQ to ZapA fully restoring the localisation of FtsK, FtsL, FtsB, FtsW and FtsI, when expressed within the *ftsA* mutant, demonstrating the ability of FtsQ to interact and recruit downstream proteins independently of FtsA. This methodology was further used to display interactions of *B.subtilis* DivIC with FtsL and *B.subtilis* DivIB with PBP2B within *E.coli* host cells, which showed that interactions were independent of other *B.subtilis* division proteins (Robichon et al., 2008).

A sensitive low-tech, scalable technique is the yeast two hybrid system (Fields and Song, 1989). The yeast transcription factors Gal4 and Gal80 have been shown to be comprised of two separable domains; a DNA binding domain and an acidic transcription activation domain (Hope and Struhl 1986; Keegan *et al* 1986). By fusing proteins of interest to each of these domains, interactions can be seen as the reconstitution of a functional transcriptional activator. Interactions can be detected by transcriptional activation of an adjacent reporter gene such as *lacZ*, and numerous interactions have been shown during yeast two hybrid screens (Bertsche *et al.*, 2006; Espeli *et al.*, 2003; Hale *et al.*, 2011; Hamoen *et al.*, 2006; Ishikawa *et al.*, 2006; Sievers and Errington, 2000). The yeast tri-hybrid assay uses the same principle but with the addition of a hybrid RNA molecule as a linker between the separated transcription domains (Young, 1998). The ability of *B.subtilis* DivIB, DivIC and FtsL to form a ternary structure in yeast was established using this method (Daniel *et al.*, 2006). The interactions seen within the yeast two hybrid system are restrained to the nucleus making it unsuitable for the investigation of large proteins, those that are membrane bound or those requiring post-translational modifications. Non-specific interactions of the separated domains have also been reported and could result in false positives (Deane *et al.*, 2002).

To overcome some of the restrictions seen within yeast two hybrid Di Lallo *et al.* (2001) developed a two-hybrid based on the dimerisation of λ repressors. A chimeric operator, constructed of two hemi-sites from phage P22 and phage 434 operators, can be recognised and bound by a hybrid repressor, again made of P22 and 434 repressors. The proteins of interest are fused to the two repressors, and thus if the proteins interact, the hybrid repressor binds to the hybrid operator and blocks the transcription of downstream reporter genes, such as *lacZ*. This method has been used to reveal large networks of interactions for division proteins in *E.coli* and *S.pneumoniae* (Di Lallo *et al.*, 2003; Fadda *et al.*, 2007; Maggi *et al.*, 2008). This technique has been further adapted to be based on the reconstitution of adenylate cyclase activity in *E.coli* (Karimova *et al.*, 1998). The catalytic domain of the *Bordetella pertussis* adenylate cyclase can be separated from the calmodulin-binding domain, into two complementary fragments T25 (residues 1-224) and T18 (residues 225-399)(Glaser *et al.*, 1988). These domains

are then fused to the proteins of interest and should an interaction occur the catalytic domain is reconstituted. The active enzyme is able to catalyse the hydrolysis of ATP to cAMP within the cytosol, which in turn can bind the transcriptional activator CAP (catabolite activator protein). The cAMP/CAP complex is a promiscuous regulator and drives the expression of a large number of genes including those involved in the catabolism of lactose and maltose. By using lactose or maltose as the unique carbon source, interactions can be easily distinguished on indicator or selective media. The use of a cytosolic regulatory molecule makes this method particularly suitable for the study of division proteins and it has been used to establish networks in a number of organisms (Claessen et al., 2008; Daniel et al., 2006; Datta et al., 2006; Ebersbach et al., 2008; Fraipont et al., 2011; Galli and Gerdes, 2010; Karimova et al., 2005; Marbouty et al., 2009a; Mazouni et al., 2004; Müller et al., 2007; Patrick and Kearns, 2008). Of particular note is its use in the establishment of an *S.aureus* interaction map including both the cytoplasmic components of the division machinery and the peptidoglycan biosynthetic apparatus (Refer to Chapter 1, Figure 1.2) (Steele *et al.*, 2011).

3.1.1 Aims of this chapter

- Bioinformatic identification of putative proteins involved in *S.aureus* WTA cell wall attachment.
- Identification of protein-protein interactions of WTA biosynthetic proteins and cell division proteins.

3.2 Results

3.2.1 Genes chosen for investigation

At the time that this investigation was undertaken a WTA biosynthetic pathway was well established (Swoboda *et al.*, 2010) with all steps having been assigned their proteins (Refer to Chapter 1.9.1, Figure 1.10). However the final step in WTA synthesis, the transfer of the cell wall polymer from their lipid-linker precursor to the cell wall peptidoglycan remained uncharacterised. It was suggested that the proteins responsible for this step were the uncharacterised LytR-CpsA-Psr (LCP) proteins, SA2103, SA1195 (MsrR) and SA0908, in personal communications with R. Daniel and the B. Bergi-Bächi group. This was later supported by evidence within *B.subtilis* that LCP proteins carried out the linkage to the peptidoglycan (Kawai *et al.*, 2011) and they were subsequently published as the hypothetical WTA ligases (Dengler *et al.*, 2012; Over *et al.*, 2011). These proteins along with TarO, the first step of the WTA biosynthetic pathway, were chosen to be investigated. In *B.subtilis* the WTA biosynthetic machinery has been shown to form a complex network of interactions through yeast and bacterial two hybrids (Formstone *et al.*, 2008), thus these four proteins were felt to be adequate to suggest if the WTA biosynthesis proteins interact with the divisome.

The topology of the LCP proteins was unknown so their protein sequences were obtained from NCBI and the topology predicted using ConPred II (Arai *et al.*, 2004). *S.aureus* TarO, SA1195 and SA0908 were all predicted to have at least one transmembrane helix with an N_{in}-C_{out} topology. SA0908 was predicted to be soluble (Table 3.1). As members of the LCP family, SA2103, SA1195 and SA0908 were expected to have a short intracellular, a transmembrane domain and a large extracellular region containing the LCP domain (Hübscher *et al.*, 2008; Kawai *et al.*, 2011). Therefore N-terminal fusions of each protein are necessary to position the adenylate cyclase fragments in the cytosol.

Penicillin binding protein 4 (PBP4) is required for the synthesis of the characteristic highly cross-linked peptidoglycan of *S.aureus* and localises to the septum, however in the absence of WTA synthesis it becomes dispersed throughout the entire cell

membrane and is unable to function normally (Atilano *et al.*, 2010). This interesting observation suggests an interaction between PBP4 and the WTA biosynthetic machinery, despite a negative result previously seen between PBP4 and TarO (Atilano *et al.*, 2010), and therefore was included within this investigation. The crystal structure of PBP4 has shown that it consists of two domains; an N-terminal domain containing its transpeptidase domain and an all β -sheet C terminal domain that is adjacent to the trans side of the cytoplasmic membrane (Atilano *et al.*, 2010; Navratna *et al.*, 2010; Scheffers and Pinho, 2005).

To fully investigate the interactions between the proteins of interest and the cell division machinery, a list of 22 *S.aureus* proteins were chosen. The list encompasses all aspects of the division process, from DNA segregation and correct septum placement, through to late division proteins involved in septum biosynthesis and synthesis of peptidoglycan-associated components. Homologues of proteins involved in *B.subtilis* elongation were also included, since *S.aureus* does not undergo any cell elongation, these proteins may play an alternative role in division of cocci (Steele *et al.*, 2011).

3.2.2 Construction of BACTH plasmids

The genes of interest were amplified by PCR and cloned into pKT25 and pUT18C to create in-frame protein fusions to the C-terminus of T25 and T18 (Figure 3.1). Ligation products were used to transform electrocompetent *E.coli* TOP10 with selection on LB kan 50 $\mu\text{g ml}^{-1}$ or amp 100 $\mu\text{g ml}^{-1}$. Positive clones were identified by colony PCR using the same primers used to amplify the genes of interest (section 2.9.3, data not shown) and by plasmid extraction, restriction digestion with *EcoRI* and *BamHI*, and electrophoresis on a 1% (w/v) agarose gel (Figure 3.2). DNA bands of the correct size were seen for each plasmid (Table 3.2). Plasmids were sequenced by the University of Sheffield Core Genomics Facility to exclude the possibility of errors having been introduced during PCR (data not shown). The translated plasmid sequences showed 100% identity to predicted amino acid sequences, although a synonymous mutation was seen in the third position of the codon in the case of T25-TarO twice and T25-SA0908 once.

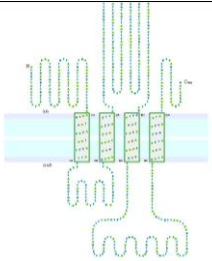
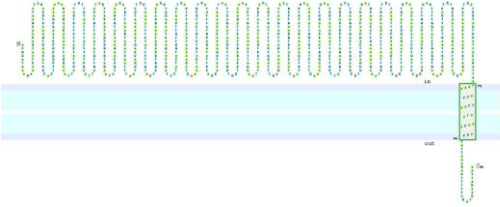
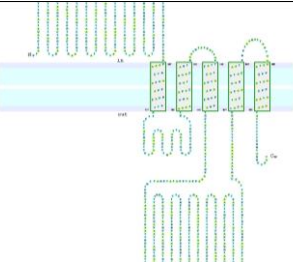
| GENE | Putative Function | Nucleotide Length (bp) | Amino acid length | Mass (kDa) | Predicted Topology |
|----------------------|---|------------------------|-------------------|------------|--|
| TarO | UDP-N-GlcNAc: UDP-P GlcNAc 1-P transferase | 1056 | 351 | 38.5 |  |
| SA2103 | Putative LCP; cell envelope-related transcriptional attenuator domain | 948 | 316 | 34.7 |  |
| SA1195 (MsrR) | Peptide methionine sulfoxide reductase regulator; Influences lytic behaviour (Dengler <i>et al.</i> , 2011) | 984 | 327 | 37.0 |  |
| SA0908 | Putative LytR; transcriptional regulator | 1218 | 405 | 45.7 | Predicted as soluble |

Table 3.1 Results obtained from bioinformatic search of proteins of interest.

Table showing the results obtained from an NCBI search of TarO, the first protein in the WTA biosynthetic pathway, and proteins suggested to be involved in the attachment of WTA, the final step in the biosynthesis of WTA. Putative function, nucleotide length and amino acid length were all obtained from NCBI (<http://www.ncbi.nlm.nih.gov/>). Weight was predicted using ExPasy tool Compute pI/Mw. Topology was predicted using ConPred II.

3.2.3 *E.coli* BTH101 as a reporter strain for the detection of protein-protein interactions

E.coli BTH101 is a non-reverting adenylate cyclase deficient reporter strain with high complementation efficiency. The frequency of spontaneous Lac⁺ revertants due to cAMP/CAP independent promoter mutations is 10⁻⁸, making BTH101 a suitable strain for detection of protein-protein interactions seen by the reconstruction of the separated adenylate cyclase (Karimova *et al.* 1998). *E.coli* BTH101 was transformed with one of the constructed plasmids and made electrocompetent. Plasmids carrying fusions of T25 or T18 to a number of *S.aureus* cell division and other proteins (FtsZ, DivIB, DivIC, EzrA, FtsA, FtsL, FtsW, PBP1, PBP2, PBP3, PBP4, ParC, ParE, YneS, YpsA, GpsB, SepF, ZapA, Noc, RodA, MreC, MreD, ypfP, LtaA, LtaA, DivIA, DnaK) were then transformed into the electrocompetent BTH101 containing one of the T18- or T25-constructed plasmid.

3.2.4 Investigating physical interactions with *S.aureus* WTA biosynthesis proteins of interest

3.2.4.1 Solid assay

To investigate positive interactions between the proteins of interest and members of the divisome, co-transformed strains were selectively grown overnight in LB with both ampicillin and kanamycin. The cells were washed three times in sdH₂O to remove media and resuspended in 5ml sdH₂O before 10µl aliquots were spotted onto minimal media agar containing 150µg ml⁻¹ X-Gal (Steele *et al.*, 2011), allowed to dry and incubated at 30°C for 26-30 hrs. The positive control strain carrying plasmids encoding T25 and T18 fused to the leucine zipper domain of GCN4 (pKT25-leucine zip or pUT18c-leucine zip)(Karimova *et al.*, 1998) and the negative control strain carrying unfused T18 and T25 fragments (pUT18c or pKT25) were also co-transformed with the opposing unfused adenylate cyclase fragment. If either negative control gave a positive result the experiment was discarded and repeated.

The WTA biosynthetic proteins will be considered first; Positive interactions were seen with many *S.aureus* division proteins (as displayed colorimetrically in Table 3.3; plates are shown in appendix I). YpfP and LtaA were constructed as both C terminal and

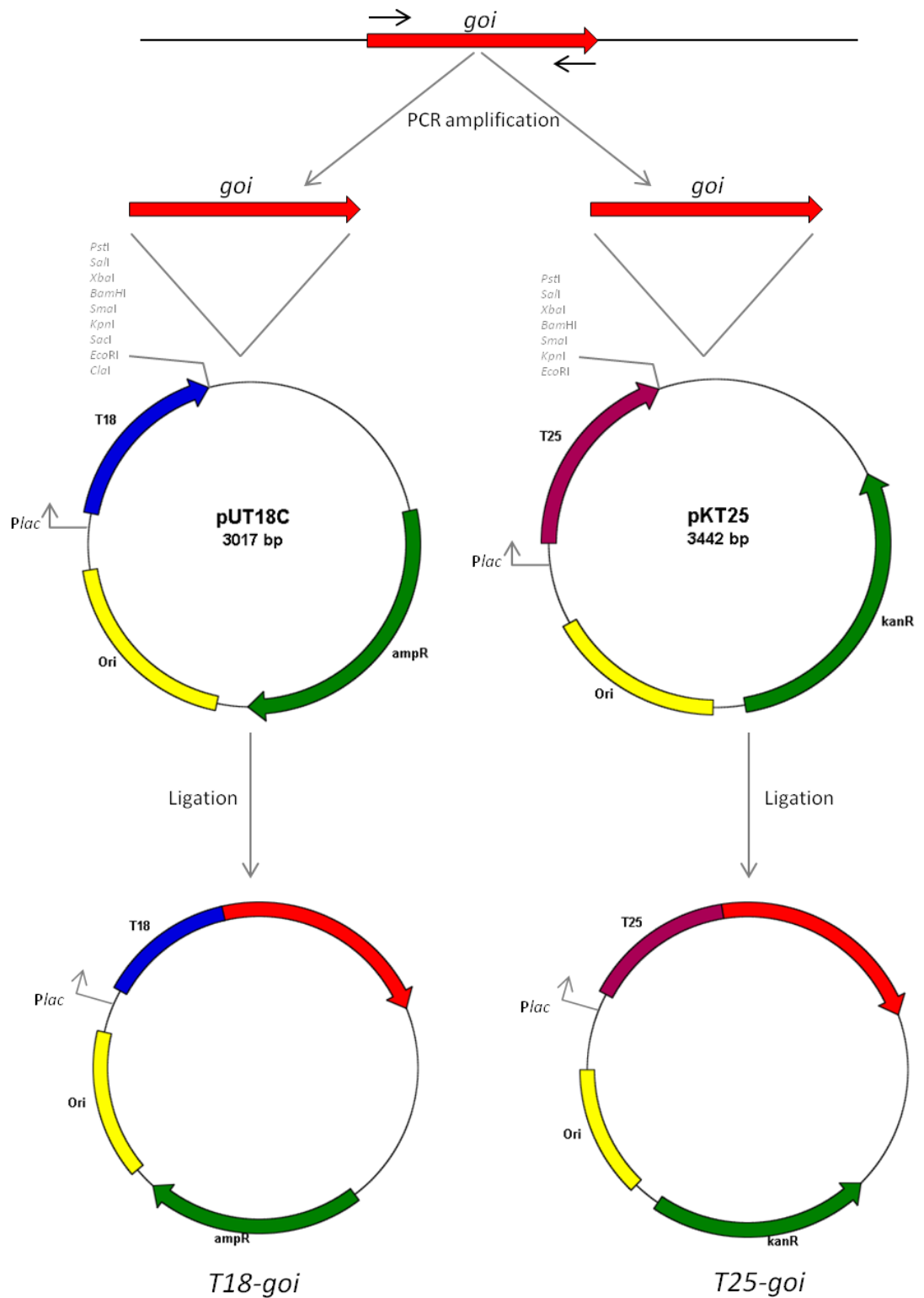
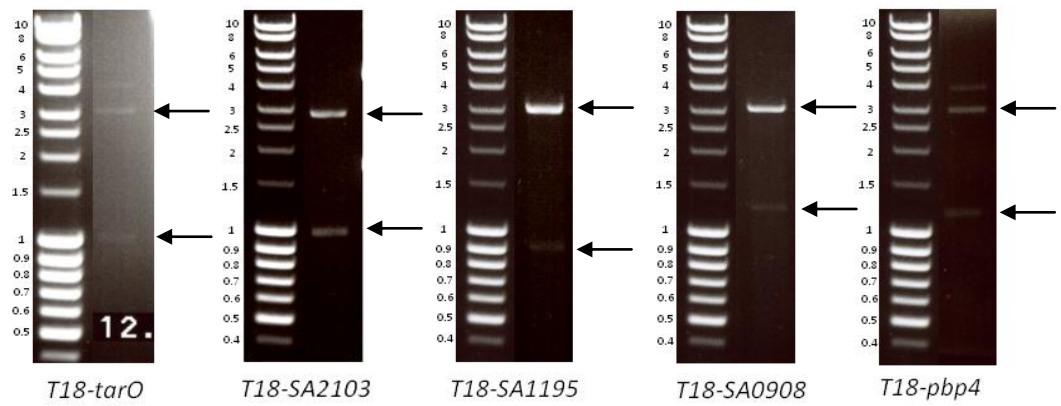


Figure 3.1 Construction of BACTH plasmids carrying C-terminal fusions

Diagrammatic representation of gene fusions of the encoding regions for the C-terminus of T18 and T25 fragments to the N-terminus of genes of interest (*goi*).

A



B

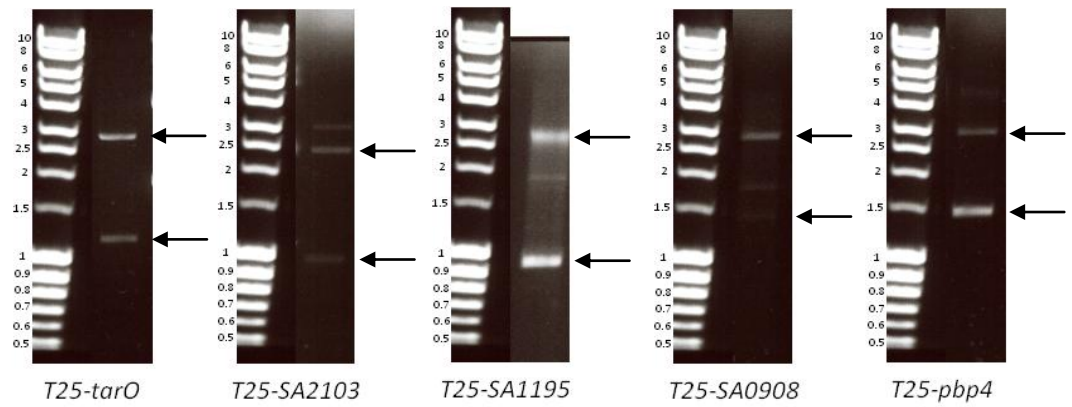


Figure 3.2 Restriction enzyme digests of BACTH plasmids

Restriction digests of BACTH plasmids with *Bam*HI and *Eco*RI carrying C-terminal fusions to a) pUT18C and b) pKT25. Bands correspond to the expected size are indicted with a black arrow. Sizes of DNA ladder shown in kb.

| Gene inserted | pUT18C | | pKT25 | |
|---------------|--------------|-------------------------|--------------|-------------------------|
| | Plasmid name | Expected band size (bp) | Plasmid name | Expected band size (bp) |
| <i>tarO</i> | pVK1 | 1056, 3017 | pVK2 | 1056, 3442 |
| <i>SA2103</i> | pVK3 | 948, 3017 | pVK4 | 948, 3442 |
| <i>SA1195</i> | pVK5 | 984, 3017 | pVK6 | 984, 3442 |
| <i>SA0908</i> | pVK7 | 1218, 3017 | pVK8 | 1218, 3442 |
| <i>pbp4</i> | pVK9 | 1296, 3017 | pVK10 | 1296, 3442 |

Table 3.1 Expected band sizes (bp) of restriction fragments of BACTH plasmids digested with *EcoRI* and *BamHI*

N terminal fusions (Bottomley, unpublished) and where interactions were seen one orientation appeared stronger than the other. The strongest orientation varied between proteins and between orientations. Of proteins that showed interactions, results could be detected with both T18 and T25 fusions (where available) for most cases. However there were some discrepancies, the T25-TarO fusion showed no interaction with many proteins that were positive with the T18-TarO, despite showing positive interactions with T18-LtaS, T18-YpfP, T18-SA2103 and T18-SA0908. T25-SA2103 gave positive interactions for T18-DivIB, T18-DivIC, T18-FtsW, T18-EzrA, T18-LtaA, T18-YpfP, T18-SA2103, T18-SA1195 and T18-SA0908 where T18-SA2103 did not. T18-SA2103 did result in a positive with T25-PBP2 where the reversed plasmids did not and with T25-PBP1, T25-PBP3 and T25-DivIA where no reciprocals were available. Both the T18 and T25-SA1195 (MsrR) were highly interactive fusions with T18-DivIB, T25-GpsB, T25-Noc, T25-ZapA, T25-MreC, T25-MreD, T25-RodA, T25-LtaA, T25-TarO and T25-SA2103 giving positive interactions where the reverse did not. T18-SA1195 also gave positive interactions with T25-PBP1, T25-ParC and T25-ParE, where reciprocal plasmids were unavailable. Finally T18-SA0908 gave positive interactions with T25-FtsA, T25-PBP1, T25-PBP3, T25-LtaA, T25-DivIVA, T25-DnaK and T25-SA2103 which were not confirmed by the T25 fusions (where available). Conversely the T25 fusion showed a positive interaction with T18-PlsY and T18-ZapA where T18-SA2103 did not. These results show that the LCP proteins; SA2103, SA1195, SA0908, and TarO do interact with divisome components and that fusion to T18 and T25 may result in only a partially functional hybrid protein.

3.2.4.2 Liquid assay

To further quantify the observed protein-protein interactions, the efficiencies of functional complementation between fusion proteins in liquid culture were examined by measuring β -galactosidase activity using MUG as a substrate. Strains were grown to mid-exponential phase ($OD_{600} \sim 0.5$) in minimal medium at 37°C in the presence of IPTG to induce expression of fusion proteins at $150\mu\text{g ml}^{-1}$. Positive interactions were assigned if the level of β -galactosidase was at least four times higher than the negative control (BTH101 co-transformed with pKT25 and pUT18C)(Karimova et al., 2005) and proved statistically significant by the students T-Test. The threshold was determined as

87.6 MUG units.

Figure 3.3 shows the interactions observed and the statistical significance of each. Almost all positive interactions seen in the solid assay with T18-TarO gave positive readings in liquid, there were however a few exceptions. T18-TarO~pKT25-YpfP gave a positive reading on the solid assay but a negative in the liquid, however as pKNT25-YpfP gave a strong positive in both solid and liquid, the interaction was determined as occurring. T18-TarO~T25-EzrA gave a positive reading on solid and its liquid reading was above the threshold but not statistically significant. The interaction with the reversed plasmids gave nothing in solid or liquid but due to the strength of the blue seen on solid medium, this was still considered a positive interaction. T18-SA2103 gave negative readings with T25-FtsZ, T25-FtsA, T25-FtsL, T25-PBP3, however the majority gave readings 3 times the negative control, performed with this experiment, with only 1 (T25-FtsL) giving just double. FtsA, and FtsL both showed positive interactions with their reciprocal fusions in both solid and liquid. Of the remaining positive interactions (PBP1, PBP2, SepF, PBP4 and DivIVA) all gave positive interactions but only T25-PBP1 and T25-PBP4 were considered statistically significant. All positive interactions seen on solid medium for T18-SA1195 also gave statistically significant positive results in liquid medium. For T18-SA0908, despite giving positive readings on solid medium, T25-LtaS and T25-YpfP both gave negative readings. T18-SA0908~T25-FtsA gave a positive reading but was not statistically significant.

When examining the T25-TarO (shown in Figure 3.4), of the 6 positive interactions seen in the solid medium only T18-SA2103 and T18-SA0908 gave positive readings and neither were considered statistically significant. In the case of T25-SA2103 only T18-PBP4 did not register the positive seen on the solid medium and a statistically significant interaction was seen with T18-GpsB, which was not observed in the solid medium. Like its reciprocal, T25-SA1195 showed positive readings for all positive interactions seen in the solid medium. T25-SA0908 gave no positive readings with either of the T18-YpfG fusions or the T18-SA2103 despite producing a positive within the solid assay.

| | TarO T18 | TarO T25 | SA2103 T18 | SA2103 T25 | SA1195 T18 | SA1195 T25 | SA0908 T18 | SA0908 T25 |
|-----------------------------------|-------------|-------------|---------------|---------------|---------------|---------------|---------------|---------------|
| FtsZ _{(pKT25N)(pUT18)} | Red | Red | Red | Red | Green | Green | Red | Red |
| DivIB _{(pKT25)(pUT18C)} | Green | Red | Red | Red | Red | Green | Red | Red |
| FtsA _{(pKT25)(pUT18C)} | Red | Red | Green | Red | Green | Green | Green | Red |
| FtsL _{(pKT25)(pUT18C)} | Green | Red | Green | Red | Green | Green | Red | Red |
| DivIC _{(pKT25)(pUT18C)} | Red | Green | Red | Red | Green | Green | Red | Red |
| FtsW _{(pKT25)(pUT18C)} | Green | Red | Red | Red | Green | Green | Red | Red |
| EzrA _{(pKT25N)(pUT18)} | Green | Red | Red | Red | Green | Green | Red | Red |
| PBP1 _{(pKT25)(pUT18C)} | Green | White | Green | White | Green | White | Green | White |
| ParC _{(pKT25)(pUT18C)} | Green | White | Red | White | Green | White | Red | White |
| ParE _{(pKT25)(pUT18C)} | Red | White | Red | Red | Green | Green | Red | White |
| YneS _{(pKT25)(pUT18C)} | Green | Green | Red | Red | Green | Green | Red | Green |
| PBP2 _{(pKT25)(pUT18C)} | Green | Red | Red | Red | Red | Red | Red | Red |
| GpsB _{(pKT25)(pUT18C)} | Green | Red | Red | Red | Green | Red | Red | Red |
| YpsA _{(pKT25)(pUT18C)} | Red | Red | Red | Red | Green | Green | Red | Red |
| SepF _{(pKT25)(pUT18C)} | Red | Red | Green | Red | Red | Red | Red | Red |
| Noc _{(pKT25)(pUT18C)} | Red | Red | Red | Red | Green | Red | Red | Red |
| PBP3 _{(pKT25)(pUT18C)} | Red | White | Green | White | Red | White | Green | White |
| ZapA _{(pKT25)(pUT18C)} | Red | Red | Red | Red | Green | Red | Red | Green |
| MreC _{(pKT25)(pUT18C)} | Green | Red | Red | Red | Green | Red | Red | Red |
| MreD _{(pKT25)(pUT18C)} | Green | Red | Red | Red | Green | Red | Red | Red |
| RodA _{(pKT25)(pUT18C)} | Red | Red | Red | Red | Green | Red | Red | Red |
| PBP4 _{(pKT25)(pUT18C)} | Green | Red | Red | Red | Red | Red | Red | Red |
| LtaA _{(pKT25N)(pUT18)} | Red | Red | Red | Red | Green | Red | Red | Red |
| LtaA _{(pKT25)(pUT18C)} | Red | Red | Red | Red | Red | Red | Green | Red |
| LtaS _{(pKT25)(pUT18C)} | Red | Green | Red | Red | Red | Red | Green | Green |
| YpfP _{(pKT25N)(pUT18)} | Green | Red | Red | Red | Red | Green | Red | Green |
| YpfP _{(pKT25)(pUT18C)} | Red | Green | Red | Red | Green | Green | Red | Green |
| DivIA _(pKT25N) | Green | White | Green | White | Red | White | Green | White |
| DnaK _(pKT25) | Red | White | Red | Red | Red | White | Green | White |
| TagO _{(pKT25)(pUT18C)} | Red | Red | Red | Red | Green | Red | Red | Red |
| SA2103 _{(pKT25)(pUT18C)} | Green | Green | Red | Green | Green | Red | Red | Green |
| SA1195 _{(pKT25)(pUT18C)} | Red | Red | Red | Green | Red | Red | Red | Red |
| SA0908 _{(pKT25)(pUT18C)} | Red | Green | Red | Red | Green | Green | Green | Green |
| T25/T18 | Red | Red | Red | Red | Red | Red | Red | Red |



An example of a positive interaction



An example of a negative interaction

Table 3.3 Summary of β -galactosidase activity of bacterial WTA biosynthesis two hybrid fusions on solid media

Activity was determined by the colour of colonies grown on minimal media plates containing $150\mu\text{g ml}^{-1}$ X-gal. Green cells represent positive interactions whilst red cells represent negative interactions.

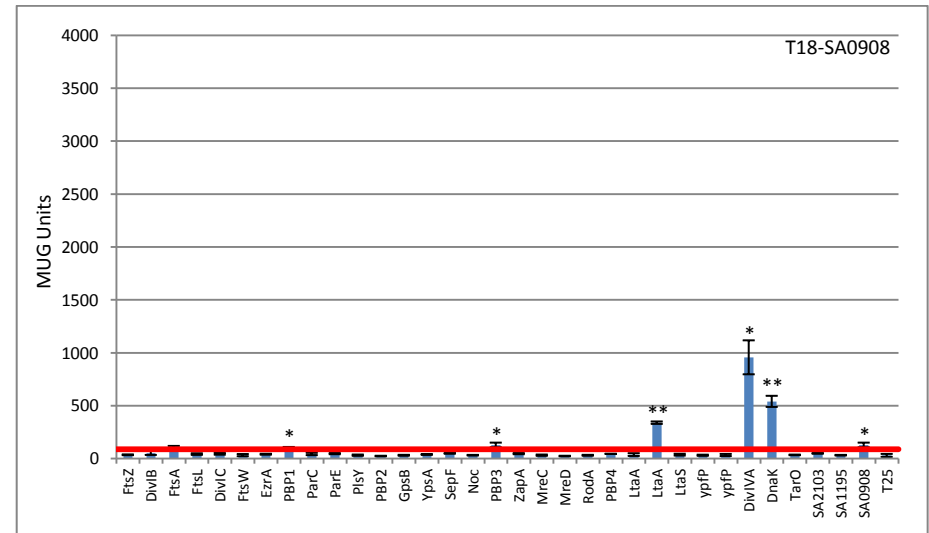
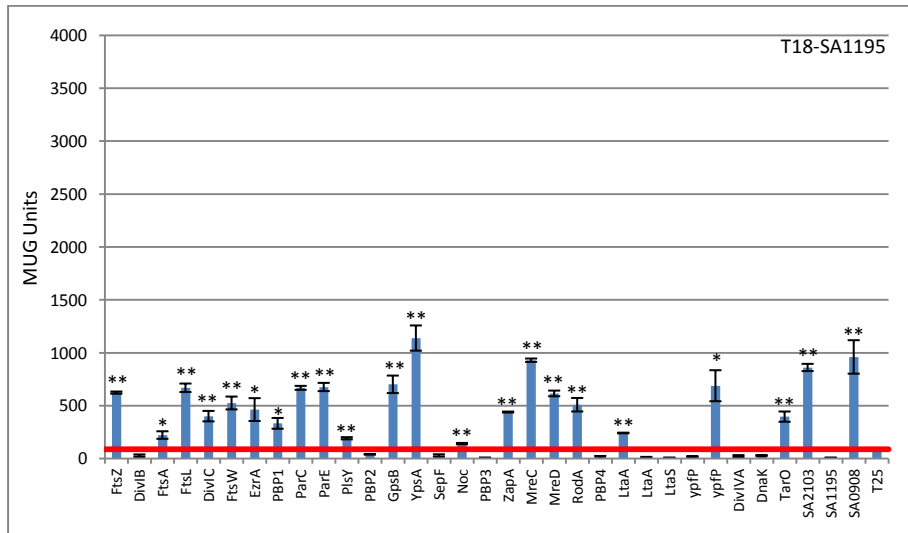
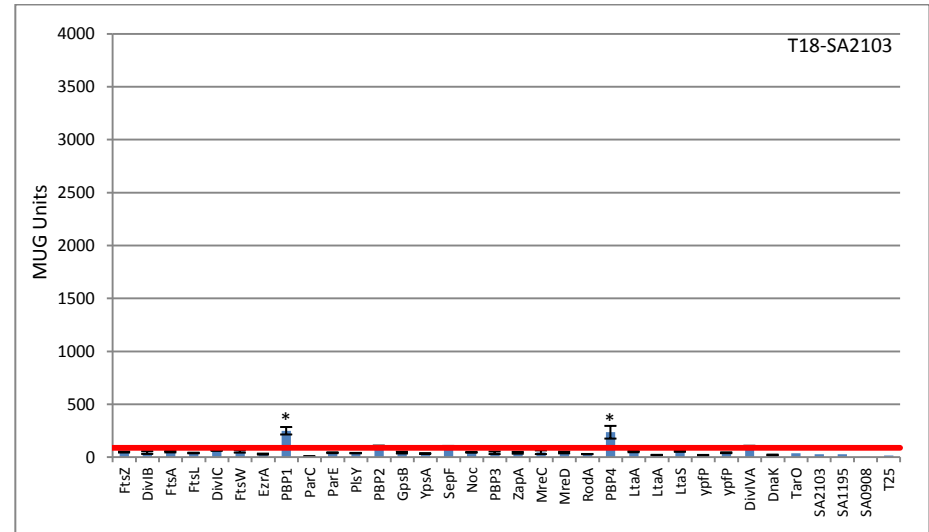
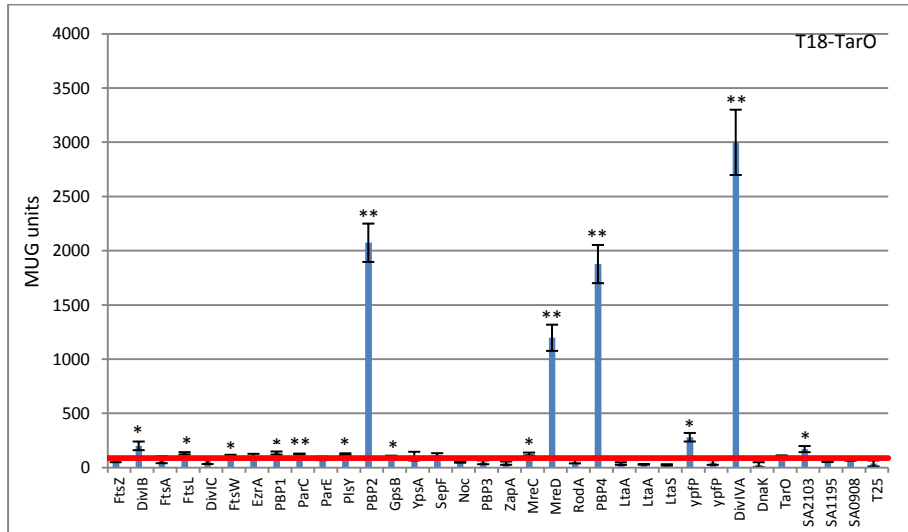


Figure 3.3 β -Galactosidase activity of T18 fused proteins of interest with T25 division proteins

Interactions of the proteins of interest fused to T18 were quantified by measuring β -galactosidase activity of *E.coli* BTH101 cells expressing complementary fusion proteins. Activity is displayed as the mean of three independent measurements of β -galactosidase activity for each co-transformant. Error bars represent the standard deviation. Values that are significantly different from the negative control, as determined by a student's T-test, are indicated by asterisks. ** denotes $p < 0.01$, * denotes $0.01 < p < 0.05$. Positive interactions are considered to be at least four times higher than the activity level for the negative control and this cut-off level (87.6 MUG units) is represented by the red line in each bar chart.

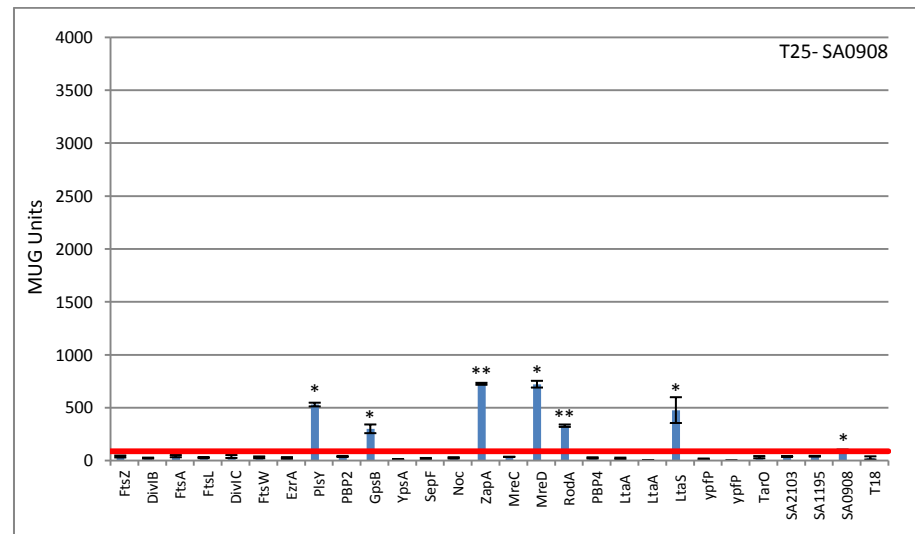
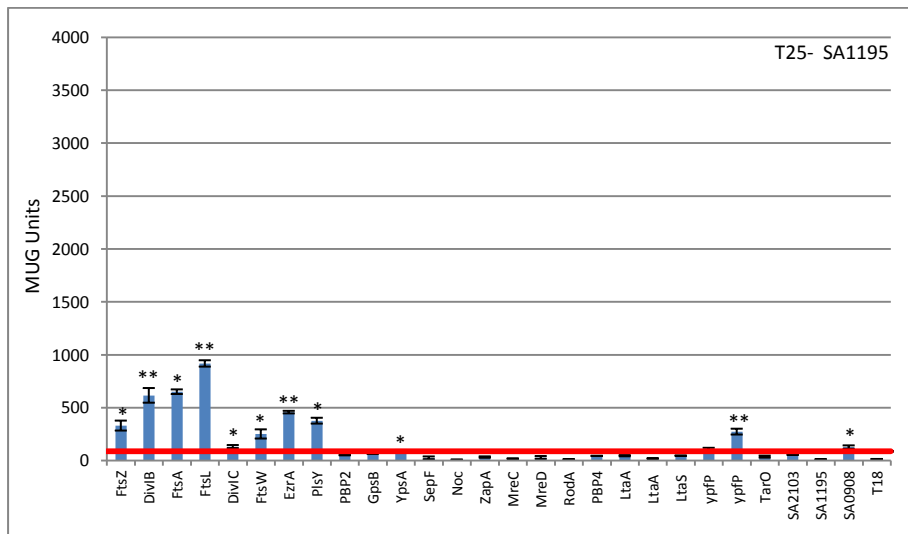
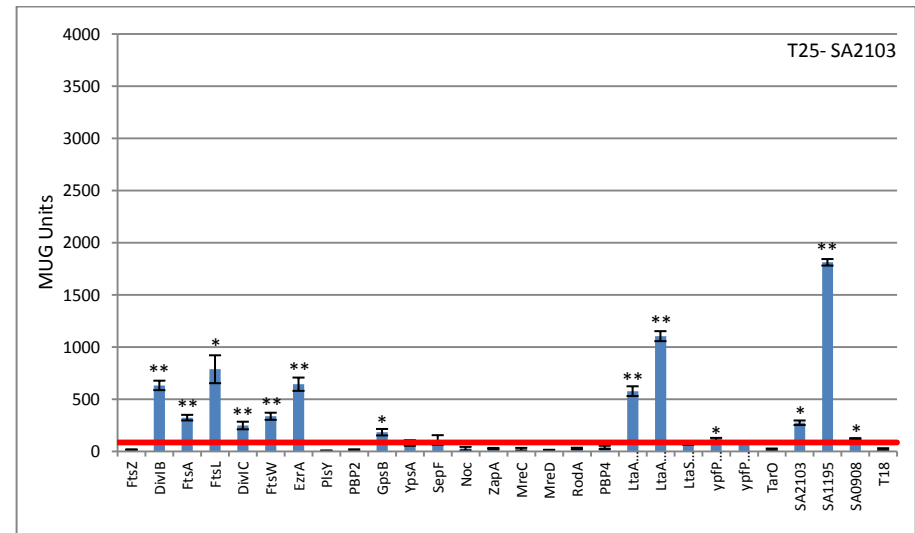
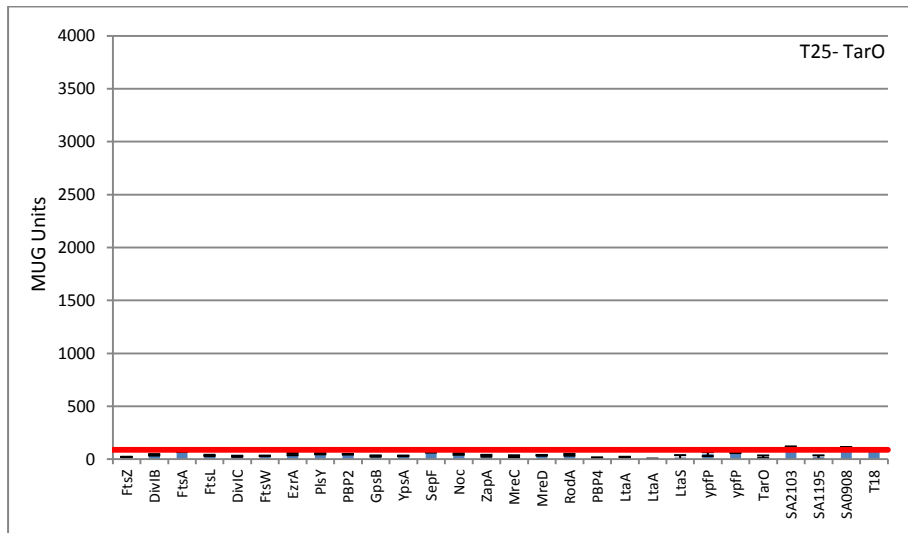


Figure 3.4 β -galactosidase activity of T25 fused proteins of interest with T18 division proteins

Interactions of the proteins of interest fused to T25 were quantified by measuring β -galactosidase activity of *E.coli* BTH101 cells expressing complementary fusions. Activity is displayed as the mean of three independent measurements of β -galactosidase activity for each co-transformant. Error bars represent the standard deviation. Values that are significantly different from the negative control, as determined by a student's T-test, are indicated by asterisks. ** denotes $p < 0.01$, * denotes $0.01 < p < 0.05$. Positive interactions are considered to be at least four times higher than the activity level for the negative control and this cut-off level (87.6 MUG units) is represented by the red line in each bar chart.

| | PBP4 T18 | PBP4 T25 |
|--|---------------------|---------------------|
| FtsZ _{(pKT25N)(pUT18)} | Green | Green |
| DivIB _{(pKT25)(pUT18C)} | Green | Green |
| FtsA _{(pKT25)(pUT18C)} | Green | Green |
| FtsL _{(pKT25)(pUT18C)} | Red | Green |
| DivIC _{(pKT25)(pUT18C)} | Red | Green |
| FtsW _{(pKT25)(pUT18C)} | Red | Green |
| EzrA _{(pKT25N)(pUT18)} | Green | Green |
| PBP1 _{(pKT25)(pUT18C)} | Green | White |
| ParC _{(pKT25)(pUT18C)} | Green | White |
| ParE _{(pKT25)(pUT18C)} | Red | White |
| YneS _{(pKT25)(pUT18C)} | Red | Green |
| PBP2 _{(pKT25)(pUT18C)} | Red | Red |
| GpsB _{(pKT25)(pUT18C)} | Green | Green |
| YpsA _{(pKT25)(pUT18C)} | Red | Green |
| SepF _{(pKT25)(pUT18C)} | Green | Green |
| Noc _{(pKT25)(pUT18C)} | Red | Green |
| PBP3 _{(pKT25)(pUT18C)} | Green | White |
| ZapA _{(pKT25)(pUT18C)} | Green | Green |
| MreC _{(pKT25)(pUT18C)} | Green | Green |
| MreD _{(pKT25)(pUT18C)} | Green | Red |
| RodA _{(pKT25)(pUT18C)} | Green | Green |
| PBP4 _{(pKT25)(pUT18C)} | Green | Green |
| LtaA _{(pKT25N)(pUT18)} | Green | Green |
| LtaA _{(pKT25)(pUT18C)} | Green | Green |
| LtaS _{(pKT25)(pUT18C)} | Green | Green |
| YpfP _{(pKT25N)(pUT18)} | Green | Green |
| YpfP _{(pKT25)(pUT18C)} | Red | Green |
| DivIA _(pKT25N) | Green | White |
| DnaK _(pKT25) | Green | White |
| TagO _{(pKT25)(pUT18C)} | Red | Red |
| SA2103 _{(pKT25)(pUT18C)} | Red | Green |
| SA1195 _{(pKT25)(pUT18C)} | Red | Green |
| SA0908 _{(pKT25)(pUT18C)} | Red | Green |
| T25/T18 | Red | Red |

Table 3.4 Summary of β -galactosidase activity of PBP4 two hybrid fusions on solid media

Activity was determined by the colour of colonies on minimal media plates containing $150\mu\text{g ml}^{-1}$ X-gal. Green cells represent positive interactions whilst red cells represent negative interactions.

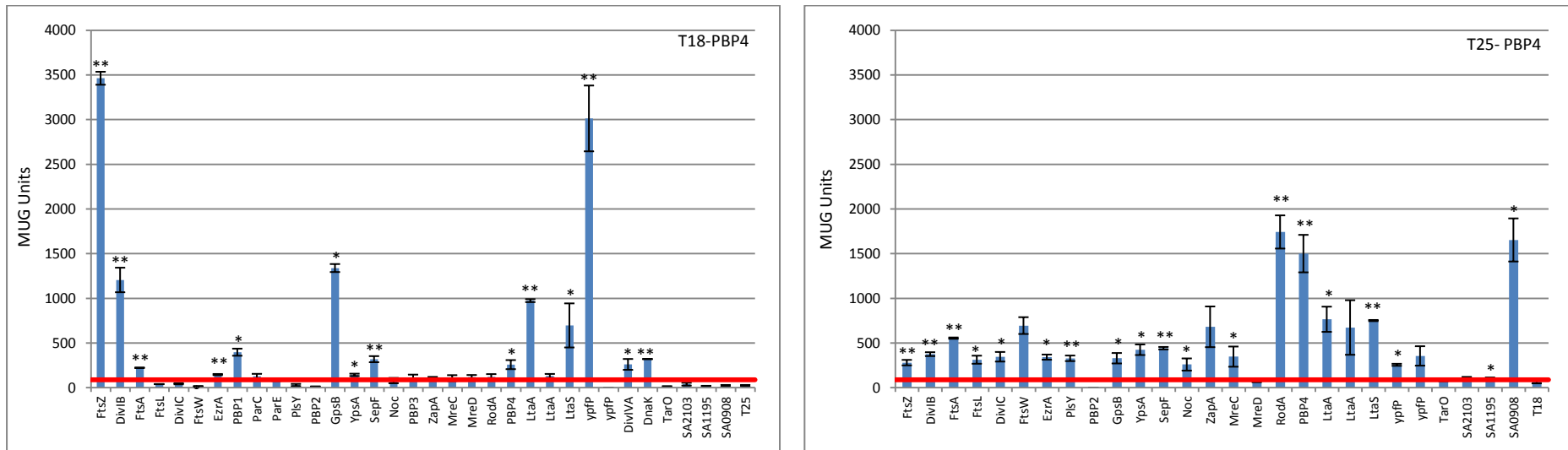


Figure 3.5 β -Galactosidase activities of T18 and T25 fused *S.aureus* PBP4 with T25 and T18 division proteins, respectively

Interactions of the PBP4 fused to T18 and T25 were quantified by measuring β -galactosidase activity of *E.coli* BTH101 cells expressing complementary fusion proteins. Activity is displayed as the mean of three independent measurements of β -galactosidase activity for each co-transformant. Error bars represent the standard deviation. Values that are significantly different from the negative control, as determined by a student's T-test, are indicated by asterisks. ** denotes $p < 0.01$, * denotes $0.01 < p < 0.05$. Positive interactions are considered to be at least four times higher than the activity level for the negative control and this cut-off level (87.6 MUG units) is represented by the red line in each bar chart.

3.2.5 Investigating physical interactions with *S.aureus* PBP4

3.2.5.1 Solid assay

Table 3.4 shows the PBP4 interactions on solid medium; the T25-PBP4 interacted with nearly all T18 divisome fusions only giving negative results with T18-PBP2, T18-MreD and T18-TarO. The T18-PBP4 fusion gave a negative reading with T25-FtsL, T25-DivIVC, T25-FtsW, T25-PlsY, T25-YpsA, T25-Noc, T25-SA2103, T25-SA1195 and T25-SA0908 when the reciprocal plasmid gave a positive. T18-PBP4~T25-MreD gave a positive reading which was not present in the T25-PBP4 screen. T18-PBP4 also gave a positive interaction with T25-PBP1, T25-ParC, T25-PBP3, T25-DivIVA and T25-DnaK, where no reciprocal plasmid was available.

3.2.5.2 Liquid assay

Almost all the interactions seen on the solid media gave matching readings in the liquid media (shown in Figure 3.5); however T18-PBP4 with T25-ParC, T25-PBP3, T25-ZapA, T25-MreC, T25-MreD, T25-RodA and one of the T25-LtaA fusions gave positive interactions but were not considered statistically significant. T25-ZapA, T25-MreC and T25-RodA gave positive interactions in the reversed screen. A positive reading was seen with T18-PBP4~T25-YpsA despite it registering negative in solid medium. The T25-PBP4 gave positive solid interactions for all fusions that gave positive interactions on the solid medium. However T18-FtsW, T18-ZapA, T18-YpfP, T18-SA2103 and one of the T18-LtaA were not considered statistically significant.

3.3 Discussion

Bacterial two-hybrid analysis has been used extensively for the investigation of protein-protein interactions in a wide variety of organisms; for example *Pseudomonas* (Goodman *et al.*, 2009), *Bacillus* (Szurmant *et al.*, 2007), *Streptomyces* (Hudson and Nodwell, 2004), *Mycobacteria* (Pearce *et al.*, 2008), human cells (Yamada *et al.*, 2003) and viruses (Dautin *et al.*, 2003). A range of cellular processes have been examined from cell wall synthesis (White *et al.*, 2010) to virulence factors involved in invasion of eukaryotic cells (Darwin *et al.*, 2001). Within *S.aureus* the bacterial two hybrid has allowed the development of a complex interaction map of cell division proteins (Steele *et al.*, 2011; A.Bottomley, 2012). The *S.aureus* studies confirmed a total of 29 interactions which had been previously detected in *E.coli*, *S.pneumoniae* and *B.subtilis* and showed several novel interactions, building up a core of 16 proteins involved in the divisome.

The work performed by Steele and Bottomley (Steele *et al.*, 2011) generated a list of 22 cell division proteins that were believed to be involved in cell division and were used to screen the proteins of interest for interactions with the divisome. This list of proteins includes those involved at each step of the division process, ranging from chromosome segregation and septum placement to peptidoglycan and cell surface protein synthesis (Figure 3.6c). Results of this study identified that all 4 proteins showed multiple partners with which they interacted, suggesting a strong presence in the division complex. The weight of interaction lines has been selected to indicate the number of confirmations this interaction has seen from the four possibilities; T25 or T18 orientations and liquid or solid assays

TarO showed many interactions across all stages of the division cycle but notably little interaction with proteins involved in Z-ring formation or nucleoid placement. The protein TarO (TagO) has not been extensively studied within *S.aureus*, the only direct interaction that has been investigated is between TarO and PBP4 which was negative (Atilano *et al.*, 2010). Within this screen T18-TarO and T25-PBP4 gave a strong positive interaction in both liquid and solid media however, the reciprocal fusion (T25-TarO~T18-PBP4) was negative suggesting a true interaction but that it might be affected by the orientation of the fusion. Preventing the expression of WTA, with a $\Delta tagO$ mutant, results in the production of round, severely defective progeny in *B.subtilis* (Pollack and Neuhaus, 1994).

The link between TagO and elongation machinery has been further confirmed by interactions seen between Tag proteins and MreB, an actin like protein that is suggested to be involved in synthesis and insertion of new peptidoglycan thereby controlling the width of rod-shaped cells (Kawai *et al.*, 2011). It is therefore unsurprising that there were many interactions seen with homologues of *B.subtilis* elongation. The conserved presence of these proteins in the divisome of a cocci, which does not undergo elongation suggests that they may have a further role (Steele *et al.*, 2011). The defects of a TarO mutant in *S.aureus* are less pronounced, with no change in morphology bar a slight increase in diameter, which suggests no specific roles in cell growth and division (Swoboda *et al.*, 2010). Therefore this implies that the many interactions seen with PBP's and essential division components indicate the site of WTA biosynthesis. Furthermore, Formstone *et al.* (2008) have shown in *B.subtilis* that the Tag proteins form a complex network of interactions which suggests that this entire pathway is linked to the divisome. My study has also shown that TarO interacts with the three putative ligases, proposing that insertion of these polymers happens at the same site as synthesis. Interactions were also seen with LTA synthetic machinery suggesting that this occurs in juxtaposition to WTA biosynthesis.

The LCP proteins have only recently been characterised in *S.aureus* and their interactions not yet studied. Within *B.subtilis* bacterial two hybrid analysis of members of the LCP family, TagT (previously known as YwtF) and TagU (LytR), have been confirmed to interact with MreB. Localisation of GFP fusions with TagT and TagU has also showed a distribution reminiscent of MreB (Kawai *et al.*, 2011). It is therefore unsurprising that SA1195 (MsrR) interacts with the homologues of elongation proteins and GpsB, which in *B.subtilis* is involved in the shuttling of PBP's between elongation and division. Interestingly though, there was only an interaction with one PBP (PBP1). SA1195 appeared to show interactions with proteins involved in all other stages of the division process. In *S.aureus*, the expression of *msrR* has been shown to peak in early exponential growth phase which further supports the divisome interactions seen here (Rossi *et al.*, 2003). Contrary to SA1195, SA2103 shows interactions with none of the elongation homologues but all the PBP's. SA0908 also showed interactions with 3 (MreD, RodA and GpsB) of the 4 elongation related homologues. Interactions between these proteins thought to be elongation specific and the ligases again suggesting that they may have another role. Indeed MreC and MreD have been researched

extensively and shown to be involved in organisation of peptidoglycan, control of cell division and morphology in *S.aureus* (Ma, unpublished).

ParC and ParE are subunits of the DNA topoisomerase IV which mediates chromosome segregation and only revealed interactions with SA1195. Noc is a nucleoid exclusion effector and like ParC and ParE only showed an interaction with SA1195. DivIA has no role in *S.aureus* (Pinho and Errington, 2004) but still interestingly showed interactions with two LCP proteins in *B.subtilis*. This suggests that the LCP proteins, alongwith the Tar's, are present at with the divisome from an early stage and that perhaps SA1195 is the first to arrive. All three LCP proteins and TarO showed interactions with at least one protein involved in Z-ring formation and late division (in this case SA0908 was an exception), suggesting that the LCP ligases maintain their presence at the divisome. Furthermore interactions were seen with LtaS by all of my proteins except SA1195 and with YpfP by all of my proteins, this could suggest that the LTA synthesis occurs alongside that of WTA. Furthermore PBP interactions were seen with all my proteins and there was a strong link with PlsY, which is involved in membrane lipid synthesis. Taken together we can suggest that WTA biosynthesis occurs at the septum alongside peptidoglycan incorporation and LTA synthesis.

The LCP proteins are members of the cell wall stress stimulon (CWSS), which is activated in response to the inhibition of cell wall synthesis, cell damage or depletion of essential cell wall biosynthesis enzymes (Belcheva and Golemi-Kotra, 2008; Campbell *et al.*, 2012; Dengler *et al.*, 2011). The stimulon contains genes encoding enzymes involved with the synthesis of the cell wall, such as PBP2 a bifunctional, transpeptidase and transglycosylase enzyme and FmtA, which plays a part in cell wall biosynthesis and may modulate the activity of the major autolysin (AtIA) (Qamar and Golemi-Kotra, 2012; Reed *et al.*, 2011). It is therefore unsurprising that the LCP proteins studied here show interactions with PBP's and other cell wall biosynthetic machinery components.

A link between WTA biosynthesis and PGN biosynthesis has been established with the study of WTA and PBP4, a LMW transpeptidase with little D,D-carboxypeptidase activity (Atilano *et al.*, 2010; Navratna *et al.*, 2010). PBP4 was therefore included within the BACTH screen and revealed multiple interactions with cell division components. PBP4 interactions

within *S.aureus* have not been thoroughly investigated, although the protein itself is fairly well characterised in laboratory and clinical strains alike. PBP4 is a β -lactamase ubiquitously expressed across strains, it is non essential but the knockout mutant shows a marked reduction in cross-linked muropeptides and increased vancomycin resistance (Navratna *et al.*, 2010). It has been shown to be present on a staphylococcal chromosome cassette (SCC*pbp4*) alongside the *tagF* gene (Mongkolrattanothai *et al.*, 2004), supporting a link between PBP4 action and WTA biosynthesis. Using immunolabelling and GFP fusions PBP5, the PBP4 homologue in *E.coli*, has shown localisation to sites of ongoing peptidoglycan synthesis in a substrate dependent manner and that it requires membrane attachment (Harris *et al.*, 1998; Potluri *et al.*, 2010). This link has been suggested as acting through FtsZ (Potluri *et al.*, 2010, 2012; Yang *et al.*, 2011). Within *S.aureus*, the only study of PBP4 interactions has been by Atlano *et al.*, where they looked at PBP4 interactions with TarO and showed no interactions (2010). However the other 3 PBP's of *S.aureus* have been studied, and they each showed a high number of interactions with the division machinery demonstrating that they have a role within the divisome (Steele *et al.*, 2011; Bottomley, 2012). PBP4 was shown to interact with almost all of the divisome proteins tested (Figure 3.7), except TarO, ParE, PBP2 and PBP3, suggesting that it too is involved with the divisome. Although an interaction was not seen with ParE a weak one was with ParC, which suggests that PBP4 can be found loosely associated with the early divisome. ParC and ParE have also been tested for interactions with one other PBP, PBP2, and none were seen (Steele *et al.*, 2011). PBPs have been shown to participate in dynamic multienzyme complexes (Sauvage *et al.*, 2008) so it is possible that interactions occur through other PBPs. No interaction was seen with TarO, supporting the work of Atlano *et al.*, but contradicting what this study saw with T18-TarO and T25-PBP4.

The bacterial two hybrid is not without flaws and therefore there is the possibility of false positives. Endogenous levels of *S.aureus* proteins are much lower than the expression levels of the hybrid proteins in *E.coli*, which can be as many as several thousand copies per cell versus a much more reserved ~150 copies per cell in the case of PBP1 (Karimova *et al.*, 2005; Pucci and Dougherty, 2002). This difference in expression level allows for the detection of weak interactions that would not necessarily be seen at lower protein concentrations. The protein concentration at the division septum is likely to be higher

which will also facilitate transient and weak interactions too. There have also been examples of heterologous interactions, seen between *S.pneumoniae* and *E.coli* division proteins, which could result in false positives (Maggi *et al.*, 2008). However the lower expression levels of *E.coli* native proteins and the use of unfused T18 or T25 plasmids means that the interactions seen are likely to be valid direct *S.aureus* interactions. All fusions made were tested with reciprocal empty plasmids which gave negative results thereby allowing us to be fairly confident in the truth of the positive interactions seen. With this it is possible to adapt previous division models to show the interactions of the WTA biosynthetic machinery (Figure 3.8). This BACTH only gives an indication of the possible interactions and verification with other methods would be preferred. Indeed this may elucidate other interactions not seen here.

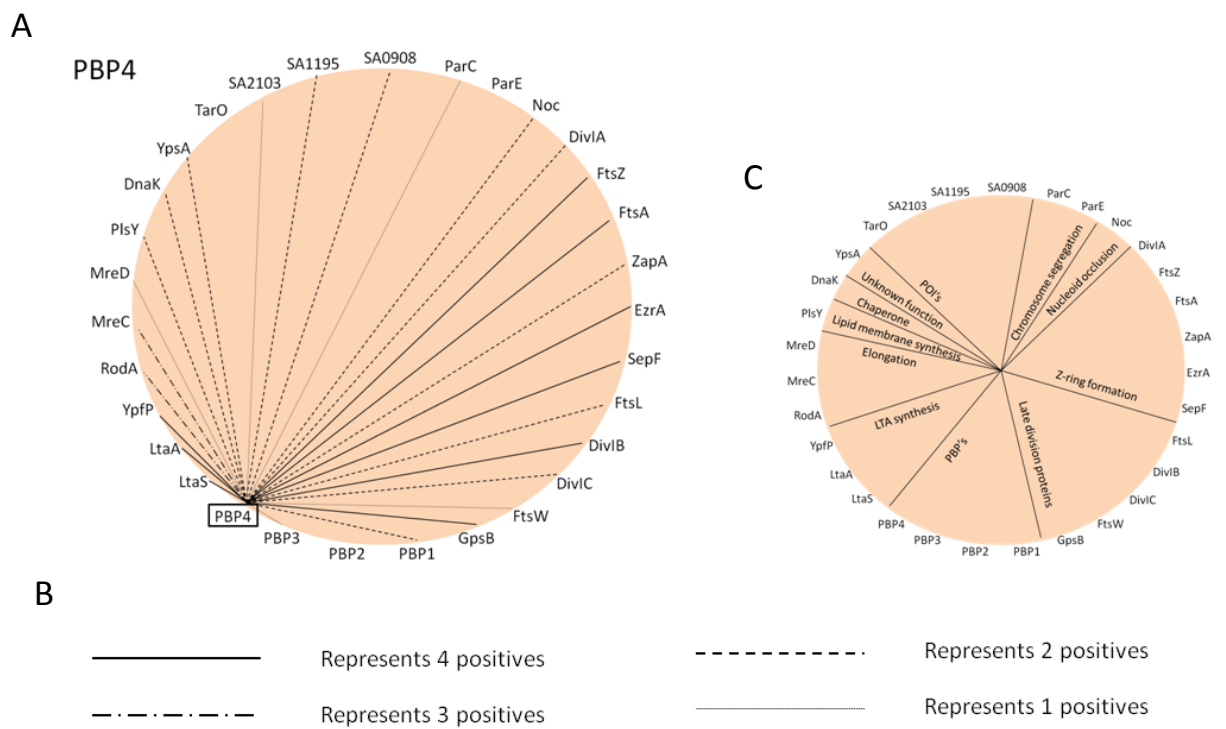


Figure 3.7 Interaction maps of PBP4

a) Interactions between PBP4 and cell division proteins as determined by BACTH are shown. b) Weight of line represents how many positives each interaction gave, either from the T18, T25, solid assay or liquid assay. c) The cell division proteins are separated into their functions.

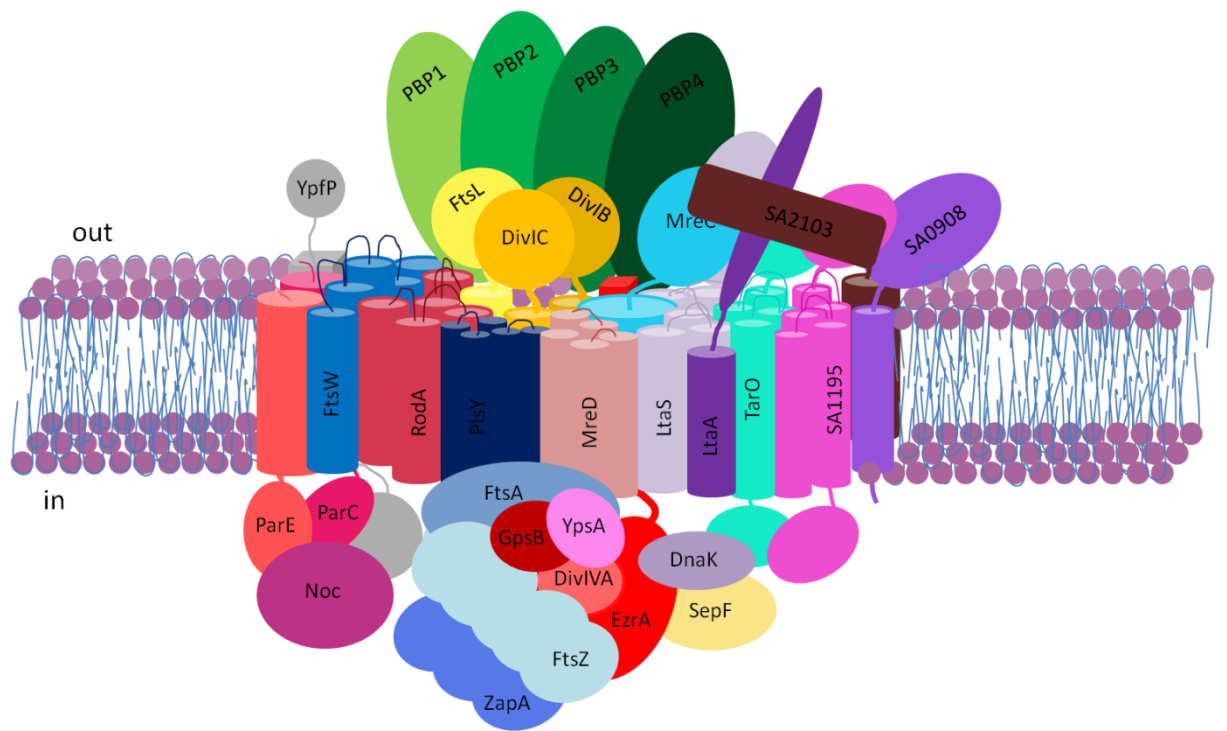


Figure 3.8 Schematic representation of the *S.aureus* divisome

Interacting components of the *S.aureus* divisome were identified using the BACTH assay, both previously and within this study (Steele *et al.*, 2011; Bottomley, 2011). This complex is dynamic thus not all divisome interactions are represented.

CHAPTER 4

The localisation of wall teichoic acids in *S.aureus*

4.1 Introduction

Several early studies of wall teichoic acid (WTA) localisation have been performed in *B.subtilis* (Clarke-Sturman *et al.*, 1989; Pooley *et al.*, 1978; Schlaeppi and Karamata, 1982; Schlaeppi *et al.*, 1985). These suggested that WTA localise at the division septa and either in patches or uniformly along the cell cylinder but none were conclusive. Subsequently, the primase TagB was localised to the cytoplasmic membrane in a dispersed manner (Bhavsar *et al.*, 2005) which led Formstone *et al.*,(2008) to systematically analyse functional GFP fusions WTA biosynthesis components (TagO, TagB, TagF, TagG and TagH). These fusions were all seen to localise at division septa and in apparent helical patterns along the cylinder consistent with the insertion of nascent peptidoglycan. This localisation was further supported by interactions seen between the elongation proteins MreD and MreC within two hybrid screens. Yeast two hybrid revealed interactions between MreD/TagH and MreD/ TagO and Bacterial two hybrid revealed interactions between both MreC and MreD with each of TagH, -O, -A, -B and -F (Formstone *et al.*, 2008) thereby further suggesting that WTA are produced alongside peptidoglycan biosynthesis. In contrast to this, in *S.aureus* Schlag *et al.*, (2010) performed binding studies using ConA-FITC, a lectin that has been shown to bind teichoic acids (Doyle and Birdsell, 1972). They observed dividing cells as two facing crescents with a free crosswall, deducing that this region was inaccessible to ConA either because WTA is not present or it is not yet fully polymerized. This conclusion seemed contradictory to the localisation and biosynthetic mechanism seen in other organisms and the results seen with the BACTH analysis.

Fluorescence microscopy has been widely used in bacterial cell biology. In particular wide field, although limited by optical resolution (approximately 0.2 μm), remains a powerful tool (Leung and Chou, 2011; Petty, 2007). To increase image resolution, the signal-to-noise ratio can be improved by applying deconvolution to captured images. This computational post-processing uses the point-spread-function (PSF) (how a point-like object becomes spread out in the image) to assign out-of-focus intensity back to its originating position in space, thus restoring the most probable object. Deconvolution typically requires a series of

z-stacks, images taken at 200nm steps in the z-direction (the resolution in the z-plane of standard light microscopy) extending from the top of the cell to the bottom, examples are shown in figures 4.9 and 4.10. The z-stack itself is useful to analyse how the fluorescence extends around the surface of a cell; for example an incomplete septal ring (doughnut shape) is viewed as two dots on either side of the cell when the centre of the cell is in focus, however when able to scroll up/down the cell the true ring shape is seen. With deconvolution the limit of resolution for wide field microscopy is 180nm-250nm in the X-Y plane and 500-700nm in the Z dimension (Schermelleh *et al.*, 2010; Wallace *et al.*, 2001).

The advent of super-resolution fluorescence microscopy techniques such as; 3D-structured illumination microscopy (3D-SIM); stimulated emission depletion microscopy (STED) and photoactivated localisation microscopy (PALM)/stochastic optical reconstruction microscopy (STORM) have improved this limit by up to a factor of 10 (Binnig *et al.*, 1986; Huang *et al.*, 2010). SIM measures the pattern of interference (known as a moiré pattern) created by the overlaying of two patterned light grids with different angles, one known and one unknown. The known pattern is typically generated by laser light passing through a movable optical grating and projected via the objective as a bar-code like pattern onto the sample. If this lined known pattern has a higher spatial frequency, more details can be obtained from the specimen (Figure 4.1 A) (Leung and Chou, 2011). The spatial frequencies that can be created are limited by diffraction therefore SIM can only improve resolution by a factor of 2 (Gustafsson, 2000; Leung and Chou, 2011). However, multicoloured 3D-SIM illuminates the sample with three interference patterns in all three planes and remains the easiest super-resolution technique to be expanded to three or more colours. STED acquires images point-by-point, scanning the specimen with a small focal point, allowing an easy reconstruction of a complex 3D object. STED selectively deactivates the fluorescence of the sample, leaving a central focal spot active which emits red shifted fluorescence that is easily distinguished from any incidental fluorescence (Figure 4.1 B). The resolution capable with STED depends on the intensity of the depletion beam, as the intensity increases the resolution improves. In practice, photodamage of the sample sets the intensity limit and a lateral spatial resolution of 50nm appears to be the minimum (with axial spatial resolution receiving no improvement from the doughnut depletion beam) (Leung and Chou, 2011; Willig *et al.*, 2006). PALM and STORM both work on the principle that the position of a

spatially isolated fluorophore can be determined with accuracy higher than the width of the PSF, if the fluorescence is known to come from a single molecule. In biological samples proteins have a high density so to achieve this spatial distinction photoactivatable fluorescent labels are used. These labels allow a controlled activation of a very small subset of the fluorescent molecules, thus the chance of having two or more located within the diffraction limit is low (Figure 4.1C). A statistical fit is used to determine precise lateral localisation and the complete image can then be built up by adding a series of images together. PALM uses specific irradiation wavelengths to optically convert the fluorescent particles from one wavelength to another. When the number of converted proteins is small, spatial distinction is capable and as this subset is photobleached another subset can be converted (Leung and Chou, 2011). A resolution of $\sim 30\text{nm}$ laterally is commonly achieved, and when combined with a beam-splitter to form two detection planes $\sim 75\text{nm}$ axially can also be achieved (Juetten *et al.*, 2008). Furthermore in 2009 interferometric PALM (iPALM) was introduced and provided sub-20nm 3D protein localisation (Shtengel *et al.*, 2009). STORM uses a fluorophore which can be reversibly switched between a fluorescent and dark state in a controlled manner by differing light wavelengths. This 'optical on-off switch' can be cycled many hundred or thousand times before the fluorophore is permanently photobleached (Leung and Chou, 2011). Three-dimensional STORM reached a laterally resolution of $\sim 30\text{nm}$ and axially resolution of $\sim 50\text{nm}$ with an incredibly fast time resolution of 1-2 s/image (Jones *et al.*, 2011). Direct STORM (dSTORM) does not require special fluorophore pairs but rather conventional photoswitchable fluorescent dyes and in 2008 used to reach resolution of approximately 20nm (Heilemann *et al.*, 2008). Figure 4.1 outlines the key principles and differences of SIM, STED and PALM/STORM (Schermele *et al.*, 2010).

As well as fluorescence microscopy the non-optical atomic force microscopy (AFM) has also yielded important insights into bacterial structure and function (a schematic describing AFM imaging is shown in Figure 4.2)(Dorobantu and Gray, 2010). The AFM can generate two types of image, height or phase. The tip can remain in constant contact with the sample, known as 'scanning mode' or oscillated at a high frequency, known as 'tapping mode'. To generate a 'height image' a cantilever with a very sharp tip ($\sim 10\text{nm}$ across) scans back and forth, known as a raster scan, across the sample surface. The deflection of the tip

by the surface is recorded by a laser beam reflected from the cantilever to a photodetector which translates the deflection into a topographical image. To create a 'phase image' weak or strong interactions between the tip and sample surface cause the tip to move out of phase with the motor and this shift is converted into an image (Zlatanova *et al.*, 2000). Phase images are excellent at highlighting topographical features and is the only mode shown within this study.

4.1.1 Aim of this chapter

- Localisation of WTA in *S.aureus* using fluorescent molecules and AFM.

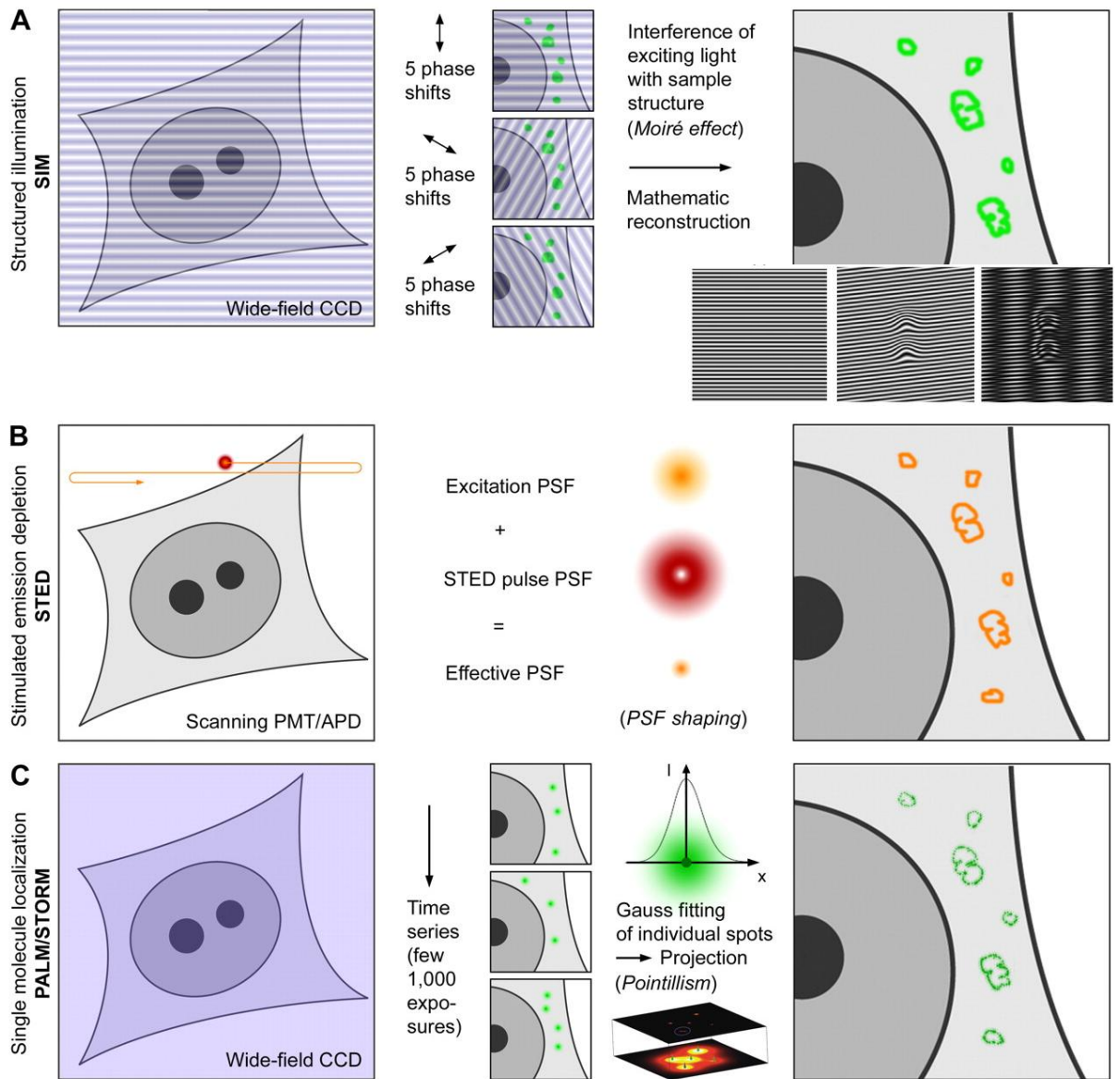


Figure 4.1 Super resolution imaging principles (Schermelleh *et al.*, 2010).

(A) In SIM the sample is excited by a striped pattern which combines with the sample information originating from structures below the diffraction limit to generate moiré pattern (shown in inset; left image shows a known structured pattern; middle shows an unknown pattern; right shows the moiré pattern of interference revealing extra sample details. A mathematical reconstruction allows, from a series of raw images a high resolution with doubled xy resolution compared with wide-field resolution.

(B) In STED the focal plane is scanned with time delayed overlapping laser beams. The first excites the fluorophores and the second depletes fluorophores in a doughnut shape, leaving only a small volume from which light can be emitted and detected.

(C) In STORM/PALM a relatively low number of fluorophores are in the emitting state. These molecules are detected on a CCD camera as diffraction-limited spots, whose lateral position is determined with a very high accuracy by a fit. Single molecule positions from thousands of images, each with a different subset of emitting molecules, then generate a density map.

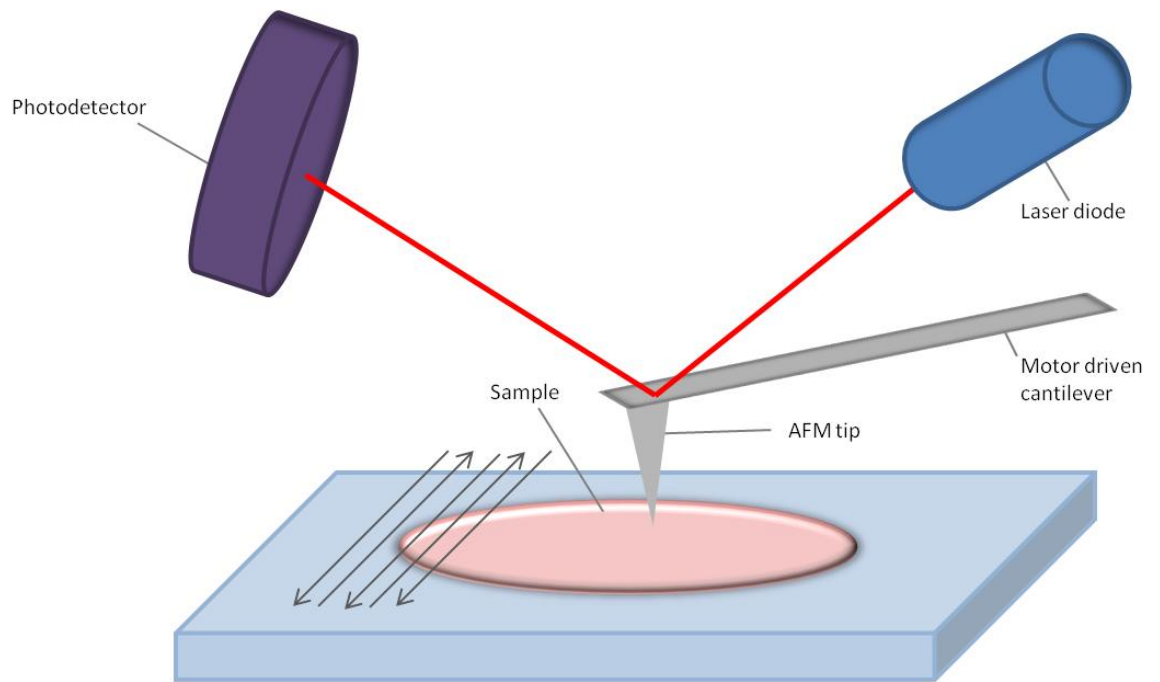


Figure 4.2 Schematic representative of Atomic Force Microscopy (AFM)

The AFM tip is moved back and forth across the sample surface (as shown by the arrows) either in contact or tapping, both to give a height or phase image.

4.2 Results

4.2.1 Identification of the localisation of WTA using AFM.

This part of the study was carried out with Dr Emma Ratcliffe.

Previous work has shown it is necessary to purify cell walls to allow pertinent features to be observed by AFM. This is due to cell contents limiting the utility of AFM due to their height and non-covalently bound materials obscuring other features (Turner *et al.*, 2010). Cells are gently broken to release the cytoplasmic contents, allowing imaging of flattened sacculi. Non-covalently bound components are then extracted by boiling cells in SDS and covalently bound proteins removed by a cocktail of proteases (pronase). Extracted cell walls are dried onto a freshly cut mica sheet and imaged in 'tapping mode' using silicon tips (Olympus) under ambient conditions (Sections 2.17-2.18). Sacculi were further purified to remove wall polymers covalently anchored to the C6 group of MurNAc, namely teichoic acids. This was achieved by weak acid treatment with hydrofluoric acid (HF), a compound used to hydrolyse the phosphodiester linkage (as described in chapter 2.15.6; Atrih *et al.*, 1999). This method of peptidoglycan purification is generally accepted to leave the unstressed peptidoglycan chemically unaffected, whilst removing all polymers.

Extracted cell walls retained the overall morphological characteristics of the cell (Figure 4.3 and Figure 4.4). Septal bands are seen as thick bands of material in circular arcs (labelled in Figure 4.3), and have been reported in *S.aureus* (as 'piecrusts'), *E.coli* and *P.aeruginosa* (Yao *et al.*, 1999; Turner *et al.*, 2010). SH1000 sacculi are shown in Figure 4.3, pre HF cell walls are completely covered with a 'furry layer'. This layer extends right up to and over the septal band with no apparent breaks. Cell walls post HF treatment and $\Delta tarO$ cell walls (Figure 4.4), which no longer produce WTA, did not have this layer and therefore we can assume it is WTA. Cell walls without WTA allow the peptidoglycan architecture to be distinguished. As previously reported, the concentric rings seen (Figure 4.3 post HF; Figure 4.4) are associated with nascent peptidoglycan which becomes the 'knobbed' as it is hydrolysed to maturity. Both peptidoglycan architectures are seen here and clearly labelled (Amako and Umeda, 1978; Giesbrecht *et al.*, 1998; Turner *et al.*, 2010).

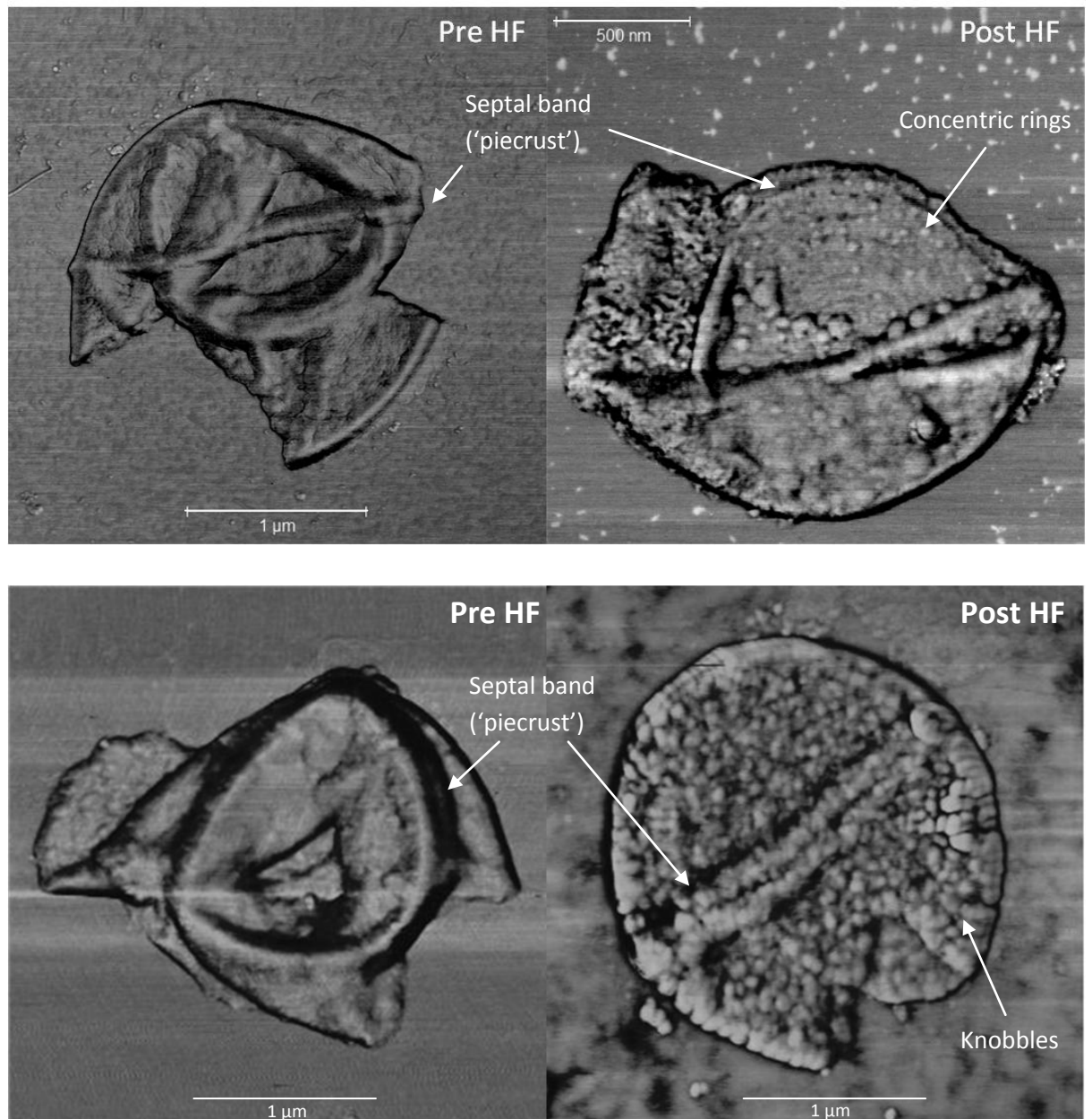


Figure 4.3 AFM images of purified sacculi from exponentially growing *S.aureus* SH1000.

AFM phase images showing broken sacculi of *S.aureus* before HF treatment (left) and after HF treatment (right). Septal rings are indicated by arrows. Pre HF treatment sacculi show a 'fuzzy' layer over the entire surface, including the septum. Post HF treatment sacculi, the removal of the WTA allows the peptidoglycan architecture to be distinguished. Concentric rings (top right image) are associated with nascent peptidoglycan. Knobbles (bottom right image) are associated with mature peptidoglycan. Images were taken by Dr. Emma Ratcliffe.

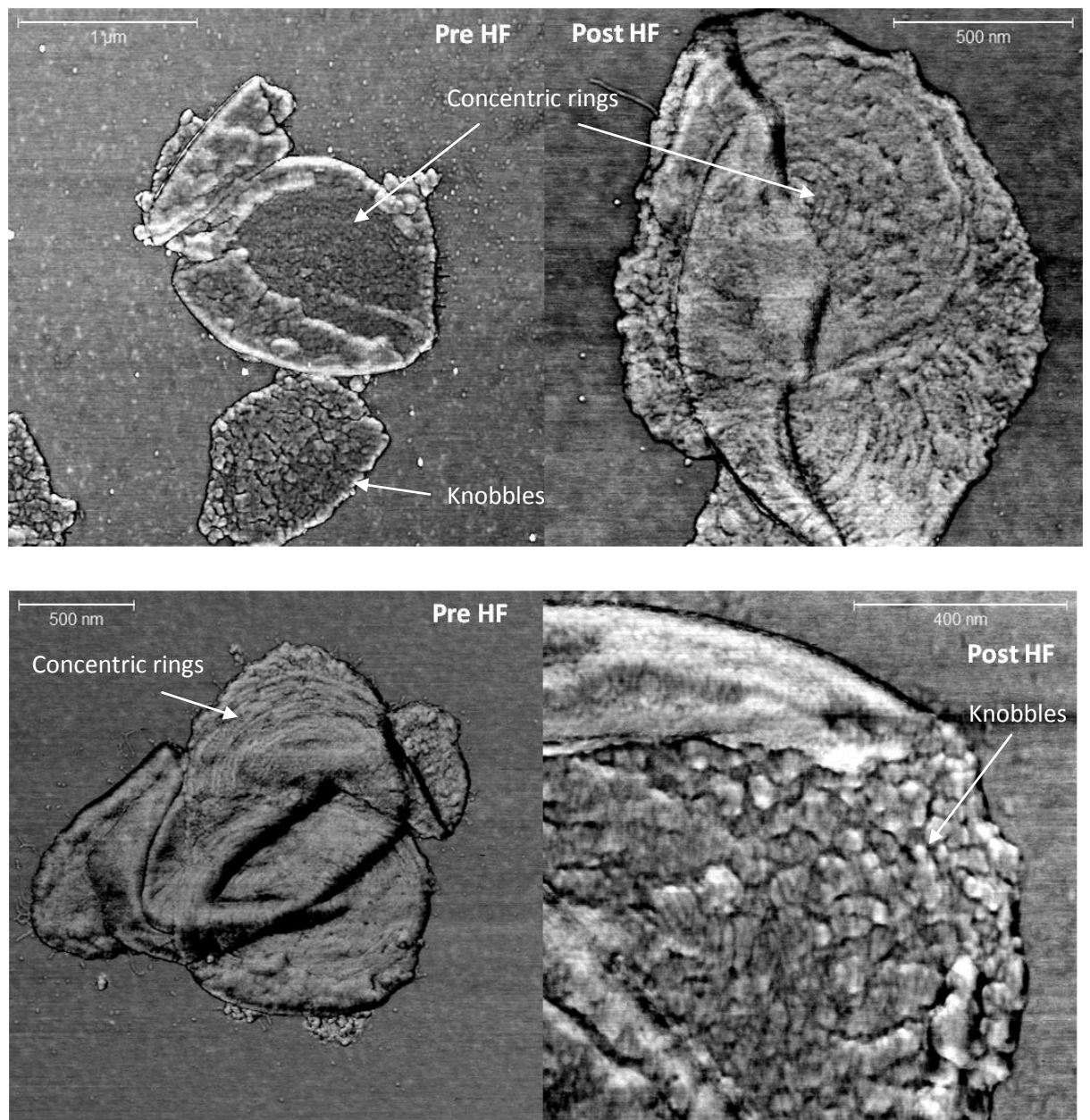


Figure 4.4 AFM images of purified sacculi from exponentially growing *S.aureus* $\Delta tarO$.

AFM images showing broken sacculi of *S.aureus* $\Delta tarO$ before HF treatment (left) and after HF treatment (right). $\Delta tarO$ mutants do not produce WTA. No difference is seen between pre HF and post HF sacculi, with no WTA the peptidoglycan architecture can be clearly distinguished in both. Concentric rings (labelled) are associated with nascent peptidoglycan. Knobbles (labelled) are associated with remodelled mature peptidoglycan. Images were taken by Dr. Emma Ratcliffe.

4.2.2 Analysis of the binding of ConA

ConcanavalinA (ConA) is isolated from Jack bean (*Canavalia ensiformis*) (Agrawal and Goldstein, 1967). It selectively binds polysaccharides containing α -mannopyranosyl or α -glucopyranosyl substituents in which hydroxyl groups at position 3, 4 and 6 are unsubstituted (Archibald and Coapes, 1971; So and Goldstein, 1969). ConA binding to carbohydrate requires CaCl_2 and MnCl_2 and results in a conformational change (Hardman and Ainsworth, 1976). It exists as a dimer of 52kDa but becomes primarily a tetramer above pH 7, however neither configuration alters the carbohydrate binding specificity (Gunther *et al.*, 1973; Mandal and Brewer, 1993). Archibald and Coapes (1971) demonstrated that ConA interacts with the α -D-N-acetylglucosaminyl residues (which have the free hydroxyl groups at position 3, 4 and 6) present in *S.aureus* teichoic acids and ConA has previously been used to localise WTA on *S.aureus* (Schlag *et al.*, 2010). SDS extraction was performed on all samples to remove any ionically bound surface proteins (Chapter 2.15.4). The cells were then subjected to a range of conditions; pronase treatment (to remove surface exposed proteins), HF (to remove WTA) and both (to remove both surface proteins and WTA) (sections 2.15.5-2.15.6). Cells were then labelled with a ConA Alexaflour 594 conjugate. Wheat Germ Agglutinin (WGA) binds to GlcNAc residues and will bind peptidoglycan ubiquitously, therefore a WGA Alexaflour 488 conjugate was used as a secondary stain to highlight the presence of bacterial cell wall (section 2.15.10, describes labelling with lectins). Samples were visualised and processed as described in Chapter 2.16.

4.2.2.1 Lectin labelling of *S.aureus* SH1000

WGA was found to bind uniformly around the cell wall and less across the septum (Figure 4.5), as has previously been observed (Endl *et al.*, 1983; Pinho and Errington, 2003). Some cells are seen to label poorly with WGA, which can be explained if they are in a different plane or by the bleaching effect very well labelled cells have (a well labelled cell is saturated in fluorescence which means that the surrounding cells appear poorly labelled by comparison). In 'untreated' samples (Fig 4.5A) ConA bound strongly across the cell surface, in an almost 'fuzzy' texture, with no specific binding seen within the cell. Binding was absent or much weaker across the septum of some cells, seen as two facing crescents in the fluorescence pattern. However it was seen at the septum of others, in contradiction with previous reports (Schlag *et al.*, 2010). Where cells were pronase treated leaving only WTA

present (Fig 4.5B), binding of ConA became comparably weaker and slightly more punctate although there still remained a high degree of binding. Again binding was seen at the septum in a number of cases. Where cells were HF treated (Fig 4.5C), unexpectedly binding was seen. The binding was again weaker than the 'untreated' sample and highly punctate. As expected when WTA and proteins were both removed (Fig 4.5D), no ConA binding was seen. Similar binding was seen in an SA113 wild type background, data not shown.

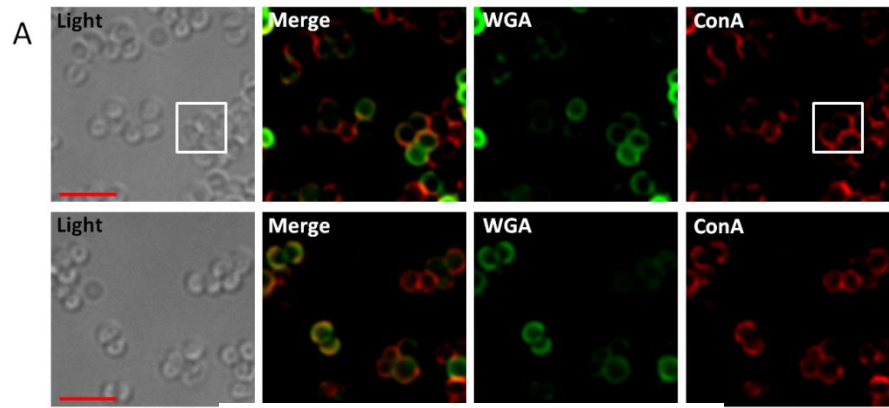
4.2.2.2 Lectin labelling of *S.aureus* $\Delta tarO$

To confirm that the unexpected binding seen in an SH1000 background was not due to insufficient treatment or damage to the cells, labelling was performed in a $\Delta tarO$ mutant background (Figure 4.6), which no longer produces WTA. It was found that the $\Delta tarO$ cells had a slightly larger diameter than SH1000 ($\Delta tarO$: $0.749\mu\text{m} \pm 0.08$; SH1000: $0.709\mu\text{m} \pm 0.07$), in agreement with previous reports (Schlag *et al.*, 2010). In 'untreated' samples (Fig 4.6A), binding was seen across the whole cell surface. Binding was seen at the septum in some cells while in others gaps were seen. In pronase treated samples (Fig 4.6B), proteins were removed and WTA no longer produced, no binding was seen. Where surface proteins were present only (Fig 4.6C), the binding was in a punctate pattern. This punctate pattern was similar to that seen in the HF treated SH1000 sample, but slightly hazier. Binding was again absent from the sample missing both WTA and surface protein (Fig 4.6D).

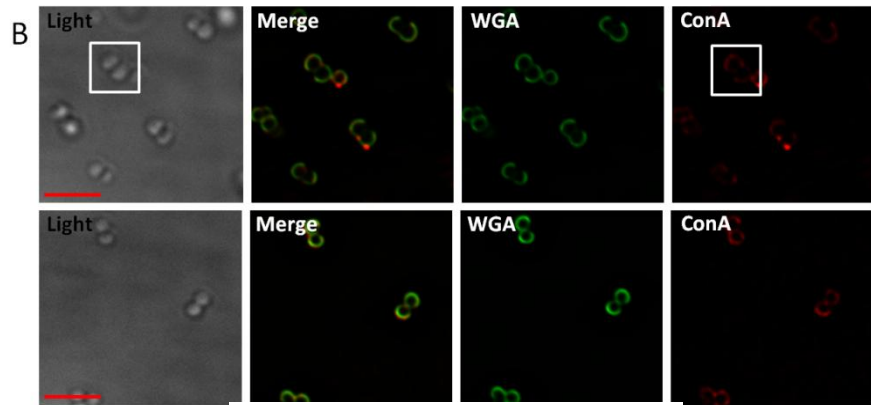
4.2.2.3 Lectin labelling in *S.aureus* $\Delta srtA$

To confirm that the unexpected binding seen in the SH1000 and $\Delta tarO$ samples was due to surface protein, labelling was performed in a $\Delta srtA$ mutant background (Figure 4.7), which no longer produces sortase A. Sortase A is the extracellular transpeptidase which catalyses the covalent attachment of proteins to the cell wall envelope (Chapter 1.10). The second sortase, Sortase B, is responsible for the attachment of only one protein, *isdB* (Chapter 1.10). The mutant no longer performs this transpeptidation and so surface proteins are unattached (Ton-That *et al.*, 2004). The $\Delta srtA$ cells had a slightly smaller diameter than SH1000 ($\Delta srtA$: $0.569\mu\text{m} \pm 0.08$; SH1000: $0.709\mu\text{m} \pm 0.07$). Where WTA are present in the 'untreated' (Fig 4.7A) and pronase treated (Fig 4.7B) samples, a hazy punctate pattern can be seen, as expected in samples (Fig 4.7C) and (Fig 4.7D) where WTA has been removed and surface proteins aren't attached no binding was seen.

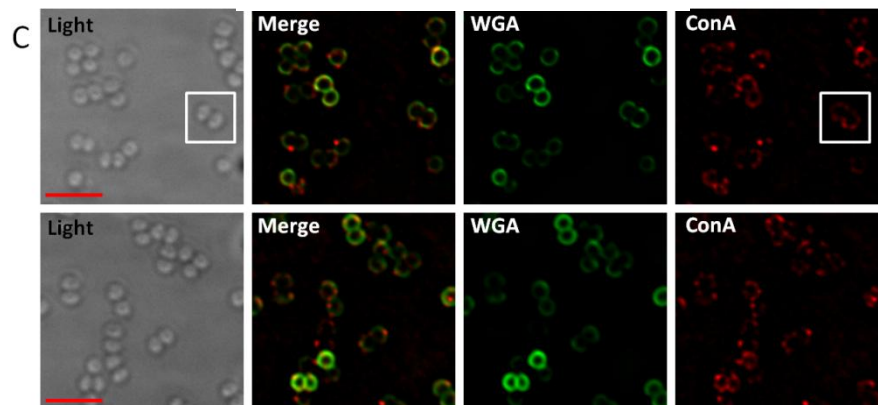
S.aureus SH1000



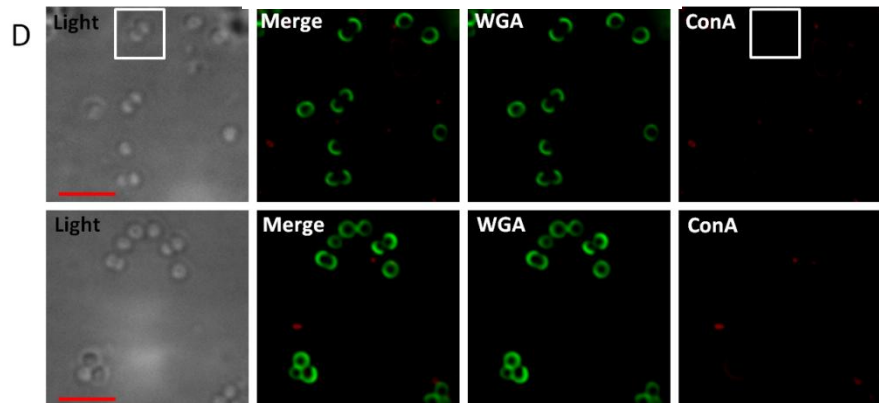
Untreated: WTA and surface proteins present



Protease treated: WTA present



HF treated: Surface proteins present



Pronase and HF treated: Nothing attached to PGN

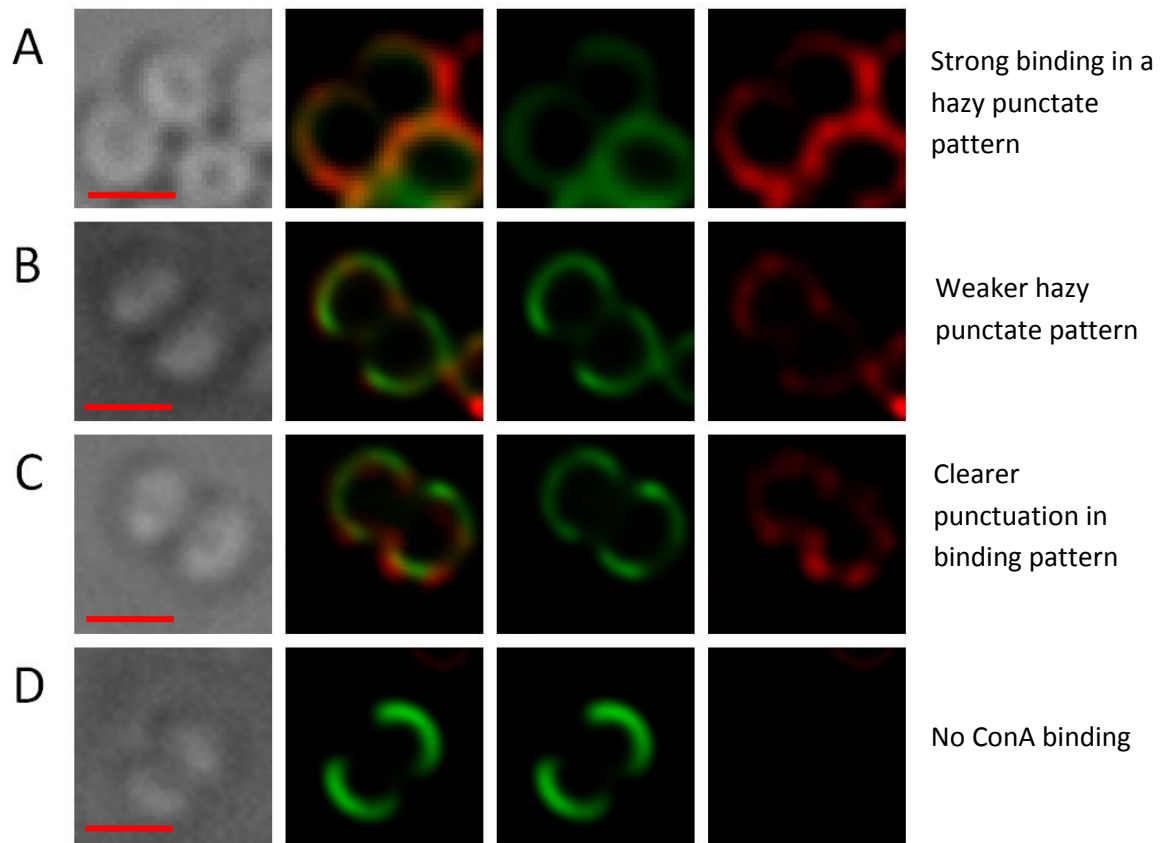
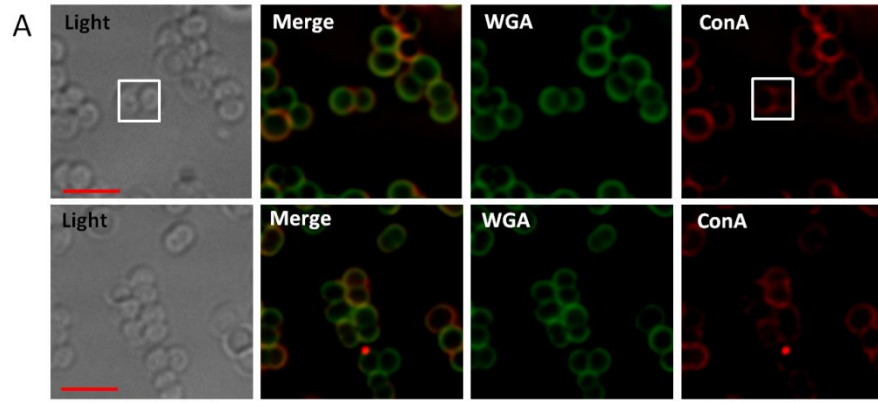


Figure 4.5 Lectin labelling of *S.aureus* SH1000

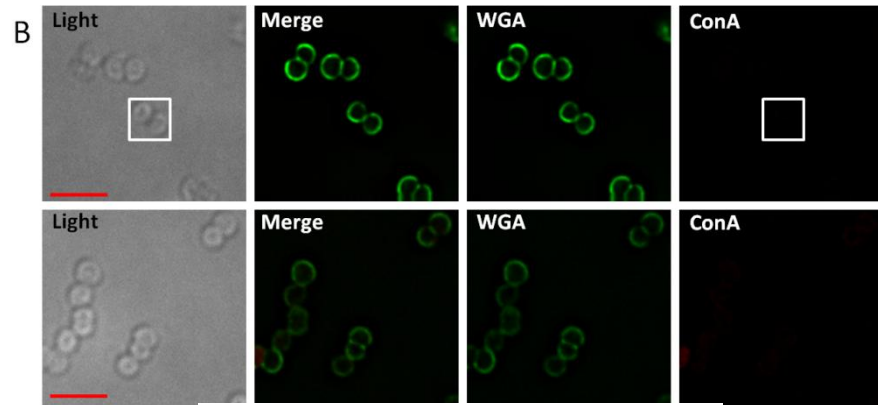
SH1000 cells were treated so that surface proteins and WTA (A), only WTA (B), only surface proteins (C) and neither (D) remained present on the cell surface. Brightfield light and fluorescence images show that whilst all the cells are strongly labelled with WGA, the labelling of ConA is absent (D) or weaker and patterned (B) and (C) when compared to 'untreated' (A). This labelling pattern suggests that ConA binds surface proteins on the cell surface as well as the expected WTA. Each row of images represents a different sample; Scale bars represent 2 μ m.

Enlarged cells (inset boxes) show differences in ConA labelling: (A) has a complete cell binding in a hazy punctate pattern with; (B) binding of WTA is weaker in a hazy slightly punctate pattern; (C) binding of surface proteins is weaker in a clearly punctate pattern. Scale bar represents 1 μ m.

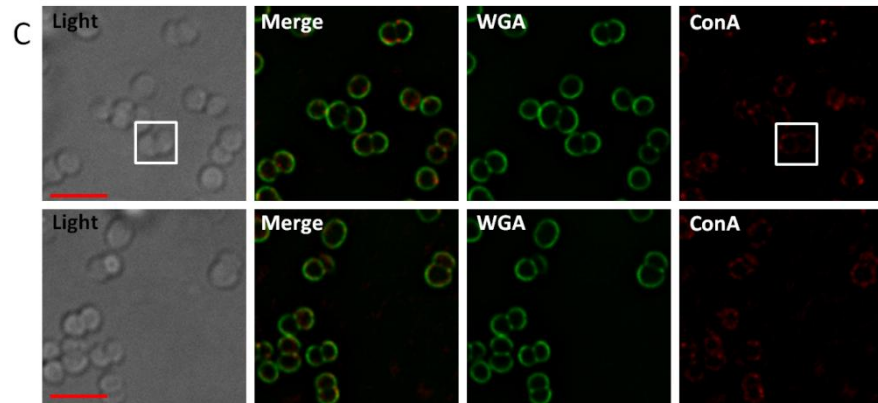
S.aureus $\Delta tarO$



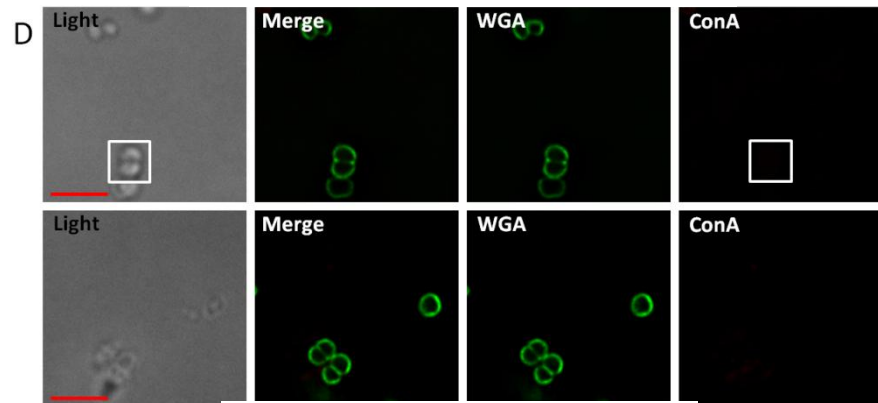
Untreated: Surface proteins present



Pronase treated: No surface proteins or WTA present



HF treated: Surface proteins present



Pronase and HF treated: Nothing attached to PGN

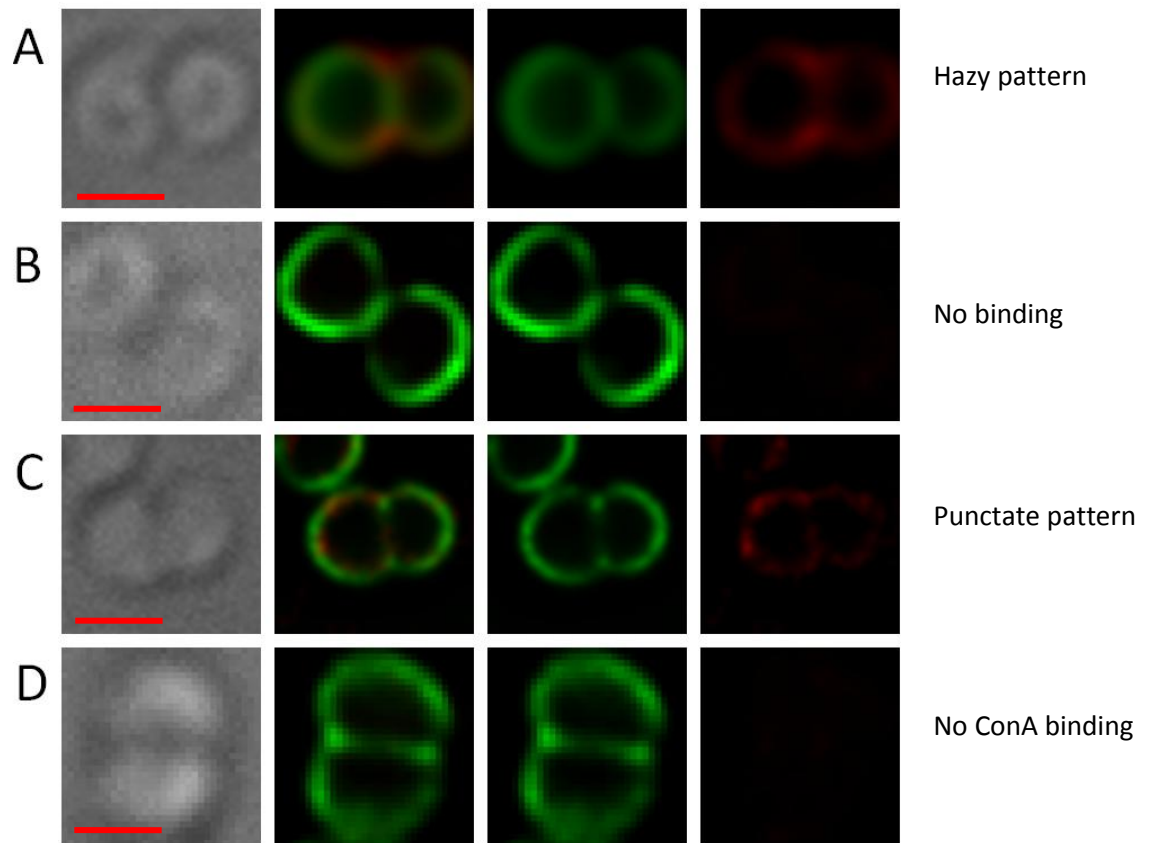
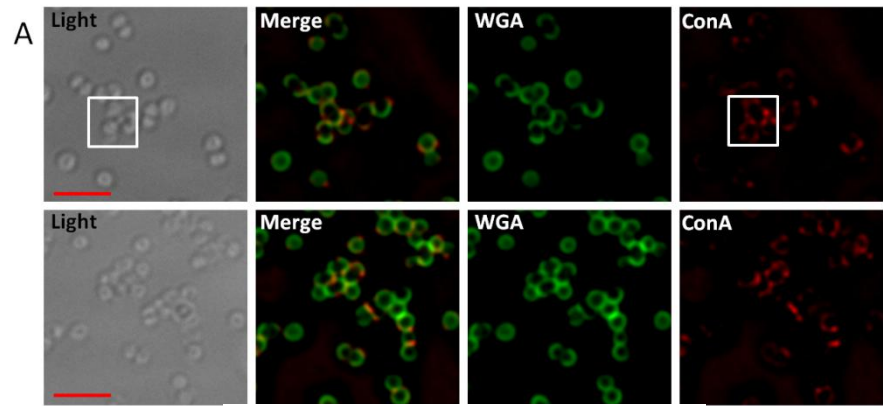


Figure 4.6 Lectin labelling of *S.aureus* $\Delta tarO$

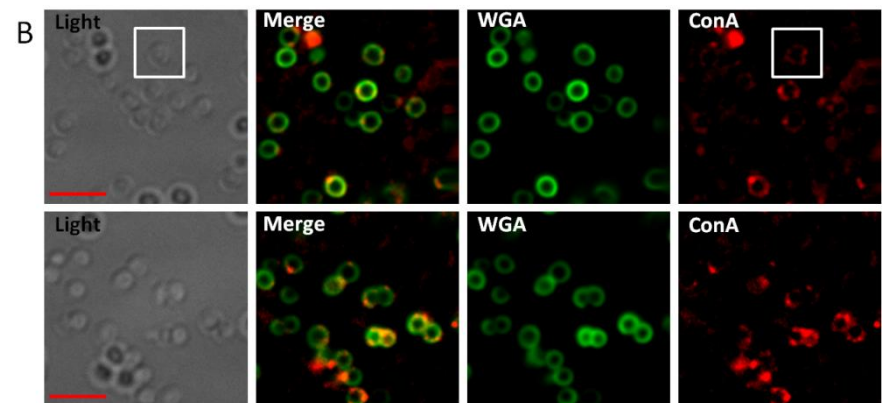
$\Delta tarO$ cells no longer produce WTA. They were treated so that surface proteins, (A) and (C), or nothing, (B) and (D), was present on the cell surface. Brightfield light and fluorescence images show that whilst all the cells are strongly labelled with WGA, the labelling of ConA is absent (D) and (B) or weaker (A) and (C) when compared to 'untreated' SH1000. This labelling pattern suggests that ConA does not exclusively bind WTA but surface proteins as well. Each row of images represents a different sample; Scale bars represent 2 μ m.

Enlarged cells (inset boxes) show that binding to surface proteins when the cells are untreated (A) is still hazy and that treatment of the cells (C) removes this blur. The punctate binding is similar to the pattern seen in SH1000 samples containing only surface proteins. Scale bar represents 1 μ m.

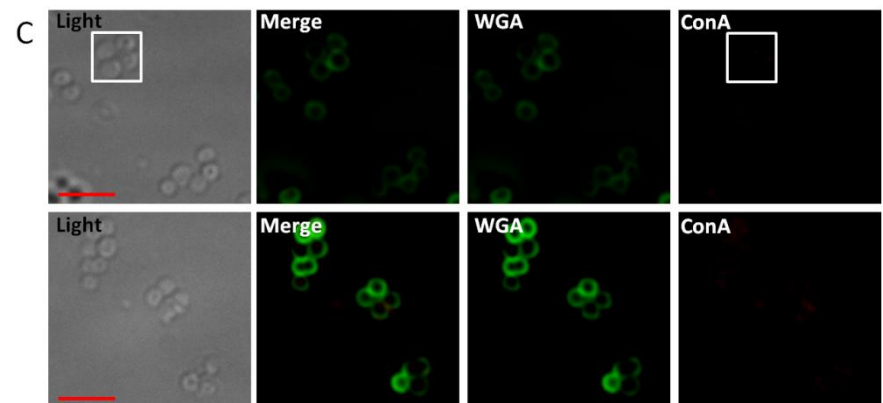
S.aureus Δ srta



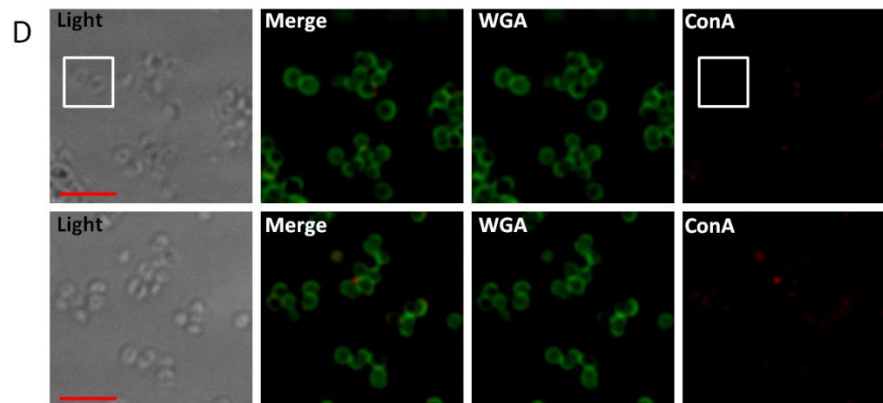
Untreated: WTA present



Pronase treated: WTA present



HF treated: Nothing attached to PGN



Pronase and HF treated: Nothing attached to PGN

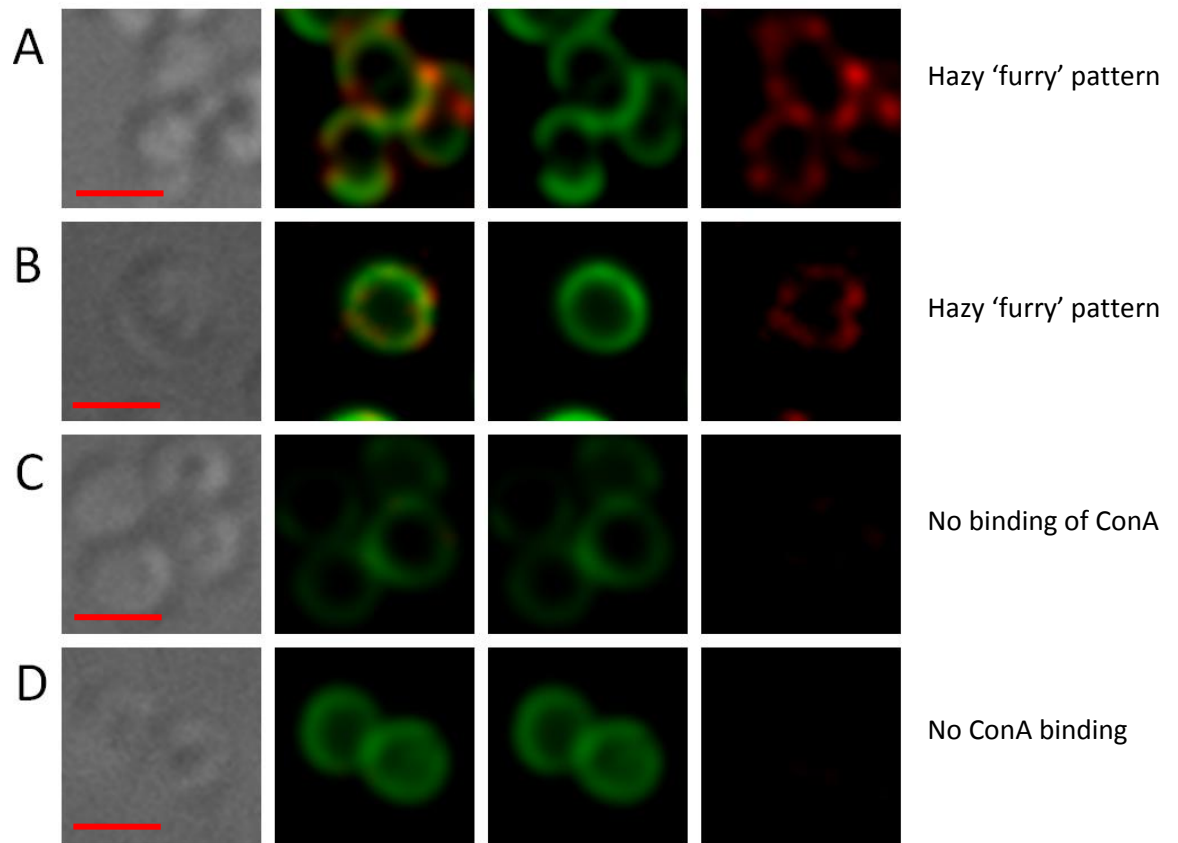


Figure 4.7 Lectin labelling of *S.aureus* Δ srtA

Δ srtA cells can no longer attach surface proteins to the cell wall. They were treated so that only WTA, (A) and (B), or nothing (C) and (D) was present on the cell surface. Brightfield light and fluorescence images show that whilst all the cells are strongly labelled with WGA, the labelling of ConA is absent in (C) and (D) or weaker in (B) when compared to 'untreated' (A). This labelling pattern supports the observation that ConA binds surface proteins as well as WTA. Each row of images represents a different sample; Scale bars represent 2 μ m.

Enlarged cells (inset boxes) show the same hazy punctate pattern seen in SH1000 samples containing WTA. Scale bar represents 1 μ m.

4.2.3 Is WTA present at the septum?

Schlag *et al* (2010) used ConA to localise WTA and reported no binding at septal regions. In my study binding of ConA has been seen at the septum and across some cell walls, although examples of binding aberration were seen. It is suspected that the high cross-linking of the nascent peptidoglycan at the septum causes an access problem for lectin preventing binding to WTA. Therefore cells were broken, SDS and pronase treated and half HF treated prior to labelling and viewing as before (Figure 4.8). Binding was seen across the septum in broken pre HF samples.

4.2.4 Analysis of ConA binding patterns

So that the localisation of both WTA and surface protein could be examined more closely, Z stack images were taken of the specific ConA binding to the different substrates. Figure 4.9 shows the binding patterns seen specifically with WTA. WTA appears to localise in a hazy punctate pattern, foci of strong labelling with weaker labelling in between. The Z stacks show that this binding is across the entire surface in this pattern. The pattern was less distinct in Δsrt 'untreated'. When examining surface protein binding (Figure 4.10) there is a difference in patterning. Surface proteins appear to localise in a distinct punctate pattern. This pattern was less distinct in $\Delta tarO$ pre HF. In both Figures, SH1000 'untreated' samples have a binding which is noticeably hazier and reminiscent of the 'furry' layer seen with AFM.

4.2.4.1 Investigation into surface protein binding of ConA

Within our laboratory SH1000 cell lysates have been applied to a ConA sepharose column and eluted using-D-glucopyranoside. Proteins purified from the eluted fragments were identified, using Mass spectrometry, as SdrC, SdrD, ClfB and ClfA (McAulay, 2011). ClfA and ClfB are high molecular-mass fibrinogen-binding proteins that are anchored to the cell surface of *S.aureus* (McDevitt *et al.*, 1994). They are members of the MSCRAMM family of virulence factors and mediate bacterial attachment to indwelling devices or damaged tissue coated in fibrinogen (McDevitt *et al.*, 1994; Ní Eidhin *et al.*, 1998). SdrC and SdrD, along with SdrE, were found to be tandemly arrayed and to show both organisational and sequence similarity to ClfA and ClfB (Josefsson *et al.*, 1998). All five proteins contain

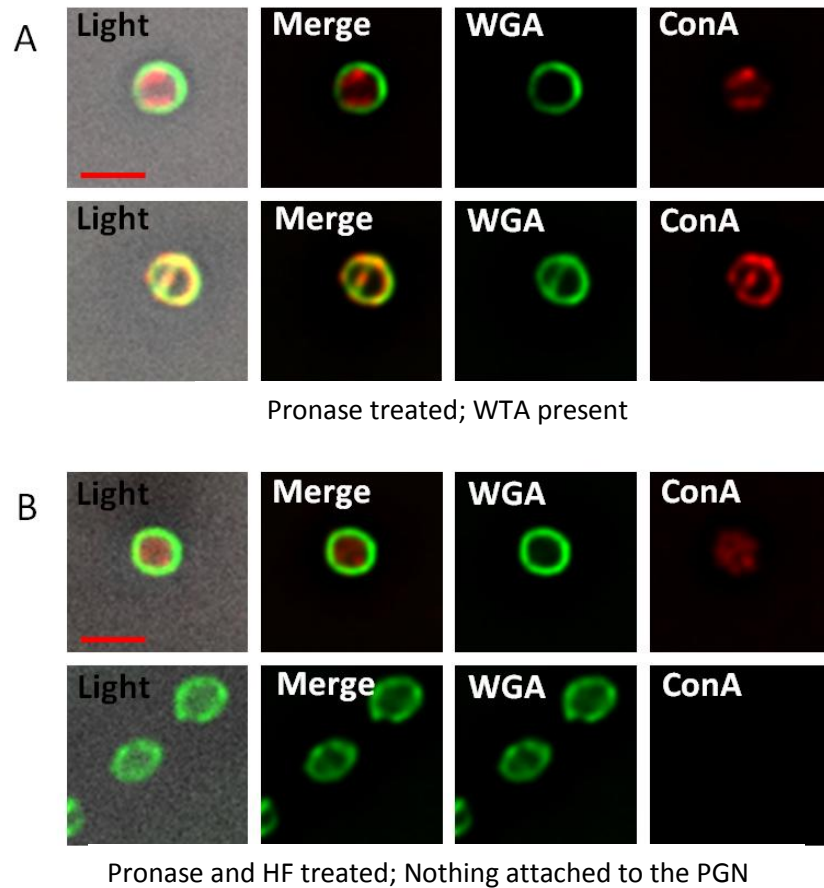


Figure 4.8 ConA labelling of *S.aureus* sacculi

Broken SH1000 cells were treated with SDS and pronase, to remove LTA and surface proteins. (A) cells were not treated with HF leaving WTA on the surface, while (B) cells were HF treated leaving nothing present on the surface. Fluorescence images show that binding can be seen at the septum of the broken cells where WTA are present and access is now no longer an issue. Light images have been merged with fluorescence because the collapsed cells are difficult to see. Scale bars represent 1 μ m.

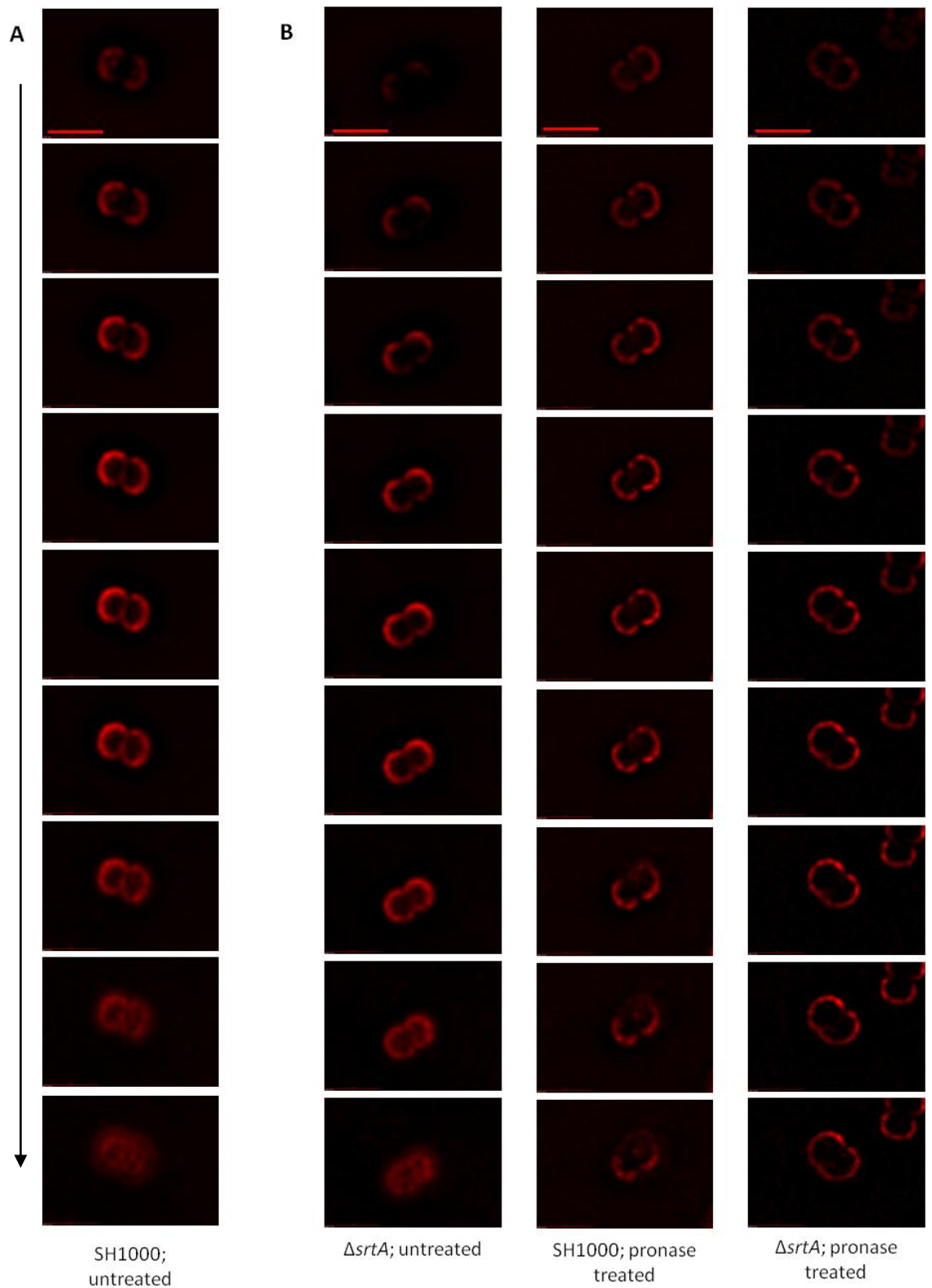


Figure 4.9 ConA binding pattern to *S. aureus* WTA

(A) SH1000 Z-stack images showing the binding of ConA to both WTA and surface proteins. (B) Z-stack images showing the binding of ConA to WTA only.

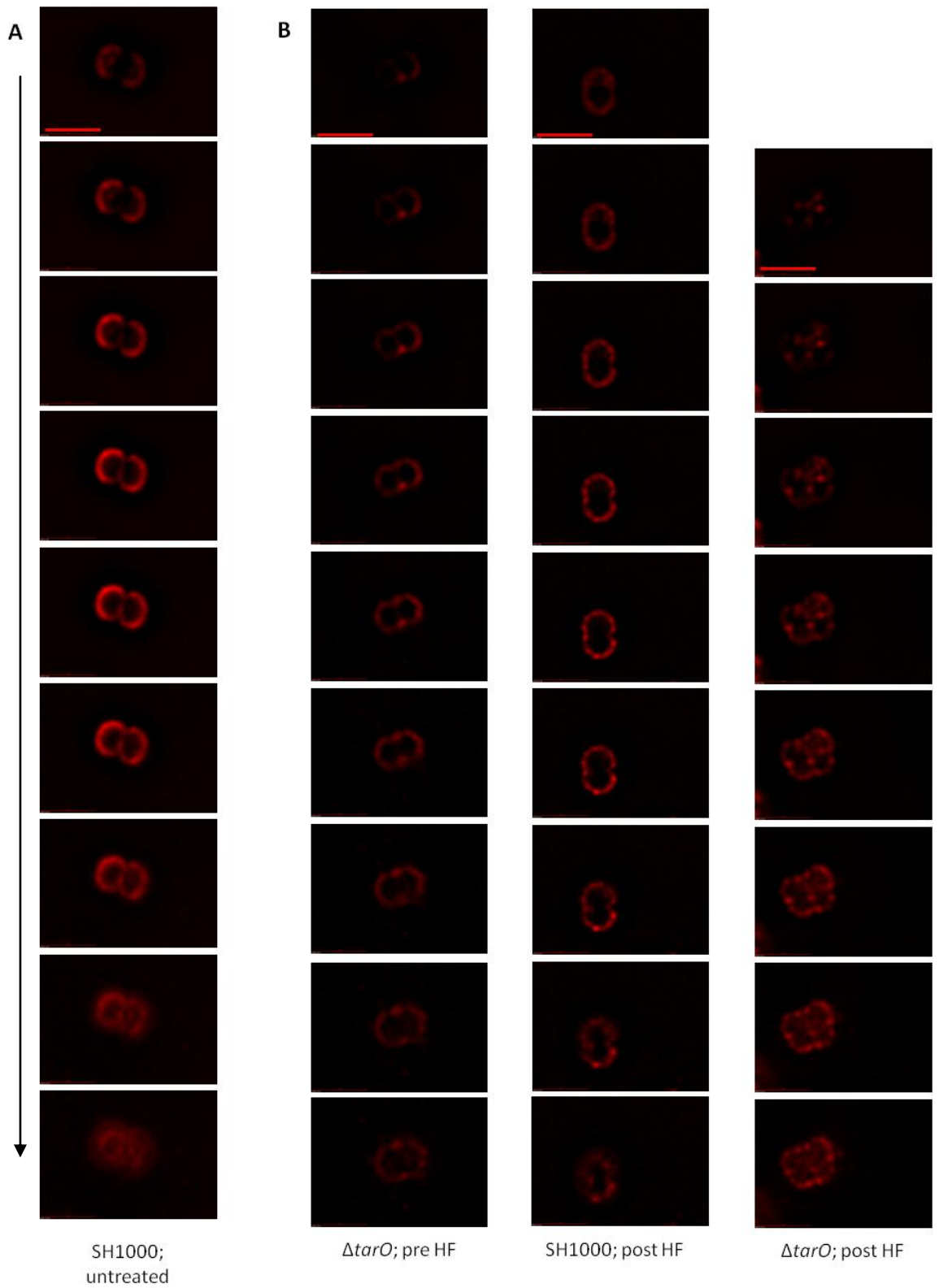


Figure 4.10 ConA binding pattern to *S. aureus* surface proteins

(A) SH1000 Z-stack images showing the binding of ConA to both WTA and surface proteins. (B) Z-stack images showing the binding of ConA to surface proteins only.

serine-aspartate repeats which have been shown to span the cell wall allowing functional expression of the protein (Hartford *et al.*, 1997). Further work within our lab identified that ClfA was the major glycoprotein of *S.aureus*, and its loss resulted in the loss of most glycoproteins detectable via Schiff staining. However, results suggested that in the absence of ClfA, the other minor surface proteins ClfB, SdrC and SdrD are glycosylated (McAulay, 2011). GtfA and GtfB are the glycosyltransferase enzymes responsible for the glycosylation of these proteins (McAulay, 2011). They have also been shown to be essential for glycosylation of a *S.aureus* homolog of GpsB, SraP (Takamatsu *et al.*, 2004). A knockout mutant in which both *gtfA* and *gtfB* are replaced by a kanamycin resistance gene was available (Mohamed, 2007).

To examine the role glycoproteins played in the binding of ConA seen in Figures 4.5-4.7, cells were SDS extracted as before and then treated under a range of conditions. Samples were prepared as described in section 2.14.4- 2.14.6

4.2.4.2 Lectin labelling in *S.aureus* Δ clfA2

To investigate whether ClfA was responsible for the punctate binding of surface proteins seen in Figure 4.11, a Δ clfA2 strain was used. In 'untreated' samples (Fig 4.11A) a low level of ConA binding was seen across the cell surface, which can be seen in enlarged cells, to maintain the diffuse punctate pattern previously pictured (Figure 4.5A and 4.7A). In pronase treated samples (Fig 4.11B), binding was seen across the cell surface much the same as the WTA patterns seen before. In HF treated samples (Fig 4.11C), binding was still observed but at a lower level and much less specifically (binding not just to the peptidoglycan but within the cell was seen in several examples). The low levels of background fluorescence indicate that this is still true binding and suggests that although it plays a large part ClfA is not the only protein binding ConA. No specific binding was observed where cells had been both HF and pronase treated (Fig 4.11D).

4.2.4.3 Lectin labelling in *S.aureus* Δ gtfAB

Specific binding to protein was still seen within the ClfA mutant, which indicates that other proteins are likely labelled. As ClfB, SdrC and SdrD were successfully purified with ConA (McAulay, 2011) and been suggested as being glycosylated a Δ gtfAB strain was examined

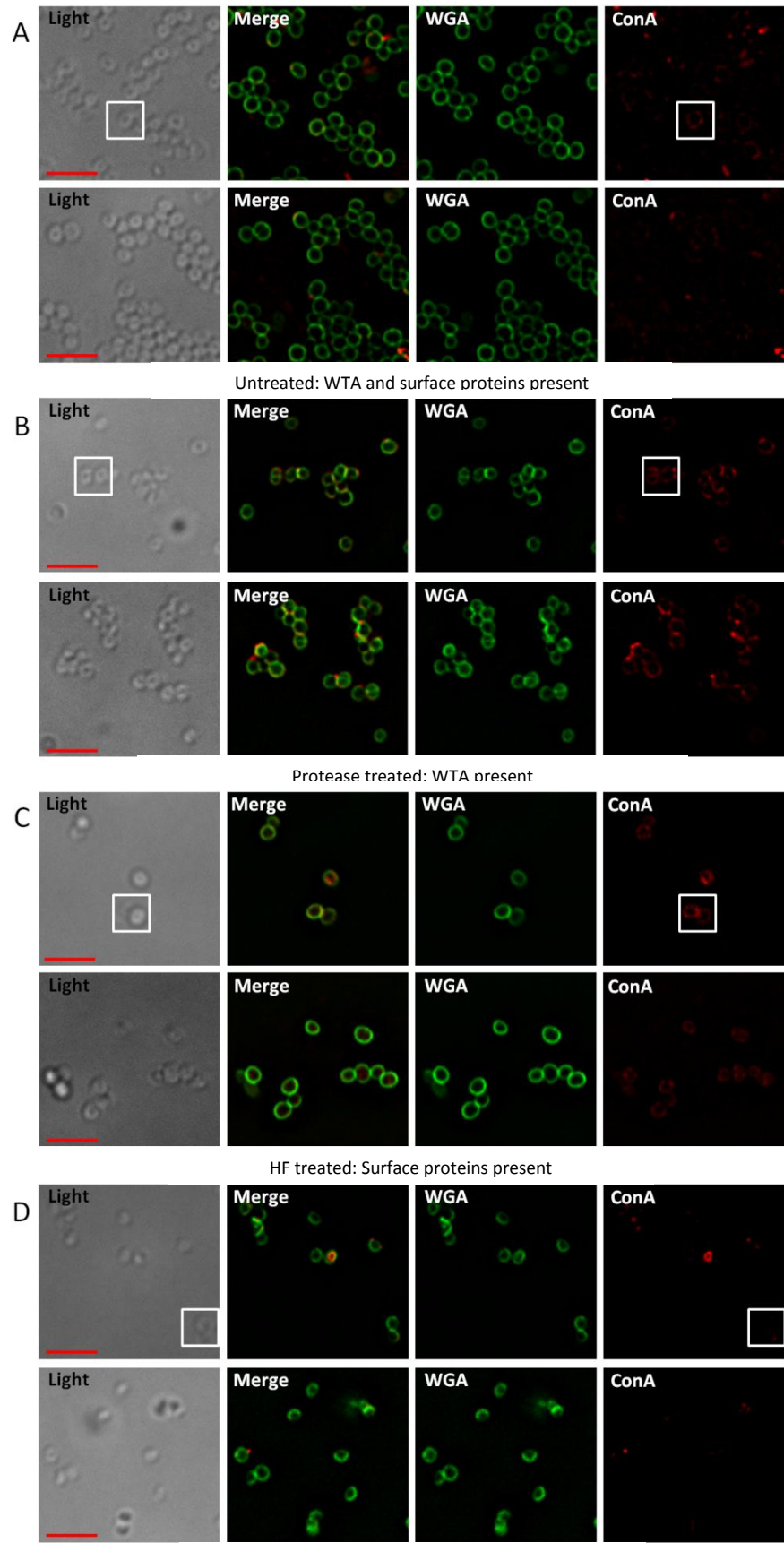
(Figure 4.12). In both 'untreated' (Fig 4.12A) and pronase treated (Fig 4.12B), where WTA was still present, binding was seen across the surface. Background levels of binding were seen in (Fig 4.12C), which suggests that glycosylation is required for ConA binding. As expected no binding is seen when both protein and WTA are removed (Fig 4.12D).

4.2.4.4 Lectin labelling in *S.aureus* Δ *gtfAB* Δ *clfA2*

A strain with both *gtfAB* and *clfA* mutation was examined (Figure 4.13). As was to be expected, binding was seen where WTA was still present, (Fig 4.13A) and (Fig 4.13B) while background levels (Fig 4.13C) or no binding (Fig 4.13D) was seen where WTA were not present.

This series suggests that the binding of ConA to surface proteins is dependant on them being glycosylated and that ClfA is the largest but not the only glycosylated surface protein.

S.aureus Δ clfA



Pronase and HF treated: Nothing attached to the PGN

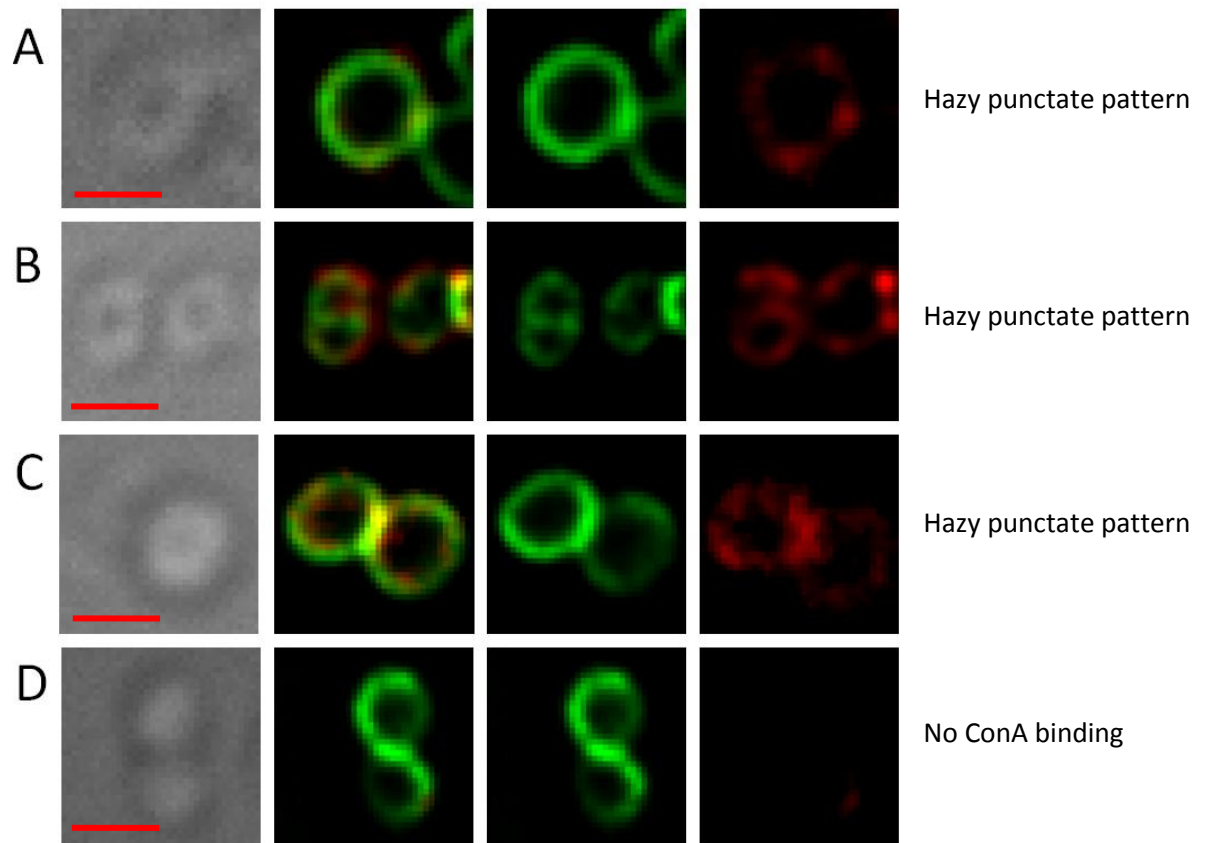
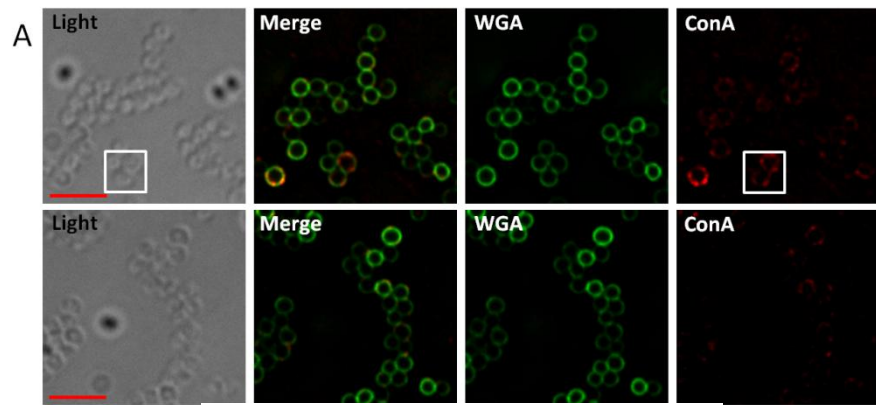


Figure 4.11 Lectin labelling of *S.aureus* Δ *clfA*

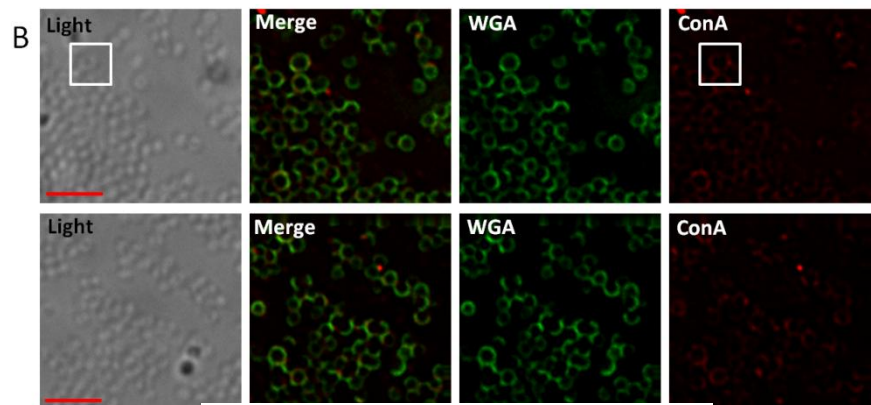
ΔclfA cells were treated so that surface proteins and WTA (A), only WTA (B), only surface proteins (C) and neither (D) remained present on the cell surface. Brightfield light and fluorescence images show that whilst all the cells are strongly labelled with WGA, the labelling of ConA is weaker in all when compared to 'untreated' SH1000. The binding in (A) and (B) had a hazy punctate pattern and a weaker similar pattern was observed in (C). This labelling pattern suggests that the major surface glycoprotein ClfA is not the only surface protein ConA binds. Each row of images represents a different sample; Scale bars represent 2 μ m.

Enlarged cells (inset boxes) show that the binding pattern observed in (C) is hazier than previously observed for surface proteins. Scale bar represents 1 μ m.

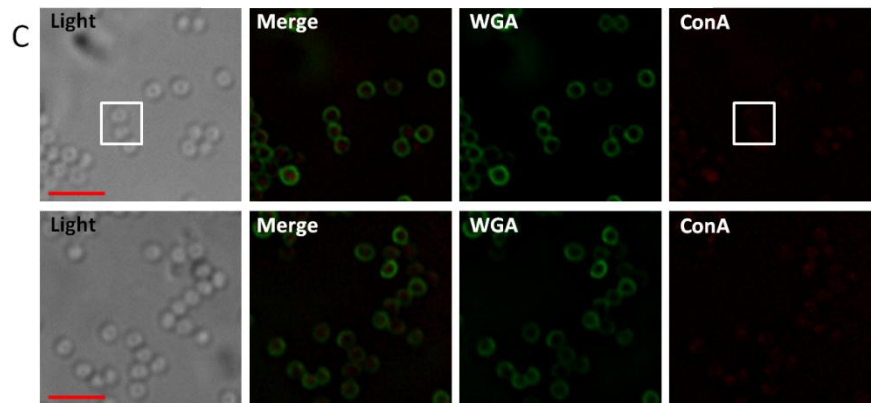
S. aureus Δ gtfAB



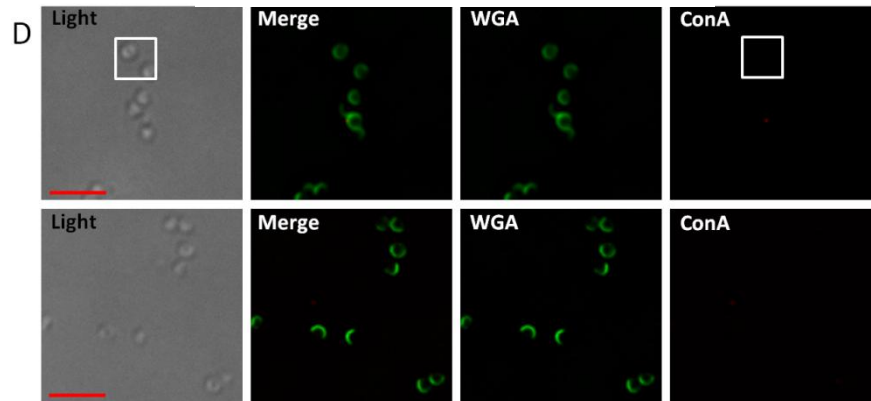
Untreated: WTA and Surface proteins present



Pronase treated: WTA present



HF treated: Surface proteins present



Pronase and HF treated: Nothing attached to the PGN

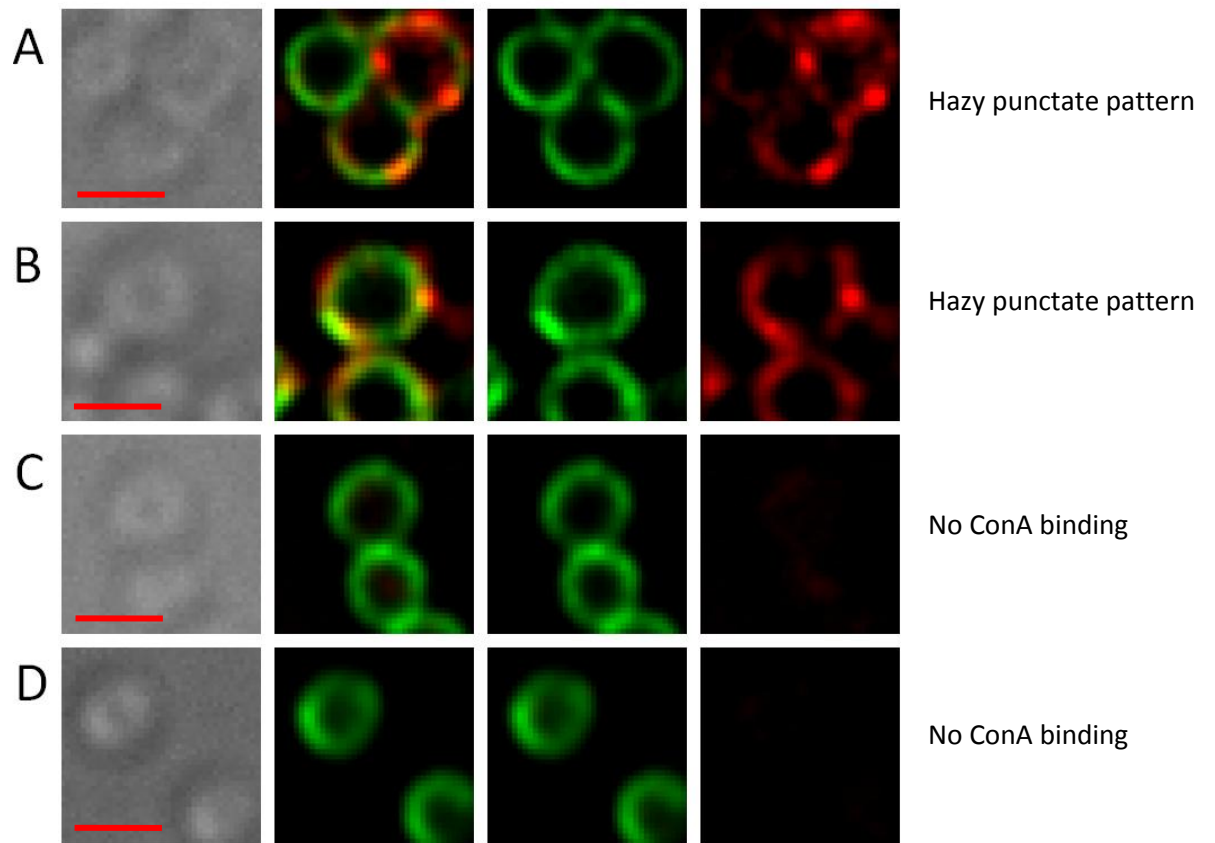


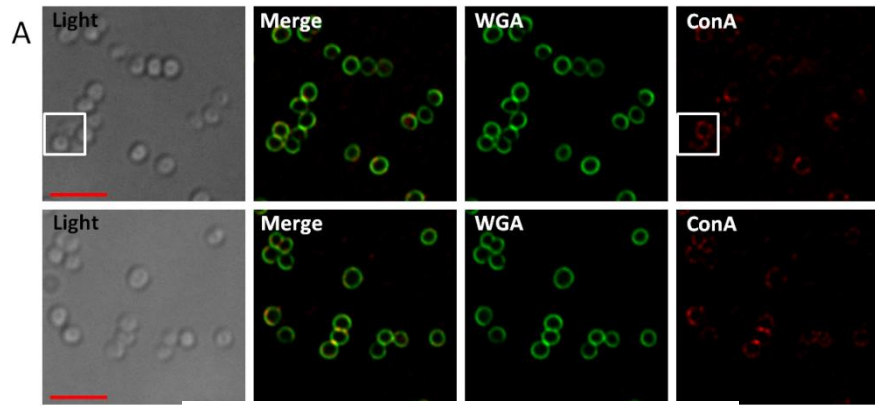
Figure 4.12 Lectin labelling of *S.aureus* Δ gtfAB

Δ gtfAB cells were treated so that non-glycosylated surface proteins and WTA (A), only WTA (B), only non-glycosylated surface proteins (C) and neither (D) remained present on the cell surface.

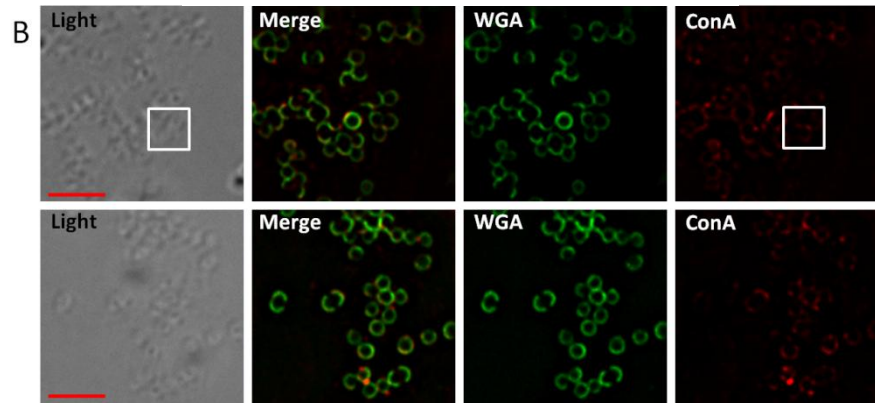
Brightfield light and fluorescence images show that whilst all the cells are strongly labelled with WGA, the labelling of ConA is absent (C) and (D). This labelling pattern suggests that ConA binds to proteins glycosylated by GtfA and/or GtfB. Each row of images represents a different sample; Scale bars represent 2 μ m.

Enlarged cells (inset boxes) (A) and (B) show the hazy punctate pattern seen previously and associated with WTA. Scale bar represents 1 μ m.

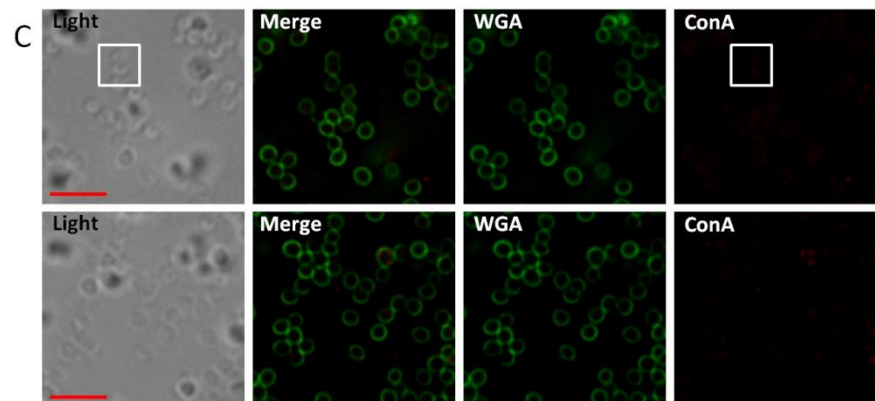
S.aureus Δ clfA Δ gtfAB



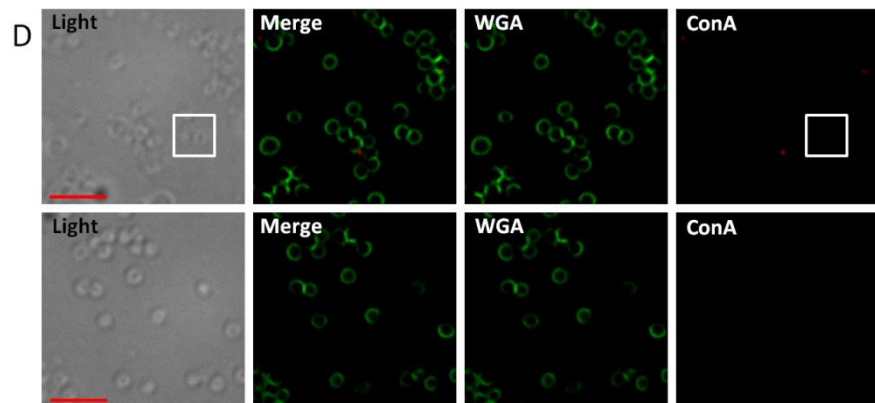
Untreated: WTA and surface proteins present



Pronase treated: WTA present



HF treated: Surface proteins present



Pronase and HF treated: Nothing attached to the PGN

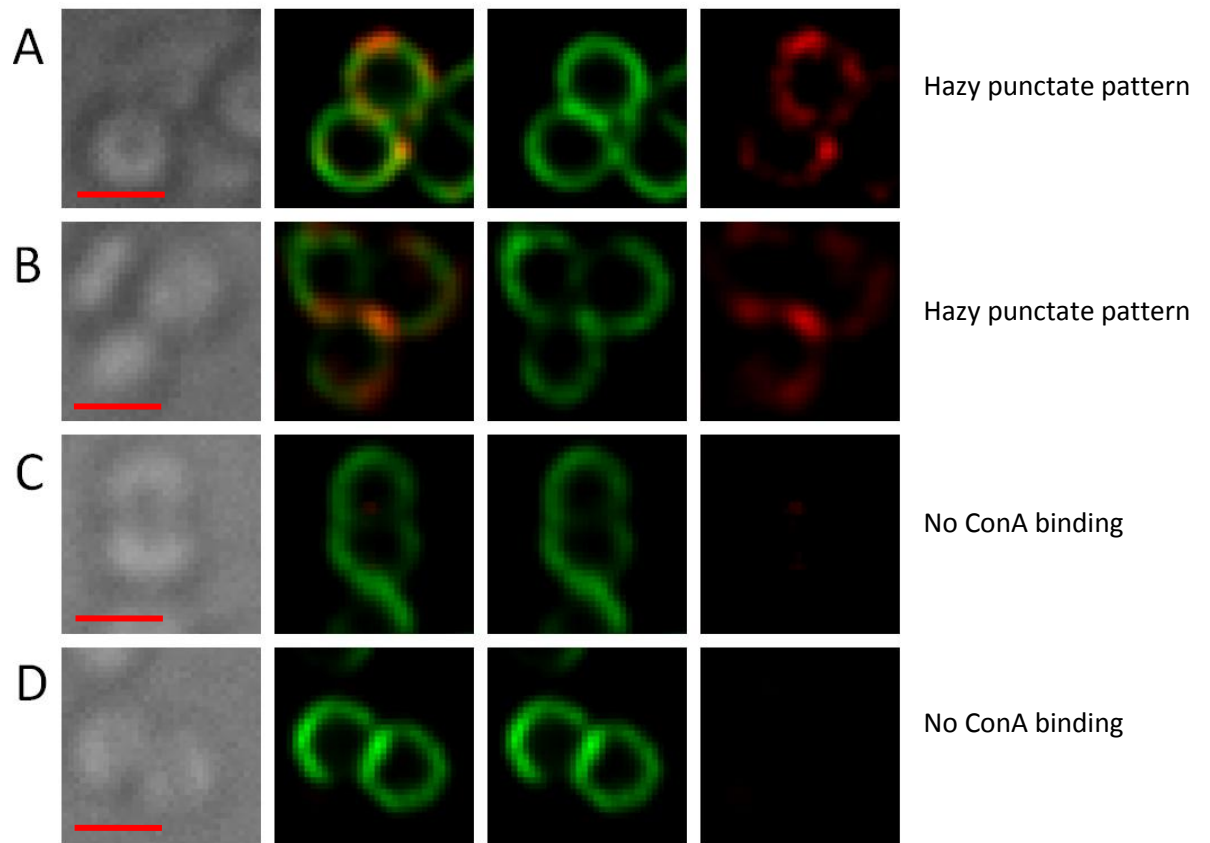


Figure 4.13 Lectin labelling in *S.aureus* Δ clfA Δ gtfAB

*Δ*clfA *Δ*gtfAB cells were treated so that surface proteins un-glycosylated and WTA (A), only WTA (B), only surface proteins un-glycosylated (C) and neither (D) remained present on the cell surface.

Brightfield light and fluorescence images show that whilst all the cells are strongly labelled with WGA, the labelling of ConA is absent (C) and (D) when compared to 'untreated' (A) and (B) where cells are still exhibiting WTA. This labelling pattern confirms that ConA binds to proteins glycosylated by GtfA and/or GtfB. Each row of images represents a different sample; Scale bars represent 2 μ m.

Enlarged cells (inset boxes) show the same hazy punctate pattern associated with WTA in (A) and (B). Scale bar represents 1 μ m.

4.3 Discussion

Although the localisation of WTA hasn't been extensively studied it is fairly well established that it is present across the entire peptidoglycan moiety (Swoboda et al., 2010; Umeda et al., 1992; Wheeler R., 2012; Xia et al., 2010a). The recent suggestion that it is not present at the septum or that if present it is not yet fully polymerised (Schlag *et al.*, 2010) is controversial. My work has suggested that WTA biosynthesis machinery is associated with the divisome (Chapter 3). Upon AFM microscopy it was seen that the WTA appear to form a 'furry' layer across the entire cell surface including the 'piecrust' ribs that dictate the septum (Turner *et al.*, 2010). Indeed Umeda *et al* (1987) have described a 'fuzzy coat that consists of fine fibres or an electron dense mass' on the *S.aureus* surface that they identified as being made of teichoic acids and proteins. This layer was also been seen in *L.lactis*, *E.faecalis* and *S.pneumoniae* and had to be removed by weak HF treatment to more clearly observe the peptidoglycan structure and annular features (septa and equatorial rings) (Wheeler *et al.*, 2011). Furthermore AFM images and interaction maps using ConA functionalised tips, showed that the cylinder of *Lactobacillus plantarum* was abundant in WTAs and 'rough', whilst cell poles were much poorer in WTA and had a smooth architecture (Andre *et al.*, 2011).

As ConA has been shown to bind the WTA backbone it was possible that a ConA-fluorophore conjugate could be used to detect WTA on the surface of *S.aureus* cells. Microscopy of SH1000 indicated that ConA binds both wall teichoic acids and surface proteins, with HF stripped and pronase treated cells acting as suitable controls. This observation was confirmed by using Δ *srtA* and Δ *tarO* which respectively exhibit no covalently bound surface proteins and WTA. Schlag *et al.* (2010) showed that ConA binds only to cells expressing *tarO*, whereas this study only observed abrogation of binding where both teichoic acids and proteins were removed; this may be due to a higher level of sensitivity in my study.

The absence of binding at the septum seen in several cells within this study and reported in *S.aureus* by Schlag *et al* (2010), could be explained either by a lack of sensitivity of the fluorescent probe, the presence of immature WTA or because it has no access to its binding partner. My study has shown that enzymes involved with the final step (in which fully

polymerised WTA are linked to the peptidoglycan), interact with the divisome suggesting that mature WTA are present at the septum. The latter offers a likely explanation because peptidoglycan is more cross linked at the septum, reducing ConA access. Peptidoglycan then undergoes processing and remodelling after cell division (Turner *et al.*, 2010). Cells were broken, allowing the fluorophore access to the septum, and then stained for WTA. Binding was seen at the cross-wall which confirms the hypothesis that absence of binding was due to access. Similar binding aberration is seen with WGA, both within this study and previously (Endl *et al.*, 1983; Pinho and Errington, 2003), and again most likely explained by nascent peptidoglycan having tight cross linking and this decreases permeability.

The binding pattern to ConA of both surface proteins and WTA was analysed. A hazy punctate pattern was seen with the binding of WTA, this pattern was seen across all conditions where only WTA was present on the cell surface (SH1000, pronase; Δ srt, 'untreated'; Δ srt pronase). The patterning was seen to extend around the entire cell surface. In Δ srtA, the 'untreated' sample binding was slightly hazier, than seen with either SH1000 pronase or Δ srt pronase. This could be explained by unglycosylated surface proteins or surface proteins which although aren't covalently attached to the surface are still associated with the cell wall and not be fully extracted by SDS interfering with clear binding. Once treated with pronase, all proteinacious material is degraded and therefore only WTA binds. Surface protein binding was in a different pattern to WTA; it was seen as a distinct punctate pattern across the entire cell surface. The number of dots did not appear to be uniform although it was not seen to exceed 6, when the cells were in focus. Once again where Δ tarO, displaying only surface protein, was left 'untreated' the binding pattern seen was slightly hazier when compared to 'treated' samples.

The data gathered from the microscopy of treated SH1000 cells and mutant cells allowed the development of a schematic representation of the localisation of surface proteins and wall teichoic acids (Figure 4.11). This schematic shows that when compared with each other, WTA forms a complete layer across the entire cell with denser patches whilst surface proteins (proven to be glycoprotein) produce distinct foci.

A 'line and dot' pattern was described for DivIB localisation and used to help suggest its localisation to piecrust and rib features (Bottomley, 2011) (Chapter 1.6; Figure 1.8B for

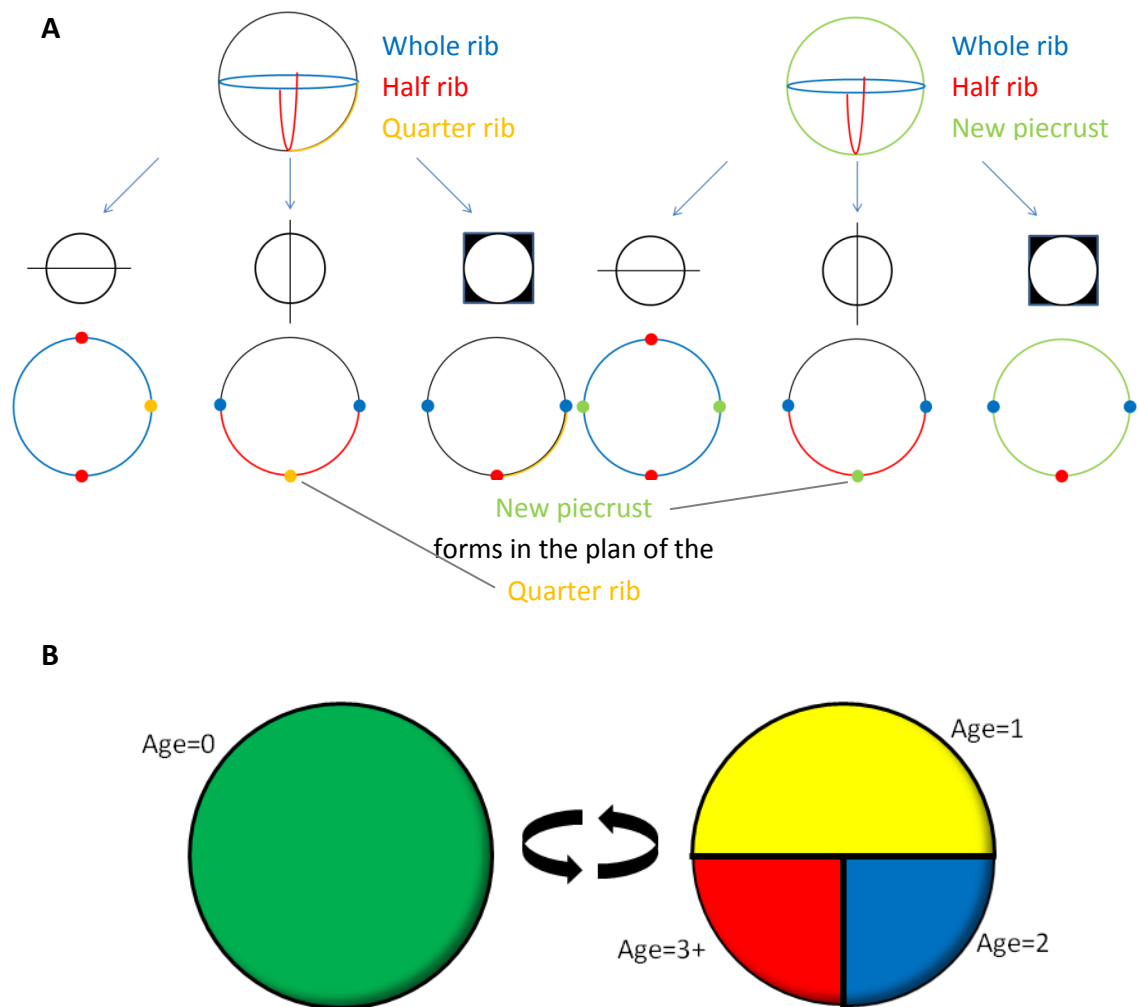


Figure 4.15 Peptidoglycan patterning models

A) Line and Dot model (Bottomley, 2011). Location of piecrust and rib features in x, y and z sections of cells, showing potential 'line and dot' patterns. Half ribs (red) and quarter (orange) are remnants of piecrusts from previous divisions that occurred in an orthogonal plane, whilst whole ribs (blue) represent the most recent plane of division. A new piecrust (green) is then formed in the plane of the quarter rib

B) Sector model (Wheeler R., 2012). Ageing of peptidoglycan by inheritance of cell wall sectors over multiple generations. Two hemispheres represent the entire cell. Age is shown as number of generations. One eighth of the cell is at least three generations old (red). Black lines indicate the peptidoglycan ribs which divide each segment.

piecrust and rib features) (Figure 4.15A). Although the WTA pattern seen here is non-uniform (the brighter spots within the complete binding are not uniform), large unlabelled segments cannot be seen in the binding to fit it to 'line and dot' model. However it could be that the peptidoglycan features distort the WTA distribution, resulting in areas of bright binding and regions of little binding. The sectoring model describes the age distribution of peptidoglycan within *S.aureus* resulting from its sequential division in three planes (Figure 4.15B). The cell wall is divided into: a half segment (green), representing nascent peptidoglycan of age 0; a quarter (yellow) representing age 1 peptidoglycan from the previous generation; an eighth (blue) dating from 2 generation previous; and the final eighth (red) must be 3 or more generations old (Turner *et al.*, 2010). There does not appear to be clear sectors within WTA binding and therefore a pure sector model does not explain the observed pattern. However WTA binding may appear brightest in mature peptidoglycan sectors when the action of hydrolases has allowed the lectin more access. As the peptidoglycan ages and becomes more hydrolysed the amount of WTA is decreased. The binding pattern observed could be the result of this sectoring model which is bisected by 'piecrusts' rib features.

The binding of ConA to surface proteins has been previously reported (McAulay, 2011). A ConA sepharose column was able to purify surface glycoproteins from *S.aureus*. When the elute was tested against a panel of lectins with varying carbohydrate specificities, only ClfA was shown to bind to ConA (McAulay, 2011). Therefore binding seen in a $\Delta clfA$ mutant was surprising but supports the conclusion, drawn by McAulay (2011), that in the absence of ClfA other surface proteins such as SdrCD and ClfB are glycosylated to a greater extent. This is supported by reduced binding in $\Delta gtfAB$ and $\Delta gtfAB\Delta clfA2$ backgrounds and shows that ConA binding is due to glycosylated surface proteins. A logical further step to confirm that the binding seen in HF stripped cells is due to ClfA and the binding in $\Delta clfA$ is due to the glycosylation of other surface proteins would be to co-localise ConA binding with specific antibodies raised against the proteins. DeDent *et al.* (2008) used antibodies against ClfA, SdrC and SdrD to show a ring-like distribution across the cell surface in a similar pattern to what is observed here (DeDent *et al.*, 2008, 2007). The pattern was suggested to be due to a YSIRK/GS motif within their signal peptides which directs the protein to the cross wall where massive peptidoglycan synthesis ensures that assembly sites for surface protein

deposition are mobile within the peptidoglycan as the sacculus expands (DeDent et al., 2008). The surface protein pattern observed in my study is uniformly punctate with no significantly greater binding at septal regions contrary to the DeDent model. However this patterning cannot be accounted for with either the 'line and dot' model' (no lines of binding) or the sector model (no differing in binding intensity in any segment), which supports the DeDent model. In all glycosylated proteins are labelled and it is likely that the overlap between ClfA, SdrCD and others led to a uniform punctate pattern. Furthermore in a ClfA mutant the localisation of glycosylated proteins was very similar to that observed by DeDent. This suggests there are a range of localisation patterns dependent on the individual surface proteins, however together they form a characteristic protein array. Overall it appears as though the WTA are not associated with the peicrust, it is important now to establish the location of cell wall hydrolases.

CHAPTER 5

Localisation of peptidoglycan hydrolases in *S.aureus*

5.1 Introduction

Peptidoglycan hydrolases are required to remodel the bacterial cell wall during growth and division. The *S.aureus* COL genome has been shown through bioinformatics to contain at least 20 putative peptidoglycan hydrolases. There are a variety of bond cleavage targets however, no putative lysozymes were detected and only two putative lytic transglycosylases were identified (Table 5.1) (Stapleton *et al.*, 2007; Wheeler, 2012).

5.1.1 Atl

The Atl autolysin is the major peptidoglycan hydrolase in both *S.aureus* and *S.epidermidis*; respectively AtlA and AtlE, they share a high degree of sequence similarity and are functionally interchangeable (Biswas *et al.*, 2006). Atl has been identified as a bifunctional enzyme tandemly encoded by the *atl* gene. This gene has an open reading frame of 3768bp, encoding a deduced protein of 1256 amino acids and molecular size of 137,381 kDa (Foster, 1995; Oshida *et al.*, 1995). This polypeptide undergoes processing steps to yield a 62 kDa *N*-acetylmuramyl-l-alanine amidase and a 51kDa endo- β -acetylglucosaminidase. The amidase (ami) domain extends from 2588bp to 4300bp or from Ala¹⁹⁹ to Lys⁷⁷⁵ in the polypeptide, while glucosaminidase (glu) stretches from 4031bp to 5743bp or from Ala⁷⁷⁶ to Lys¹²⁵⁶ in the polypeptide (Oshida *et al.*, 1995). The two catalytic domains are separated by three direct repeats, which show 31% identity between the three repeats (Foster, 1995). Repeat regions 1 and 2 remain attached to the C-terminal of Atl(ami) and repeat 3 is found at the N-terminal of Atl(glu). When sequence aligned each repeat can be further subdivided into an a-type and a b-type subunit, however both subunit types contain a highly conserved glycine-tryptophan (GW) motif (Marino *et al.*, 2002). Both *S.aureus* and *S.epidermidis* have the same modular organisation which is shown alongside the cleavage steps in Figure 5.1. The *atl* mutant forms large clusters of improperly separated cells in which individual cells appear to be interlinked with others. The outer surface of mutant cells appears much rougher than parent cells, indicating the vital role of Atl in cell separation (Foster, 1995).

| Protein | TIGR Locus Name | Putative identification | Gene length (bp) | Molecular weight (kDa) | pI | % GC | References |
|-----------------|-----------------|---------------------------------------|------------------|------------------------|------|------|--|
| Atl | SACOL1062 | Bifunctional autolysin | 3771 | 137.3 | 10.1 | 35 | (Foster, 1995; Oshida et al., 1995) |
| SagA | SACOL2298 | Putative Glucosaminidase | 779 | 29.7 | 9.6 | 32 | (Murray, 2001) |
| SagB | SACOL1825 | Putative Glucosaminidase | 855 | 32.5 | 9.3 | 31 | (Mohamed S.A.S, 2007) |
| ScaA (Sle1/Aaa) | SACOL0507 | Amidase, CHAP domain | 1005 | 35.8 | 9.7 | 37 | (Heilmann et al., 2005; Pourmand et al., 2006) |
| ScaB | SACOL0723 | CHAP domain | 798 | 28.2 | 6.1 | 38 | (Pourmand et al., 2006) |
| ScaC | SACOL2581 | CHAP domain | 768 | 27.6 | 7.8 | 37 | (Pourmand et al., 2006) |
| ScaD | SACOL2291 | CHAP domain | 804 | 29.3 | 8.9 | 39 | (Pourmand et al., 2006) |
| ScaE | SACOL0820 | CHAP domain | 840 | 30.2 | 10.0 | 35 | (Pourmand et al., 2006) |
| ScaF | SACOL0270 | CHAP domain | 894 | 33.0 | 5.9 | 37 | (Pourmand et al., 2006) |
| ScaG | SACOL2557 | CHAP domain | 432 | 16.8 | 10.2 | 35 | (Pourmand et al., 2006) |
| ScaH | SACOL2666 | Putative glucosaminidase, CHAP domain | 1860 | 69.3 | 6.0 | 33 | (Mohamed, 2007; Pourmand et al., 2006) |
| ScaI | SACOL1576 | CHAP domain | 1047 | 70.3 | 9.4 | 35 | (Pourmand et al., 2006) |
| ScaJ | SACOL2295 | CHAP domain | 501 | 17.4 | 5.6 | 38 | (Pourmand et al., 2006) |
| IsaA | SACOL2584 | Putative lytic transglycosylase | 702 | 24.2 | 6.1 | 42 | (Stapleton et al., 2007) |
| LytM | SACOL0263 | Lysostaphin | 969 | 35.0 | 6.0 | 40 | (Ramadurai and Jayaswal, 1997) |
| LytN | SACOL1264 | Amidase/Endopeptidase | 1152 | 43.2 | 9.5 | 29 | (Sugai et al., 1998; Frankel et al., 2011) |
| SceD | SACOL2088 | Putative lytic transglycosylase | 696 | 24.0 | 5.5 | 39 | (Stapleton et al., 2007) |
| SA0191 | SACOL0191 | Putative lysostaphin | 579 | 21.9 | 9.1 | 36 | (Wheeler et al., 2012) |
| SA1687 | SACOL1687 | Putative amidase | 876 | 32.7 | 7.8 | 33 | (Wheeler et al., 2012) |
| SA2195 | SACOL2195 | Putative lysostaphin | 855 | 32.8 | 7.1 | 31 | (Wheeler et al., 2012) |

Table 5.1 List of putative peptidoglycan hydrolases identified by an *in silico* screen of the *S.aureus* COL genome

Putative peptidoglycan hydrolase class is indicated based on highest homology scores to characterised autolysins. (+) Putative activity based on homology to the stated autolysin of known activity. Table adapted from (Hayhurst, 2006; Mohamed, 2007; Wheeler, 2012).

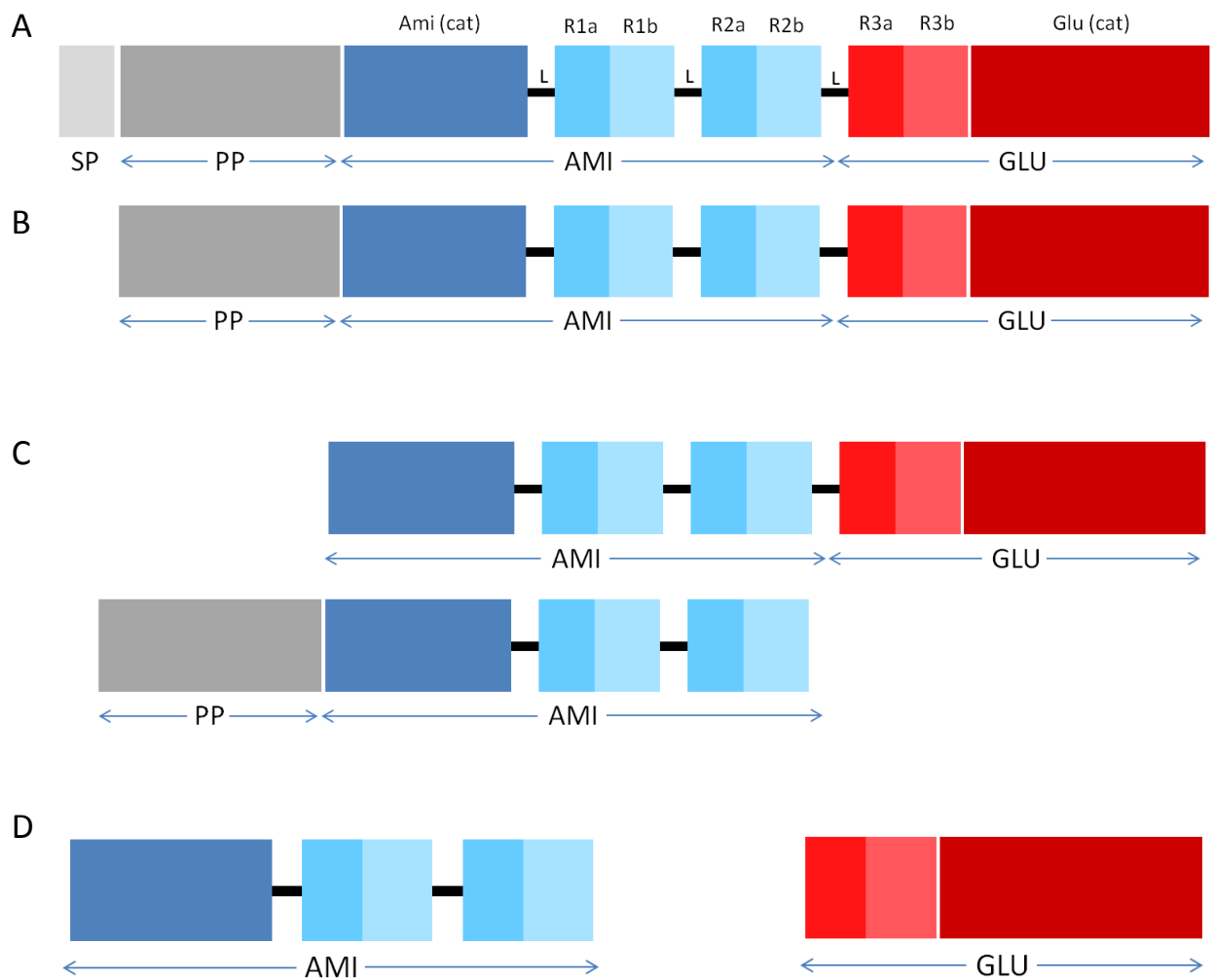


Figure 5.1 Domain structure of AtI of *S.aureus*

(Adapted from (Komatsuzawa et al., 1997; Zoll et al., 2012))

A, The translated AtI gene product; **B**, During secretion via the Sec pathway, the signal peptide is removed leaving the 138kDa pro-AtI; **C**, 115kDa (top) and 85kDa (bottom) intermediates; **D**, Fully processed products, 62kDa amidase and 51kDa glucosaminidase.

SP, Signal peptide; **PP**, pro-peptide of unknown function; **R(1/2/3)a/ R(1/2/3)b**; a-type and b-type of the R? Module; **L**, Linker.

Anti-immunoglobulin G (IgG) generated against purified Atl amidase or glucosaminidases each inhibited cell separation forming giant cell clusters, indicating that both enzymes have a function (Sugai et al., 1995). Interestingly an AtIA mutant did not significantly affect the ability of *S.aureus* to provoke an acute infection in a mouse sepsis model (Takahashi et al., 2002) but AtIE mutants had an attenuated virulence in a rat-catheter-associated infection model (Rupp et al., 2001). Levels of *atl* expression remained consistent during growth phase and when oxygen availability, KCL concentration or growth medium changes were studied. However *atl* gene expression was threefold higher at 37°C compared to 25°C and increased by twofold in the presence of NaCl (Foster, 1995).

Both Atl gene products were shown, by immunoelectron microscopy, to localise to the equatorial ring on the cell surface at septal regions of the future cell division site (Yamada et al., 1996). Pro-Atl, amidase and glucosaminidase have all been confirmed to localise to the cell surface (Baba and Schneewind, 1998). Targeting of Pro-Atl was shown to occur prior to proteolytic cleaving and the three repeat regions have been shown to be necessary and sufficient for correct localisation (Baba and Schneewind, 1998). The repeat regions exhibit a higher affinity for peptidoglycan than the catalytic amidase domain itself (Biswas et al., 2006). WTA has been shown to prevent binding of the repeats, which was proposed to direct Atl(ami) away from old cell wall material, and suggests the repeats have a strong role in targeting (Schlag et al., 2010). Indeed synthetic peptides based upon the amino acid sequence of R1 were capable of inhibiting and/or inducing autolysis which may be the result of the modification of *S.aureus* autolysin activities (Takano et al., 2000). Recently, the crystal structure of R2 has been determined, revealing that each repeat folds into two half-open β -barrel subunits and has the ability to bind both LTA and peptidoglycan (Zoll et al., 2012). It was suggested that LTA act as a receptor for the repeats allowing Atl to rebind as it hydrolyses peptidoglycan (Zoll et al., 2012). This supports the observation that LTA prevents penicillin-induced autolysis in *S.aureus* (Suginaka et al., 1979) and that the majority of autolytic enzymes were not attached to the cell wall in an LTA mutant (Corrigan et al., 2011). Small-angle X-ray scattering identified the linker regions between repeats as differing in flexibility and allowed a model where Atl amidase is anchored to LTA in the septum via repeats, here it would be able to assume several conformational states that would facilitate cell wall cleavage at a large number of sites (Zoll et al., 2012). Further to

repelling Atl, WTA has been shown to create a 'cation-exchanger like mesh' that is required to create a local acidified pool around the Gram-positive cell envelope (Biswas et al., 2012). This governs the pH-dependent activity of autolysins, in particular Atl whose activity is known to decline at acidic pH values (Biswas et al., 2012; Lützner et al., 2009).

5.1.2 Amidases (Sle1/Aaa (ScaA) and SA1687)

SA1687 has been labelled a putative amidase based on homology with the *B.subtilis* amidase, LytC (Wheeler, 2012). Sle1/Aaa is the only other known amidase of *S.aureus* and has been shown to be involved in cell separation (Heilmann et al., 2005; Kajimura et al., 2005). It is homologous to the *S.epidermidis* autolysin Aae, with both possessing bacteriolytic activity and adhesive properties (Heilmann et al., 2005, 2003). The *aaa* gene encodes a deduced protein of 334 amino acids with a predicted molecular mass of 35.8 kDa (Heilmann et al., 2005). Sle1 was purified from the *atl* mutant as a 32 kDa lytic band and identified as identical to Aaa (Kajimura et al., 2005). Characterisation of the enzyme has shown that it is an *N*-acetylmuramyl-L-alanine amidase, which preferentially cleaves dipeptide cross-bridges that interlink the two murein strands in peptidoglycan (Kajimura et al., 2005). The enzyme lacks a C-terminal LPTXG anchor region, typical of gram-positive surface proteins (Schneewind et al., 1993), but instead contains an N-terminal signal peptide that is followed by three peptidoglycan-binding LysM domains (Heilmann et al., 2005). It also contains a C-terminal CHAP domain which has the bacteriolytic activity and recently been shown to have a novel adhesive function to ECM (Extracellular matrix) proteins (Hirschhausen et al., 2012; Zou and Hou, 2010). Sle1 (Aaa) interacts with fibrinogen, fibronectin and vitronectin, and knockout mutants showed reduced adherence to surface-absorbed fibrinogen and fibronectin (Heilmann et al., 2005). A *sle1 (aaa)* insertional mutant impaired cell separation and induced the formation of clusters (Kajimura et al., 2005). Furthermore there was a significant decrease in mutant strain pathogenesis in an acute infection mouse model (Kajimura et al., 2005). Immunofluorescence microscopy revealed a cell surface localisation and like Atl a staphylococcal *tarO* mutant abolished localisation to the cross wall (Frankel and Schneewind, 2012; Heilmann et al., 2005). Recently a model has been proposed in which the LysM domain ensures septal localisation followed by cleavage of peptidoglycan, thereby exposing new LysM binding sites in the cross-wall of separating bacterial cells (Frankel and Schneewind, 2012).

5.1.3 The CHAP family

Members of the CHAP family have been found in a wide variety of bacteria and have also been detected in bacteriophage, archaea and the *Trypanosomatidae* family of eukaryotes (Rigden *et al.*, 2003). The CHAP domain is named after the acronym cysteine, histidine-dependent amidohydrolases/peptidases. It has been suggested to have amidase activity and is the invariant cysteine and histidine residues which form the putative active site (Bateman and Rawlings., 2003; Rigden *et al.*, 2003). The domain is between 110 and 140 amino acids and structural predictions have shown the N-terminal as largely alpha helices and the C-terminal comprised mainly of beta strands, putting it into the $\alpha+\beta$ structural class (Rigden *et al.*, 2003). It is commonly associated with other domains that cleave peptidoglycan and it has been suggested that this indicates a cooperative manner of action to cleave specialised substrates (Bateman and Rawlings., 2003).

5.1.4 Glucosaminidases (SagA, SagB and ScaH)

Atl(glu) plus three additional putative glucosaminidases, SagA, SagB and ScaH, has been identified via bioinformatics of *S.aureus* COL (Mohamed, 2007; Wheeler, 2012). All four glucosaminidases have been found to be maximally expressed in exponential phase, however they are under the influence of different gene regulator mechanisms (Mohamed, 2007). They also differ in modular structure. Unlike Atl, ScaH contains two domains, an N-terminal glucosaminidase domain and a C-terminal CHAP domain (which designates ScaH as a member of the Sca family) (Bateman and Rawlings, 2003; Rigden *et al.*, 2003). SagA and SagB have both been shown to have hydrolase activity (Wheeler, 2012) but their modular arrangement has not been determined. All four enzymes have a function in cell separation, with SagB having the major role (Mohamed, 2007). Evidence that *N*-acetylglucosaminidase activity is involved in *S.aureus* glycan chain length determination was observed using RP-HPLC (reverse phase high pressure chromatography) (Boneca *et al.*, 2000) and SagB mutant studies (Wheeler, 2012). Further mutant studies indicated that the archetypal short glycan strands of *S.aureus* are the product of glucosaminidase activity, primarily mediated by SagB. The remodelling of the nascent long glycan stands to the short strands of mature peptidoglycan is vital to allow the cells to expand and growth (Wheeler, 2012).

Halotolerance appears to be another function of glucosaminidases, with SagB activity again proving critical for survival under high salt concentrations (Wheeler, 2012).

5.1.5 Lytic transglycosylases (IsaA and SceD)

Lytic transglycosylases are a further class of autolysins, whose role is largely unknown. They have been proposed to play a role in cell wall turnover and subsequent β -lactamase induction in *E.coli* (Kraft *et al.*, 1999), in cell division and induction of the inflammatory immune response via release of peptidoglycan fragments in *N.gonorrhoeae* (Cloud and Dillard, 2004, 2002), and in facilitating the assembly of pili and flagella of *C.crescentus* (Roure *et al.*, 2012; Viollier and Shapiro, 2003). Two putative lytic transglycosylases have been characterised in *S.aureus*, IsaA and SceD. IsaA and SceD are translated into ionically bound proteins of 24.2kDa and 24kDa respectively, with the lytic transglycosylase domains found in the C-terminal region (Stapleton *et al.*, 2007). IsaA (Immunodominant staphylococcal antigen A) has been identified as a major antigen of *S.aureus* and was found to be highly detectable in serum from patients with staphylococcal infections (Clarke *et al.*, 2006; Pourmand *et al.*, 2006). A mouse model has also been used to confirm that the presence of IsaA antibodies augments a host immune response (Lorenz *et al.*, 2011). Similarly, an elevated titer of SceD antibodies has been associated with non-carriage of *S.aureus* (Clarke *et al.*, 2006), explained when SceD was found to be essential for nasal colonisation in cotton rats (Burian *et al.*, 2010; Stapleton *et al.*, 2007). It is also regulated by SaeRS, a two-component sensor involved in the regulation of multiple virulence factors (Goerke *et al.*, 2005; Liang *et al.*, 2006), suggesting a role in pathogenicity (Stapleton *et al.*, 2007). SceD and IsaA can be mutually compensatory when they behave differently. SceD upregulation has been noted in an *isaA* mutant but not the reverse, which indicates overlapping but distinct roles (Stapleton *et al.*, 2007). Cell separation was also impaired in a *sceD* mutant and was exacerbated in an *isaAsceD* double mutant (Stapleton *et al.*, 2007). Localisation of IsaA, using immunoelectron microscopy, showed distribution mainly at the septal region (Sakata *et al.*, 2005).

5.1.6 Lysostaphins (LytM, SA0191 and SA2195)

LytM is the only confirmed lysostaphin of *S.aureus*. Both SA0191 and SA2195 have been assigned as putative lysostaphins based on a 46% or 36% identity, respectively, with LytM

(Wheeler, 2012). LytM is a glycylglycine endopeptidase which is expressed during exponential growth phase (Ramadurai *et al.*, 1999). It is 948bp that encodes a polypeptide of 316 amino acids and calculated molecular mass of 34.4kDa (Ramadurai and Jayaswal, 1997). Doubt has been cast on the peptidoglycan hydrolyzing activity of the full length LytM, with suggestions that the N-terminus occludes the active site (Odintsov *et al.*, 2004; Singh *et al.*, 2010). Nevertheless, the C-terminal catalytic fragment has been clearly confirmed as cleaving the pentaglycine crossbridges (Firczuk *et al.*, 2005; Odintsov *et al.*, 2004). It remains unclear as to whether the catalytic domain can be released as only full length inactive LytM was identified in the cell wall envelope (Pieper *et al.*, 2006; Sabala *et al.*, 2012). LytM is under the control of the two component system WalkR, which is thought to play a role in virulence and cell wall metabolism (Dubrac and Msadek, 2004). Localisation studies using LytM antibodies showed no specific pattern across the cell surface, suggesting that LytM may play a role in actively growing and dividing cells (Ramadurai *et al.*, 1999)

LytN is only produced by certain strains of staphylococci and specifically digests the gly-gly bond in interpeptide chains of *S.aureus* (Sugai *et al.*, 1997a, 1997b). LytN is 1152 amino acids which fold into two domains, a C-terminal active domain and an N-terminal binding domain, which contains both LysM and CHAP domains (Frankel *et al.*, 2011; Sugai *et al.*, 1998). The LytN precursor is secreted via a YSIRK(G/S) motif signal peptide (DeDent *et al.*, 2008), which directs the protein into the cross-wall compartment separating the peptidoglycan from the inside (Frankel *et al.*, 2011). The LysM domain, like in Sle1, is WTA dependent for septal localisation with *tagO* mutants showing all over binding (Frankel and Schneewind, 2012). Although originally reported to have no discernible defects (Sugai *et al.*, 1998), *lytN* mutants have since been shown to have structurally damaged cross-walls and altered growth (rate and yield). Overexpression of *lytN* also affects growth rate and triggers rupture of the cross-wall (Frankel *et al.*, 2011). LytN producing strains are resistant to its own action, by altering the amino acid composition of their interpeptide chains (increasing serine content and decreasing glycine content). The gene involved in this alteration, *eprh*, is tandemly encoded with *lytN* (Sugai *et al.*, 1997a).

5.1.7 Aims of this investigation

- Localise Atl amidase and glucosaminidase using antibodies and identify their dynamics
- Investigate the role of WTA in Atl localisation
- Map the localisation of other hydrolases

5.2 Results

5.2.1 Atl amidase

5.2.1.1 Generation of recombinant Atl amidase

An *E.coli* overexpression construct, pSRC002 (Chapter 2; Table 2.5) was previously developed within our laboratory (Clarke *et al.*, 2006). The pSRC002 plasmid contains a pET21a overexpression vector with a His-tagged Atl amidase domain inserted under the control of an IPTG inducible promoter (Clarke *et al.*, 2006). Previous characterisation work showed that the purified recombinant protein was capable of hydrolysis of *B.subtilis* and ovocoid peptidoglycan (Hayhurst *et al.*, 2008; Wheeler *et al.*, 2011).

5.2.1.2 Overexpression and purification of Atl amidase

As described in Chapter 2.14.2 overexpression of Atl was carried out by IPTG induction. Successful overexpression of the recombinant protein was indicated by the presence of a high yield protein band at approximately 62 kDa four hours after induction (Figure 5.2A). This band was absent in the pre-IPTG induction sample and solubility was determined as described in 2.14.2 using SDS-PAGE. Overexpressed Atl amidase (Atl(ami)) was deduced as being soluble (Chapter 2.14.2; Figure 5.2A). However attempts to purify the soluble protein were unsuccessful and it was necessary to purify Atl(ami) under denaturing conditions. This property has been observed previously by Hayhurst and Wheeler, and it was suggested that Atl(ami) becomes insoluble when overexpressed (Hayhurst *et al.*, 2008; Wheeler *et al.*, 2011). The insoluble fraction was separated (Chapter 2.14.3) and the protein purified by nickel-affinity chromatography using the HiTrap system (Chapter 2.14.4). Proteins were purified in the presence of urea and eluted using an imidazole gradient. Fractions containing protein were indicated by UV detection at 280nm and pooled. The fractions were dialysed with stepwise (2M-0.5M) decreases in urea concentrations, from 8 to 0 M over a 24 hour period (Chapter 2.14.5). Decreasing urea concentrations incrementally helps to prevent the recombinant protein precipitating. The final Atl(ami) concentration was determined, using the BioRad protein concentration assay (Chapter 2.13.6), as 0.38 mg/ml (Figure 5.2B). Protein was concentrated in further experiments for consistency with other samples using a Millipore column.

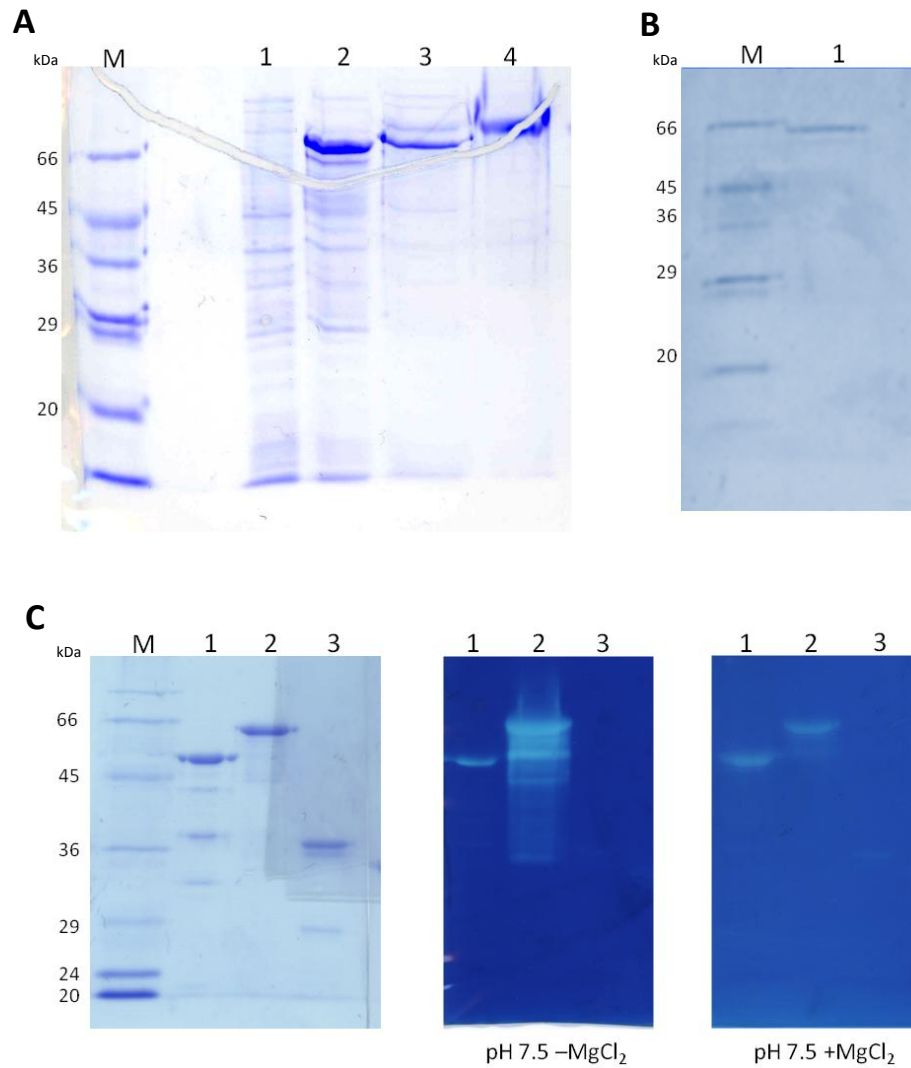


Figure 5.2 Recombinant Atl amidase protein production

(A) Overexpression of Atl(ami) and its solubility. Lane 1, pre-IPTG induction sample; lane 2, post-IPTG induction sample; lane 3, soluble sample; lane 4, insoluble sample.

(B) Purification of insoluble recombinant Atl(ami) after dialysis. Lane 1, Atl(ami)

(C) Coomassie and zymograms of Atl(ami). Lane 1, AtI(glu) 0.5 µg/ml; Lane 2, AtI(ami) 0.5 µg/ml; Lane 3, DivIB 0.5 µg/ml. Gels were incubated in the renaturing conditions listed below each gel overnight, stained for 3 hours and then destained for ~5hrs. Recombinant Atl(ami) and AtI(glu) both retain their hydrolytic activity.

Standards at sizes indicated in kDa (Sigma, Dalton Mark VII-L).

5.2.1.3 Confirmation of Atl amidase activity

Previous work within our laboratory has demonstrated that the overexpression of recombinant C-terminal His tagged proteins does not affect their autolysin activity. This was shown by zymogram for SagA, SagB and ScaH (Hayhurst, 2006; Mohamed, 2007; Murray, 2001). Zymogram analysis detects digestion of substrate by enzymes under non-reducing conditions, and has been shown to detect subpicogram amounts of activity (Gogly et al., 1998; Kleiner and Stetler-Stevenson, 1994). The zymograms use purified cell walls stripped of teichoic acids incorporated into the resolving gel, as a substrate. The gel is incubated in renaturing solution, renaturing gel stain (containing Methylene Blue) and destained until zones of clearing are seen where hydrolase activity has occurred (as described in 2.13.4). Figure 5.2C shows the purified Atl(ami) protein tested by zymogram using *S.aureus* SH1000 cell wall as a substrate. A negative control (DivIB) and a positive control (Atl(glu)) (Wheeler, 2012) for hydrolase activity were used. Atl(ami) and Atl(glu) gave distinct zones of clearing both with and without MgCl₂. A slight zone of clearing was seen in the negative control in the presence of MgCl₂, this is due to the protein binding peptidoglycan, but not hydrolysing, therefore blocking the dye and has previously been reported for DivIB (Bottomley, 2011).

5.2.1.4 Generation of antibodies

Pure recombinant protein was provided to Bioserv and antibodies were generated. The final serum was tested for specificity against whole cell lysate, mutant lysate and recombinant Atl(ami) (Figure 5.3). The Western blot revealed significant non-specific binding so the serum was affinity purified and tested again. A band of specific binding was seen at the correct size (amidase; 62kDa) in both lanes 1-2, containing pure recombinant protein, and lane 4, containing whole cell lysate.

5.2.1.5 Localisation of Atl amidase in SH1000 *spa::kan*

Immunolocalisation was performed in a strain where the gene encoding Protein A was replaced with a kanamycin resistance cassette (Girbe Buist, unpublished), SH1000 *spa::kan* (s2978), thus preventing non-specific binding of Atl(ami) antibodies to *S.aureus* Protein A. Protein A is a (Chapter 1.10) surface protein that is well characterised for its ability to bind immunoglobulin (DeDent et al., 2007; Sjodahl, 1977). Cells were grown to exponential

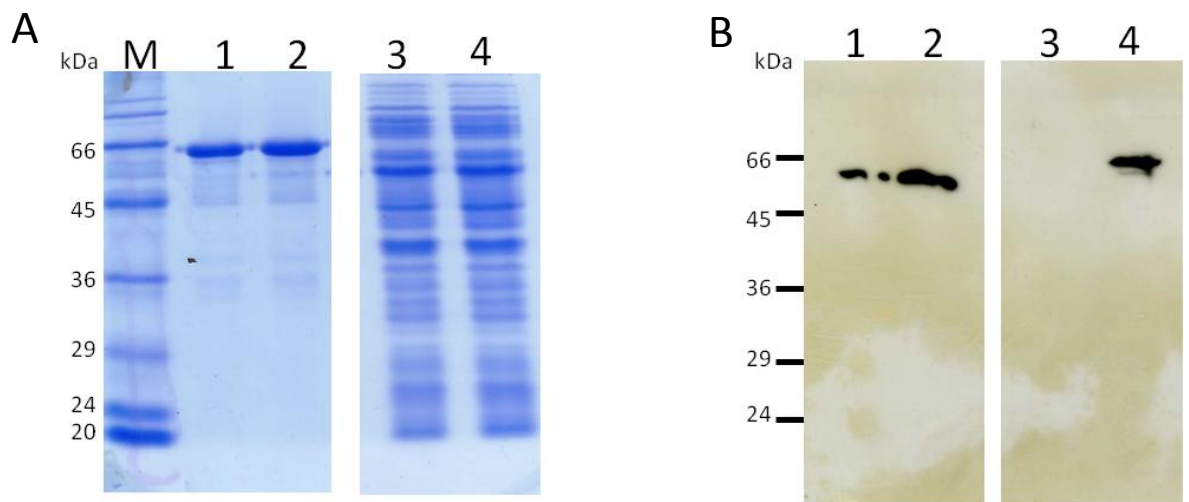


Figure 5.3 Purification of Atl amidase

Lane 1, 0.02mg ml^{-1} amidase; Lane 2, 0.04mg ml^{-1} amidase; Lane 3, Δatl whole cell lysate; Lane 4, SH1000 whole cell lysate.

A) Western blot using affinity purified α -Atl(ami) (antibodies). Binding is seen specifically to Atl(ami) in lanes 1-2 and lane 4. (1° antibody 1:5000; 2° antibody 1:20000).

B) Standards at sizes indicated in kDa (Sigma, Dalton Mark VII-L).

phase and stained with vancomycin (in tube staining was determined to give the best results) (2.17.11), to allow cells to be assigned growth stages. Cells were dried onto poly-L-lysine and immunostained as described in 2.17.12. A range of α -Atl(ami) concentrations were tested, with optimum results observed at 1:1000 dilution. The secondary antibody used was Alexa-Fluor 594-conjugated α -rabbit IgG (Invitrogen) at a dilution of 3:1000.

No fluorescence was observed in controls without primary antibody (Figure 5.4A) or in an *Atl* mutant (Figure 5.4B). Specific binding was seen on the surface of SH1000 *spa::kan* cells (Figure 5.4C and Figure 5.4D). Where septal plates had completely formed, a ring of binding was most often seen (75% of cells) (Figure 5.5A). As the cells began to separate strong binding was seen associated with the dividing septum, as expected. This was observed as a Y shape at the start (Figure 5.5B) and a deep V or a double ring towards the completion of cytokinesis (Figure 5.5C and D). When looking at the Z-stack images the 'double-ring' binding seen was in fact a V shape imaged mid way through (Figure 5.5D and Figure 5.5F). Only rarely were 'double-rings' seen but these were always still touching at one point. X shape binding, which would indicate separation occurring simultaneously from both sides of the cell, was not seen. There was no bulk labelling of the newly exposed cell surface instead binding remained on marginal regions of the split. In many cases Atl(ami) was seen to localise at sites where peptidoglycan synthesis had started to occur but a complete septal disc had not yet formed (Figure 5.5E). There was minimal binding not linked to sites of peptidoglycan synthesis and this can be attributed to Atl(ami) still bound from previous rounds of division.

Cells were assigned a cell cycle stage according to vancomycin labelling (Turner et al., 2010). Atl(ami) binding was then characterised in current or different plane and shape; as a ring, Y, X or different plane (Figure 5.6A shows the cell plane and vancomycin stages). 382 cells from 3 different fields of vision in two separate experiments were analysed (Figure 5.6B). The statistics were used to develop a schematic model of Atl(ami) localisation throughout the cell cycle (Figure 5.7). When the septum is incomplete Atl(ami) is present at both the current plane of synthesis and the previous plane. As the septal plate forms Atl(ami) forms a ring around the cell in the current plane and becomes Y shaped as the cells begin to split. This Y becomes a deep V as the cell proceeds through its cell cycle. As orthogonal growth commences, small amounts of Atl(ami) begin to appear at the new

division plane. Although in most cases an indentation was seen opposite splitting, the cell separation always appeared at one side.

5.2.1.6 Re-emergence of Atl amidase after trypsination

To reveal where Atl(ami) first localises and how quickly this occurs, all existing proteins, including existing Atl(ami), were removed. SH1000 *spa::kan* cells were incubated with trypsin for 60mins, washed with PBS and resuspended in media containing protease inhibitor to quench all further proteolysis (as described in chapter 2.17.8). At time intervals, staphylococci were fixed and labelled with vancomycin prior to revealing localisation of Atl(ami) by immunofluorescence (2.17.11-2.17.12). Primary and secondary antibodies were at the same concentration as before (1°, 1:1000; 2°, 3:1000). Any binding seen was characterised into dot, ring, Y/V in the same plane as peptidoglycan synthesis, binding in two planes (current and different) or binding in different plane than peptidoglycan synthesis. 382 cells were characterised from 2 separate experiments (Figure 5.8 shows a graph of the cell binding and examples of cells at each stage).

At 0 min no binding was seen which showed that all protein had been removed by trypsination. Atl(ami) was not seen to reappear until 10 min after treatment when 71% of cells showed binding. The binding appeared as a single dot on the cell (30%) or as a ring in the plane of synthesis (29%). When dots appeared they were often in planes that were not actively synthesising peptidoglycan. By 15 min 93% of cells showed binding and were seen as predominantly rings. At 20 min 94% of cells had produced Atl(ami) and the ring remained the predominant binding pattern seen. At 30 min a greater amount of cells had Atl(ami) in both the plane of peptidoglycan synthesis and another plane. By 60 min 39% of cells had Atl(ami) at a different plane of peptidoglycan synthesis. It appears as though Atl(ami) is produced rapidly by the cell and localises to peptidoglycan ribs (see below, Figure 5.9) from previous divisions or new sites of peptidoglycan synthesis. From here as the cells continue to grow Atl(ami) localises with growth, is left behind and gradually falls off.

5.2.1.7 Does Atl amidase localise to cell surface features?

The piercrust (as discussed in Chapter 1.6; Figure 1.7) is laid down in the plane of division

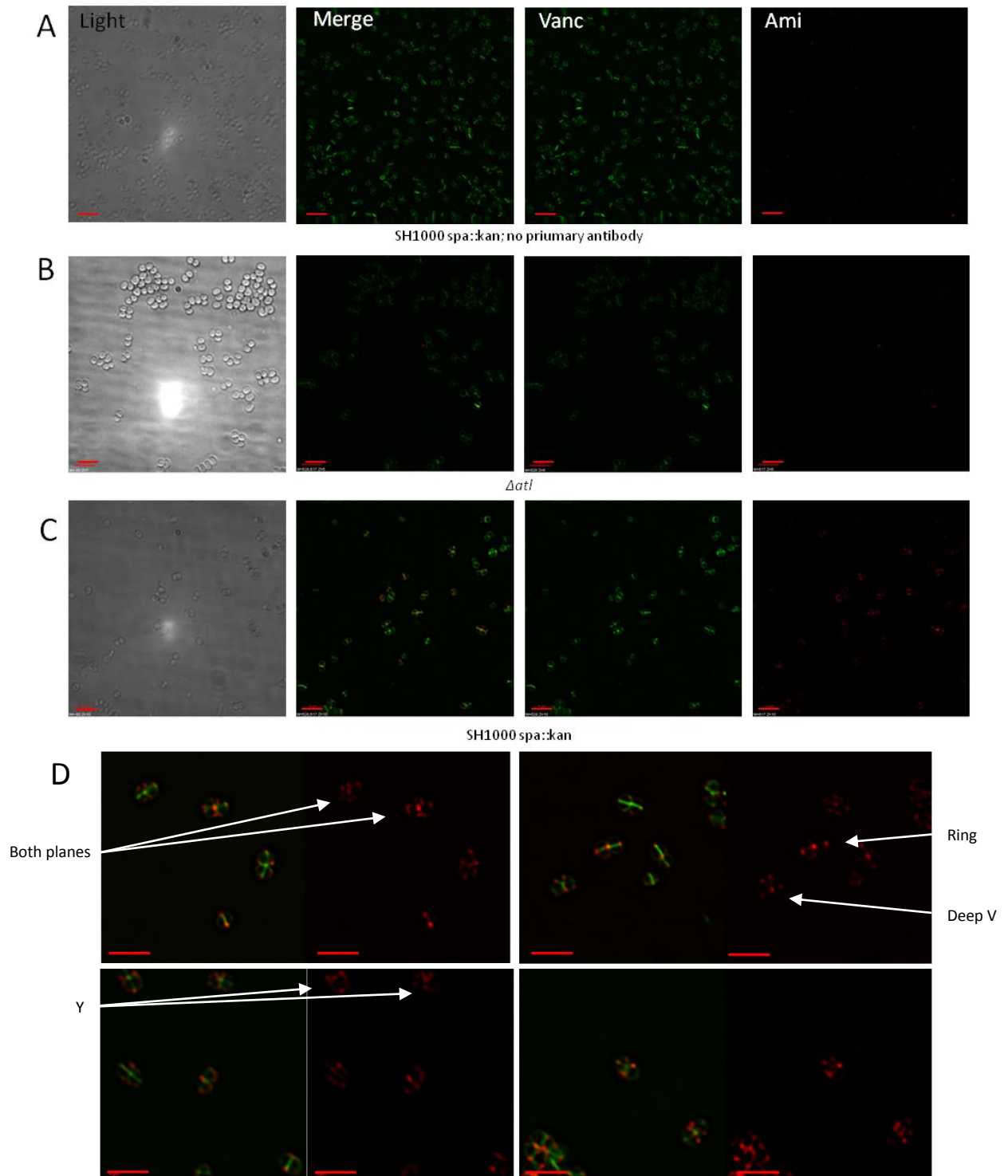


Figure 5.4 Localisation of Atl amidase

(A) SH1000 *spa::kan* with no primary antibody, no binding is seen; (B) Δatl no Atl(ami), no binding is seen; (C) SH1000 *spa::kan*, binding is seen at sites of new peptidoglycan incorporation; (D) Enlarged SH1000 *spa::kan* cells from separate experiments show binding at sites of new peptidoglycan synthesis and where cells are splitting. Scale bar represents 4 μ m.

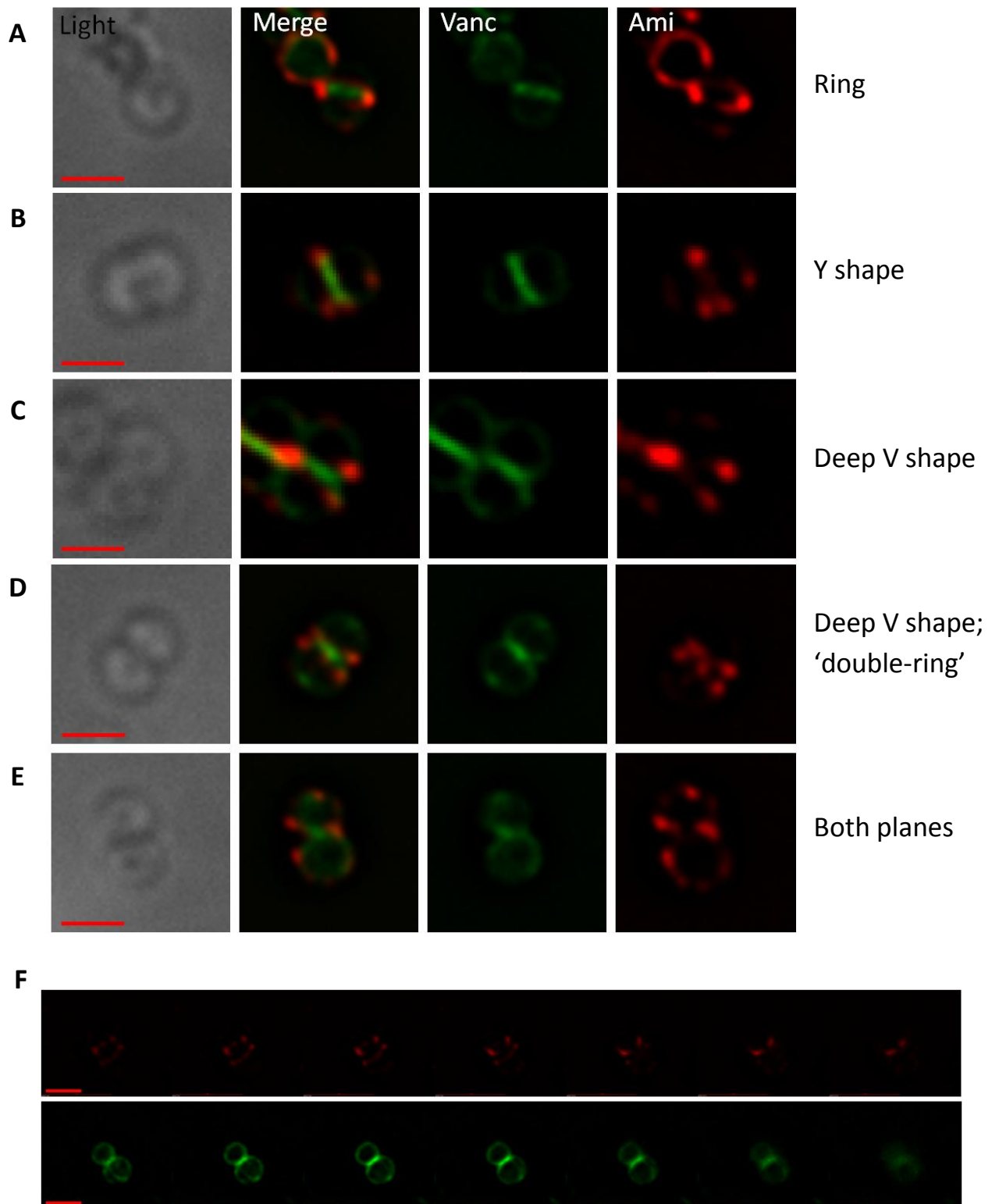


Figure 5.5 Expanded images showing SH1000 *spa::kan* Atl amidase localisation

Ring shape can be seen with complete septal disc (A); Y shape is seen as the cell splits (B); the Y shape becomes a deep V as the cells split (C); when seen from above the V shape can appear as a 'double-ring' (D); as orthogonal growth begins in the next plane Atl(ami) appears in two planes (E). Z stack of deep V (F). A-E scale bar represents 1 μ m; F scale bar represents 2 μ m.

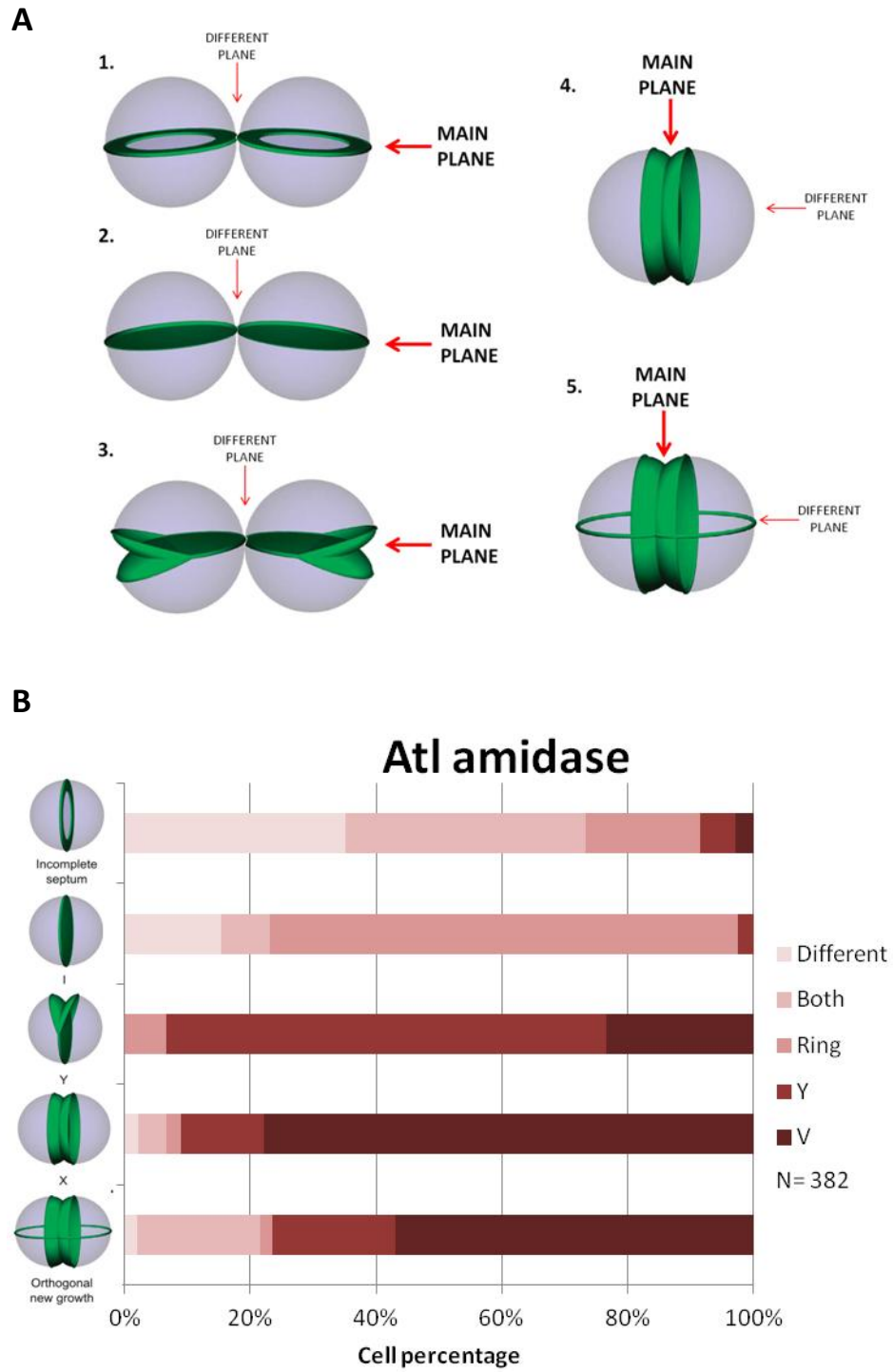


Figure 5.6 Analysis of Atl amidase localisation

(A) Schematic of vancomycin labelling throughout the cell cycle and classification of main plane at each stage. (B) Percentage of Atl amidase localisation at each stage of the cell cycle.

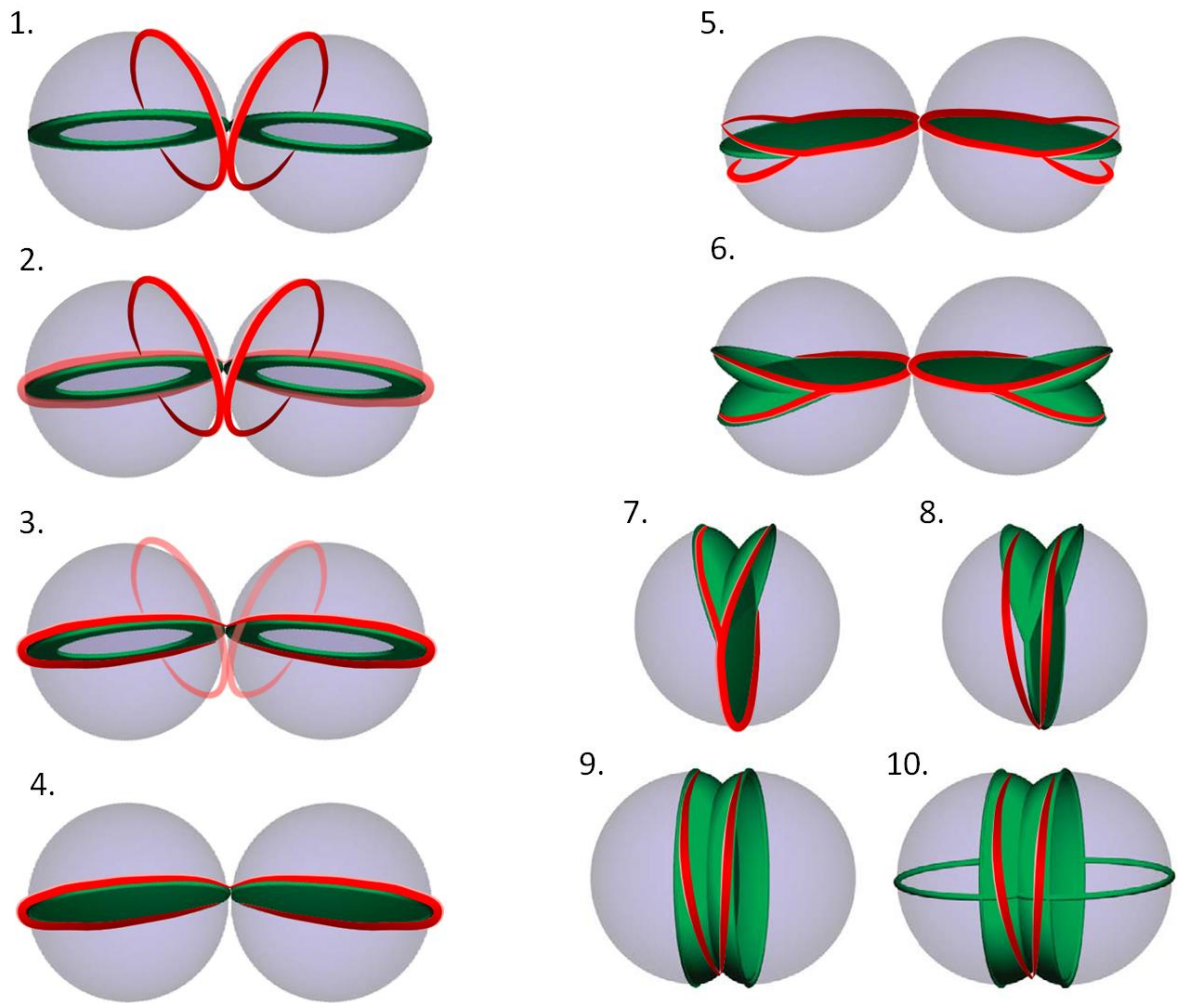


Figure 5.7 Schematic model of Atl amidase throughout the cell cycle

Green indicates vancomycin. Red indicates Atl(ami) localisation.

A deep V of binding is seen where two cells have split and as they commence their next cycle of division (1). As the septal plate is formed Atl(ami) is produced and bound in a ring around the current plane (2). Atl(ami) from the previous planes is lost (3). When a complete septum is formed the Atl(ami) ring (4) splits at one side forming a Y shape (5). This allows peptidoglycan growth to continue (6 and 7). Atl(ami) splits further into a deep V (8). Peptidoglycan synthesis continues as the cells split (9) and orthogonal growth begins (10). Indentations are seen into the septum at the base of the V but the shape does not change from a V to X.

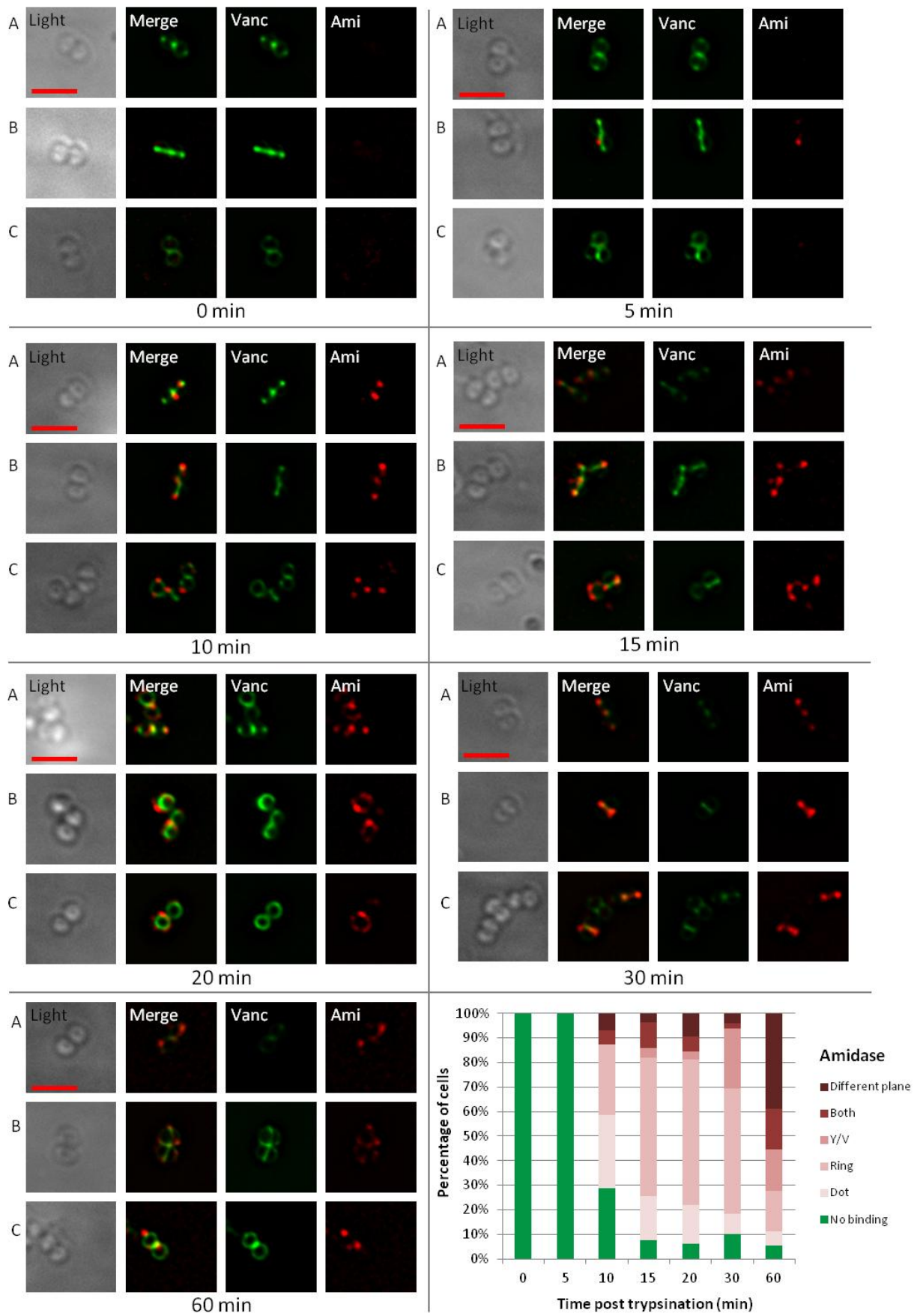


Figure 5.8 Re-emergence of Atl amidase after trypsination of cells

Each panel shows the time post-trypsination, 0-60 min from top left to bottom. Row A, shows cells beginning septal growth; Row B, shows cells with complete septal plates and Row C shows cells beginning orthogonal growth (where found). Distribution patterns were assigned one of five classes. Scale bar represents 2 μ m.

Atl(ami) reappears after 10 min, predominantly as a dot(s) or ring pattern. By 60 min cells are beginning show localisation in planes different from current growth.

before the septal plate has completely formed. It remains in place and is divided between the two cells as they split forming ribs (Turner *et al.*, 2010). Atl(ami) appears to remain on the outside of the cell in a ring either side of the splitting cells, therefore it seemed likely that Atl(ami) could bind ribs. During division, older ribs are dissected by the new piecrust placement and subsequent division, resulting in cells containing whole ribs, half ribs and quarter ribs. Z-stacks of cells were analysed in detail and quarter ribs were able to be distinguished in numerous cells. Figure 5.9A shows two cells with incomplete septal plates (orthogonal growth) still splitting from the previous division. Atl(ami) is still bound in a deep V (point facing towards the viewer) from the previous division, but can also be seen in the left hand cell as a quarter line. This binding is highly reminiscent of the piecrust pattern suggesting that Atl(ami) is indeed binding this feature (Figure 1.7A). This is the current plane so a new piecrust would be expected to form, however the binding is distinctly in the old peptidoglycan. Figure 5.9B shows a cell with a complete septal disc and ring of Atl(ami). There is faint binding also seen perpendicular to the current plane, which only appears half way through the Z stack. This suggests binding to the old quarter rib.

Analysis of the dot patterns seen at 10mins after trypsination as Atl(ami) started to appear on the cell surface further suggested binding to the peptidoglycan piecrusts. As discussed in chapter 4.3, a 'dot and line' model has been used to suggest localisation to piecrust and rib features ('dot and line' model Figure 4.13B). It is important to note that not all cells displayed a dot pattern upon re-emergence. Those that did were cells undergoing active septal growth, which is the plane of the quarter rib, and so only half and whole ribs could be seen. Figure 5.9C i and ii show binding in the old peptidoglycan segment, vancomycin labelling was aligned with the new piecrust of the model and dots suggested binding to half and whole ribs from previous divisions. In Figure 5.9C iii Atl(ami) is seen at the current plane but also with the half rib from the previous division.

5.2.1.8 Colocalisation of peptidoglycan features and immunofluorescence

It was hoped to combine STORM and AFM technologies to align immunofluorescence and peptidoglycan features but time restraints for this thesis meant that this was not possible (both microscopy techniques are discussed in Chapter 4.1). In preparation for work with STORMforce (STORM and AFM) the immunofluorescence protocol was adapted for work

with the STORM microscope. To facilitate focusing and allow correction of drift, gold nanoparticles were dried to the slide using nitrogen gas. Cells were applied on top and also dried to the slide using nitrogen gas. The primary antibody was applied at a range of concentrations (5:1000- 1:20000) overnight and the secondary antibody of Alexafluor 532 also at a range of concentrations (1:1000- 10:1000) for 2hrs. Cells were mounted in cysteamine in PBS, to increase the length of time fluorescent molecules were in the 'off' state, and completely sealed to prevent drying (Chapter 2.21 and 2.22). Unfortunately, despite several attempts only one usable image was obtained (Figure 5.10). There was a high level of background binding, which all attempts to lower removed significant specific binding. Low levels of Atl(ami) binding across the entire cell surface was seen. The patterns seen with fluorescence were similar to those observed with deltaposition, however when switched to STORM they became more difficult to distinguish. This is most likely due to further protocol refinement needed. Nevertheless some details were able to be examined and one cell in particular (Figure 5.10). It appears as if the Atl(ami) is localised in a line, which appears to be one or two layers of peptidoglycan thick. This line is also not uniform and appears to be beginning to split from one side.

5.2.1.9 Atl amidase localisation in SH1000 $\Delta tarO$

A relationship between WTA and Atl localisation has been previously reported (Schlag et al., 2010). Atl(ami) was shown to accumulate at the septal region of SH1000 *spa::kan* cells, while in WTA deficient cells the amidase is evenly distributed across the cell surface. To examine this relationship, a protein A negative strain of $\Delta tarO$ had to be made. A *spa::kan* transduction into $\Delta tarO$ cells was not possible as WTAs are the phage (ϕ) attachment sites. A strain containing a *tarO* complementation plasmid (*S.aureus* SA113 $\Delta tarO::ermB$ pRB473-*tarO*) was used to make a ϕ lysate (donated by A.Peschel). This ϕ lysate was used to transduce SH1000 *spa::kan*, the resulting cells were plated onto erythromycin and kanamycin plates for selection. Cells that grew were also patched onto plates containing chloramphenicol (pRB473-*tarO*) and those that did not grow on this plate were selected. Selected strains were verified by Western blot using α -protein A (appendix II). Immunolocalisation was performed on SH1000 $\Delta tarO::ermB$ *spa::kan* cells and similar results to those previously reported (Schlag et al., 2010) were seen (Figure 5.11B and C). Atl(ami) distribution was completely disrupted in $\Delta tarO$ cells and was seen to be uniformly

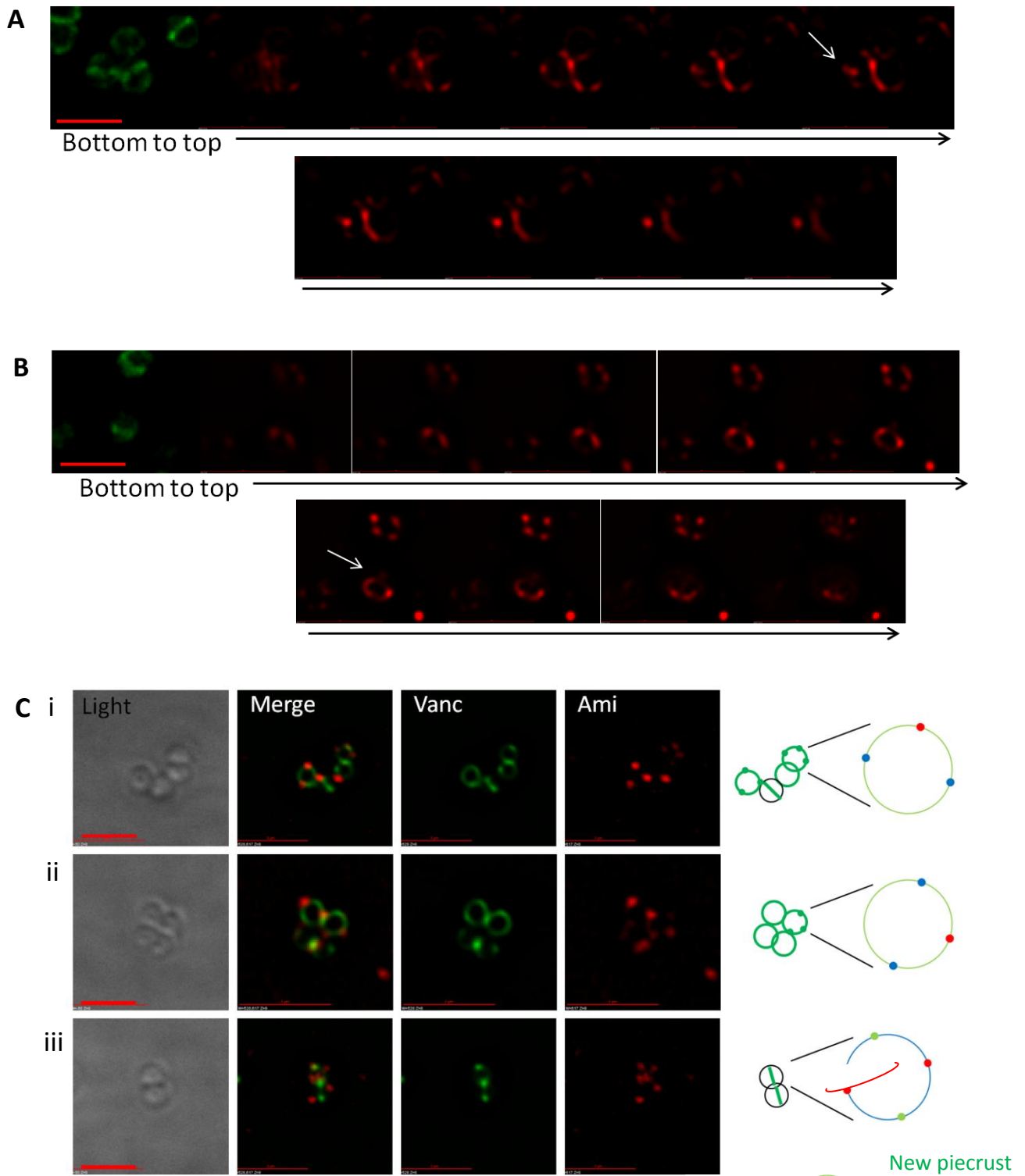


Figure 5.9 Atl amidase binds piecrust

(A) and (B) Z stacks of cells show Atl(ami) binding to a quarter rib indicated by the arrow. Scale bar represents 2 μ m.

(C) After trypsination Atl(ami) binds in a dot pattern that indicates binding to previous ribs. Interpretative diagrams are shown to the right of cells and an overall diagram shown in (D). Refer to text for in depth description. Scale bar

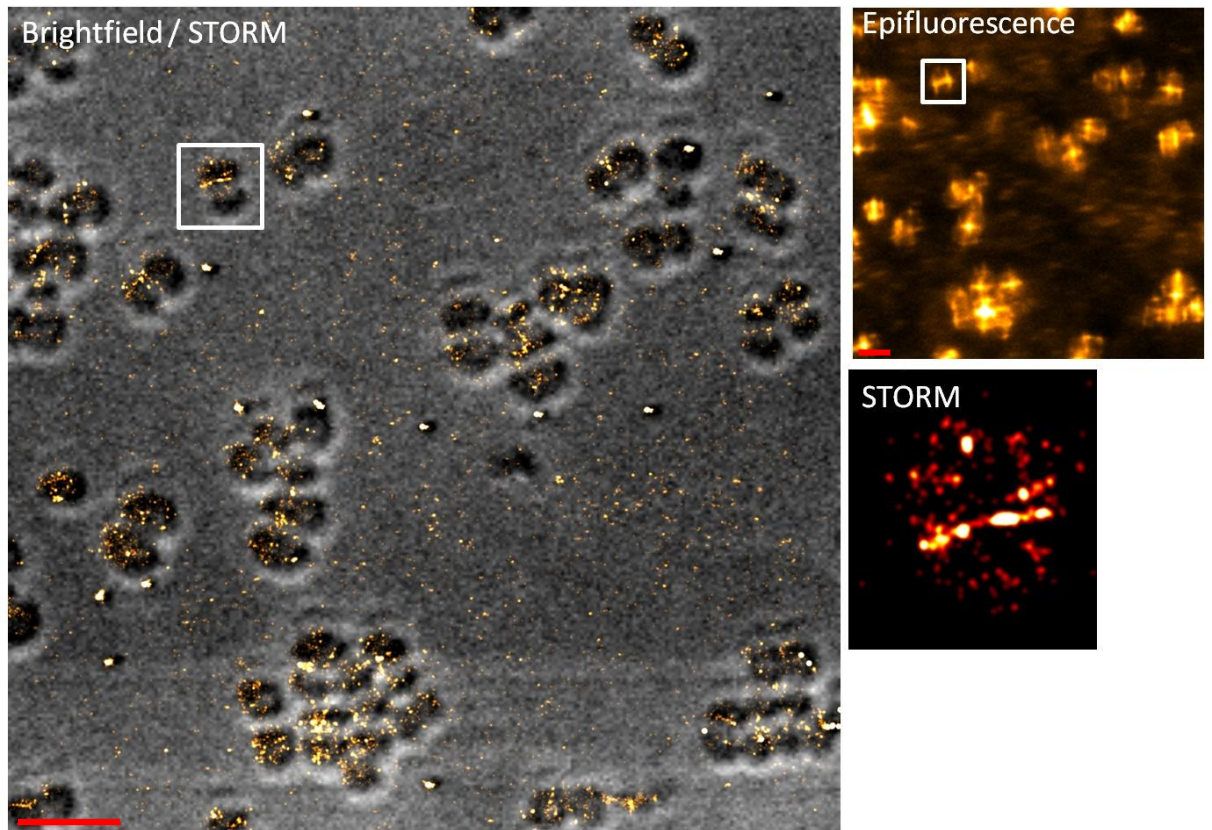


Figure 5.10 Atl amidase localisation viewed by STORM microscopy

Immunolocalisation of Atl(ami) viewed with STORM microscopy. Epifluorescence image shows similar binding patterns as seen with DeltaVision. STORM and brightfield were overlaid because structures were difficult to distinguish due to the high level of background. Enlarged cell shows a ring of Atl (ami) across the septum of the cell that appears to be 1-2 layers of peptidoglycan thick. Scale bar represents 2 μ m.

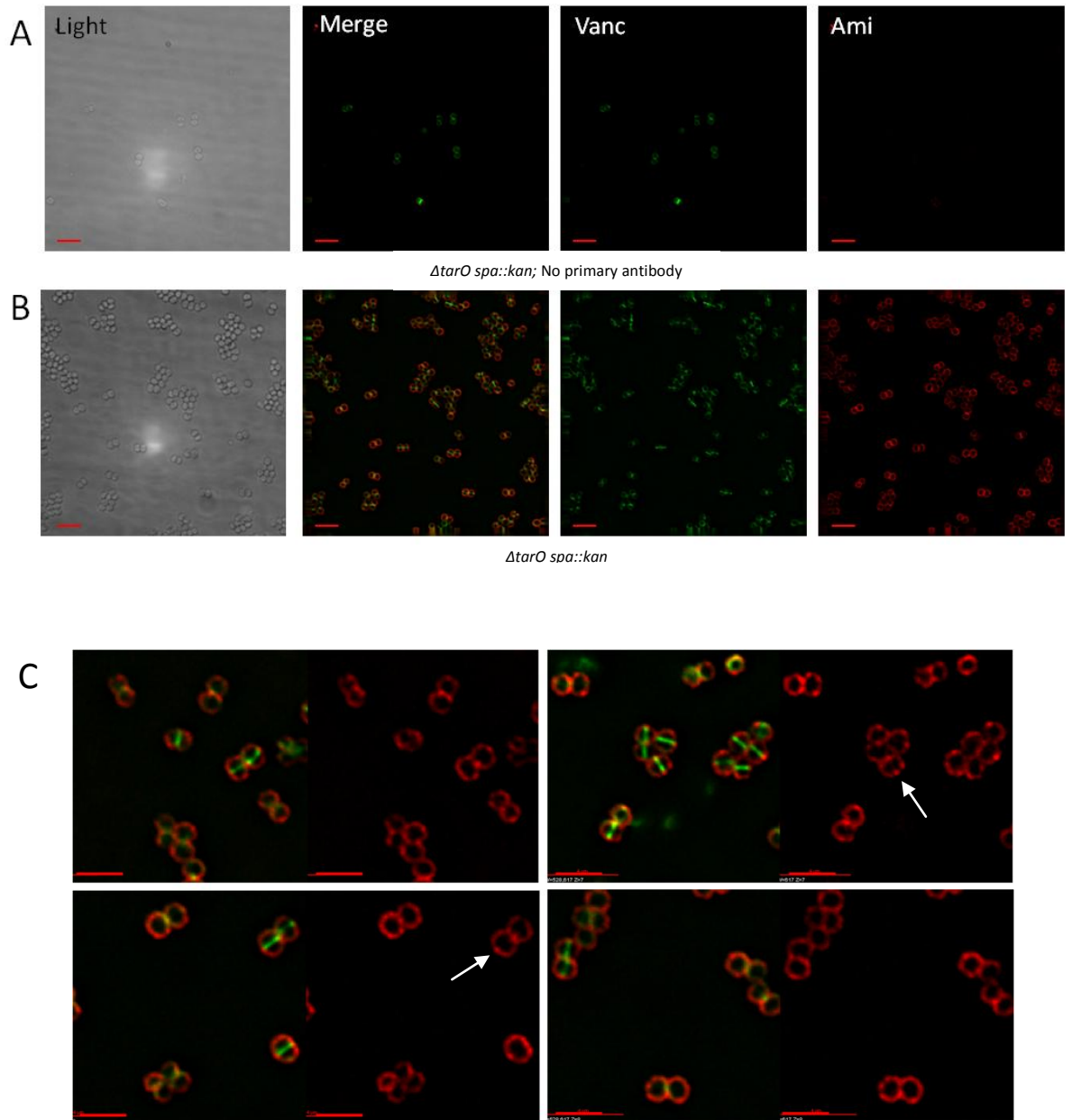


Figure 5.11 Localisation of Atl amidase in $\Delta tarO$

(A) *SH1000 tarO::ermB spa::kan* with no primary antibody, no binding is seen; (B) *SH1000 tarO::ermB spa::kan*, AtII(ami) binding is across the entire cell surface; (C) Expanded images of *SH1000* cells from separate experiments show binding across the cell surface with several cells showing bright foci. Faint cross-wall binding can be seen, indicated by arrows. Scale bar represents 4μm.

bound across the cell surface. Occasionally foci of strong binding were seen at the edges of complete septal discs but not in all cases. Examples of faint crosswall binding were also seen. No fluorescence was observed in controls without primary antibody (Figure 5.11A).

5.2.1.9. Colocalisation of Atl amidase and ConA

Data here suggests that Atl(ami) binds to the peptidoglycan rib features and that the WTA inhibits binding to the rest of the wall. It was hypothesised that labelling WTA and Atl(ami) might help to further examine the relationship between WTA and Atl. This study has already proven that ConA binds both WTA and surface proteins (chapter 4) and therefore the experiment was performed in a SH1000 Δ *srtA* background. SH1000 Δ *srtA* was transduced with a *spa::kan* lysate and the resultant strain tested by Western blotting (appendix II). For labelling, cells were grown to exponential phase and stained with vancomycin (2.17.11), before being dried to slides and immunostained (2.17.12). Primary antibody was applied at 1:1000 dilution, washed 8 times and the secondary was applied at 3:1000 dilution along with ConA at 1:4 dilution. The final cell wash was only repeated three times, to limit the loss of ConA.

No Atl(ami) signal was seen in controls not containing primary antibody (Figure 5.12A). Following the above protocol SH1000 Δ *srtA spa::kan* cells were labelled with only Atl(ami) and with only ConA, similar patterns were seen to those within Chapter 5 (Figure 5.4) and Chapter 4 (Figure 4.8) respectively. However when cells were also labelled with vancomycin and/or antibody, the ConA observed binding pattern was different (Figure 5.12); there was strong crosswall binding (no apparent access issue as seen in Chapter 4)(Figure 5.12B and C); smooth binding across the cell surface (Figure 5.12B , C and D); and bright foci which often aligned with antibody binding (Figure B and D). When cells were probed with antibodies against a protein found across the whole cell surface, SceD (shown later in section 5.2.5), foci were not seen. Together this suggested that ConA was binding both vancomycin (cross wall binding and smooth cell surface) and antibody (aligned bright foci) in favour/aswell as its desired target WTA.

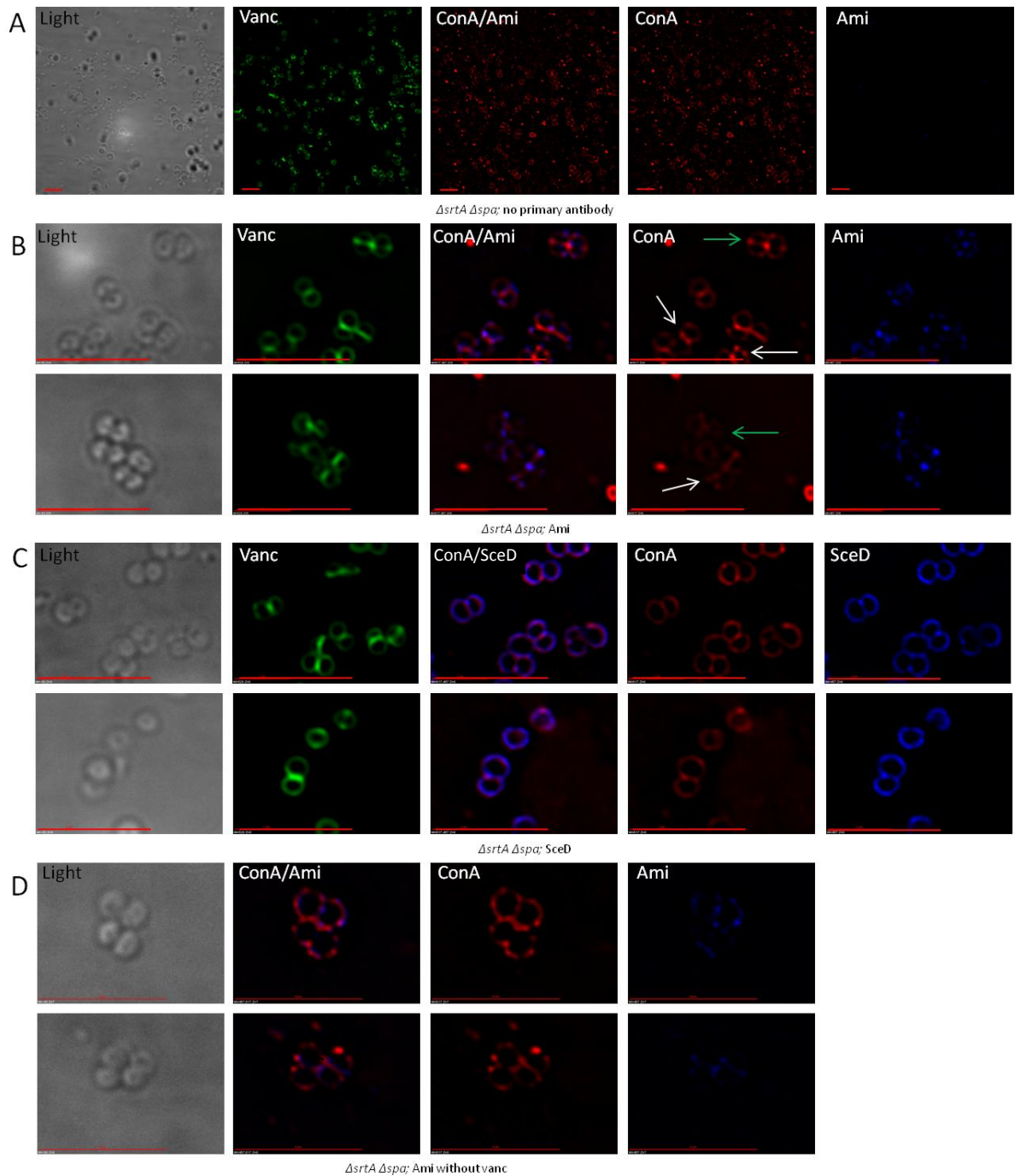


Figure 5.12 Binding of ConA to antibodies and vancomycin

(A) SH1000 $\Delta srtA \Delta spa::kan$ cells with no primary antibody show no binding and expected binding patterns of conA. (B) ConA binding pattern is altered by vancomycin and antibodies. White arrows show foci of conA binding that align with antibodies. Green arrows show cross wall binding that aligns with vancomycin labelled septal growth. (C) ConA shows fewer foci when antibody binding is all over. (D) ConA shows foci that align with antibody binding. Scale bar represents 6 μ m.

5.2.2. Atl glucosaminidase

5.2.2.1. Generation of Atl glucosaminidase antibodies

An *E. coli* overexpression construct, pSRC003 (Chapter 2; Table 2.5) was previously developed within our laboratory. The pSRC003 plasmid contains a pET24d overexpression vector with a His-tagged Atl glucosaminidase domain inserted under the control of an IPTG inducible promoter (Clarke et al., 2006). Purified Atl(glu) generated using this vector was obtained from Wheeler (2012) and shown to be active by zymogram (Chapter 2.13.4) (Figure 5.2C). Pure recombinant protein was provided to Bioserv and antibodies were generated. The final serum was tested for specificity against whole cell lysate, mutant lysate and recombinant Atl(glu) (Figure 5.13A). The Western blot revealed significant non-specific binding so the serum was affinity purified and tested again (Figure 5.13B). A band of specific binding was seen at the correct size (glucosaminidase; 51kDa) in both lanes 1-2, containing pure recombinant protein, and lane 4, containing whole cell lysate. Breakdown products were also observed in lanes 1-2.

5.2.3.2 Localisation of Atl glucosaminidase in SH1000 *spa::kan*

Immunolocalisation was again performed in SH1000 *spa::kan*, grown to exponential and stained with vancomycin (2.17.11) prior to immunostaining (2.17.18). A range of α -Atl(glu) concentrations were tested and again 1:1000 found to be the best. The secondary antibody used was Alexa-Fluor 594-conjugated α -rabbit IgG (Invitrogen) at a dilution of 3:1000.

No fluorescence was observed in controls without primary antibodies (Figure 5.14A) or in an Δ atl mutant (Figure 5.14B). Specific binding was seen on the surface of SH1000 *spa::kan* cells (Figure 5.14C and D). The same binding patterns seen for Atl(ami) were observed for Atl(glu) but they did not appear to occur at the same cell cycle stages or within the same time frames. As before, no bulk labelling was seen on the nascent peptidoglycan and no X structures were found. Unlike Atl(ami), cells in early division most commonly showed binding only associated with the previous division cycle. Furthermore, the ring structure appeared more transient with Atl(glu) binding rarely found without binding in another plane. Y and V shapes were more common and binding in multiple planes was seen at all stages. It was also noted that V shapes did often take on an almost double ring shape however in all cases examined the two rings maintained contact at one point.

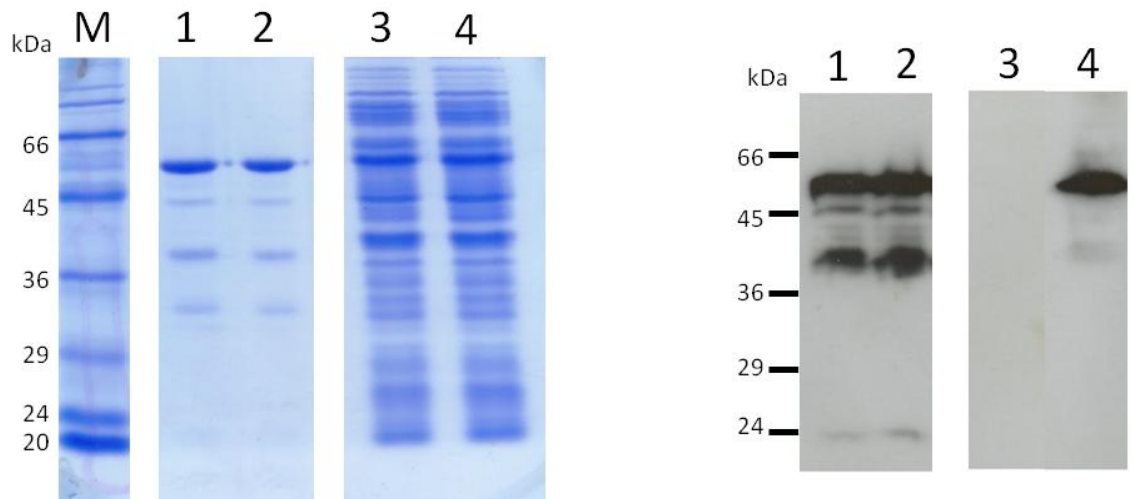


Figure 5.13 Purification of Atl glucosaminidase

Lane 1, 0.02mg ml^{-1} glucosaminidase; Lane 2, 0.04mg ml^{-1} glucosaminidase; Lane 3, Δatl whole cell lysate; Lane 4; SH1000 whole cell lysate.

Western blot using affinity purified α -Atl(glu). Binding is seen to Atl(glu) and breakdown products in lanes 1-2 and to Atl(glu) in lane 4 .

Standards at sizes indicated in kDa (Sigma, Dalton Mark VII-L).

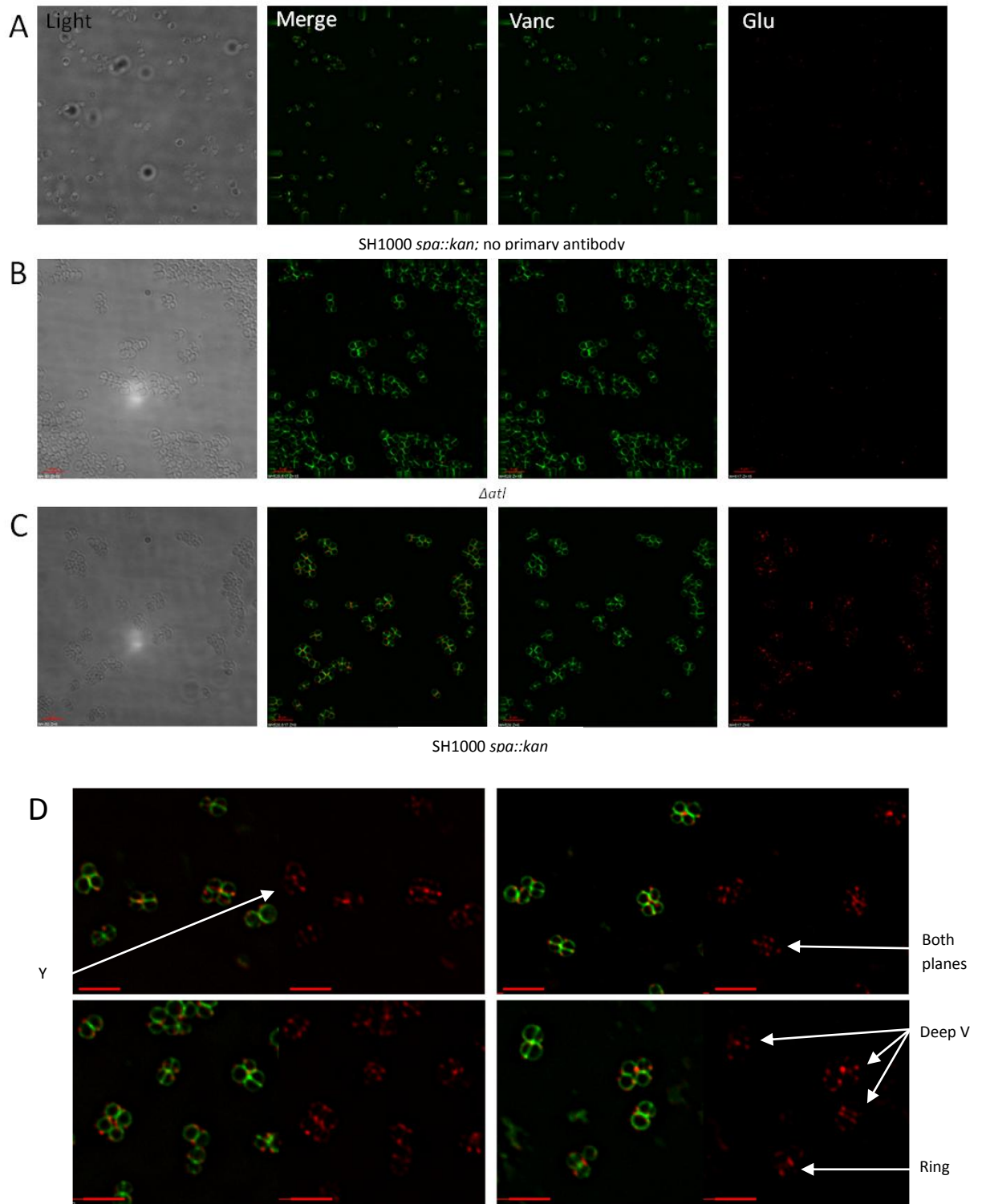


Figure 5.14 Localisation of Atl glucosaminidase

(A) SH1000 *spa::kan* with no primary antibody, no binding is seen; (B) Δatl no longer produce Atl(glu), no binding is seen; (C) SH1000 *spa::kan*, binding is seen at sites of new peptidoglycan incorporation and on the outside of cell splits; (D) Enlarged SH1000 *spa::kan* cells from separate experiments show binding at sites of new peptidoglycan synthesis and where cells are splitting. Localisation appears less specific than Atl(ami).

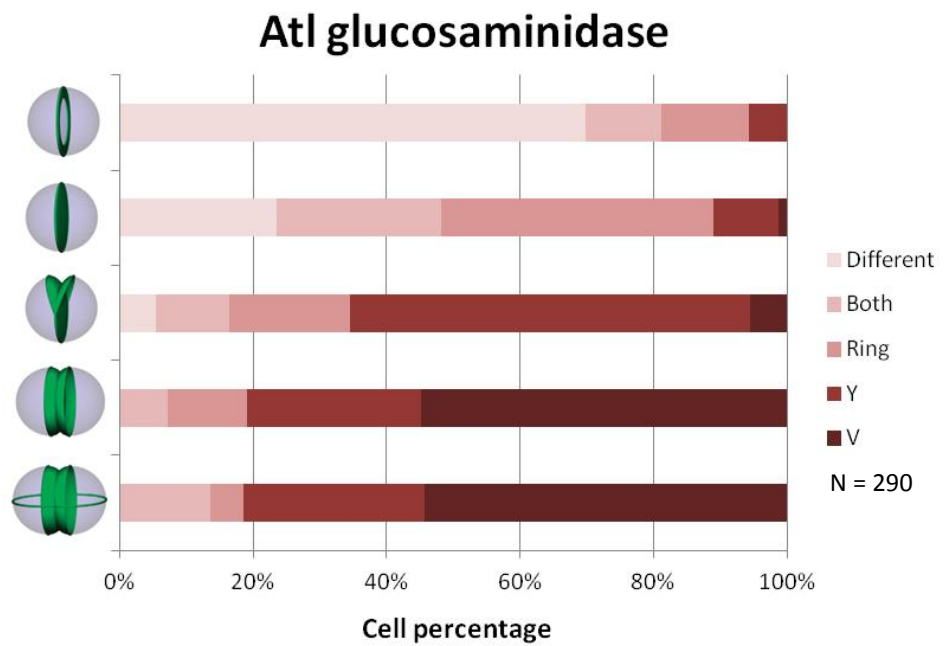
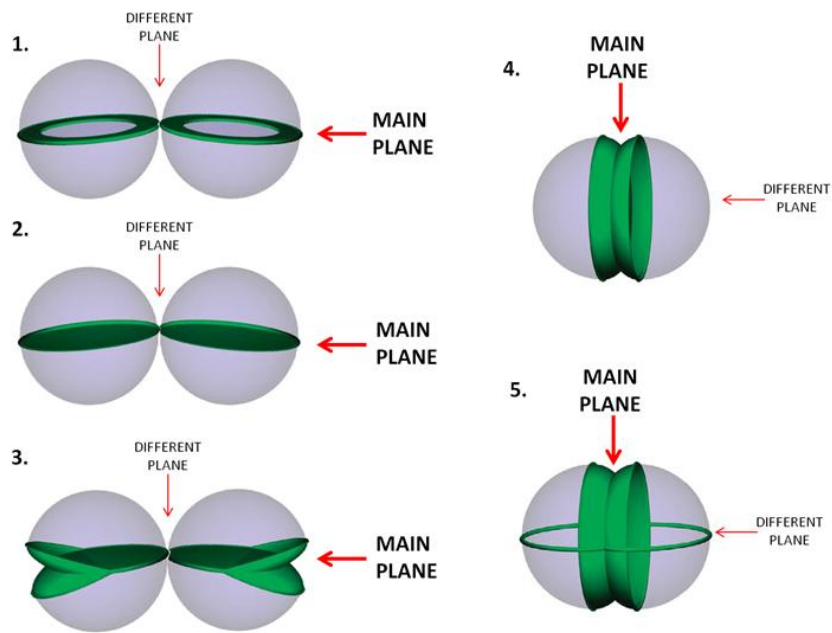


Figure 5.15 Analysis of Atl glucosaminidase localisation

(A) Schematic of vancomycin labelling throughout the cell cycle and classification of main plane at each stage. (B) Percentage graph of Atl glucosaminidase localisation at each stage of the cell cycle.

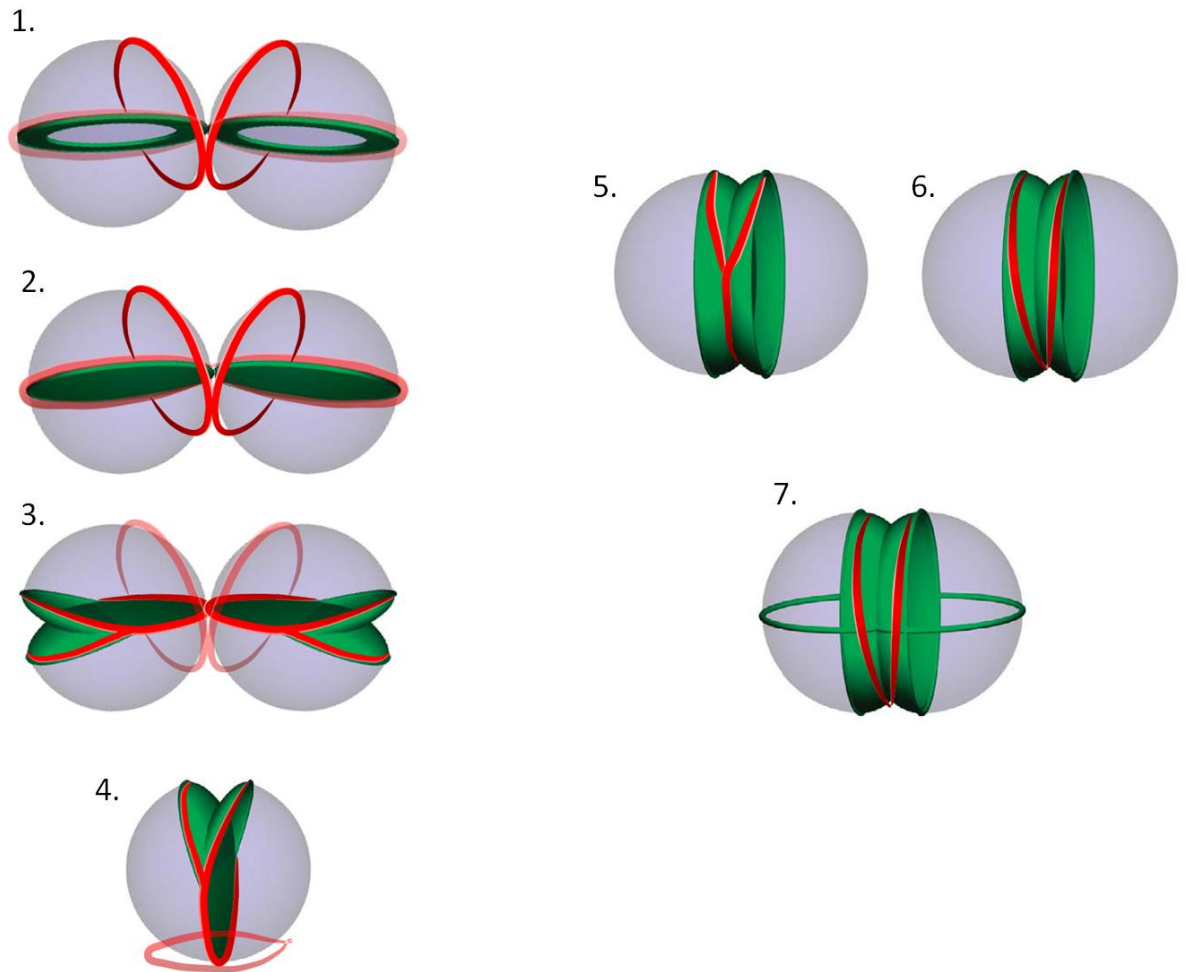


Figure 5.16 Schematic model of Atl glucosaminidase throughout the cell cycle

Green indicates vancomycin labelling; Red indicates Atl(glu) binding.

As cells commence division Atl(glu) remains associated with the previous round (1). A few cells may have Atl(glu) attached in both planes. As the septal disc completes the majority of binding is still associated with the previous round of division or with both rounds (2). As the cells begin to split, Atl(glu) is found in a Y shape alongside the new cell wall synthesis (3 and 4). Atl(glu) is still found associated with previous division cycles. As the cell continues growth the Y shape deepens to a V and localisation associated with previous rounds is not found (5 and 6). As orthogonal growth begins Atl(glu) remains in line with the previous round (7).

Cells were again assigned a cell cycle stage according to vancomycin labelling (Turner et al., 2010) and the Atl(glu) binding characterised (Figure 5.15A shows the cell plane and vancomycin stages). 290 cells from 3 different fields of vision in two separate experiments were analysed (Figure 5.15B). This again allowed the development of a model of Atl(glu) localisation throughout the cell cycle (Figure 5.16). When the septum is incomplete Atl(glu) was found most often in the previous plane and only rarely to associate with both planes of division. Binding is not found mainly at the current plane until the cell begins to split. As the cell continues growth (seen as X vancomycin labelling) Y and deep V shapes predominate with only 15.6% of cells showing the ring structure and only 9% of cells still also localised in the previous plane. The amount of cells showing two planes of localisation started to increase with the beginning of orthogonal growth. The predominant shape present with orthogonal growth is the deep V, as with Atl(ami).

5.2.3.3 Re-emergence of Atl glucosaminidase after trypsination

Initial localisation of Atl(glu) and how quickly this occurs were also analysed. The cells were trypsinated as before and the reappearance of Atl(glu) analysed at specific timepoints (2.17.8 for trypsination and 2.17.11-2.17.12 for immunofluorescence). 290 cells were characterised from 2 separate experiments (Figure 5.17). At 0 min no binding was seen which showed that all Atl(glu) had been removed by trypsin treatment. Atl(glu) began to reappear at low levels at 10 min but did not fully reappear until 20 min. As with Atl(ami) the reappearance was mainly as (a) dot/s (41% cells). At 20 min 94% of cells showed binding and by 30 min 100% Atl(glu). The ring binding pattern was clearly seen at 20, 30 and 60 min stages. There was also less Atl(glu) found in different planes to active growth than previously observed which again implies that Atl(glu) left behind after division remains attached.

5.2.3.4 Does Atl glucosaminidase localise to peptidoglycan features?

Half and quarter rib binding is seen frequently with Atl(ami) (Chapter 5; Figure 5.9) however Atl(glu) appears more frequently in multiple planes and therefore these structures were much harder to see. A few examples of half ribs were found but quarter ribs were not observed. Figure 5.18A -B show examples of half ribs. Figure 5.18A shows a faint line of Atl(glu) perpendicular to septal growth which is most clearly viewed at the apex of the cell.

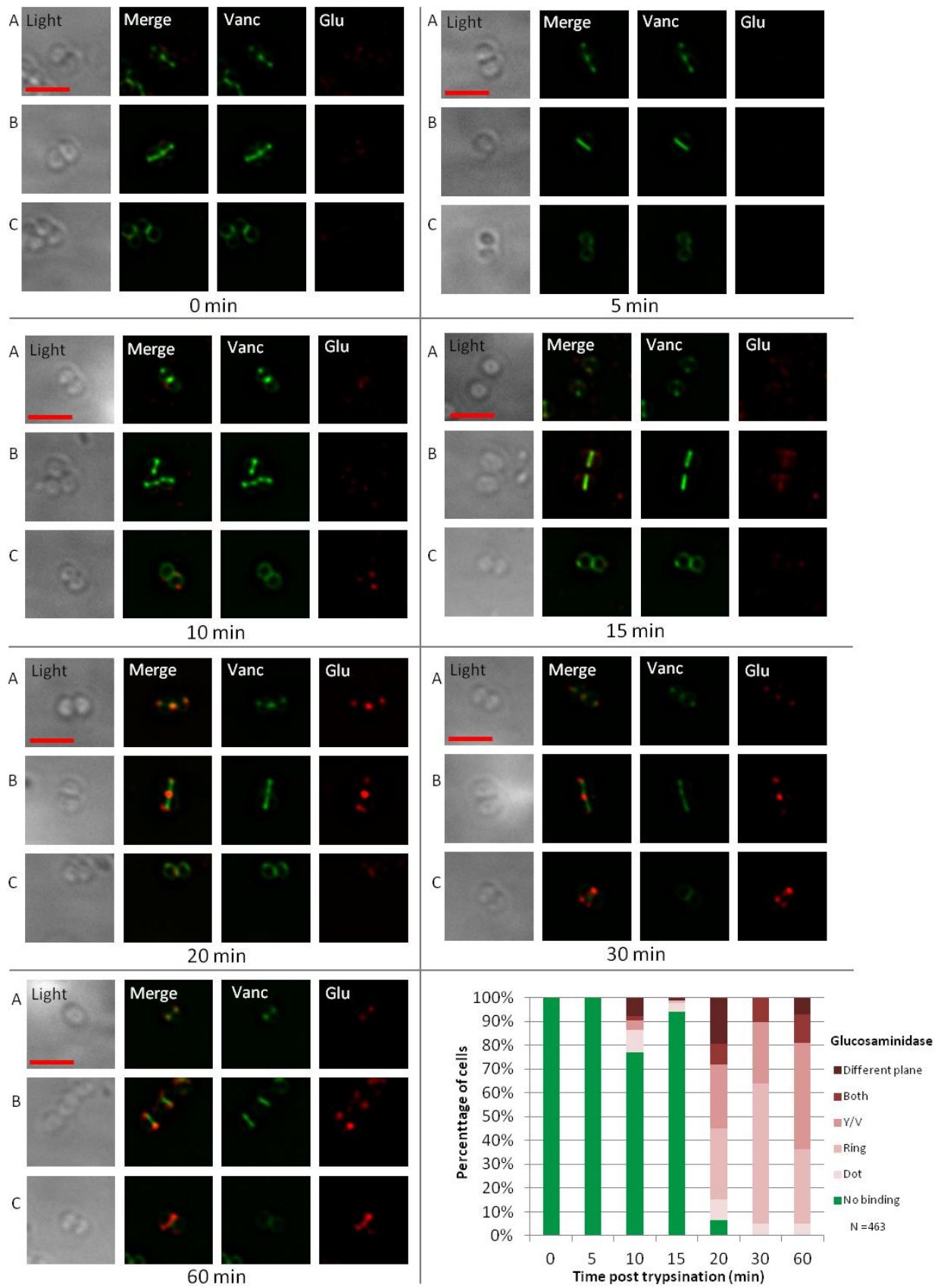


Figure 5.17 Re-emergence of Atl glucosaminidase after trypsination

Each panel shows a trypsination time point, 0-60 min from top left to bottom. Row A, shows cells beginning septal growth; Row B, shows cells with complete septal plates and Row C shows cells beginning orthogonal growth (where found). Distribution patterns were assigned one of five classes. Scale bar represents 2 μ m.

Atl(glu) reappears after 20 min and shows an array of patterns. It does not reappear in the dot/ring pattern seen with Atl(ami) but can be seen in the Y/V of later stage and in different planes of growth as soon as it begins to reappear after trypsination.

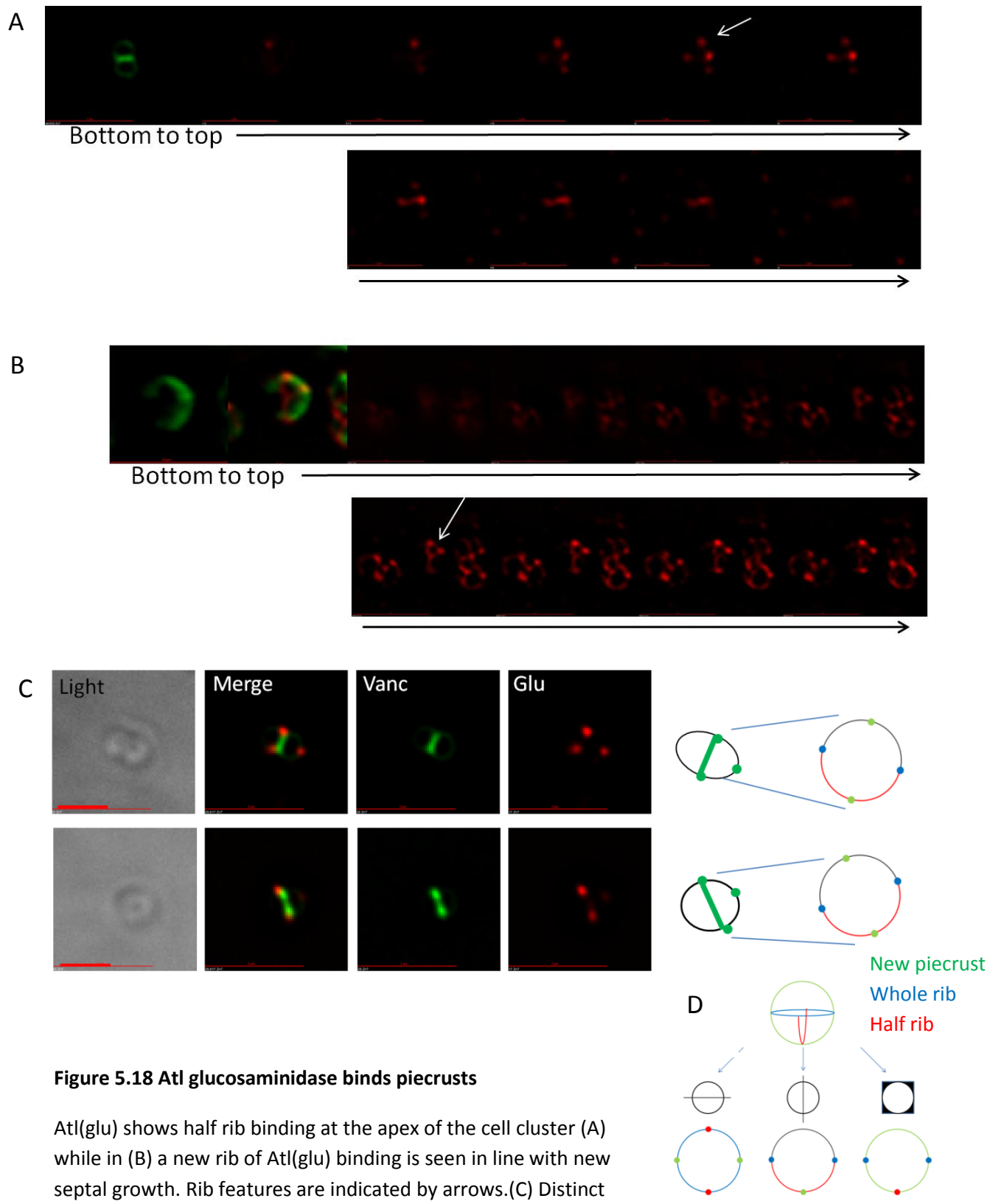


Figure 5.18 Atl glucosaminidase binds piecrusts

Atl(glu) shows half rib binding at the apex of the cell cluster (A) while in (B) a new rib of Atl(glu) binding is seen in line with new septal growth. Rib features are indicated by arrows. (C) Distinct dot patterning after trypsination is associated with one side of peptidoglycan rib features. Interpretative diagrams of the cells is shown to the right of each image and an overall diagram of the theoretical location of rib features is shown in (D).

Figure 5.18B shows the most recent plane of division as a ring of Atl(glu) around the cell, septal growth has begun in the next plane and a rib of Atl(glu) is forming starting with old peptidoglycan. By examining cells recovering from trypsination it was hypothesised that more evidence could be found however dot structures were not prevalent. As Atl(glu) began to re-emerge it formed structures in the plane of peptidoglycan synthesis and nowhere else, and dot patterns indicating piecrust localisation were not often found. Those that were seen were difficult to fit to the 'line and dot' model. When three dots were seen, two were associated with new septal growth and the third was potentially bound to one side of a whole rib (Figure 5.18C).

5.2.3.5 Atl glucosaminidase localisation in SH1000 $\Delta tarO$

The delocalisation of Atl(ami) in WTA deficient cells has previously been reported and this study saw similar results (Schlag et al., 2010). However the relationship between Atl(glu) and WTA has not previously been examined. It is likely to respond in a similar way to Atl(ami) because the absence of WTA disrupted exogenous R1-2 septal localisation. R3 of Atl(glu) shares 31% identity and ligand binding specificity (Foster, 1995; Zoll et al., 2012). Immunolocalisation was performed in the constructed strain SH1000 $\Delta tarO::ermB spa::kan$ and similar results were seen as with Atl(ami). No fluorescence was seen in controls (Figure 5.19A) and distribution was completely disrupted in the absence of WTA (Figure 5.19B and C). Atl(glu) was seen to bind across the entire cell surface however the patterning appeared hazier than in Atl(ami). No evidence of crosswall binding was seen.

5.2.4 Co-localisation of Atl amidase and Atl glucosaminidase

Whilst performing immunolocalisation of Atl(ami) and Atl(glu) it became apparent that their localisation throughout the cell cycle varies. This was reflected when comparing the statistics and models built for each enzyme (Figure 5.7 and Figure 5.16). Dual labelling of cells for both Atl(ami) and Atl(glu) would be useful to further analyse this difference. To do this monoclonal α -Atl(glu) raised in mouse were kindly donated by the Schwarz group (Varrone et al., 2011).

5.2.4.1 Co-localisation in SH1000 $spa::kan$

Cells were prepared the same as in prior immunolocalisation experiments (2.17.11-

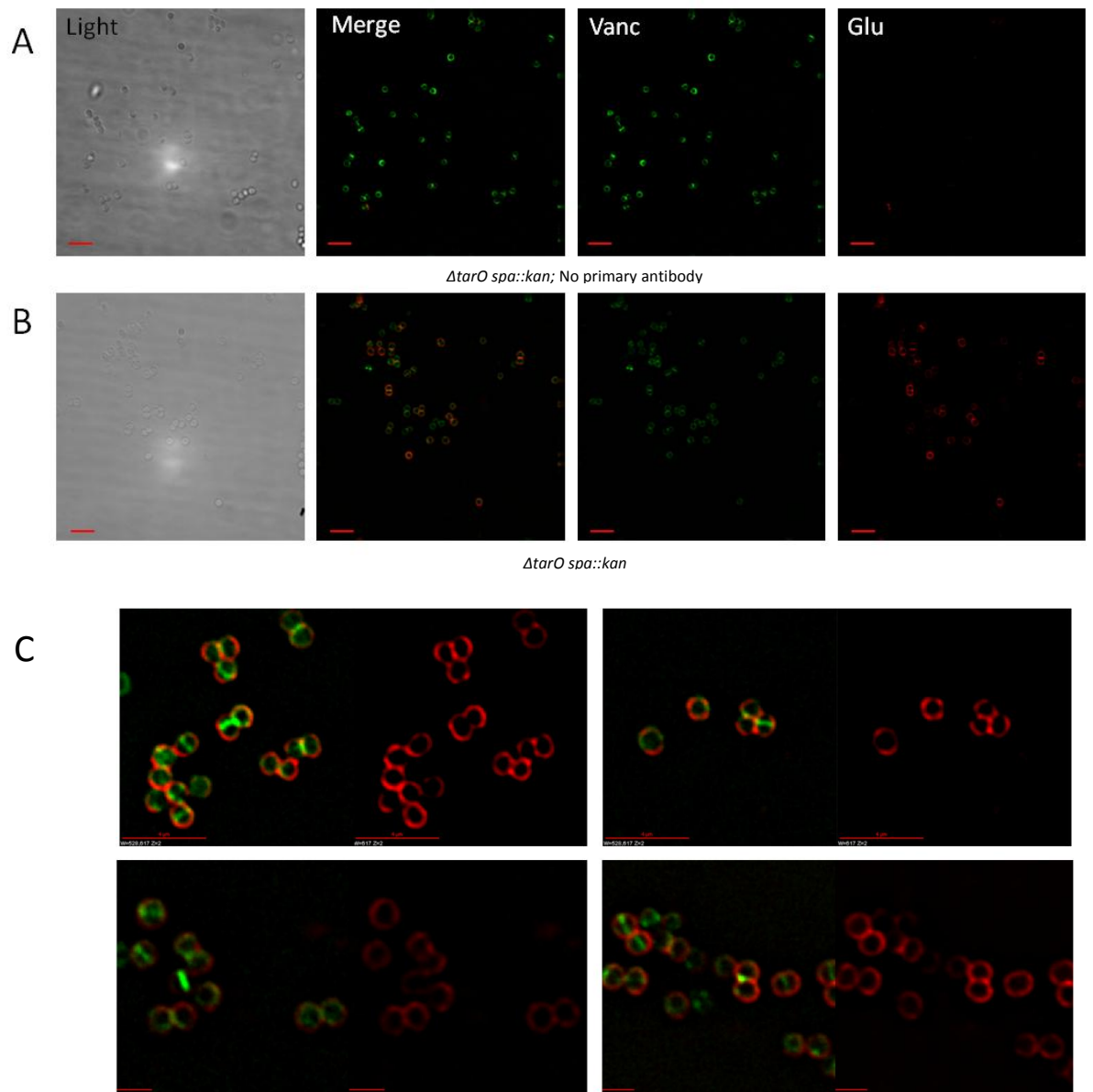


Figure 5.19 Localisation of Atl glucosaminidase in $\Delta tarO$

(A) SH1000 *tarO::ermB spa::kan* with no primary antibody, no binding is seen; (B) SH1000 *tarO::ermB spa::kan*, binding is across the entire cell surface; (C) Expanded images of SH1000 cells from separate experiments show binding across the cell surface with bright foci. Scale bar represents 4 μm .

2.17.12) with primary antibodies being applied together at 1:1000 concentration. Secondary antibodies of anti-mouse Alexa-Fluor 594 conjugate and anti-rabbit Alexa-Fluor 350 conjugate were also applied together each at a concentration of 3:1000. Merged images show Atl(ami) as blue and Atl(glu) as red, however Atl(ami) alone was saved in greyscale because the images were easier to view.

Dual labelling was not seen to affect the localisation of either antibody. Although much of the antibody localisation overlaps (seen as purple in merged images), there are still clear areas in which a specific antibody is localised (Figure 5.20B). Enlarged cells show the difference in localisation throughout the cell cycle previously observed. Figure 5.20C i shows cells with incomplete septa, Atl(glu) is seen to localise solely at the previous site of division whilst Atl(ami) is also forming rings around the current plane. When septa have completely formed (Figure 5.20C ii) Atl(glu) is found in line with current growth however Atl(ami) still has a greater presence in the current plane. Interestingly, it was observed that as cells split (Figure 5.20C iii-v) Atl(ami) appears to be on the inside of Atl(glu). Figure 5.20C iii and iv show cells splitting with both antibodies in a Y/V shape, however the binding of Atl(ami) appears narrower. Figure 5.20C v again shows cells splitting yet to commence orthogonal growth however in this instance Atl(ami) is seen as complete rings in a Y/V shape whilst Atl(glu) appears as 'double-rings' and to bind outside of Atl(ami).

Combining the previous models for each a schematic representation of the localisation of both Atl(ami) and Atl(glu) was established (Figure 5.21). As cells begin to form septa, both Atl(ami) and Atl(glu) are found predominately in the previous division plane. Atl(ami) forms a complete ring in line with the completing septa while still being found in line with previous division alongwith Atl(glu). Upon completion of the septal plate, Atl(ami) is found only in a ring at the current plane and Atl(glu) still being found in the previous plane. As Atl(ami) begins to split into a Y shape Atl(glu) is found as a ring around the septal plate. When cells move to the Y shape growth pattern, both antibodies are found in the Y shape. Atl(ami) again precedes Atl(glu) forming a V shape. As the cells then begin to further grow in preparation for splitting Atl(glu) joins Atl(ami) in a deep V shape. When the new cells begin orthogonal growth both Atls remain at the most recent plane of growth in a deep V, and as before Atl(ami) is seen at the new plane prior to Atl(glu). It is important to note that

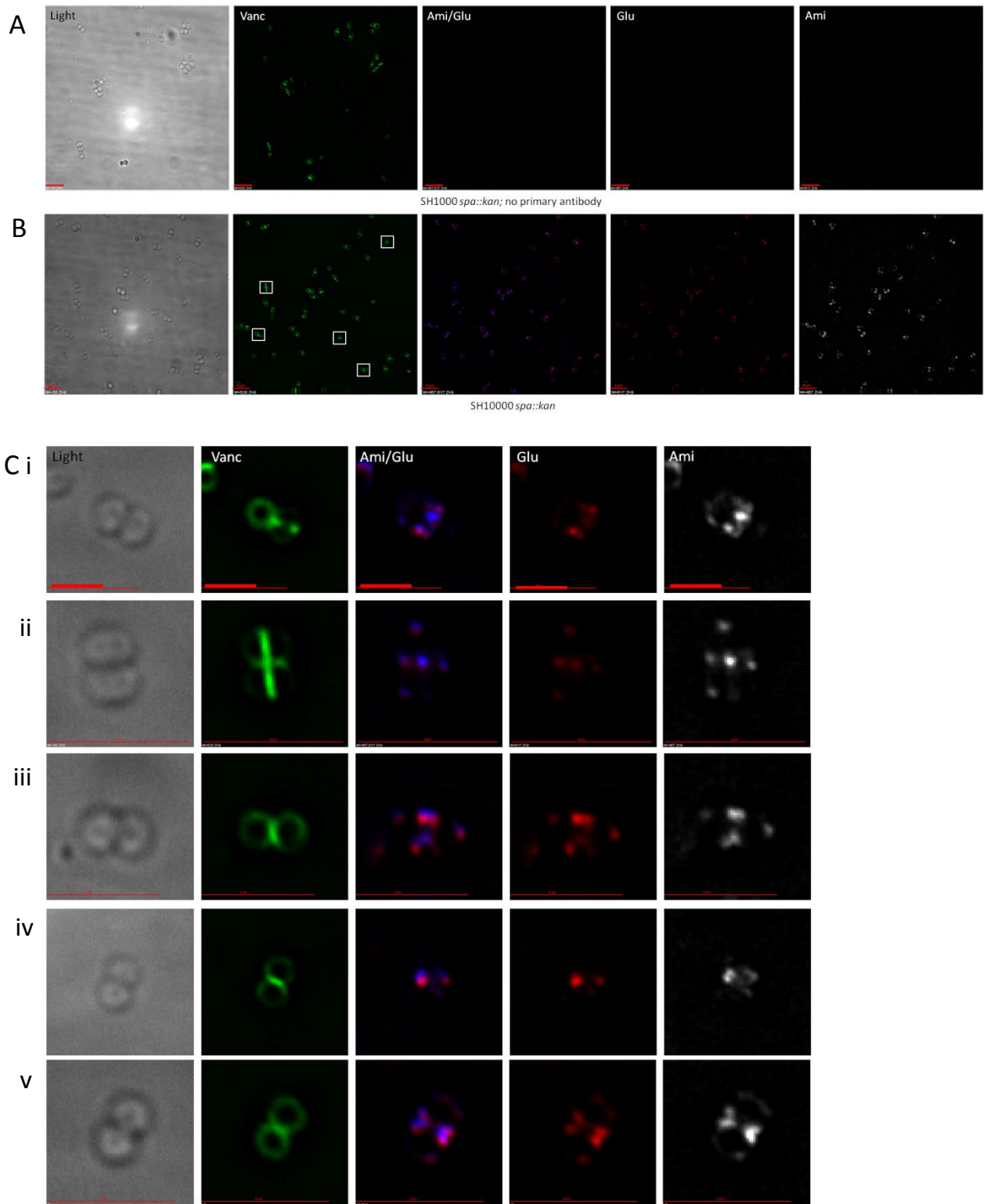


Figure 5.20 Co-localisation of Atl(ami) and Atl(glu) in SH1000 cells

(A) SH1000 *spa::kan* with no primary antibody, no binding is seen; (B) SH1000 *spa::kan*, Atl(ami) and Atl(glu) binding is seen at sites of new peptidoglycan incorporation and on the outside of cell splits; Boxes enlarged in (C). SH1000 *spa::kan* cells from separate experiments show binding of Atl(ami) and Atl(glu) in different patterns at sites of new peptidoglycan synthesis and where cells are splitting. Scale bars represent 4µm in A-B and 2µm in C.

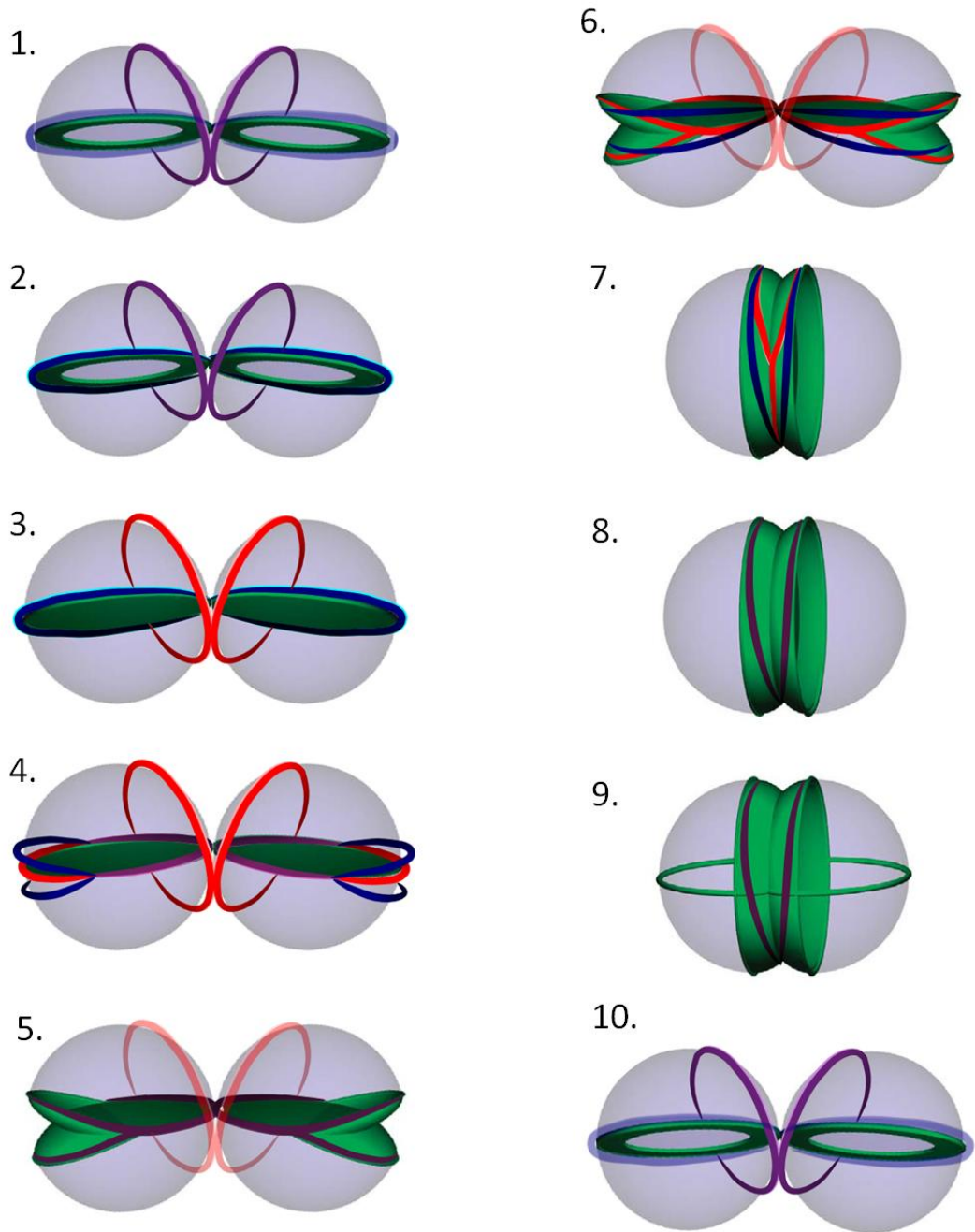


Figure 5.21 Schematic model of Atl(ami) and Atl(glu) localisation throughout the cell cycle

Atl(ami) is represented in blue; Atl(glu) is represented in red; Atl(ami) and Atl(glu) co-localisation is represented in purple. Atl(ami) is found to precede Atl(glu) localisation throughout cell growth. However both follow the same localisation pattern. Atl(ami) is found at the current plane of growth before the septal plate has completed (1-2). When the septal plate is complete, Atl(glu) forms a ring and Atl(ami) splits to form a Y shape (3-4). Atl(ami) and Atl(glu) both show Y shape localisation at the same time the cell shows Y shape growth (5). Atl(ami) forms a deep V before Atl(glu) or cell growth has progressed (6). As cell growth does progress Atl(glu) forms a deep V (7-8). Atl(ami) does not localise with orthogonal growth but its delayed (9-10).

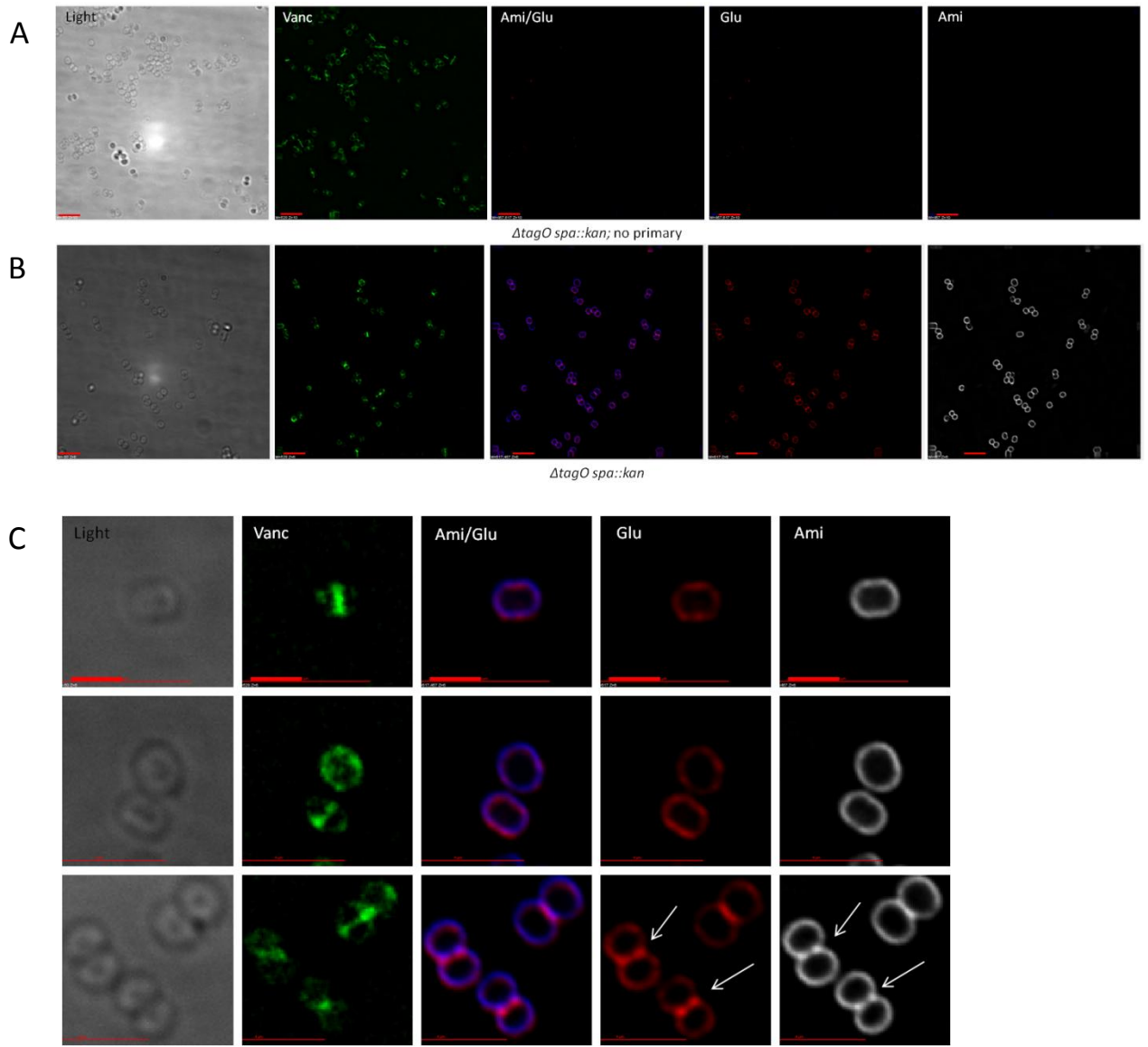


Figure 5.22 Co-localisation of Atl(ami) and Atl(glu) in $\Delta tarO$

(A) SH1000 *tarO::ermB spa::kan* with no primary antibody, no binding is seen; (B) SH1000 *tarO::ermB spa::kan*, Atl(ami) and Atl(glu) binding is seen across the entire cell surface; (C) Enlarged cells from separate experiments show binding of Atl(ami) and Atl(glu) across the cell surface with Atl(glu) binding being more patchy. Arrows indicate foci where Atl(ami) and Atl(glu) binding overlap. Scale bars represent 4 μ m in A-B and 2 μ m in C.

both Atl(ami) and Atl(glu) can be found associated with the previous plane of growth throughout the life cycle, however the amount of Atl(glu) was much greater than Atl(ami).

5.2.4.2 Co-localisation in SH1000 $\Delta tarO$

The delocalisation of both Atl(ami) and Atl(glu) in the absence of WTA was further analysed to determine if the location of bright foci revealed any details. SH1000 $\Delta tarO::ermB spa::kan$ cells were prepared for immunofluorescence as described in section 5.2.3.1. Atl(glu) was seen to contain more foci than Atl(ami) which shows a nearly completely smooth binding (Figure 5.22). The Atl(glu) patterning was patchy across the cell surface as previously seen and clearly differed from the smooth binding of Atl(ami). The few instances of Atl(ami) binding showing foci were found to be at the same site as foci in Atl(glu) binding (Figure 5.22C; white arrows indicate foci).

5.2.5 Other hydrolases (SagB, ScaH and SceD)

Similar localisation experiments were performed on other hydrolases to highlight any similarities between their localisation and that of Atl(ami) and Atl(glu), to further our understandings of specific functions.

SagB and ScaH are both glucosaminidases and SceD is a lytic transglycosylase. Within our lab antibodies against each of these had previously been raised in rabbit and mutant strains created. They were therefore deemed to be appropriate proteins to study. Mutant strains *scaH::tet* and *sceD::tet* were transduced with $\phi spa::kan$ lysate and *sa1825::kan* (SagB) was transduced with $\phi spa::tet$ lysate to make them compatible with immunofluorescence as negative controls. Transduced strains were checked with antibiotic selection and Western blots using α -protein A antibodies (shown in appendix II) and shown to be successful.

5.2.4.1 SagB localisation

Cells were prepared the same as prior immunolocalisation experiments (2.17.11- 2.17.12) with primary antibody applied at 1:1000 concentration and secondary antibody of anti-rabbit Alexa-Fluor 594 conjugate applied at 3:1000.

No fluorescence was seen in negative controls with no primary antibody (not shown) and *sagB::kan spa::tet* (Figure 5.23A). SH1000 *spa::kan* showed a punctate patterning of SagB

across the cell surface (Figure 5.23B and Figure 5.23A). In most cases this punctate pattern was regimented and extended across the entire surface. Cross-wall binding was not seen although strong foci in line with active peptidoglycan synthesis suggest SagB encircles active growth. Several clear ribs were found and T junctions (Figure 5.24Biii) could be seen, which to our knowledge are unique to peptidoglycan ribs. In many cases the dot patterning was reminiscent of the 'line and dot' model, used to imply association with rib features, and several cells could be fitted to this (Figure 5.24B). However the basic model allows a maximum of four dots and this was not the case in most cells, suggesting that they bind elsewhere also. No difference in localisation or patterning was seen in the absence of Atl (Figure 5.23C and E). However $\Delta tarO$ cells showed complete disruption of patterning with binding seen smoothly across the whole cell surface (Figure 5.23D and E). This suggests that SagB binds in a similar manner to Atl however this binding pattern is not dependent on Atl. As with Atl(ami) and Atl(glu) cells were trypsinated to remove existing SagB and allowed to recover, timepoints taken, fixed and stained (2.17.8 for trypsination and 2.17.11-2.17.12 for immunofluorescence) (Figure 5.25). SagB began to reappear at 10 min but only 29% showed binding and it wasn't until 20 min when 88% were labelled. It emerged most often in line with active peptidoglycan synthesis either as a single dot or a ring. Rarely, SagB was seen perpendicular to the active plane of growth in dots.

5.2.4.2 ScaH localisation

Cells were prepared the same as in prior immunolocalisation experiments (2.17.11-2.17.12) with primary antibody applied at 1:1000 concentration and secondary antibody of anti-rabbit Alexa-Fluor 594 conjugate applied at 3:1000.

No fluorescence was seen when no primary antibody was added (not shown) or in *scaH::tet spa::kan* cells (Figure 5.26A). SH1000 *spa::kan* cells showed a punctate pattern of binding across the entire cell surface which looked to be similar to that of SagB (Figure 5.26B and Figure 5.27). However the punctate pattern was less regimented with strong foci unequally distributed across the surface. Furthermore unlike SagB, cross-wall binding was seen in many cases (Figure 5.27A) and the 'line and dot' model could not be easily assigned to cells. However ribs were distinguished in a number of cases (Figure 5.27B). Localisation was slightly disrupted in Δatl *spa::kan* cells, with binding appearing slightly clearer and slightly

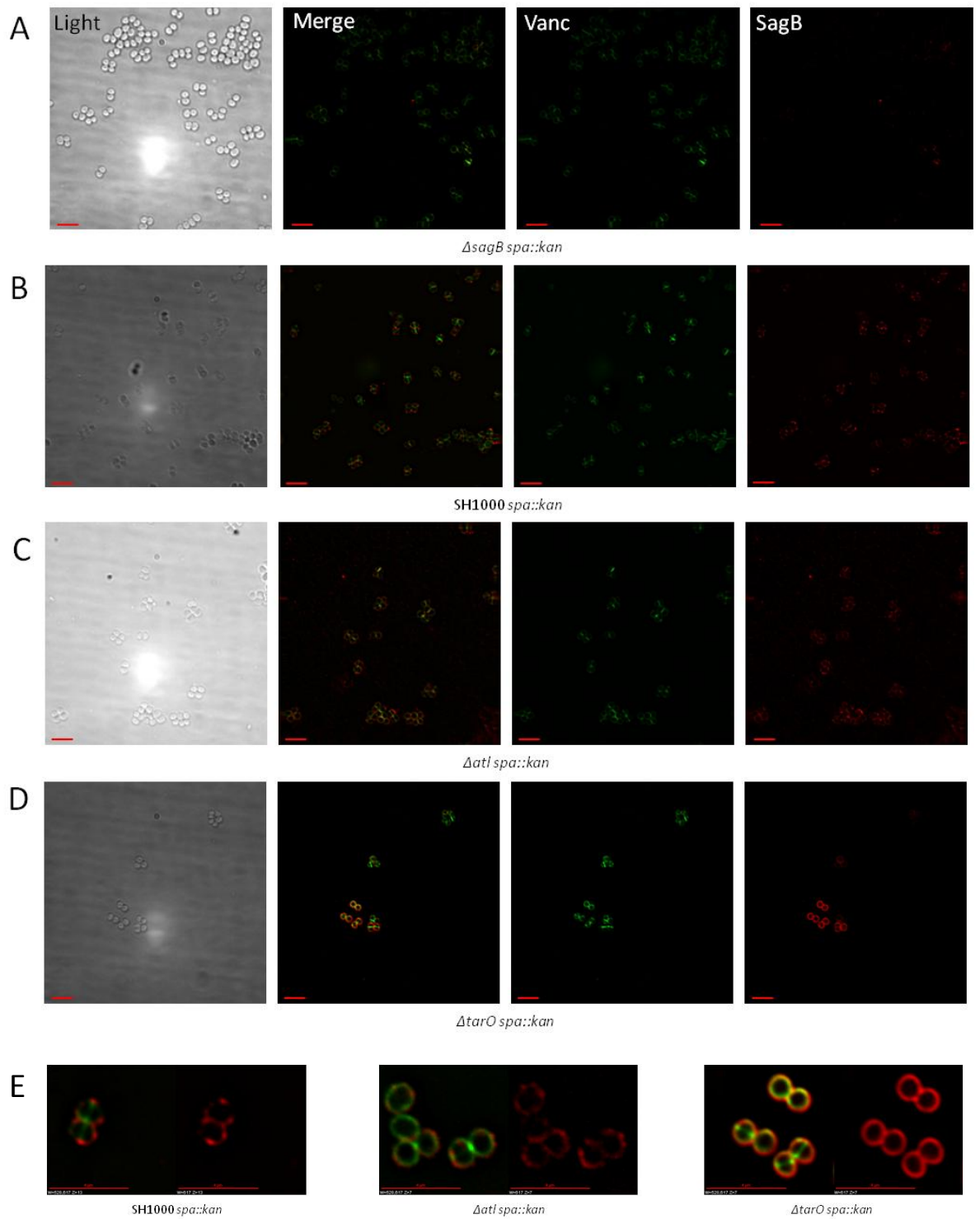


Figure 5.23 Localisation of SagB

(A) *sagB::kan spa::tet* no longer produces SagB, no binding is seen (B) SH1000 *spa::kan*, binding is seen in a punctate pattern across the entire cell surface; (C) *Δatl spa::kan* cells show similar binding patterns to WT cells. (D) *ΔtarO spa::kan* cells show complete disruption of the binding patterns. (E) Enlargements of SagB localisation in each strain show differences in binding patterns. Scale bar indicates 4 μ m

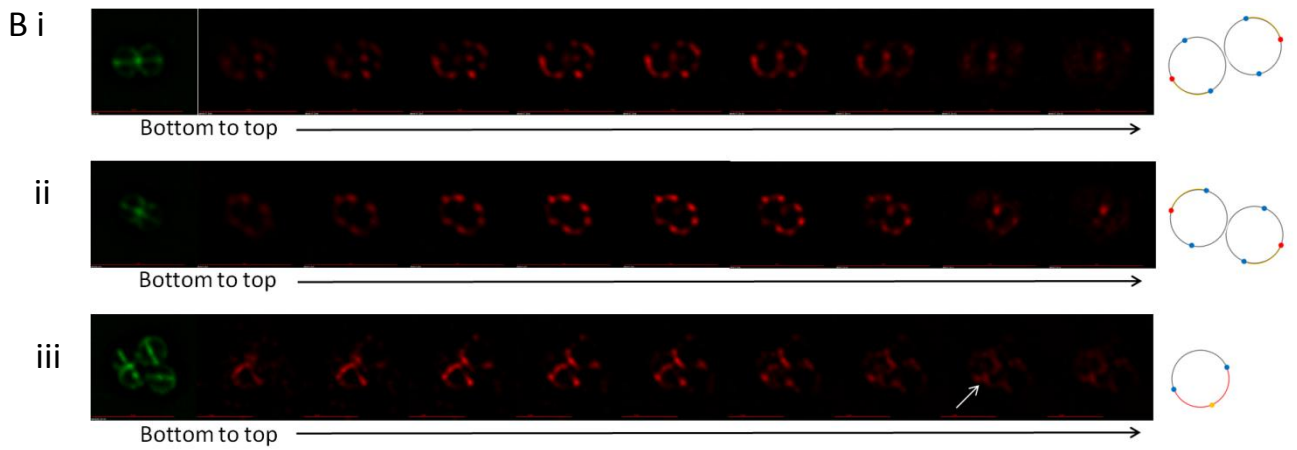
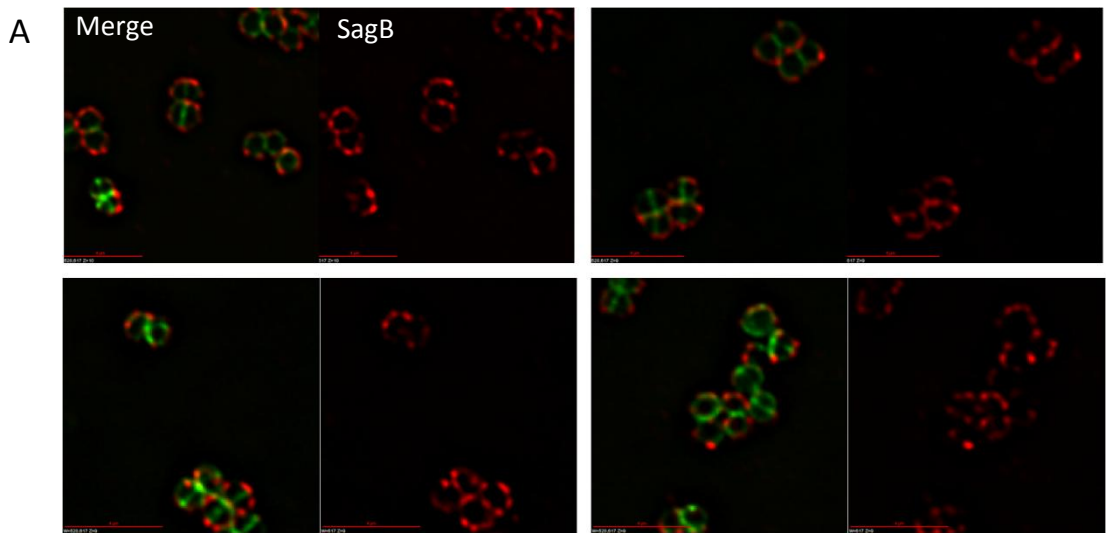
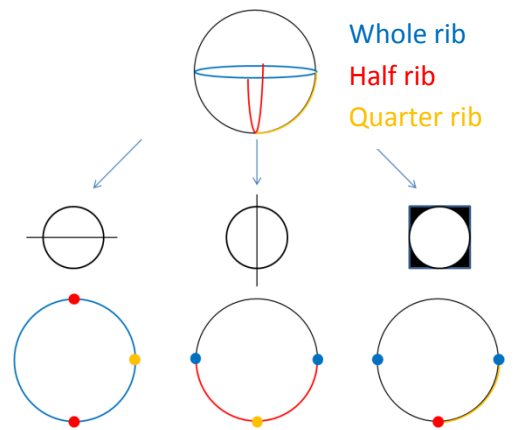


Figure 5.24 SagB localisation pattern

(A) Expanded images of SagB localisation in SH1000 *spa::kan* show the punctate patterning, reminiscent of 'line and dot' model but more disordered. No cross-wall binding is seen but strong foci are seen in line with peptidoglycan synthesis. (B) Z stacks of cells showing matched line and dot model schematics. (Biii) shows a clear rib and T junction. Matched models are shown to the right of images and an overall diagram of the location of rib features is shown in (C). Note in this case vancomycin labelling was not used to guide the 'line and dot' model because quarter ribs were seen.



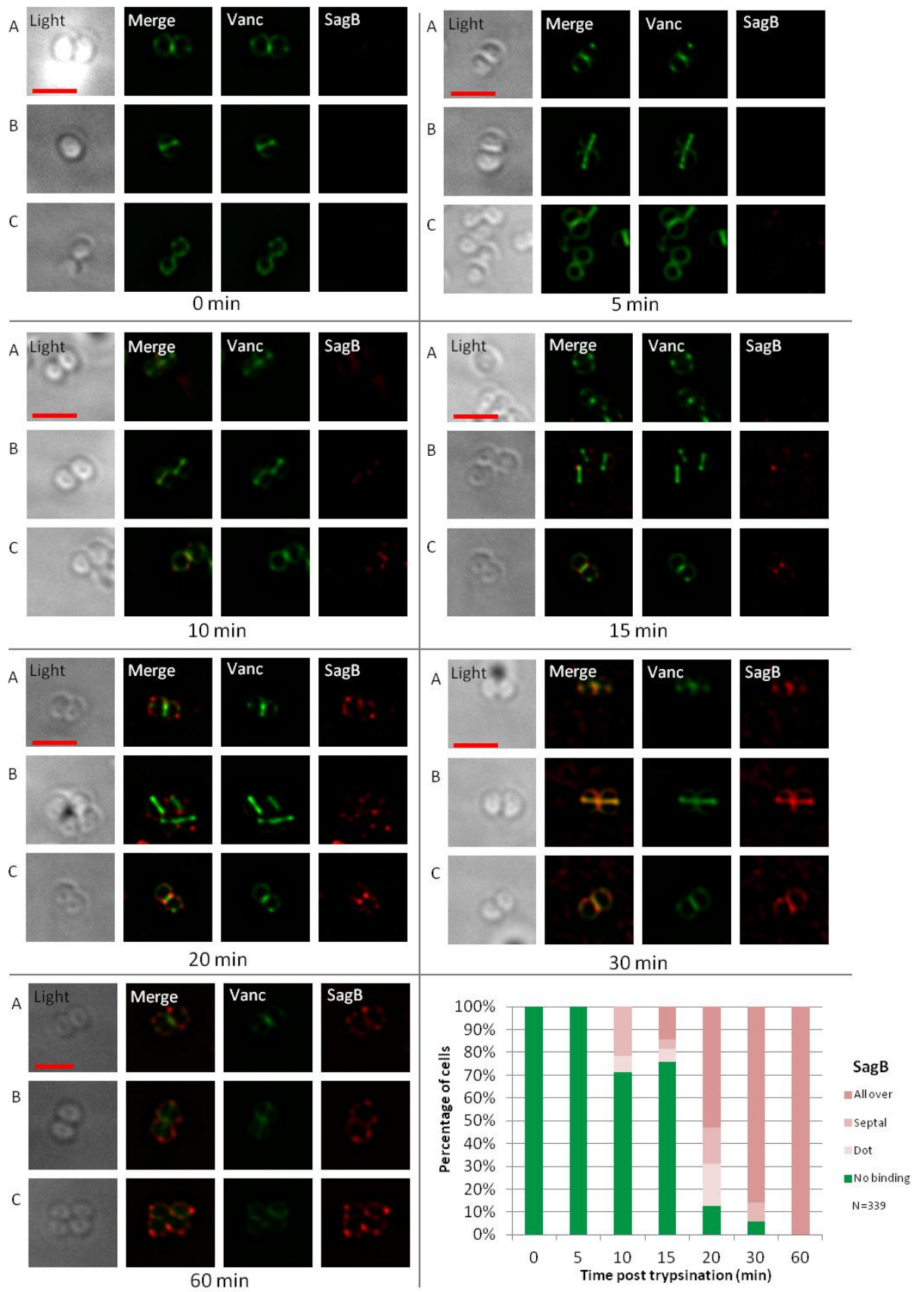


Figure 5.25 Re-emergence of SagB after trypsination

Each panel shows a trypsination time point, 0-60 min from top left to bottom. Row A, shows cells beginning septal growth; Row B, shows cells with complete septal plates and Row C shows cells beginning orthogonal growth (where found). Distribution patterns were assigned one of three classes. Scale bar represents 2 μ m.

SagB began to reappear after 10 min, primarily at the septum or as a dot. Cells are very quickly show SagB localisation across the entire cell surface.

more extensive across the cell surface.

When cells were trypsinated and labelled for ScaH re-emergence (2.17.8 for trypsination and 2.17.11-2.17.12 for immunofluorescence), it was seen to emerge more rapidly than SagB (Figure 5.28). At 10 min 11% of cells showed labelling and by 15 min 100% of cells were labelled whilst in SagB 29% showed labelling at 10 min but all cells were not labelled until 60 min. Furthermore very few cells showed dot labelling and only slightly more showed septal labelling, cells appeared to express ScaH across the entire cell surface.

5.2.4.3 SceD localisation

Cells were prepared the same as in prior immunolocalisation experiments (2.17.11-2.17.12) with primary antibody applied at 1:1000 concentration and secondary antibody of anti-rabbit Alexa-Fluor 594 conjugate applied at 3:1000. No fluorescence was seen when no primary antibody was added (not shown) or in *sceD::tet spa::kan* cells (Figure 5.29A). SH1000 *spa::kan* cells showed binding across the entire cell surface in a hazy pattern, with irregular bright foci within the binding and very few gaps (Figure 5.29B and Figure 5.30A). The bright foci were often in line with new peptidoglycan synthesis but not in all case and cross-wall binding was seen (Figure 5.30). Localisation was not disrupted in Δatl *spa::kan* cells and was very similar to that of WT cells (Figure 5.29C). The absence of WTA only had a mild effect, making the binding smoother (Figure 5.29D).

As before cells were trypsinated to observe SceD re-emergence (2.17.8 for trypsination and 2.17.11-2.17.12 for immunofluorescence)(Figure 5.31). Unfortunately trypsination was not complete in this experiment as 18% of cells at 0mins still showed binding however several inferences can still be drawn. Labelled cells at 0mins showed septal or dot labelling which suggests that cells were aggregated during the incubation and contact surface remained un-trypsinated. Cells are vortexed before dried onto slides revealing the un-trypsinated surfaces. Re-emergence of SceD was more rapid than all other hydrolases studied as only 2% of cells remained unlabelled after 5mins and all cells were labelled by 10mins. The majority of cells showed all over binding, however septal localisation and dot labelling were both seen at early as well as late timepoints.

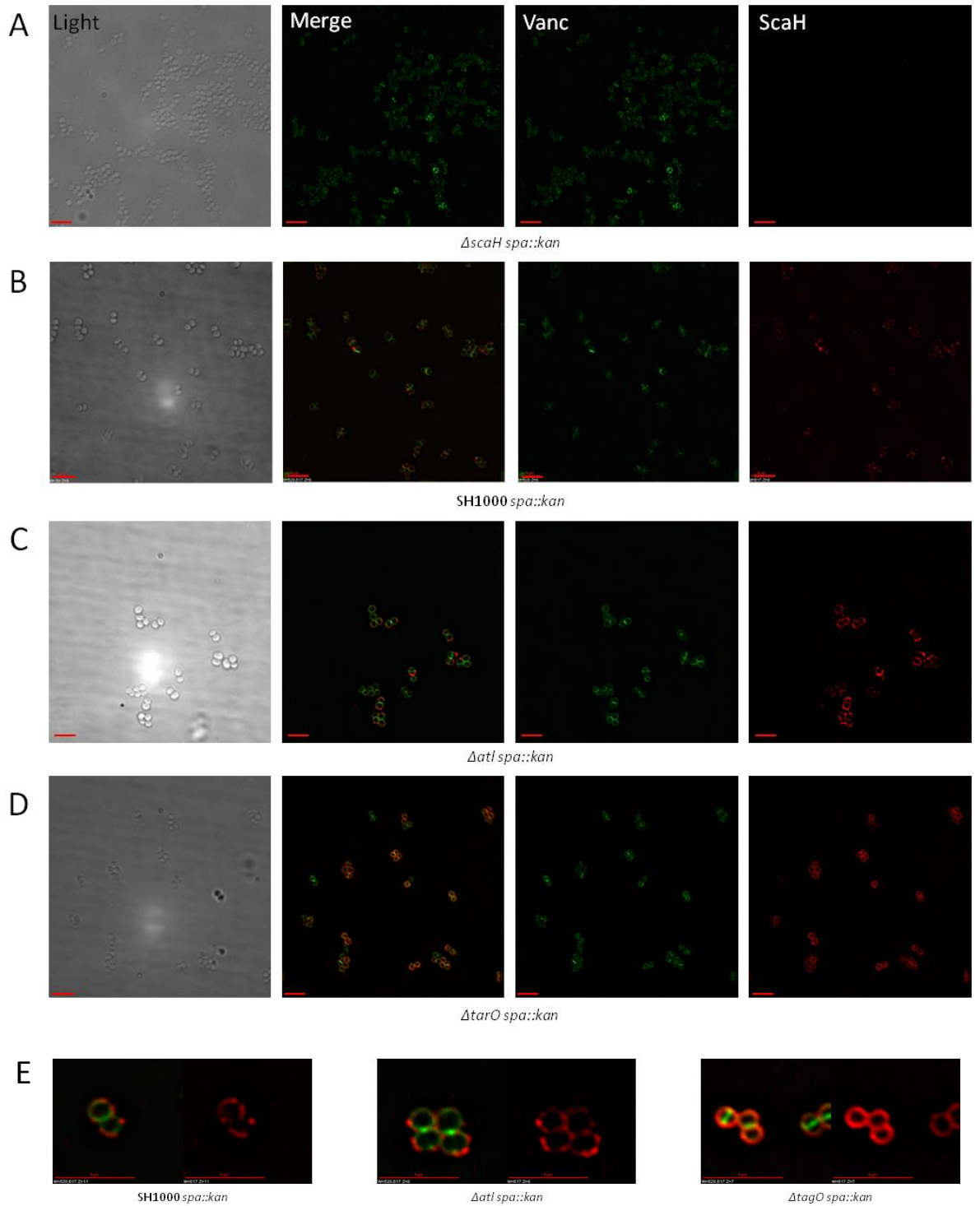


Figure 5.26 Localisation of ScaH

(A) $\Delta scaH spa::kan$ no longer produces ScaH, no binding is seen (B) SH1000 $spa::kan$, binding is seen in a punctate pattern across the entire cell surface similar to that of SagB; (C) $\Delta atl spa::kan$ cells show similar binding patterns to WT cells. (D) $\Delta tarO spa::kan$ cells show complete disruption of the binding patterns. (E) Enlargements of ScaH localisation in each strain showing differences. Scale bar indicates 4 μm .

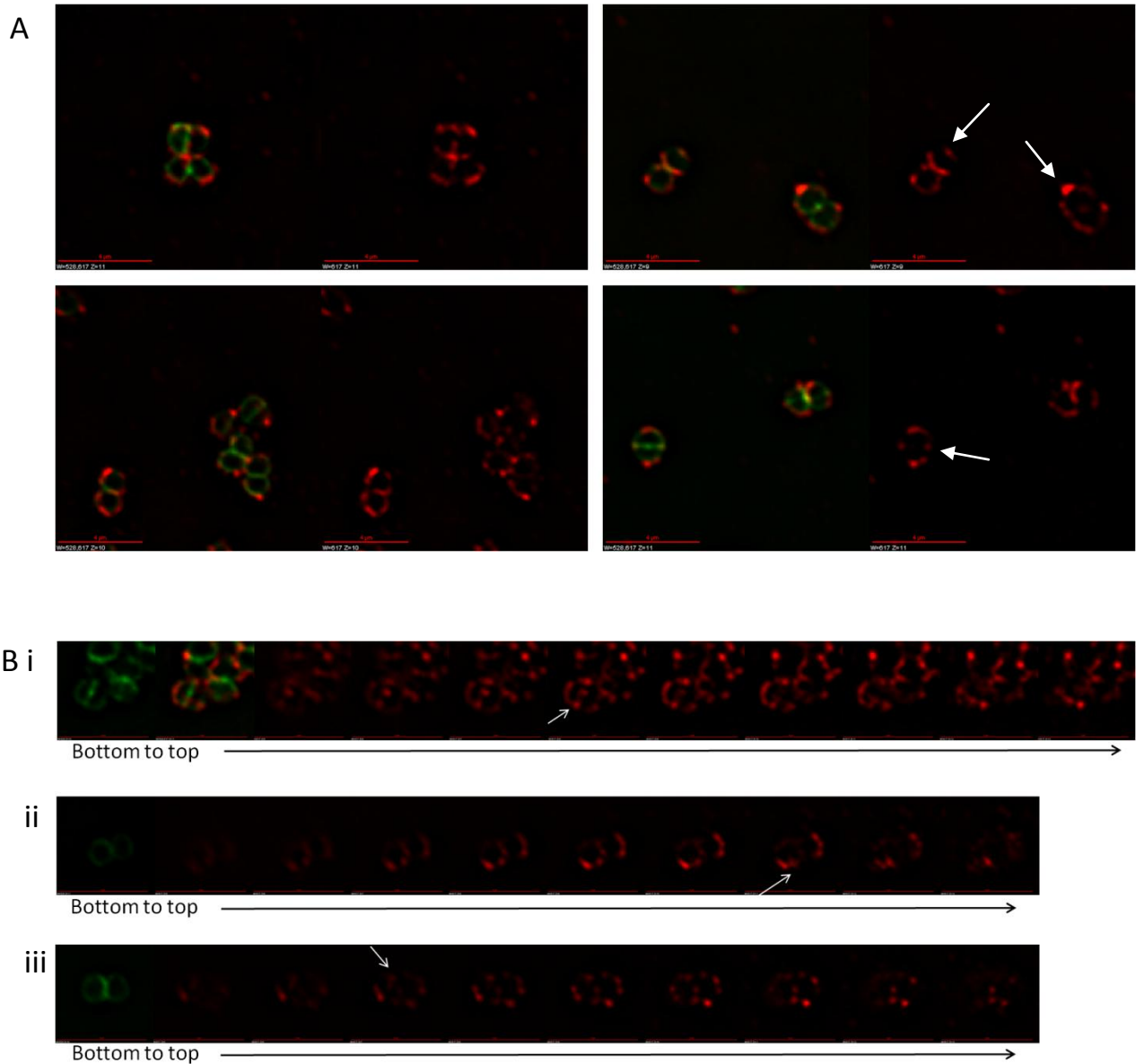


Figure 5.27 ScaH localisation pattern

(A) Expanded images show binding reminiscent of the 'line and dot' model but more disordered. No cross-wall binding is seen but strong foci are seen in line with peptidoglycan synthesis (arrows); (B) Z stacks of cells show the presence of ribs (indicated with arrows); (Bi) shows a T junction; (Bii) shows a quarter rib; (Biii) shows a quarter rib and shows a clearly defined punctate pattern.

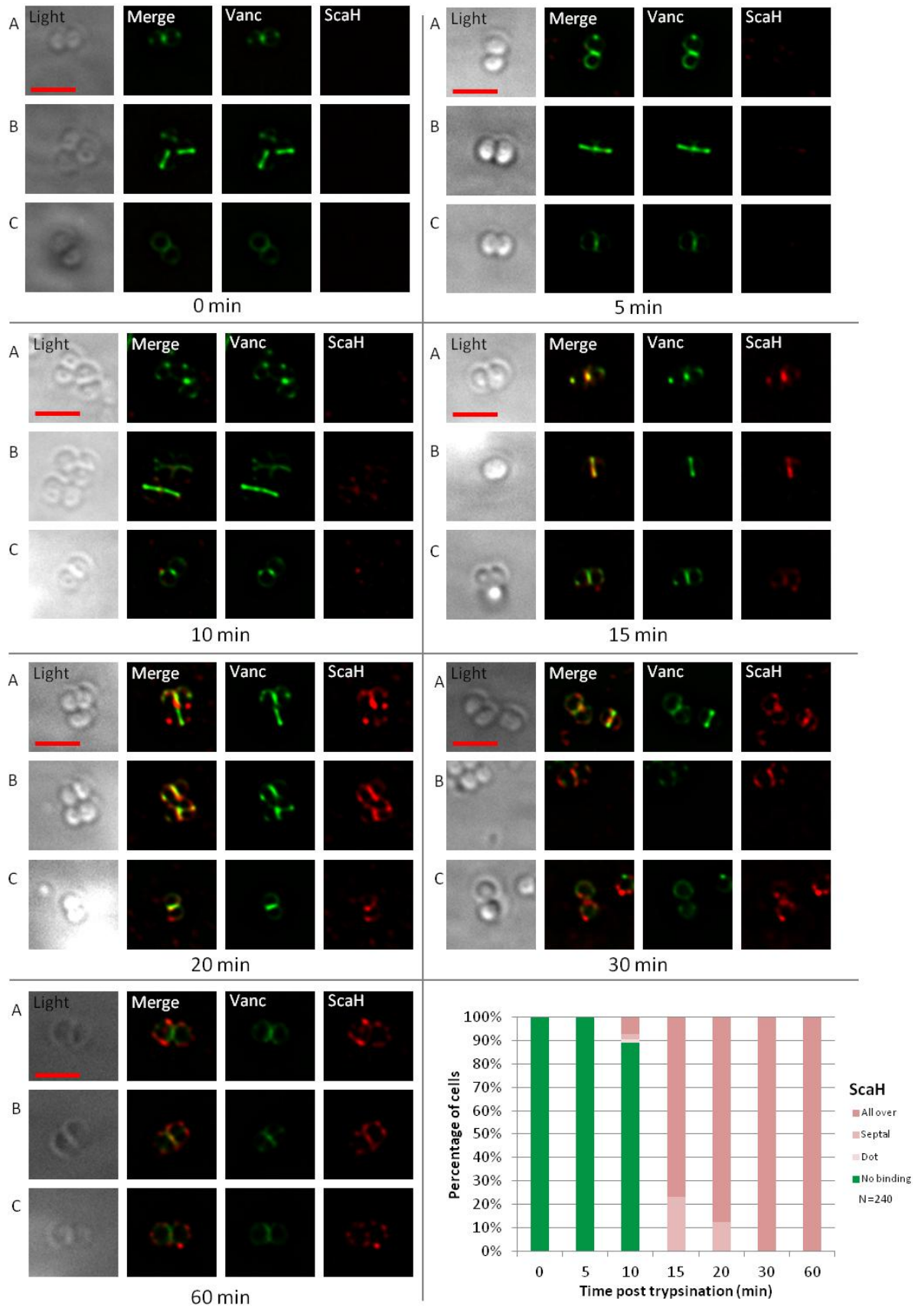


Figure 5.28 Re-emergence of ScaH after trypsination

Each panel shows a trypsination time point, 0-60 min from top left to bottom. Row A, shows cells beginning septal growth; Row B, shows cells with complete septal plates and Row C shows cells beginning orthogonal growth (where found). Distribution patterns were assigned one of three classes. Scale bar represents 2 μ m.

ScaH begins to reappear at 10mins and all cells are labelled by 15mins. Very few cells showed dot patterning (1.5%) and only at 10mins. Septal localisation was seen at 10, 15 and 20 min but only in small amounts. The majority of labelling was all over the cell surface.

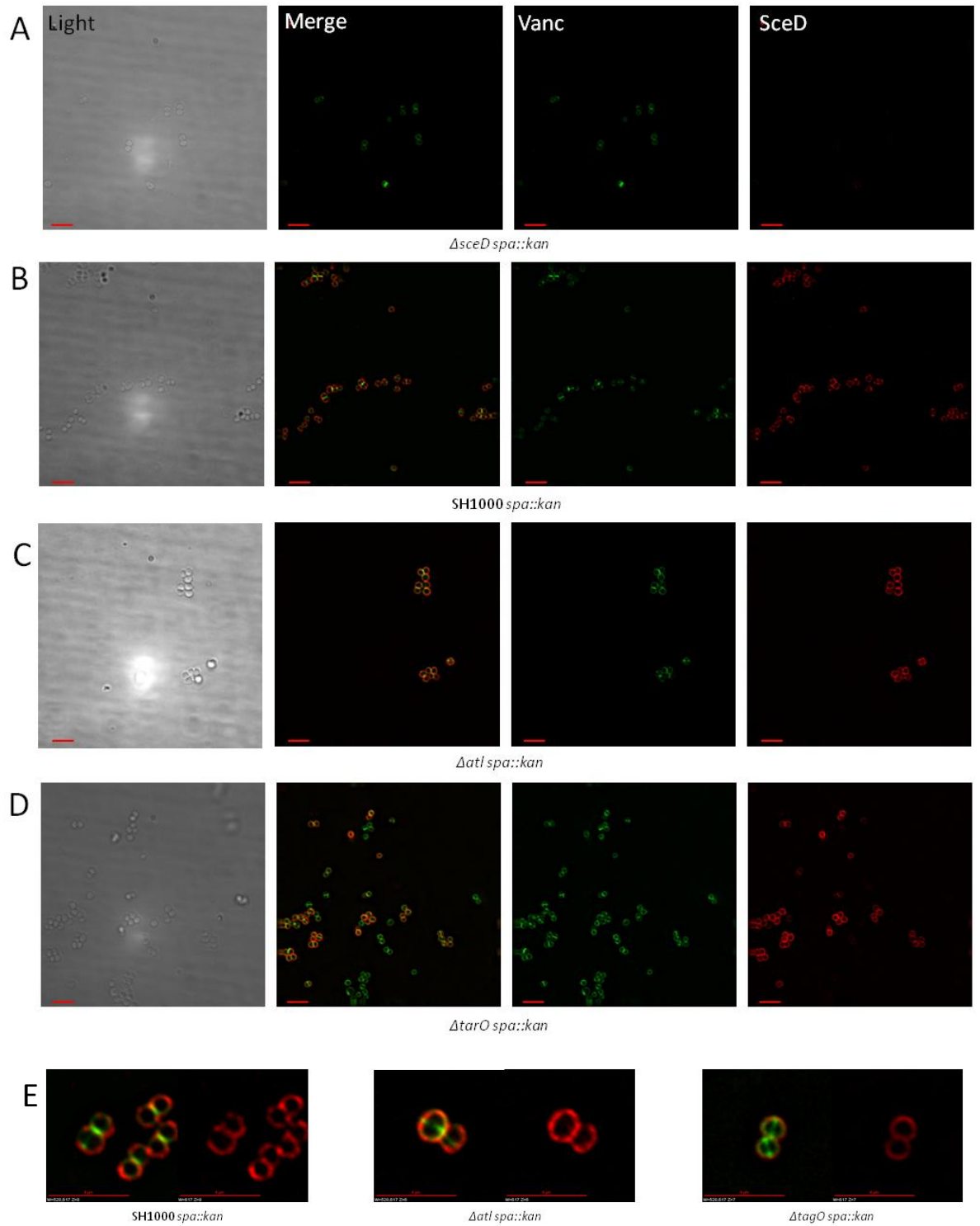


Figure 5.29 Localisation of SceD

(A) *sceD::kan spa::tet* no longer produces SceD, no binding is seen (B) SH1000 *spa::kan*, binding is seen across the entire cell surface with irregular bright foci; (C) $\Delta atl spa::kan$ cells show similar binding patterns to WT cells but slightly hazier. (D) $\Delta tarO spa::kan$ cells show complete binding to the entire cell surface which is smoother than WT cells. (E) Enlargements of SagB localisation in each strain show the differences in binding patterns. Scale bar indicates 4 μm .

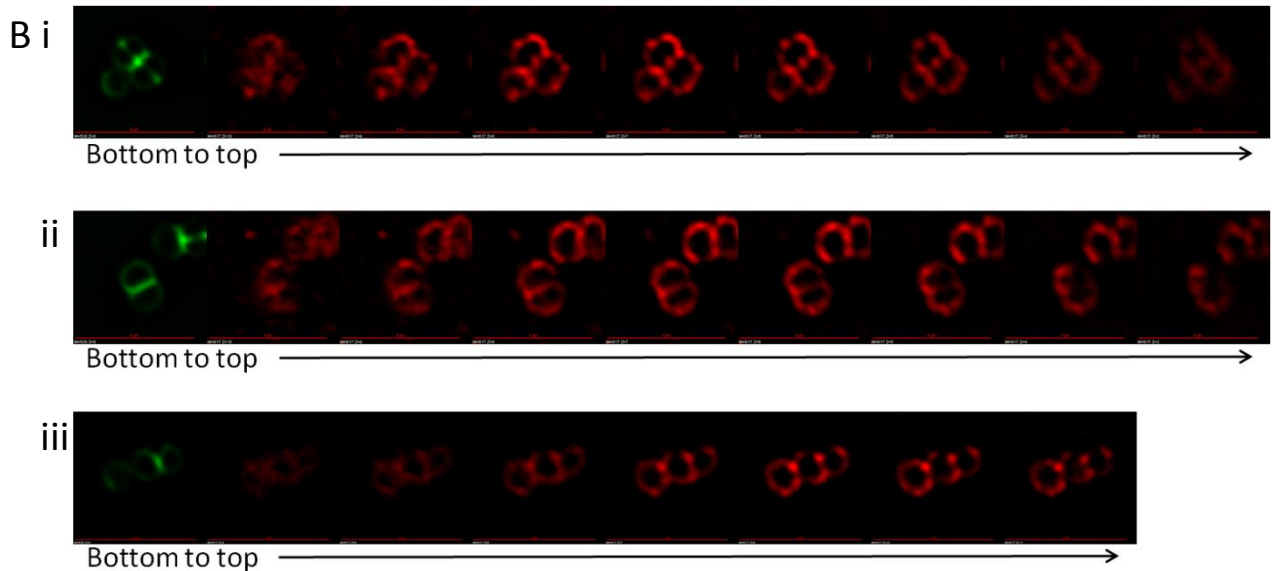
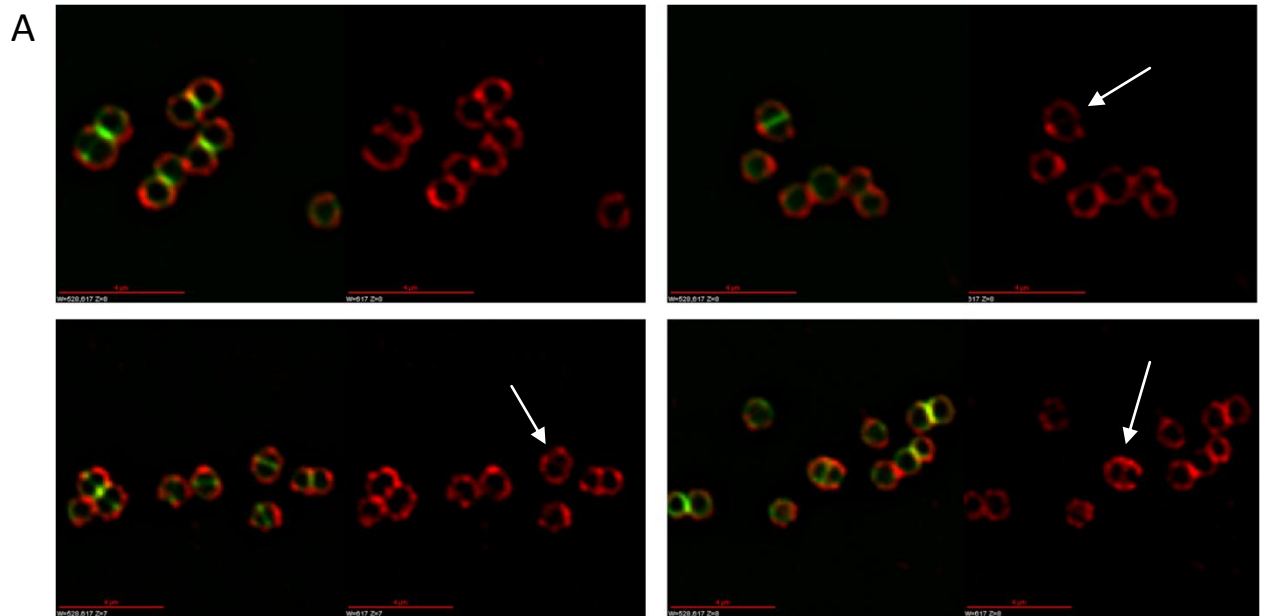


Figure 5.30 SceD localisation patterns

(A) Enlarged images show hazy binding which covers the entire cell surface. Cross-wall binding is seen in a number of cases (arrows) and strong foci are often in line with peptidoglycan synthesis; (B) Z stacks of cells from bottom to top showing binding around the entire cell; (Bi) Strong foci are in line with peptidoglycan synthesis; (Bii) Clear cross-wall binding; (Biii) Strong foci are not always in line with peptidoglycan synthesis.

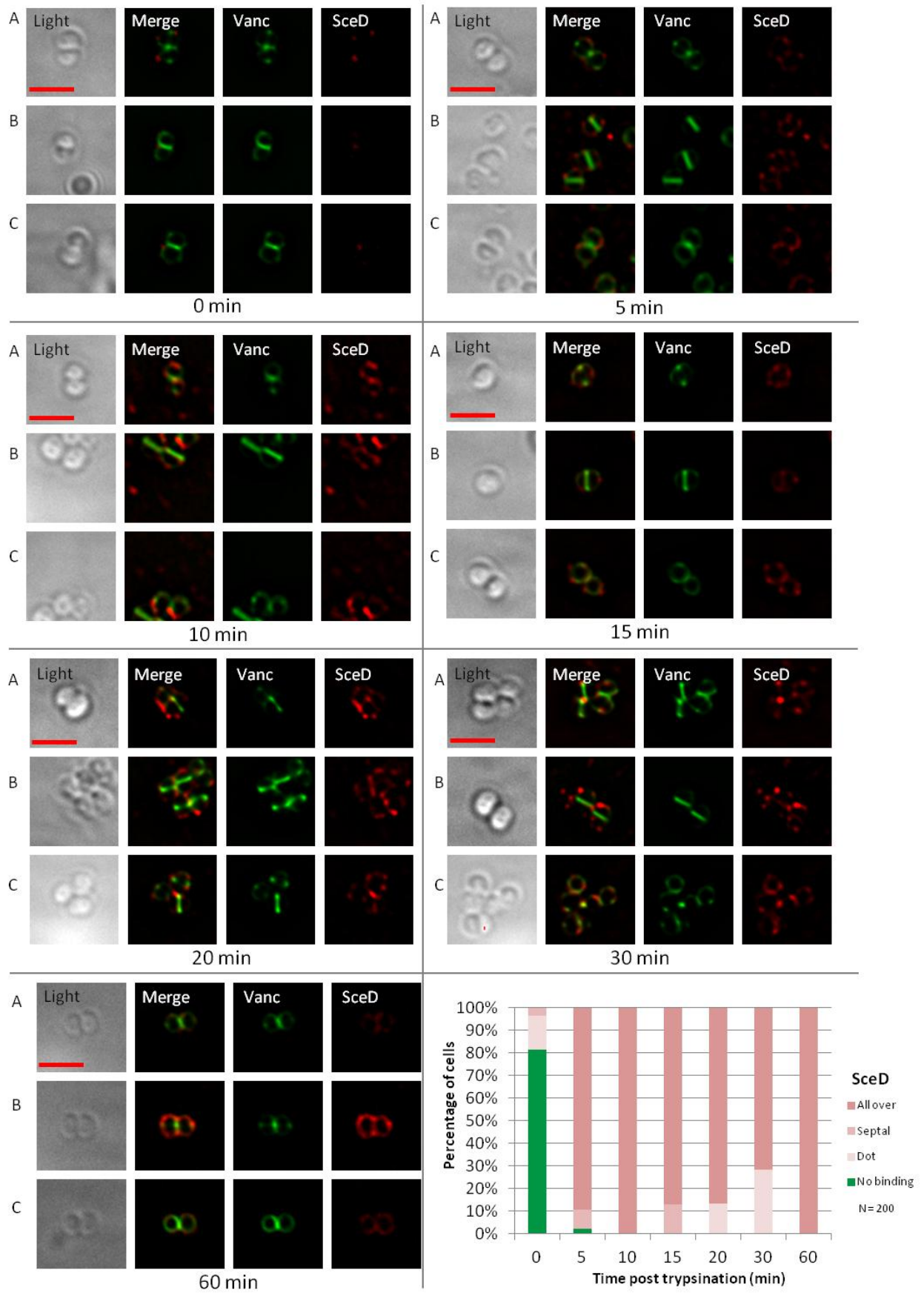


Figure 5.31 Re-emergence of SceD after trypsination

Each panel shows a trypsination time point, 0-60 min from top left to bottom. Row A, shows cells beginning septal growth; Row B, shows cells with complete septal plates and Row C shows cells beginning orthogonal growth (where found). Distribution patterns were assigned one of three classes. Scale bar represents 2 μ m.

SceD trypsination was incomplete as binding is seen at 0 min. However almost all cells (97.6%) showed labelling at 5mins and predominately across the whole cell surface.

5.3 Discussion

Yamada *et al.*, (1996) extensively studied the localisation of Atl amidase and glucosaminidase using immunoelectron microscopy. They described a 'double-ring-like' structure forming prior to complete septum formation and division. This double-ring was seen to split into two as the cells divide ending as mirror images at the marginal regions of two adjacent cells. They described a 'ribbon-like' arrangement from former cell divisions and proposed a cell-cell separation model (Figure 5.32) (Yamada *et al.*, 1996). Both Atl(ami) and Atl(glu) have been confirmed as binding staphylococcal cell wall (Komatsuzawa *et al.*, 1997; Schlag *et al.*, 2010) and the specific septal localisation of Atl(ami) studied by Schlag *et al.*, (2010). Here we also observed septal localisation of Atl(ami) and Atl(glu) as rings. We observed that as cells split the rings of Atl split to a Y and then to a V shape. We did not observe two completely separate rings as the cells were splitting. On occasion Atl(glu) showed an almost 'double-ring' however they remained in contact at one side of the splitting cells at all times. It is possible that the rings seen surrounding the septum are double width and that limitations in the resolution of the deltatvision microscope is unable to detect this. However when using the higher resolution STORM microscope the Atl(ami) line of binding appeared to only be a single fluorophore wide. It is therefore more likely that more Atl is produced as the cell and its site of attachment splits. The cell-cell separation model also implies that cell separation occurs simultaneously from both sides of the dividing cells. An X shaped binding pattern would indicate this and was not observed at any point with either antibody. It is likely that pits are made into the completed septum by Atl(ami) and Atl(glu) leading to instability and physical splitting from a single point of weakness.

What are the sites of attachment? Yamada *et al.*, (1996) noted that the gold particles used to detect Atl(glu) were not attached directly to the dense rim of the cell wall. The particles were an average distance of 20-50nm from the cell rim and appeared to be associated with fibrous material extending from the cells. Although they found colocalisation difficult, a potential candidate of LTA was proposed (Yamada *et al.*, 1996). This has been supported by evidence that R1 and R2 can bind LTA, which lead to a model whereby Atl(ami) is readsorbed by LTA as it hydrolyses through the septum (Zoll *et al.*, 2012). This model does not account for the ring structures which remain at marginal regions. Work within our lab

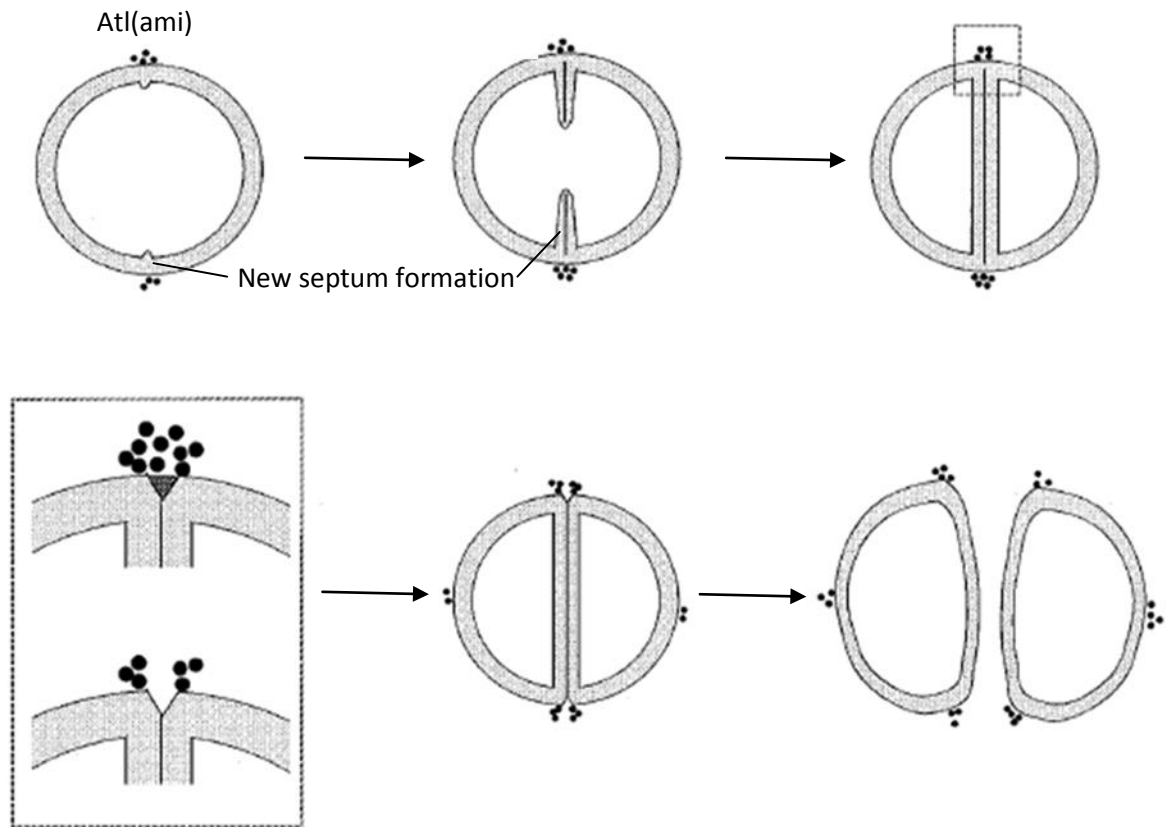


Figure 5.32 Cell-Cell separation model (adapted from Yamada *et al.*, 1996)

Yamada *et al.*, (1996) propose the *atl* gene products form a ring structure on the cell surface at a potential septal site where processing of the Atl protein presumably takes place. Following the completion of the septum formation, mature forms of Atl(ami) and Atl(glu) start to digest the peripheral peptidoglycan connecting the daughter cells. Completion of separation produces two daughter cells which have already started to align the *atl* gene products at the site of the new septum formation (Yamada *et al.*, 1996).

has established that *S.aureus* lays down a thick piecrust (Chapter 1.6; Figure 1.7) before completion of the septal plate. As the cells divide this piecrust is split in two and half is inherited by each daughter (Turner *et al.*, 2010). This concurs with Atl(ami) localisation and to a lesser extent Atl(glu). Indeed when looking at Z stacks of Atl localisation, examples of rib and piecrust features can be found. Furthermore when analysing dot patterns seen as either Atl re-emerged after trypsination they could often be fitted to the 'line and dot' model, which has been used to show piecrust localisation (Bottomley, 2011). Binding was seen as a quarter rib in line with new peptidoglycan growth in cases of both Atl(ami) and Atl(glu) (Figure 5.9A and Figure 5.18Aii). As a current plane, a new piecrust would have formed however the binding is seen in old peptidoglycan. It is unlikely that the Atl has remained attached for the previous three generations and indeed this is not seen. Thus Atl is likely newly binding the quarter rib from previous generations made more prominent by the formation of the new piecrust underneath.

In this study cells were labelled with vancomycin so that cell cycle stages could be assigned to binding patterns. This allowed us to build up models of how both Atl(ami) and Atl(glu) localise throughout the cell cycle (Figure 5.7 and Figure 5.16 respectively). Comparison of these models and colocalisation studies allowed us to distinguish a slight shift in localisation of the two hydrolases throughout the cell cycle (Figure 5.21). It appears as though Atl(glu) localises later than Atl(ami) to septal regions. Furthermore comparison of the re-emergence of each hydrolase after complete trypsination showed that they have different timings. Atl(ami) took 10 min to reappear whilst Atl(glu) took 20 min. This difference in re-emergence and cell cycle timing is surprising as both hydrolases are expressed together as a propeptide before their joint signal sequence is cleaved and further external processing forms the enzymes, Ami-R1-R2 and R3-Glu (Heilmann *et al.*, 2003, 1997). Studies have shown that the repeat regions are responsible and sufficient for the targeting of the enzymes to the septal region (Baba and Schneewind, 1998; Schlag *et al.*, 2010; Zoll *et al.*, 2012). Atl(glu) only has one repeat region it is therefore possible that it is less sensitive to the piecrust than Atl(ami).

Colocalisation of Atl with the peptidoglycan rib features using STORMForce was hampered by time constraints for this thesis. However preparatory work for this new microscope began with STORM protocol refinement. Unfortunately efforts to get images were largely

unsuccessful, primarily due to a high background level which attempts to resolve resulted in no significant binding.

More Atl and differently processed Atl forms were observed to bind the cell wall in SA113 $\Delta tarO$ strains (Schlag *et al.*, 2010). This leads to the observation that Atl(ami) loses its septal localisation in the absence of WTA (Schlag *et al.*, 2010). This localisation has been attributed to the repeat regions and they too were observed to be better recruited in a $\Delta tarO$ strain (Schlag *et al.*, 2010). Furthermore externally applied Atl repeat regions were shown to localise separately to WTA and bind uniformly in a WTA deficient mutant (Biswas *et al.*, 2012; Schlag *et al.*, 2010; Zoll *et al.*, 2012). We also observed complete delocalisation of Atl(ami) and also Alt(glu) in the absence of WTA. Bright foci were seen with both antibodies in line with septal growth in a number of cases which could be attributed to rib 'bulges' in the cell wall. Work performed within Chapter 4 showed that in a $\Delta srtA$ strain WTA can be specifically labelled and it was hoped that dual labelling with antibody and lectin would show differences in localisation. This was not possible because ConA appears to be very 'sticky' and bound both vancomycin and antibody, creating artefacts in its binding pattern. However work within Chapter 4 suggested that the hazy punctate/dotty pattern of WTA localisation could be due to the piecrust features intersecting its binding. This suggests that the piecrust peptidoglycan is unmodified by WTA, although we have no biochemical data to support this.

Interestingly when studying the glucosaminidases ScaH and SagB, we found their localisation to be very similar. Although more disordered, the binding was reminiscent of Atl binding and septal/rib binding was commonly seen. Although no crosswall binding was seen, exposed nascent peptidoglycan was bound. Furthermore bright foci were commonly seen at the septum. These observations support the recent discovery that glucosaminidases are responsible for peptidoglycan maturation and therefore expected to localise with sites of synthesis and bind nascent peptidoglycan. Quarter rib binding suggests that glucosaminidases are present before new piecrusts have formed, however both showed a low level of binding across the cell surface. Binding was fully delocalised in WTA deficient mutants. Other *S.aureus* hydrolases, Sle1 and LytN, have also been shown to be unable to bind peptidoglycan in the presence of WTA and to bind uniformly across the cell

surface in the absence of WTAs (Frankel and Schneewind, 2012). This further supports our hypothesis that ribs do not contain WTA.

The lytic transglycosylase SceD was seen to localise uniformly across the entire cell surface. Lytic transglycosylases have been proposed as having a role in cell wall turnover and this localisation pattern supports this (Kraft *et al.*, 1999). However, the only other lytic transglycosylase in *S.aureus*, IsaA, localises predominately to the septal region (Sakata *et al.*, 2005). SceD was the fastest of the studied hydrolases, taking only 5 mins to reappear after trypsination. Faint cross-wall binding was seen in a number of cases. SceD's role in peptidoglycan maturation is vital for cell growth and therefore it is unsurprising that it rapidly reappears. Cross-wall localisation suggests that it has the ability to bind nascent peptidoglycan or that it is delivered directly to the cross-wall compartment. Several other known hydrolases, LytN and Sle1, have been shown to be produced here via their LysM domains (Frankel and Schneewind, 2012).

CHAPTER 6

General discussion

The understanding of cellular functions requires detailed knowledge of all factors, the specific interactions and modifications as well as their distribution in the cell and the dynamic cell cycle changes thereof. From the very beginning, microscopy has played a key role in cell biology. However early attempts to characterise the architecture of the peptidoglycan network and the distribution of associated surface proteins were hampered by the limitations of the available technology. This led to the general view of a simplistic, homogenous network of peptidoglycan studded with uniform surface proteins. However, thanks to the development and application of nanometre resolution imaging technologies it has begun to be possible to overcome this barrier, and has led to rapid developments in our understanding.

6.1 *S.aureus* peptidoglycan architecture

Although relatively early studies showed that the sacculus of *S.aureus* was heterogeneous in thickness (Giesbrecht *et al.*, 1998; Gilbo *et al.*, 1967; Touhami *et al.*, 2004), only recently has this been closely examined. The sacculus architecture has been found to transition from ring-like to knobbly as it ages, and to be dissected by thicker equatorial bands of piecrust peptidoglycan as well as the orthogonal ribs left from previous piecrust features (Turner *et al.*, 2010; Wheeler, 2012; observed in Chapter 4). The ring architecture itself is not new and has been observed in the septa of gram-positive rods, cocci and ovococci (Amako and Umeda, 1978; Andre *et al.*, 2011; Hayhurst *et al.*, 2008; Turner *et al.*, 2010; Wheeler *et al.*, 2011). It is known to be associated with nascent cell wall, and was shown in *S.aureus* by scanning electron imaging of daughter cells (Giesbrecht *et al.*, 1998). To account for the changing architecture of peptidoglycan a novel growth by hydrolysis model was recently proposed (Turner *et al.*, 2010; Section 1.6; Figure 1.7B). When combined with piecrust features, the model of growth is as follows and schematically shown in Figure 6.1. The plane of division selected contains the quarter rib where the cell lays down a new belt of thick peptidoglycan (piecrust) before septal plate formation. Long, inelastic, glycan strands are centripetal orientated to make the septal plate and the cell is split by the

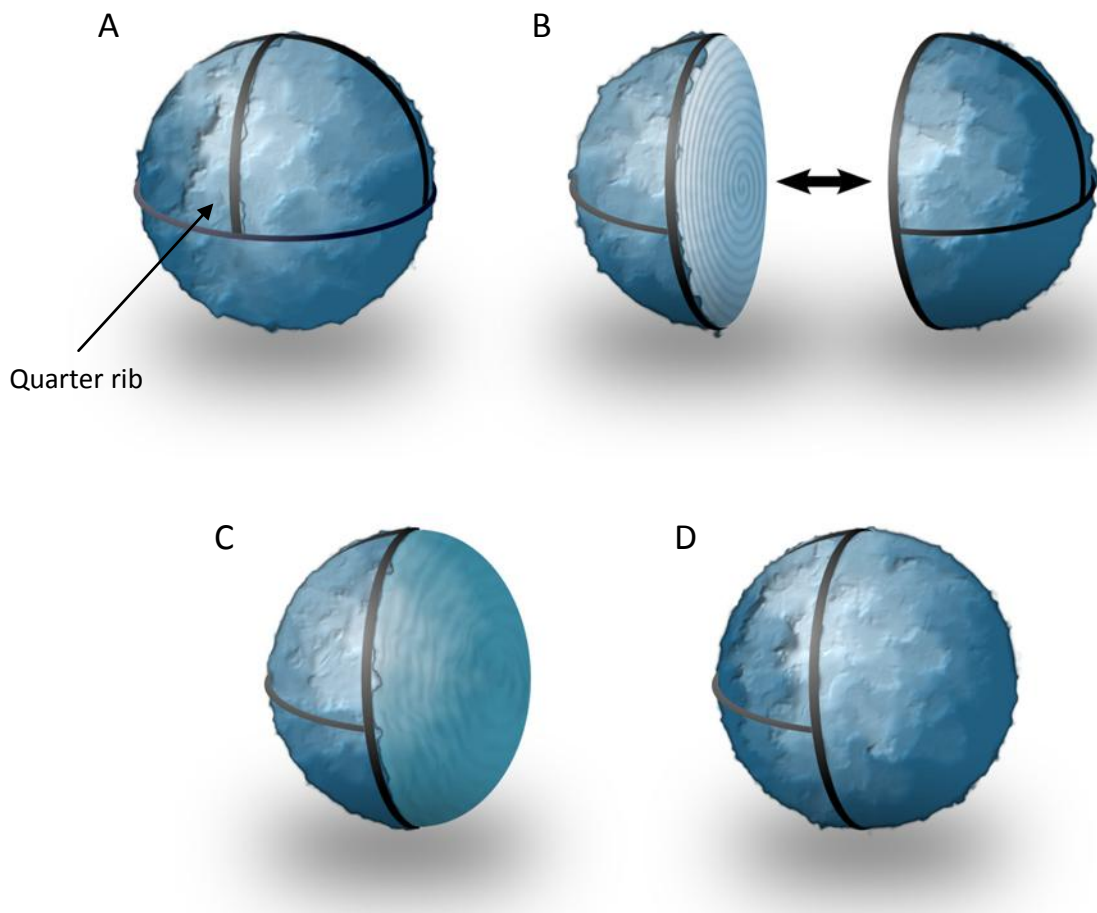


Figure 6.1 Division plane growth choice through peptidoglycan ribs and growth by hydrolysis and piecrust (Wheeler R., 2012)

Black lines indicate the orientation of peptidoglycan ribs and the two peptidoglycan architectures, ring and knobbles, are schematically represented. (A) A mature spherical *S.aureus* has knobbled peptidoglycan architecture. *S.aureus* synthesises a septal cross-wall in the plane of the quarter rib (indicated). (B) The cell divides into two daughter cells, exposing a flat cross-wall with ring architecture. (C) The densely packed glycan strands are quickly cleaved by glucosaminidases, observed as a transitioning from ring to knobby texture, and turgor pressure causes the cell to expand. (D) The ring architecture is lost as the cell wall matures.

action of hydrolases. The centripetal glycan strands radially constrain the cross-wall and prevents volume increase of daughter cells. The peptidoglycan band braces the cell and prevents collapse to a more energetically favourable smaller sphere, resulting in a brief period as a hemispherical cell. As the glycan chains are hydrolysed by glucosaminidases the stress bearing function is shared with more flexible peptide stems and the cell can expand under turgor pressure (Turner *et al.*, 2010). AFM work performed here has confirmed these peptidoglycan architectures and features (Chapter 4).

6.2 How does a sphere divide faithfully in three planes?

Unlike rod-shaped organisms, *S.aureus* does not use either the oscillating mechanism or the stable polar-localisation of the Min system to prevent cell division at the poles. Despite the gram-negative coccus *Neisseria gonorrhoeae* hypothesised to use a putative oscillatory mechanism to divide on two orthogonal planes (Ramirez-Arcos *et al.*, 2002), no Min homologues have been identified in *S.aureus* and a *divIVA* mutant had no effect (Pinho and Errington, 2004). However, it has been shown that depletion of *S.aureus* nucleoid occlusion factor, Noc results in the formation of multiple Z rings which are no longer perpendicular (Veiga *et al.*, 2011). Thus although *S.aureus* can use Noc to determine division plane and prevent Z-ring formation over the bacterial chromosome, this only accounts for two orthogonal planes. The characterisation of the peptidoglycan ‘piecrust’ features and the intersecting ribs left from previous divisions offers a means of recording previous divisions, as discussed in Section 1.6 (Figure 1.7). Together, a model in which chromosome segregation occurs parallel to the quarter rib can be established allowing orthogonal growth on three planes (Figure 6.2) (Turner *et al.*, 2010; Veiga *et al.*, 2011). It has been hypothesised that DivIB plays an important role as the link between the two processes, recognising the piecrust features and coordinating the divisome accordingly (Bottomley, 2011). However it still remains unclear whether coordination of division is driven by the division machinery, chromosome segregation machinery or both.

6.3 How are the ‘piecrust’ features recognised?

Several mechanisms of how piecrust features are ‘sensed’ by proteins have been suggested. Firstly, the ribs could be furnished during synthesis with an anchoring protein that recruits others. However with successive divisions the rib gets shorter and thus the

most recent rib would contain the most anchoring protein. Secondly, the ribs could physically impose local membrane curvature which is recognised by a protein sensor. Although several protein domains, Bar and ALPS, have been identified as capable of this none of the proteins showing 'piecrust' localisation have been shown to contain these domains (Antony, 2011). It is also possible that the ribs are close enough to the cell membrane to encourage the binding of membrane anchored proteins and/or it could potentially displace LTAs which may be inhibiting protein localisation. However this does not account for external proteins that localise in a 'piecrust' pattern. Finally the peptidoglycan chemistry of the ribs themselves could be distinct and direct recognition for protein binding. Work within this study has suggested that the peptidoglycan architectural features are devoid of WTA, thereby directing certain proteins to them. Indeed the membrane protein DivIB has shown 'piecrust' localisation and a decrease in affinity for peptidoglycan containing WTA (Bottomley, 2011). Whilst the external Atl has been shown to localise to piecrust features (chapter 5), to delocalise in a $\Delta tarO$ mutant (chapter 5) and WTA have been shown to modulate Atl autolytic activity (Biswas et al., 2006).

6.4 Where are WTAs localised?

AFM studies showed WTA as a 'fluffy' or 'furry' layer that extends across the entire cell surface (Chapter 4). Immunoelectron microscopy has also suggested that WTA are uniformly expressed across the cell wall of *S.aureus* (Umeda et al., 1992). Furthermore, EM studies showed that *S.aureus* cells have a continuous electron-dense layer at the cell surface that continues down the centre of the division plane as separation occurs and that this layer is composed of WTA-rich peptidoglycan (Matias and Beveridge, 2007). However, using the more sensitive technique of cryo-EM, it was found that the septum is comprised of two electron-dense layers separated by a less dense midzone layer (Matias and Beveridge, 2007), implying WTAs may not be uniformly localised throughout the peptidoglycan, at least during septum formation. Labelling of WTA with ConA has also shown a lack of septal binding (Schlag et al., 2010). However TarO(TagO) has previously been localised at the septum in *S.aureus* (Atilano et al., 2010) and my work has shown that TarO, along with three other WTA biosynthesis proteins (MsrR, SA2103 and SA0908), interact with a number of cell division proteins. This suggests that WTA biosynthesis machinery interacts with, and therefore likely localises with, the divisome of *S.aureus*.

Interestingly, both Schlag *et al.*, (2010) and Atilano *et al.*, (2010) have suggested that WTA are not present at the septum in their fully polymerised mature form. However work here has shown that the LCP proteins, (MsrR, SA2103 and SA0908) involved in the final ligation step of WTA synthesis (Dengler *et al.*, 2012; Over *et al.*, 2011), interact with many divisome components and thus suggesting that fully polymerised WTA are indeed produced at the septum.

Direct visualisation of WTA localisation was performed using the lectin ConA under the identified appropriate conditions for specific labelling (Δ srtA, pronase treated WT cells). The binding was not the reported uniform layer and that it was found at the septum although it did not extend into the crosswall. It has been noted that large molecules cannot access the cross-wall compartment (DeDent *et al.*, 2008; Pinho and Errington, 2003) and, although not witnessed here, may not penetrate the nascent cross-wall even after daughter cell separation (Wheeler, 2012). The gaps within the layer of WTA are proposed as being caused by piecrust and rib features intersecting the binding and we suggest that WTA are not present on the piecrust features (Figure 6.3A-B). AFM imaging of wild type sacculi did not show gaps in the WTA 'furry' layer across the piecrust features. It is likely that during preparation of the samples the long WTA have folded down across the piecrust features, obscuring a narrow bare channel. It is likely that older segments of cell wall may contain less WTA as the cell wall is hydrolysed (Figure 6.3A-B).

6.5 Which cellular processes do WTA influence?

There is much evidence linking WTA to growth, cell division, and morphogenesis. Simultaneous inhibition of TarO and native transpeptidases was synthetically lethal (Campbell *et al.*, 2011) and a *S.aureus* Δ tarO displayed defective septation, with multiple septa frequently initiated at non-orthogonal angles. This links division and WTA and suggests that the biosynthetic machinery involved is unregulated in the Δ tarO mutant (Campbell *et al.*, 2011). The aforementioned protein DivIB has been suggested as the potential division link with depletion mutants showing multiple deregulated septa (Bottomley, 2011). A functional link between elongation machinery and WTA biosynthesis has been indicated by deletion mutants of *tagO* in *B.subtilis* leading to the rounding of cells (Soldo *et al.*, 2002). The localisation of PBP4, the transpeptidase responsible for

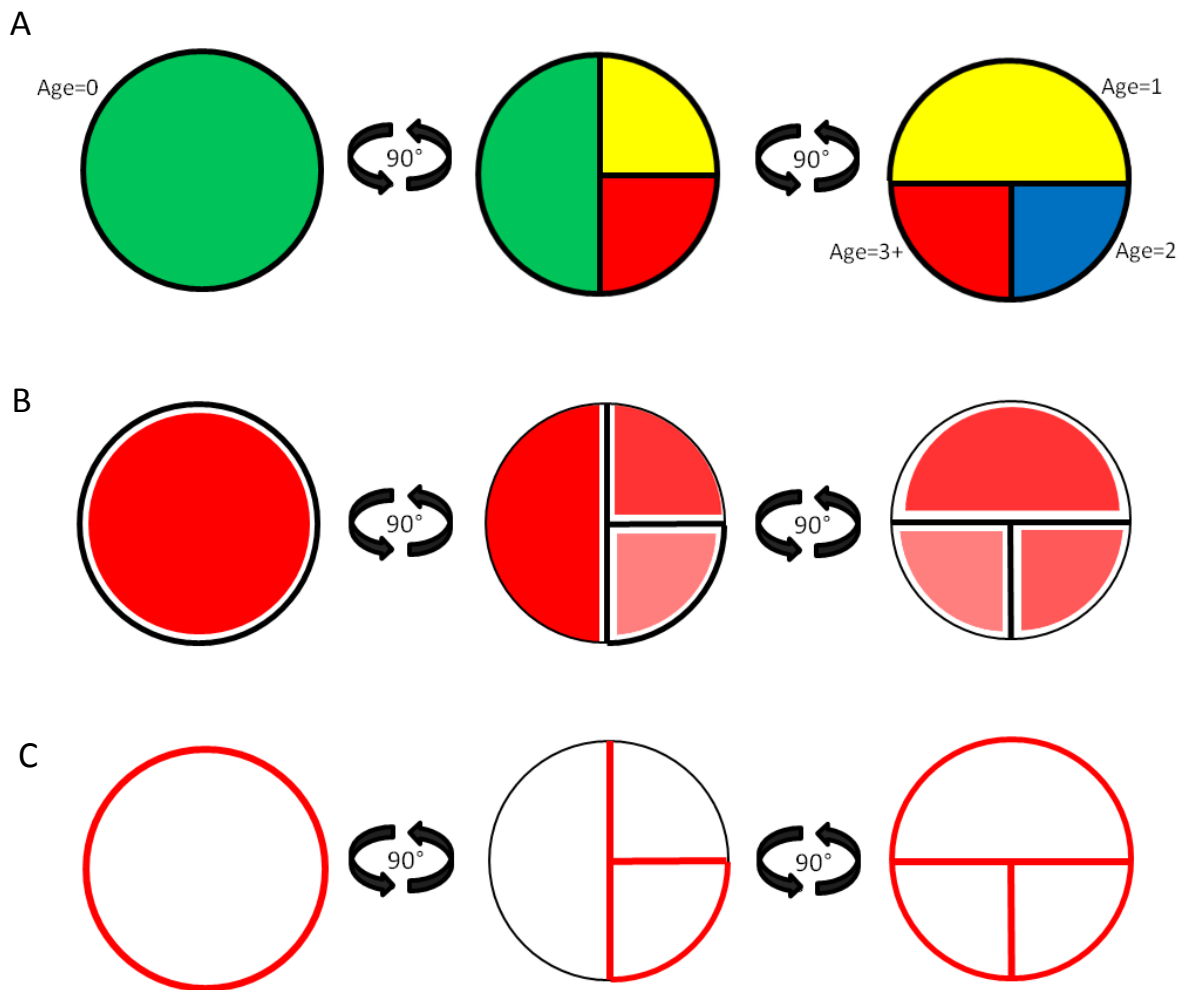


Figure 6.2 The localisation of WTA and how it directs proteins localisation

(A) The three plane orthogonal division of *S.aureus* results in a patchwork of different age peptidoglycan segment, bisected by peptidoglycan 'piecrusts' and ribs from previous divisions. Coloured segments differ in age; Green, no generations old, Yellow, one generation old; Blue, 2 generations old; Red, three+ generations old. Black lines, piecrust and rib features. (B) WTA is not present at the piecrust or ribs features. Red, WTA localisation; Thick black, piecrust and rib features (C) The lack of WTA exposes the piecrust peptidoglycan to binding by hydrolases. Red lines, binding sites of hydrolases.

the characteristic high cross-linking of *S.aureus* peptidoglycan (Memmi *et al.*, 2008), was shown to be spatially dependent on WTA (Atilano *et al.*, 2010). Furthermore, it was suggested that TagO (TarO) acted as a temporal indicator of completion of initial peptidoglycan synthesis, controlling the activity of PBP4 which leads to an increase in cross-linking (Atilano *et al.*, 2010). WTA has been shown to modulate the activity of autolysins by binding protons and maintaining an acidic pH in which hydrolases, largely Atl, decline in function thus protecting the cell from autolysis (Biswas *et al.*, 2012). In addition work, both within this study and by others, has also indicated that WTA are responsible for the localisation of several hydrolases required for cell separation; SagB (Chapter 5), Atl (Schlag *et al.*, 2010; Chapter 5), ScaH (Chapter 5) and Sle1 (Heilmann *et al.*, 2005). Such a diverse number of proteins are unlikely to have a common domain involved in localisation that is affected by WTA. Indeed if we look at the hydrolases involved in septum cleavage which are delocalised in a *tarO* mutant; Atl contains the three repeat regions for localisation (Baba and Schneewind, 1998; Biswas *et al.*, 2006; Schlag *et al.*, 2010; Chapter 5); Sle1 contains a LysM domains (Heilmann *et al.*, 2005) and ScaH a CHAP domain (Bateman and Rawlings, 2003; Rigden *et al.*, 2003; Chapter 5). This variety of binding domains supports a non-specific model of steric hindrance, where WTA block all available binding sites except the piecrust peptidoglycan (Figure 6.3C). However, we have also shown that SceD is not WTA dependant and present across the entire cell surface (Chapter 5).

6.6 How is the active division plane differentiated from others?

How are proteins directed to the septum and not all 'piecrust' features? How do hydrolases know which 'piecrust' rib feature is in the current plane of growth? It seems reasonable that in older segments there may be less WTA as peptidoglycan is hydrolysed and lost with its binding partners. Thus in older segments a loss of density and/or height may allow for the oldest piecrust, the quarter rib, to be uncovered and the correct plane of division selected for growth. As this growth commences, the newest piecrust is formed under the old piecrust, as the 'inside-to-outside' model would suggest, and could make the old piecrust quarter section more prominent (Figure 6.4). It is here that Atl binds first and then the rest of the new piecrust. If it does indeed bind this quarter rib section first then this receives hydrolysis for the longest periods and could be the point of weakness from which the cell splits. Atl binds the new piecrust preferentially because it is the largest, as all other

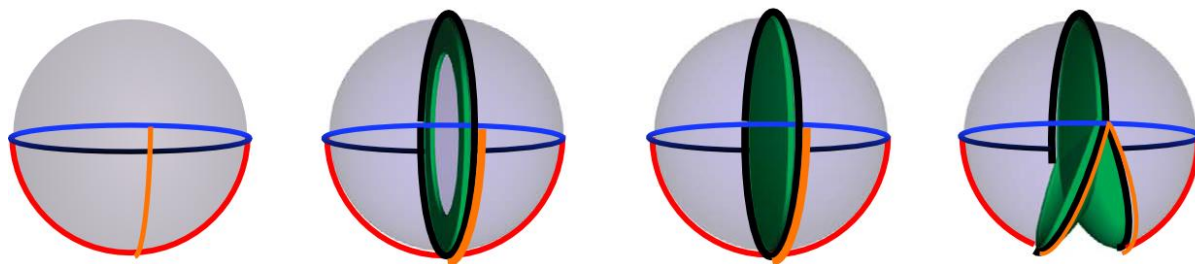


Figure 6.4 Cells split from one side only

The quarter rib section of the new piecrust has been available for action of the hydrolases for the longest and as a new piecrust forms underneath is prominent from the outside. It could therefore have received the longest and the most hydrolytic action. This section could therefore be the point of weakness from which the cell splits. Continued hydrolysis thins the quarter rib section of the new piecrust. Blue, whole rib; Red, half rib; Orange, quarter rib; Black, new piecrust; Green, peptidoglycan synthesis.

piecrusts have undergone a degree of hydrolysis. Additionally, Atl(ami), and to a much lesser extent Atl(glu), show septal localisation early on in the division process (before the completion of the septal plate) which further indicates that the piecrust peptidoglycan is produced without WTA as oppose to it being displaced. However this current plane specific localisation is not seen with hydrolases such as SagB and ScaH. This could be that they are less modulated by WTA than Atl and so able to attach and function despite WTA encroachment and the localised acidic pH, or that their LysM binding domains are less sensitive than the repeat regions. Furthermore differences in observed foci size could be explained by difference in rib thickness due to the peptidoglycan turnover with each generation's growth.

6.7 Future work

Further work with STORM would help to refine the Atl cell cycle model and its localisation patterns (Does Atl(glu) form a 'double-ring'?). Indeed video-rate SIM capable of super-resolution imaging in the tens of milliseconds time-frame could be applied for visualisation of Atl cell cycle dynamics *in vivo* (Lefman *et al.*, 2011). Both techniques could also be used to study the movements of ScaH and SagB, here we have shown that they are produced primarily at the septum is this how they arrive at all piecrusts? Although we are suggesting that the peptidoglycan 'piecrust' and rib features have a different composition to the rest of the sacculus, there is no chemical proof or direct visualisation of this. It has proven difficult to resolve individual glycan strands or peptide stems from the surrounding peptidoglycan using non-differential techniques such as AFM and EM (Elliott *et al.*, 1975; Giesbrecht *et al.*, 1998; Hayhurst *et al.*, 2008; Touhami *et al.*, 2004; Turner *et al.*, 2010). Theoretically single glycan strands could be found by observing hydrolysis with lysostaphin however the peptidoglycan network has proven too complex to examine its chemistry (Francius *et al.*, 2008). Simultaneous AFM and fluorescence imaging in *S.aureus* would show direct localisation of the Atl, SagB and ScaH to specific peptidoglycan features. The technology to do this is in the early stages of development; STORMForce combines AFM and STORM technologies and has been used to observe new growth with vancomycin alongside peptidoglycan architecture so far (Foster, unpublished). Sadly, time constraints for this thesis prevented use of this technique within my study.

As well as increased resolution microscopy, localisation studies could be addressed biologically. Cell wall synthesis is dispersed across the entire cell wall when *S.aureus* is depleted of FtsZ causing formation of enlarged spherical cells (Pinho and Errington, 2003). In such cells, it is likely that the rib architecture is disrupted and thus immunolocalisation of piecrust localising proteins would also show a dispersed pattern. In addition to disrupting the piecrust features, their generation could be observed. By creating *S.aureus* protoplasts previous ribs are erased as the cells regenerate their cell wall and re-establish orthogonal division, the hydrolase localisation can be studied. It is worth noting that regenerating protoplasts have abnormal cell division (Gruss and Novick, 1986) and the cell physiology is greatly perturbed in regenerating protoplasts (Elliott *et al.*, 1975) making the interpretation of these results very difficult.

Overall, my work provides a further insight into the localisation of WTA and a mechanism which controls the pattern of display of surface proteins. This study offers a refinement on how a spherical bacterium can faithfully divide in three orthogonal planes. The study of fundamental processes like cell division is vital to our understanding of a clinically relevant pathogen and the prokaryote specific structure peptidoglycan.

References

- Addinall, S.G., Bi, E., Lutkenhaus, J.,** 1996. FtsZ ring formation in fts mutants. *J. Bacteriol.* 178, 3877–3884.
- Agrawal, B.B., Goldstein, I.J.,** 1967. Physical and chemical characterization of concanavalin A, the hemagglutinin from jack bean (*Canavalia ensiformis*). *Biochim. Biophys. Acta* 133, 376–379.
- Ahn, S.-J., Burne, R.A.,** 2006. The atlA operon of *Streptococcus mutans*: role in autolysin maturation and cell surface biogenesis. *J. Bacteriol.* 188, 6877–6888.
- Amako, K., Umeda, A.,** 1978. Concentric circular structure of the cell wall of *Staphylococcus epidermidis* revealed by the scanning electron microscope. *J Electron Microscop (Tokyo)* 27, 147–148.
- Amieva, M.R., El-Omar, E.M.,** 2008. Host-bacterial interactions in *Helicobacter pylori* infection. *Gastroenterology* 134, 306–323.
- Anderson, D.E., Gueiros-Filho, F.J., Erickson, H.P.,** 2004. Assembly dynamics of FtsZ rings in *Bacillus subtilis* and *Escherichia coli* and effects of FtsZ-regulating proteins. *J. Bacteriol.* 186, 5775–5781.
- Andre, G., Deghorain, M., Bron, P.A., van Swam, I.I., Kleerebezem, M., Hols, P., Dufrene, Y.F.,** 2011. Fluorescence and atomic force microscopy imaging of wall teichoic acids in *Lactobacillus plantarum*. *ACS Chem. Biol.* 6, 366–376.
- Angert, E.R.,** 2005. Alternatives to binary fission in bacteria. *Nature Reviews Microbiology* 3, 214–224.
- Angert, E.R., Losick, R.M.,** 1998. Propagation by sporulation in the guinea pig symbiont *Metabacterium polyspora*. *Proc. Natl. Acad. Sci. U.S.A.* 95, 10218–10223.
- Antonny, B.,** 2011. Mechanisms of membrane curvature sensing. *Annu. Rev. Biochem.* 80, 101–123.
- Arai, M., Mitsuke, H., Ikeda, M., Xia, J.-X., Kikuchi, T., Satake, M., Shimizu, T.,** 2004. ConPred II: a consensus prediction method for obtaining transmembrane topology models with high reliability. *Nucleic Acids Res* 32, W390–W393.
- Archer, G.L.,** 1998. *Staphylococcus aureus*: A Well-Armed Pathogen. *Clin Infect Dis.* 26, 1179–1181.
- Archibald, A.R., Coapes, H.E.,** 1971. The interaction of concanavalin A with teichoic acids and bacterial walls. *Biochem J* 123, 665–667.
- Arends, S.J.R., Kustus, R.J., Weiss, D.S.,** 2009. ATP-binding site lesions in FtsE impair cell division. *J. Bacteriol.* 191, 3772–3784.
- Arends, S.J.R., Williams, K., Scott, R.J., Rolong, S., Popham, D.L., Weiss, D.S.,** 2010. Discovery and characterization of three new *Escherichia coli* septal ring proteins that contain a SPOR domain: DamX, DedD, and RlpA. *J. Bacteriol.* 192, 242–255.
- Atilano, M.L., Pereira, P.M., Yates, J., Reed, P., Veiga, H., Pinho, M.G., Filipe, S.R.,** 2010. Teichoic acids are temporal and spatial regulators of peptidoglycan cross-linking in *Staphylococcus aureus*. *Proc. Natl. Acad. Sci. U.S.A.* 107, 18991–18996.
- Atrih, A., Bacher, G., Allmaier, G., Williamson, M.P., Foster, S.J.,** 1999. Analysis of peptidoglycan structure from vegetative cells of *Bacillus subtilis* 168 and role of PBP 5 in peptidoglycan maturation. *J. Bacteriol.* 181, 3956–3966.
- B.Liedberg, C.N., I.Lundstrom,** 1983. Surface Plasmon Resonance for Gas Detection and Biosensing. *Sensors and Actuators B: Chemical* 4, 299–304.
- Baba, T., Schneewind, O.,** 1998. Targeting of muralytic enzymes to the cell division site of Gram-positive bacteria: repeat domains direct autolysin to the equatorial surface ring of *Staphylococcus aureus*. *The EMBO Journal* 17, 4639–4646.
- Baba, T., Takeuchi, F., Kuroda, M., Yuzawa, H., Aoki, K., Oguchi, A., Nagai, Y., Iwama, N., Asano, K., Naimi, T., Kuroda, H., Cui, L., Yamamoto, K., Hiramatsu, K.,** 2002. Genome and virulence determinants of high virulence community-acquired MRSA. *Lancet* 359, 1819–1827.
- Bateman, A., Rawlings, N.D.,** 2003. The CHAP domain: a large family of amidases including GSP amidase and peptidoglycan hydrolases. *Trends Biochem. Sci.* 28, 234–237.

- Beall, B., Lutkenhaus, J.,** 1989. Nucleotide sequence and insertional inactivation of a *Bacillus subtilis* gene that affects cell division, sporulation, and temperature sensitivity. *J. Bacteriol.* 171, 6821–6834.
- Beech, P.L., Nheu, T., Schultz, T., Herbert, S., Lithgow, T., Gilson, P.R., McFadden, G.I.,** 2000. Mitochondrial FtsZ in a chromophyte alga. *Science* 287, 1276–1279.
- Belcheva, A., Golemi-Kotra, D.,** 2008. A close-up view of the VraSR two-component system. A mediator of *Staphylococcus aureus* response to cell wall damage. *J. Biol. Chem.* 283, 12354–12364.
- Berger-Bächi, B.,** 1994. Expression of resistance to methicillin. *Trends Microbiol.* 2, 389–393.
- Bernhardt, T.G., Boer, P.A.J. de,** 2005. SImA, a Nucleoid-Associated, FtsZ Binding Protein Required for Blocking Septal Ring Assembly over Chromosomes in *E. coli*. *Molecular Cell* 18, 555–564.
- Bertsche, U., Kast, T., Wolf, B., Fraipont, C., Aarsman, M.E.G., Kannenberg, K., von Rechenberg, M., Nguyen-Distèche, M., den Blaauwen, T., Höltje, J.-V., Vollmer, W.,** 2006. Interaction between two murein (peptidoglycan) synthases, PBP3 and PBP1B, in *Escherichia coli*. *Mol. Microbiol.* 61, 675–690.
- Bhavsar, A.P., Truant, R., Brown, E.D.,** 2005. The TagB protein in *Bacillus subtilis* 168 is an intracellular peripheral membrane protein that can incorporate glycerol phosphate onto a membrane-bound acceptor in vitro. *J. Biol. Chem.* 280, 36691–36700.
- Bi, E.F., Lutkenhaus, J.,** 1991. FtsZ ring structure associated with division in *Escherichia coli*. *Nature* 354, 161–164.
- Binnig, Quate, Gerber,** 1986. Atomic force microscope. *Phys. Rev. Lett.* 56, 930–933.
- Biswas, R., Martinez, R.E., Göhring, N., Schlag, M., Josten, M., Xia, G., Hegler, F., Gekeler, C., Gleske, A.-K., Götz, F., Sahl, H.-G., Kappler, A., Peschel, A.,** 2012. Proton-Binding Capacity of *Staphylococcus aureus* Wall Teichoic Acid and Its Role in Controlling Autolysin Activity. *PLoS One* 7.
- Biswas, R., Voggu, L., Simon, U.K., Hentschel, P., Thumm, G., Götz, F.,** 2006. Activity of the major *staphylococcal* autolysin Atl. *FEMS Microbiol. Lett.* 259, 260–268.
- Blackman, S.A., Smith, T.J., Foster, S.J.,** 1998. The role of autolysins during vegetative growth of *Bacillus subtilis* 168. *Microbiology (Reading, Engl.)* 144 (Pt 1), 73–82.
- Boneca, I.G., Huang, Z.H., Gage, D.A., Tomasz, A.,** 2000. Characterization of *Staphylococcus aureus* cell wall glycan strands, evidence for a new beta-N-acetylglucosaminidase activity. *J. Biol. Chem.* 275, 9910–9918.
- Bork, P., Sander, C., Valencia, A.,** 1992. An ATPase domain common to prokaryotic cell cycle proteins, sugar kinases, actin, and hsp70 heat shock proteins. *Proc. Natl. Acad. Sci. U.S.A.* 89, 7290–7294.
- Boruc, J., Inzé, D., Russinova, E.,** 2010. A high-throughput bimolecular fluorescence complementation protein-protein interaction screen identifies functional *Arabidopsis* CDKA/B-CYCD4/5 complexes. *Plant Signal Behav* 5, 1276–1281.
- Bottomley,** 2011. Identification and characterisation of the cell division machinery in *Staphylococcus aureus*. University of Sheffield.
- Boyle, D.S., Khattar, M.M., Addinall, S.G., Lutkenhaus, J., Donachie, W.D.,** 1997. ftsW is an essential cell-division gene in *Escherichia coli*. *Mol. Microbiol.* 24, 1263–1273.
- Bramhill, D.,** 1997. Bacterial cell division. *Annu. Rev. Cell Dev. Biol.* 13, 395–424.
- Brown, S., Xia, G., Luhachack, L.G., Campbell, J., Meredith, T.C., Chen, C., Winstel, V., Gekeler, C., Irazoqui, J.E., Peschel, A., Walker, S.,** 2012. Methicillin resistance in *Staphylococcus aureus* requires glycosylated wall teichoic acids. *Proc. Natl. Acad. Sci. U.S.A.* 109, 18909–18914.
- Brunskill, E.W., Bayles, K.W.,** 1996. Identification and molecular characterization of a putative regulatory locus that affects autolysis in *Staphylococcus aureus*. *J. Bacteriol.* 178, 611–618.
- Bublitz, M., Polle, L., Holland, C., Heinz, D.W., Nimitz, M., Schubert, W.-D.,** 2009. Structural basis for autoinhibition and activation of Auto, a virulence-associated peptidoglycan hydrolase of *Listeria monocytogenes*. *Mol. Microbiol.* 71, 1509–1522.

- Buddelmeijer, N., Beckwith, J.,** 2004. A complex of the *Escherichia coli* cell division proteins FtsL, FtsB and FtsQ forms independently of its localization to the septal region. *Mol. Microbiol.* 52, 1315–1327.
- Buddelmeijer, N., Judson, N., Boyd, D., Mekalanos, J.J., Beckwith, J.,** 2002. YgbQ, a cell division protein in *Escherichia coli* and *Vibrio cholerae*, localizes in codependent fashion with FtsL to the division site. *Proc. Natl. Acad. Sci. U.S.A.* 99, 6316–6321.
- Burian, M., Rautenberg, M., Kohler, T., Fritz, M., Krismer, B., Unger, C., Hoffman, W.H., Peschel, A., Wolz, C., Goerke, C.,** 2010. Temporal Expression of Adhesion Factors and Activity of Global Regulators during Establishment of *Staphylococcus aureus* Nasal Colonization. *J Infect Dis.* 201, 1414–1421.
- Cabeen, M.T., Jacobs-Wagner, C.,** 2005. Bacterial cell shape. *Nat. Rev. Microbiol.* 3, 601–610.
- Calamita, H.G., Doyle, R.J.,** 2002. Regulation of autolysins in teichuronic acid-containing *Bacillus subtilis* cells. *Molecular Microbiology* 44, 601–606.
- Campbell, J., Singh, A.K., Santa Maria, J.P., Kim, Y., Brown, S., Swoboda, J.G., Mylonakis, E., Wilkinson, B.J., Walker, S.,** 2011. Synthetic lethal compound combinations reveal a fundamental connection between wall teichoic acid and peptidoglycan biosyntheses in *Staphylococcus aureus*. *ACS Chem Biol* 6, 106–116.
- Campbell, J., Singh, A.K., Swoboda, J.G., Gilmore, M.S., Wilkinson, B.J., Walker, S.,** 2012. An antibiotic that inhibits a late step in wall teichoic acid biosynthesis induces the cell wall stress stimulon in *Staphylococcus aureus*. *Antimicrob. Agents Chemother.* 56, 1810–1820.
- Carettoni, D., Gómez-Puertas, P., Yim, L., Mingorance, J., Massidda, O., Vicente, M., Valencia, A., Domenici, E., Anderluzzi, D.,** 2003. Phage-display and correlated mutations identify an essential region of subdomain 1C involved in homodimerization of *Escherichia coli* FtsA. *Proteins* 50, 192–206.
- Carlstrom, D.,** 1957. The crystal structure of alpha-chitin (poly-N-acetyl-D-glucosamine). *J Biophys Biochem Cytol* 3, 669–683.
- Carson, M.J., Barondess, J., Beckwith, J.,** 1991. The FtsQ protein of *Escherichia coli*: membrane topology, abundance, and cell division phenotypes due to overproduction and insertion mutations. *J. Bacteriol.* 173, 2187–2195.
- Cha, J.H., Stewart, G.C.,** 1997. The divIVA minicell locus of *Bacillus subtilis*. *J Bacteriol* 179, 1671–1683.
- Chang, S., Sievert, D.M., Hageman, J.C., Boulton, M.L., Tenover, F.C., Downes, F.P., Shah, S., Rudrik, J.T., Pupp, G.R., Brown, W.J., Cardo, D., Fridkin, S.K.,** 2003. Infection with vancomycin-resistant *Staphylococcus aureus* containing the vanA resistance gene. *N. Engl. J. Med.* 348, 1342–1347.
- Chatterjee, A.N.,** 1969. Use of Bacteriophage-resistant Mutants to Study the Nature of the Bacteriophage Receptor Site of *Staphylococcus aureus*. *J. Bacteriol.* 98, 519–527.
- Chen, Y., Erickson, H.P.,** 2005. Rapid in vitro assembly dynamics and subunit turnover of FtsZ demonstrated by fluorescence resonance energy transfer. *J. Biol. Chem.* 280, 22549–22554.
- Chepelev N., Chepelev L., Alamgir M.D., Golshani A.,** 2008. Large-scale protein-protein interaction detection approaches: past, present and future. *Biotechnology and Biotechnological Equipment* 22, 513–529.
- Chung, K.-M., Hsu, H.-H., Yeh, H.-Y., Chang, B.-Y.,** 2007. Mechanism of regulation of prokaryotic tubulin-like GTPase FtsZ by membrane protein EzrA. *J. Biol. Chem.* 282, 14891–14897.
- Claessen, D., Emmins, R., Hamoen, L.W., Daniel, R.A., Errington, J., Edwards, D.H.,** 2008. Control of the cell elongation-division cycle by shuttling of PBP1 protein in *Bacillus subtilis*. *Mol. Microbiol.* 68, 1029–1046.
- Clarke, S.R., Brummell, K.J., Horsburgh, M.J., McDowell, P.W., Mohamad, S.A.S., Stapleton, M.R., Acevedo, J., Read, R.C., Day, N.P.J., Peacock, S.J., Mond, J.J., Kokai-Kun, J.F., Foster, S.J.,** 2006. Identification of In Vivo-Expressed Antigens of *Staphylococcus aureus* and Their Use in Vaccinations for Protection against Nasal Carriage. *J Infect Dis.* 193, 1098–1108.

- Clarke-Sturman, A.J., Archibald, A.R., Hancock, I.C., Harwood, C.R., Merad, T., Hobot, J.A.,** 1989. Cell wall assembly in *Bacillus subtilis*: partial conservation of polar wall material and the effect of growth conditions on the pattern of incorporation of new material at the polar caps. *J. Gen. Microbiol.* 135, 657–665.
- Cloud, K.A., Dillard, J.P.,** 2002. A lytic transglycosylase of *Neisseria gonorrhoeae* is involved in peptidoglycan-derived cytotoxin production. *Infect. Immun.* 70, 2752–2757.
- Cloud, K.A., Dillard, J.P.,** 2004. Mutation of a single lytic transglycosylase causes aberrant septation and inhibits cell separation of *Neisseria gonorrhoeae*. *J. Bacteriol.* 186, 7811–7814.
- Collins, L.V., Kristian, S.A., Weidenmaier, C., Faigle, M., Van Kessel, K.P.M., Van Strijp, J.A.G., Götz, F., Neumeister, B., Peschel, A.,** 2002. *Staphylococcus aureus* strains lacking D-alanine modifications of teichoic acids are highly susceptible to human neutrophil killing and are virulence attenuated in mice. *J. Infect. Dis.* 186, 214–219.
- Corbin, B.D., Wang, Y., Beuria, T.K., Margolin, W.,** 2007. Interaction between Cell Division Proteins FtsE and FtsZ. *J. Bacteriol.* 189, 3026–3035.
- Corrigan, R.M., Abbott, J.C., Burhenne, H., Kaefer, V., Gründling, A.,** 2011. c-di-AMP is a new second messenger in *Staphylococcus aureus* with a role in controlling cell size and envelope stress. *PLoS Pathog.* 7, e1002217.
- Courvalin, P.,** 2006. Antibiotic resistance: the pros and cons of probiotics. *Dig Liver Dis* 38 Suppl 2, S261–265.
- D’Elia, M.A., Millar, K.E., Bhavsar, A.P., Tomljenovic, A.M., Hutter, B., Schaab, C., Moreno-Hagelsieb, G., Brown, E.D.,** 2009. Probing teichoic acid genetics with bioactive molecules reveals new interactions among diverse processes in bacterial cell wall biogenesis. *Chem. Biol.* 16, 548–556.
- D’Elia, M.A., Pereira, M.P., Chung, Y.S., Zhao, W., Chau, A., Kenney, T.J., Sulavik, M.C., Black, T.A., Brown, E.D.,** 2006. Lesions in teichoic acid biosynthesis in *Staphylococcus aureus* lead to a lethal gain of function in the otherwise dispensable pathway. *J. Bacteriol.* 188, 4183–4189.
- D’Ulisse, V., Fagioli, M., Ghelardini, P., Paolozzi, L.,** 2007. Three functional subdomains of the *Escherichia coli* FtsQ protein are involved in its interaction with the other division proteins. *Microbiology (Reading, Engl.)* 153, 124–138.
- Dai, K., Lutkenhaus, J.,** 1991. ftsZ is an essential cell division gene in *Escherichia coli*. *J. Bacteriol.* 173, 3500–3506.
- Dai, K., Xu, Y., Lutkenhaus, J.,** 1993. Cloning and characterization of ftsN, an essential cell division gene in *Escherichia coli* isolated as a multicopy suppressor of ftsA12(Ts). *J. Bacteriol.* 175, 3790–3797.
- Danese, P.N., Oliver, G.R., Barr, K., Bowman, G.D., Rick, P.D., Silhavy, T.J.,** 1998. Accumulation of the enterobacterial common antigen lipid II biosynthetic intermediate stimulates degP transcription in *Escherichia coli*. *J. Bacteriol.* 180, 5875–5884.
- Daniel, R.A., Errington, J.,** 2000. Intrinsic instability of the essential cell division protein FtsL of *Bacillus subtilis* and a role for DivIB protein in FtsL turnover. *Mol. Microbiol.* 36, 278–289.
- Daniel, R.A., Errington, J.,** 2003. Control of cell morphogenesis in bacteria: two distinct ways to make a rod-shaped cell. *Cell* 113, 767–776.
- Daniel, R.A., Noiro-Gros, M.-F., Noiro, P., Errington, J.,** 2006. Multiple Interactions between the Transmembrane Division Proteins of *Bacillus subtilis* and the Role of FtsL Instability in Divisome Assembly. *J. Bacteriol.* 188, 7396–7404.
- Darwin, K.H., Robinson, L.S., Miller, V.L.,** 2001. SigE Is a Chaperone for the *Salmonella enterica* Serovar Typhimurium Invasion Protein SigD. *J. Bacteriol.* 183, 1452–1454.
- Datta, P., Dasgupta, A., Singh, A.K., Mukherjee, P., Kundu, M., Basu, J.,** 2006. Interaction between FtsW and penicillin-binding protein 3 (PBP3) directs PBP3 to mid-cell, controls cell septation and mediates the formation of a trimeric complex involving FtsZ, FtsW and PBP3 in mycobacteria. *Mol. Microbiol.* 62, 1655–1673.

- Dautin, N., Karimova, G., Ladant, D.,** 2003. Human immunodeficiency virus (HIV) type 1 transframe protein can restore activity to a dimerization-deficient HIV protease variant. *J. Virol.* 77, 8216–8226.
- De Boer, P., Crossley, R., Rothfield, L.,** 1992. The essential bacterial cell-division protein FtsZ is a GTPase. *Nature* 359, 254–256.
- De Boer, P.A., Crossley, R.E., Hand, A.R., Rothfield, L.I.,** 1991. The MinD protein is a membrane ATPase required for the correct placement of the *Escherichia coli* division site. *EMBO J.* 10, 4371–4380.
- De Boer, P.A., Crossley, R.E., Rothfield, L.I.,** 1992. Roles of MinC and MinD in the site-specific septation block mediated by the MinCDE system of *Escherichia coli*. *J. Bacteriol.* 174, 63–70.
- De Leeuw, E., Graham, B., Phillips, G.J., ten Hagen-Jongman, C.M., Oudega, B., Luirink, J.,** 1999. Molecular characterization of *Escherichia coli* FtsE and FtsX. *Mol. Microbiol.* 31, 983–993.
- De Pedro, M.A., Quintela, J.C., Höltje, J.V., Schwarz, H.,** 1997. Murein segregation in *Escherichia coli*. *J. Bacteriol.* 179, 2823–2834.
- Deane, C.M., Salwiński, Ł., Xenarios, I., Eisenberg, D.,** 2002. Protein interactions: two methods for assessment of the reliability of high throughput observations. *Mol. Cell Proteomics* 1, 349–356.
- DeDent, A., Bae, T., Missiakas, D.M., Schneewind, O.,** 2008. Signal peptides direct surface proteins to two distinct envelope locations of *Staphylococcus aureus*. *EMBO J.* 27, 2656–2668.
- DeDent, A.C., McAdow, M., Schneewind, O.,** 2007. Distribution of protein A on the surface of *Staphylococcus aureus*. *J. Bacteriol.* 189, 4473–4484.
- Den Blaauwen, T., Buddelmeijer, N., Aarsman, M.E.G., Hameete, C.M., Nanninga, N.,** 1999. Timing of FtsZ Assembly in *Escherichia coli*. *J. Bacteriol.* 181, 5167–5175.
- Dengler, V., Meier, P.S., Heusser, R., Berger-Bächli, B., McCallum, N.,** 2011. Induction kinetics of the *Staphylococcus aureus* cell wall stress stimulon in response to different cell wall active antibiotics. *BMC Microbiol.* 11, 16.
- Dengler, V., Meier, P.S., Heusser, R., Kupferschmied, P., Fazekas, J., Friebe, S., Staufer, S.B., Majcherczyk, P.A., Moreillon, P., Berger-Bächli, B., McCallum, N.,** 2012. Deletion of hypothetical wall teichoic acid ligases in *Staphylococcus aureus* activates the cell wall stress response. *FEMS Microbiol. Lett.* 333, 109–120.
- Derouaux, A., Wolf, B., Fraipont, C., Breukink, E., Nguyen-Distèche, M., Terrak, M.,** 2008. The monofunctional glycosyltransferase of *Escherichia coli* localizes to the cell division site and interacts with penicillin-binding protein 3, FtsW, and FtsN. *J. Bacteriol.* 190, 1831–1834.
- Di Lallo, G., Fagioli, M., Barionovi, D., Ghelardini, P., Paolozzi, L.,** 2003. Use of a two-hybrid assay to study the assembly of a complex multicomponent protein machinery: bacterial septosome differentiation. *Microbiology (Reading, Engl.)* 149, 3353–3359.
- Din, N., Quardokus, E.M., Sackett, M.J., Brun, Y.V.,** 1998. Dominant C-terminal deletions of FtsZ that affect its ability to localize in *Caulobacter* and its interaction with FtsA. *Mol. Microbiol.* 27, 1051–1063.
- Dmitriev, B.A., Toukach, F.V., Holst, O., Rietschel, E.T., Ehlers, S.,** 2004. Tertiary Structure of *Staphylococcus aureus* Cell Wall Murein. *J. Bacteriol.* 186, 7141–7148.
- Dmitriev, B.A., Toukach, F.V., Schaper, K.-J., Holst, O., Rietschel, E.T., Ehlers, S.,** 2003. Tertiary structure of bacterial murein: the scaffold model. *J. Bacteriol.* 185, 3458–3468.
- Donachie, W.D., Begg, K.J.,** 1989. Cell length, nucleoid separation, and cell division of rod-shaped and spherical cells of *Escherichia coli*. *J. Bacteriol.* 171, 4633–4639.
- Dorobantu, L.S., Gray, M.R.,** 2010. Application of atomic force microscopy in bacterial research. *Scanning* 32, 74–96.
- Doyle, R.J., Birdsell, D.C.,** 1972. Interaction of concanavalin A with the cell wall of *Bacillus subtilis*. *J. Bacteriol.* 109, 652–658.

- Dramsi, S., Biswas, I., Maguin, E., Braun, L., Mastroeni, P., Cossart, P.,** 1995. Entry of *Listeria monocytogenes* into hepatocytes requires expression of InlB, a surface protein of the internalin multigene family. *Molecular Microbiology* 16, 251–261.
- Draper, G.C., McLennan, N., Begg, K., Masters, M., Donachie, W.D.,** 1998. Only the N-terminal domain of FtsK functions in cell division. *J. Bacteriol.* 180, 4621–4627.
- Dubrac, S., Boneca, I.G., Poupel, O., Msadek, T.,** 2007. New insights into the Walk/WalR (YycG/YycF) essential signal transduction pathway reveal a major role in controlling cell wall metabolism and biofilm formation in *Staphylococcus aureus*. *J. Bacteriol.* 189, 8257–8269.
- Dubrac, S., Msadek, T.,** 2004. Identification of Genes Controlled by the Essential YycG/YycF Two-Component System of *Staphylococcus aureus*. *J. Bacteriol.* 186, 1175–1181.
- Durand-Heredia, J.M., Yu, H.H., De Carlo, S., Lesser, C.F., Janakiraman, A.,** 2011. Identification and characterization of ZapC, a stabilizer of the FtsZ ring in *Escherichia coli*. *J. Bacteriol.* 193, 1405–1413.
- Dziarski, R., Gupta, D.,** 2005. Peptidoglycan recognition in innate immunity. *J. Endotoxin Res.* 11, 304–310.
- Dziarski, R., Gupta, D.,** 2010. Review: Mammalian peptidoglycan recognition proteins (PGRPs) in innate immunity. *Innate Immun* 16, 168–174.
- E.J. Hayhurst,** 2006. Peptidoglycan structure and dynamics in gram-positive bacteria. University of Sheffield.
- Ebersbach, G., Galli, E., Møller-Jensen, J., Löwe, J., Gerdes, K.,** 2008. Novel coiled-coil cell division factor ZapB stimulates Z ring assembly and cell division. *Mol. Microbiol.* 68, 720–735.
- Einhauer, A., Jungbauer, A.,** 2001. The FLAGTM peptide, a versatile fusion tag for the purification of recombinant proteins. *J. Biochem. and Biophys. Methods* 49, 455–465.
- Eldholm, V., Johnsborg, O., Straume, D., Ohnstad, H.S., Berg, K.H., Hermoso, J.A., Håvarstein, L.S.,** 2010. *Pneumococcal* CbpD is a murein hydrolase that requires a dual cell envelope binding specificity to kill target cells during fratricide. *Mol. Microbiol.* 76, 905–917.
- Ellermeier, C.D., Hobbs, E.C., Gonzalez-Pastor, J.E., Losick, R.,** 2006. A three-protein signaling pathway governing immunity to a bacterial cannibalism toxin. *Cell* 124, 549–559.
- Elliott, T.S., Ward, J.B., Wyrick, P.B., Rogers, H.J.,** 1975. Ultrastructural study of the reversion of protoplasts of *Bacillus licheniformis* to bacilli. *J. Bacteriol.* 124, 905–917.
- Ellwood, D.C.,** 1970. The wall content and composition of *Bacillus subtilis* var. niger grown in a chemostat. *Biochem. J.* 118, 367–373.
- Ellwood, D.C., Tempest, D.W.,** 1972. Influence of culture pH on the content and composition of teichoic acids in the walls of *Bacillus subtilis*. *J. Gen. Microbiol.* 73, 395–402.
- Endl, J., Seidl, H.P., Fiedler, F., Schleifer, K.H.,** 1983. Chemical composition and structure of cell wall teichoic acids of staphylococci. *Arch. Microbiol.* 135, 215–223.
- Erickson, H.P.,** 2001. The FtsZ protofilament and attachment of ZipA--structural constraints on the FtsZ power stroke. *Curr. Opin. Cell Biol.* 13, 55–60.
- Erickson, H.P., Anderson, D.E., Osawa, M.,** 2010. FtsZ in Bacterial Cytokinesis: Cytoskeleton and Force Generator All in One. *Microbiol Mol Biol Rev* 74, 504–528.
- Errington, J.,** 2003. Regulation of endospore formation in *Bacillus subtilis*. *Nat. Rev. Microbiol.* 1, 117–126.
- Errington, J., Daniel, R.A., Scheffers, D.-J.,** 2003. Cytokinesis in bacteria. *Microbiol. Mol. Biol. Rev.* 67, 52–65, table of contents.
- Espeli, O., Lee, C., Mariani, K.J.,** 2003. A physical and functional interaction between *Escherichia coli* FtsK and topoisomerase IV. *J. Biol. Chem.* 278, 44639–44644.
- Fadda, D., Pischedda, C., Caldara, F., Whalen, M.B., Anderluzzi, D., Domenici, E., Massidda, O.,** 2003. Characterization of divIVA and other genes located in the chromosomal region downstream of the dcw cluster in *Streptococcus pneumoniae*. *J. Bacteriol.* 185, 6209–6214.

- Fadda, D., Santona, A., D'Ulisse, V., Ghelardini, P., Ennas, M.G., Whalen, M.B., Massidda, O.,** 2007. *Streptococcus pneumoniae* DivIVA: localization and interactions in a MinCD-free context. *J. Bacteriol.* 189, 1288–1298.
- Fattom, A., Schneerson, R., Szu, S.C., Vann, W.F., Shiloach, J., Karakawa, W.W., Robbins, J.B.,** 1990. Synthesis and immunologic properties in mice of vaccines composed of *Staphylococcus aureus* type 5 and type 8 capsular polysaccharides conjugated to *Pseudomonas aeruginosa* exotoxin A. *Infect Immun* 58, 2367–2374.
- Fernández-Tornero, C., López, R., García, E., Giménez-Gallego, G., Romero, A.,** 2001. A novel solenoid fold in the cell wall anchoring domain of the *pneumococcal* virulence factor LytA. *Nat. Struct. Biol.* 8, 1020–1024.
- Feucht, A., Lucet, I., Yudkin, M.D., Errington, J.,** 2001. Cytological and biochemical characterization of the FtsA cell division protein of *Bacillus subtilis*. *Mol. Microbiol.* 40, 115–125.
- Firczuk, M., Mucha, A., Bochtler, M.,** 2005. Crystal structures of active LytM. *J. Mol. Biol.* 354, 578–590.
- Fonzé, E., Vermeire, M., Nguyen-Distèche, M., Brasseur, R., Charlier, P.,** 1999. The crystal structure of a penicilloyl-serine transferase of intermediate penicillin sensitivity. The DD-transpeptidase of streptomycetes K15. *J. Biol. Chem.* 274, 21853–21860.
- Formstone, A., Carballido-López, R., Noirot, P., Errington, J., Scheffers, D.-J.,** 2008. Localization and Interactions of Teichoic Acid Synthetic Enzymes in *Bacillus subtilis*. *J. Bacteriol.* 190, 1812–1821.
- Foster, S.J.,** 1995. Molecular characterization and functional analysis of the major autolysin of *Staphylococcus aureus* 8325/4. *J. Bacteriol.* 177, 5723–5725.
- Fraipont, C., Alexeeva, S., Wolf, B., van der Ploeg, R., Schloesser, M., den Blaauwen, T., Nguyen-Distèche, M.,** 2011. The integral membrane FtsW protein and peptidoglycan synthase PBP3 form a subcomplex in *Escherichia coli*. *Microbiology (Reading, Engl.)* 157, 251–259.
- Francius, G., Domenech, O., Mingeot-Leclercq, M.P., Dufrêne, Y.F.,** 2008. Direct observation of *Staphylococcus aureus* cell wall digestion by lysostaphin. *J. Bacteriol.* 190, 7904–7909.
- Frankel, M.B., Hendrickx, A.P.A., Missiakas, D.M., Schneewind, O.,** 2011. LytN, a murein hydrolase in the cross-wall compartment of *Staphylococcus aureus*, is involved in proper bacterial growth and envelope assembly. *J. Biol. Chem.* 286, 32593–32605.
- Frankel, M.B., Schneewind, O.,** 2012. Determinants of murein hydrolase targeting to cross-wall of *Staphylococcus aureus* peptidoglycan. *J. Biol. Chem.* 287, 10460–10471.
- Fu, G., Huang, T., Buss, J., Coltharp, C., Hensel, Z., Xiao, J.,** 2010. In vivo structure of the *E. coli* FtsZ-ring revealed by photoactivated localization microscopy (PALM). *PLoS ONE* 5, e12682.
- Fukushima, T., Szurmant, H., Kim, E.-J., Perego, M., Hoch, J.A.,** 2008. A sensor histidine kinase coordinates cell wall architecture with cell division in *Bacillus subtilis*. *Mol. Microbiol.* 69, 621–632.
- Galli, E., Gerdes, K.,** 2010. Spatial resolution of two bacterial cell division proteins: ZapA recruits ZapB to the inner face of the Z-ring. *Mol. Microbiol.* 76, 1514–1526.
- Gan, L., Chen, S., Jensen, G.J.,** 2008. Molecular organization of Gram-negative peptidoglycan. *Proc. Natl. Acad. Sci. U.S.A.* 105, 18953–18957.
- García-Lara, J., Foster, S.J.,** 2009. Anti-*Staphylococcus aureus* immunotherapy: current status and prospects. *Current Opinion in Pharmacology* 9, 552–557.
- Gérard, P., Vernet, T., Zapun, A.,** 2002. Membrane topology of the *Streptococcus pneumoniae* FtsW division protein. *J. Bacteriol.* 184, 1925–1931.
- Gerding, M.A., Liu, B., Bendezú, F.O., Hale, C.A., Bernhardt, T.G., de Boer, P.A.J.,** 2009. Self-enhanced accumulation of FtsN at Division Sites and Roles for Other Proteins with a SPOR domain (DamX, DedD, and RlpA) in *Escherichia coli* cell constriction. *J. Bacteriol.* 191, 7383–7401.
- Ghuysen, J.M.,** 1991. Serine beta-lactamases and penicillin-binding proteins. *Annu. Rev. Microbiol.* 45, 37–67.

- Ghuysen, J.-M.**, 1994. Molecular structures of penicillin-binding proteins and β -lactamases. *Trends in Microbiology* 2, 372–380.
- Gibson, C.W., Daneo-Moore, L., Higgins, M.L.**, 1983. Cell wall assembly during inhibition of DNA synthesis in *Streptococcus faecium*. *J. Bacteriol.* 155, 351–356.
- Giesbrecht, P., Kersten, T., Maidhof, H., Wecke, J.**, 1998. *Staphylococcal* cell wall: morphogenesis and fatal variations in the presence of penicillin. *Microbiol. Mol. Biol. Rev.* 62, 1371–1414.
- Gilbo, C.M., Beaton, C.D., Coles, N.W.**, 1967. Electron microscopy of the lysis of *Staphylococcus aureus* cell walls by *Aeromonas* lytic factor. *J. Bacteriol.* 93, 1972–1975.
- Girardin, S.E., Philpott, D.J.**, 2004. Mini-review: The role of peptidoglycan recognition in innate immunity. *European Journal of Immunology* 34, 1777–1782.
- Glaser, P., Ladant, D., Sezer, O., Pichot, F., Ullmann, A., Danchin, A.**, 1988. The calmodulin-sensitive adenylate cyclase of *Bordetella pertussis*: cloning and expression in *Escherichia coli*. *Mol. Microbiol.* 2, 19–30.
- Goehring, N.W., Gueiros-Filho, F., Beckwith, J.**, 2005. Premature targeting of a cell division protein to midcell allows dissection of divisome assembly in *Escherichia coli*. *Genes Dev.* 19, 127–137.
- Goerke, C., Fluckiger, U., Steinhuber, A., Bisanzio, V., Ulrich, M., Bischoff, M., Patti, J.M., Wolz, C.**, 2005. Role of *Staphylococcus aureus* global regulators *sae* and *sigmaB* in virulence gene expression during device-related infection. *Infect. Immun.* 73, 3415–3421.
- Goffin, C., Fraipont, C., Ayala, J., Terrak, M., Nguyen-Distèche, M., Ghuysen, J.M.**, 1996. The non-penicillin-binding module of the tripartite penicillin-binding protein 3 of *Escherichia coli* is required for folding and/or stability of the penicillin-binding module and the membrane-anchoring module confers cell septation activity on the folded structure. *J. Bacteriol.* 178, 5402–5409.
- Gogly, B., Groult, N., Hornebeck, W., Godeau, G., Pellat, B.**, 1998. Collagen zymography as a sensitive and specific technique for the determination of subpicogram levels of interstitial collagenase. *Anal. Biochem.* 255, 211–216.
- Goley, E.D., Yeh, Y.-C., Hong, S.-H., Fero, M.J., Abeliuk, E., McAdams, H.H., Shapiro, L.**, 2011. Assembly of the *Caulobacter* cell division machine. *Mol. Microbiol.* 80, 1680–1698.
- Gonzalez, M.D., Beckwith, J.**, 2009. Divisome under construction: distinct domains of the small membrane protein FtsB are necessary for interaction with multiple cell division proteins. *J. Bacteriol.* 191, 2815–2825.
- González-Pastor, J.E., Hobbs, E.C., Losick, R.**, 2003. Cannibalism by sporulating bacteria. *Science* 301, 510–513.
- Goodman, A.L., Merighi, M., Hyodo, M., Ventre, I., Filloux, A., Lory, S.**, 2009. Direct interaction between sensor kinase proteins mediates acute and chronic disease phenotypes in a bacterial pathogen. *Genes Dev.* 23, 249–259.
- Gross, M., Cramton, S.E., Götz, F., Peschel, A.**, 2001. Key Role of Teichoic Acid Net Charge in *Staphylococcus aureus* Colonization of Artificial Surfaces. *Infect. Immun.* 69, 3423–3426.
- Gruss, A., Novick, R.**, 1986. Plasmid instability in regenerating protoplasts of *Staphylococcus aureus* is caused by aberrant cell division. *J. Bacteriol.* 165, 878–883.
- Gueiros-Filho, F.J., Losick, R.**, 2002. A widely conserved bacterial cell division protein that promotes assembly of the tubulin-like protein FtsZ. *Genes Dev.* 16, 2544–2556.
- Guinane, C.M., Cotter, P.D., Ross, R.P., Hill, C.**, 2006. Contribution of penicillin-binding protein homologs to antibiotic resistance, cell morphology, and virulence of *Listeria monocytogenes* EGDe. *Antimicrob. Agents Chemother.* 50, 2824–2828.
- Gündoğdu, M.E., Kawai, Y., Pavlendova, N., Ogasawara, N., Errington, J., Scheffers, D.-J., Hamoen, L.W.**, 2011. Large ring polymers align FtsZ polymers for normal septum formation. *EMBO J.* 30, 617–626.
- Gunther, G.R., Wang, J.L., Yahara, I., Cunningham, B.A., Edelman, G.M.**, 1973. Concanavalin A Derivatives with Altered Biological Activities. *Proc Natl Acad Sci U S A* 70, 1012–1016.

- Gustafsson, M.G.**, 2000. Surpassing the lateral resolution limit by a factor of two using structured illumination microscopy. *J Microsc* 198, 82–87.
- Haeusser, D.P., Schwartz, R.L., Smith, A.M., Oates, M.E., Levin, P.A.**, 2004. EzrA prevents aberrant cell division by modulating assembly of the cytoskeletal protein FtsZ. *Mol. Microbiol.* 52, 801–814.
- Hale, C.A., de Boer, P.A.**, 1997. Direct binding of FtsZ to ZipA, an essential component of the septal ring structure that mediates cell division in *E. coli*. *Cell* 88, 175–185.
- Hale, C.A., de Boer, P.A.**, 1999. Recruitment of ZipA to the septal ring of *Escherichia coli* is dependent on FtsZ and independent of FtsA. *J. Bacteriol.* 181, 167–176.
- Hale, C.A., Shiomi, D., Liu, B., Bernhardt, T.G., Margolin, W., Niki, H., de Boer, P.A.J.**, 2011. Identification of *Escherichia coli* ZapC (YcbW) as a component of the division apparatus that binds and bundles FtsZ polymers. *J. Bacteriol.* 193, 1393–1404.
- Hamoen, L.W., Meile, J.-C., de Jong, W., Noirot, P., Errington, J.**, 2006. SepF, a novel FtsZ-interacting protein required for a late step in cell division. *Mol. Microbiol.* 59, 989–999.
- Hancock, L.E., Perego, M.**, 2004. Systematic inactivation and phenotypic characterization of two-component signal transduction systems of *Enterococcus faecalis* V583. *J. Bacteriol.* 186, 7951–7958.
- Hardman, K.D., Ainsworth, C.F.**, 1976. Structure of the concanavalin A-methyl alpha-D-mannopyranoside complex at 6-Å resolution. *Biochemistry* 15, 1120–1128.
- Harris, F., Demel, R., de Kruijff, B., Phoenix, D.A.**, 1998. An investigation into the lipid interactions of peptides corresponding to the C-terminal anchoring domains of *Escherichia coli* penicillin-binding proteins 4, 5 and 6. *Biochim. Biophys. Acta* 1415, 10–22.
- Harro, C.D., Betts, R.F., Hartzel, J.S., Onorato, M.T., Lipka, J., Smugar, S.S., Kartsonis, N.A.**, 2012. The immunogenicity and safety of different formulations of a novel *Staphylococcus aureus* vaccine (V710): results of two Phase I studies. *Vaccine* 30, 1729–1736.
- Hartford, O., Francois, P., Vaudaux, P., Foster, T.J.**, 1997. The dipeptide repeat region of the fibrinogen-binding protein (clumping factor) is required for functional expression of the fibrinogen-binding domain on the *Staphylococcus aureus* cell surface. *Mol. Microbiol.* 25, 1065–1076.
- Hayhurst, E.J., Kailas, L., Hobbs, J.K., Foster, S.J.**, 2008. Cell wall peptidoglycan architecture in *Bacillus subtilis*. *Proc Natl Acad Sci U S A* 105, 14603–14608.
- Heidrich, C., Templin, M.F., Ursinus, A., Merdanovic, M., Berger, J., Schwarz, H., De Pedro, M.A., Höltje, J.-V.**, 2001. Involvement of N-acetylmuramyl-l-alanine amidases in cell separation and antibiotic-induced autolysis of *Escherichia coli*. *Molecular Microbiology* 41, 167–178.
- Heidrich, C., Ursinus, A., Berger, J., Schwarz, H., Höltje, J.-V.**, 2002. Effects of multiple deletions of murein hydrolases on viability, septum cleavage, and sensitivity to large toxic molecules in *Escherichia coli*. *J. Bacteriol.* 184, 6093–6099.
- Heilemann, M., van de Linde, S., Schüttelz, M., Kasper, R., Seefeldt, B., Mukherjee, A., Tinnefeld, P., Sauer, M.**, 2008. Subdiffraction-resolution fluorescence imaging with conventional fluorescent probes. *Angew. Chem. Int. Ed. Engl.* 47, 6172–6176.
- Heilmann, C., Hartleib, J., Hussain, M.S., Peters, G.**, 2005. The multifunctional *Staphylococcus aureus* autolysin aaa mediates adherence to immobilized fibrinogen and fibronectin. *Infect. Immun.* 73, 4793–4802.
- Heilmann, C., Hussain, M., Peters, G., Götz, F.**, 1997. Evidence for autolysin-mediated primary attachment of *Staphylococcus epidermidis* to a polystyrene surface. *Mol. Microbiol.* 24, 1013–1024.
- Heilmann, C., Thumm, G., Chhatwal, G.S., Hartleib, J., Uekötter, A., Peters, G.**, 2003. Identification and characterization of a novel autolysin (Aae) with adhesive properties from *Staphylococcus epidermidis*. *Microbiology (Reading, Engl.)* 149, 2769–2778.
- Henriques, A.O., Glaser, P., Piggot, P.J., Moran, C.P., Jr**, 1998. Control of cell shape and elongation by the rodA gene in *Bacillus subtilis*. *Mol. Microbiol.* 28, 235–247.

- Heptinstall, S., Archibald, A.R., Baddiley, J.,** 1970. Teichoic acids and membrane function in bacteria. *Nature* 225, 519–521.
- Hiramatsu, K.,** 2001. Vancomycin-resistant *Staphylococcus aureus*: a new model of antibiotic resistance. *Lancet Infect Dis* 1, 147–155.
- Hiramatsu, K., Hanaki, H.,** 1998. Glycopeptide resistance in *staphylococci*. *Curr. Opin. Infect. Dis.* 11, 653–658.
- Hiramatsu, K., Hanaki, H., Ino, T., Yabuta, K., Oguri, T., Tenover, F.C.,** 1997. Methicillin-resistant *Staphylococcus aureus* clinical strain with reduced vancomycin susceptibility. *J. Antimicrob. Chemother.* 40, 135–136.
- Hirano, T., Minamino, T., Macnab, R.M.,** 2001. The role in flagellar rod assembly of the N-terminal domain of *Salmonella* FlgJ, a flagellum-specific muramidase. *J. Mol. Biol.* 312, 359–369.
- Hirschhausen, N., Schlesier, T., Peters, G., Heilmann, C.,** 2012. Characterization of the Modular Design of the Autolysin/Adhesin Aaa from *Staphylococcus Aureus*. *PLoS One* 7.
- Höltje, J.V.,** 1998. Growth of the stress-bearing and shape-maintaining murein sacculus of *Escherichia coli*. *Microbiol. Mol. Biol. Rev.* 62, 181–203.
- Höltje, J.V., Heidrich, C.,** 2001. Enzymology of elongation and constriction of the murein sacculus of *Escherichia coli*. *Biochimie* 83, 103–108.
- Höltje, J.V., Tuomanen, E.I.,** 1991. The murein hydrolases of *Escherichia coli*: properties, functions and impact on the course of infections in vivo. *J. Gen. Microbiol.* 137, 441–454.
- Horsburgh, G.J., Atrih, A., Foster, S.J.,** 2003. Characterization of LytH, a differentiation-associated peptidoglycan hydrolase of *Bacillus subtilis* involved in endospore cortex maturation. *J. Bacteriol.* 185, 3813–3820.
- Horsburgh, M.J., Aish, J.L., White, I.J., Shaw, L., Lithgow, J.K., Foster, S.J.,** 2002. sigmaB modulates virulence determinant expression and stress resistance: characterization of a functional rsbU strain derived from *Staphylococcus aureus* 8325-4. *J. Bacteriol.* 184, 5457–5467.
- Hu, Z., Lutkenhaus, J.,** 2000. Analysis of MinC reveals two independent domains involved in interaction with MinD and FtsZ. *J. Bacteriol.* 182, 3965–3971.
- Hu, Z., Saez, C., Lutkenhaus, J.,** 2003. Recruitment of MinC, an Inhibitor of Z-Ring Formation, to the Membrane in *Escherichia coli*: Role of MinD and MinE. *J. Bacteriol.* 185, 196–203.
- Huang, B., Babcock, H., Zhuang, X.,** 2010. Breaking the diffraction barrier: super-resolution imaging of cells. *Cell* 143, 1047–1058.
- Hübscher, J., Lüthy, L., Berger-Bächi, B., Stutzmann Meier, P.,** 2008. Phylogenetic distribution and membrane topology of the LytR-CpsA-Psr protein family. *BMC Genomics* 9, 617.
- Hudson, M.E., Nodwell, J.R.,** 2004. Dimerization of the RamC morphogenetic protein of *Streptomyces coelicolor*. *J. Bacteriol.* 186, 1330–1336.
- Huecas, S., Andreu, J.M.,** 2004. Polymerization of nucleotide-free, GDP- and GTP-bound cell division protein FtsZ: GDP makes the difference. *FEBS Lett.* 569, 43–48.
- Huecas, S., Llorca, O., Boskovic, J., Martín-Benito, J., Valpuesta, J.M., Andreu, J.M.,** 2008. Energetics and geometry of FtsZ polymers: nucleated self-assembly of single protofilaments. *Biophys. J.* 94, 1796–1806.
- Huecas, S., Schaffner-Barbero, C., García, W., Yébenes, H., Palacios, J.M., Díaz, J.F., Menéndez, M., Andreu, J.M.,** 2007. The interactions of cell division protein FtsZ with guanine nucleotides. *J. Biol. Chem.* 282, 37515–37528.
- Hughes, A.H., Hancock, I.C., Baddiley, J.,** 1973. The function of teichoic acids in cation control in bacterial membranes. *Biochem. J.* 132, 83–93.
- Ishikawa, S., Kawai, Y., Hiramatsu, K., Kuwano, M., Ogasawara, N.,** 2006. A new FtsZ-interacting protein, YlmF, complements the activity of FtsA during progression of cell division in *Bacillus subtilis*. *Molecular Microbiology* 60, 1364–1380.
- Jacobs, C., Frère, J.M., Normark, S.,** 1997. Cytosolic intermediates for cell wall biosynthesis and degradation control inducible beta-lactam resistance in gram-negative bacteria. *Cell* 88, 823–832.

- Jones, S.A., Shim, S.-H., He, J., Zhuang, X., 2011. Fast, three-dimensional super-resolution imaging of live cells. *Nat. Methods* 8, 499–508.
- Jones, T., 2002. StaphVAX (Nabi). *Curr Opin Investig Drugs* 3, 48–50.
- Josefsson, E., McCrea, K.W., Eidhin, D.N., O'Connell, D., Cox, J., Hook, M., Foster, T.J., 1998. Three new members of the serine-aspartate repeat protein multigene family of *Staphylococcus aureus*. *Microbiology* 144, 3387–3395.
- Juette, M.F., Gould, T.J., Lessard, M.D., Mlodzianoski, M.J., Nagpure, B.S., Bennett, B.T., Hess, S.T., Bewersdorf, J., 2008. Three-dimensional sub-100 nm resolution fluorescence microscopy of thick samples. *Nat. Methods* 5, 527–529.
- Kajimura, J., Fujiwara, T., Yamada, S., Suzawa, Y., Nishida, T., Oyamada, Y., Hayashi, I., Yamagishi, J., Komatsuzawa, H., Sugai, M., 2005. Identification and molecular characterization of an N-acetylmuramyl-L-alanine amidase Sle1 involved in cell separation of *Staphylococcus aureus*. *Mol. Microbiol.* 58, 1087–1101.
- Kallipolitis, B.H., Ingmer, H., 2001. *Listeria monocytogenes* response regulators important for stress tolerance and pathogenesis. *FEMS Microbiol. Lett.* 204, 111–115.
- Karamanos, Y., 1997. Endo-N-acetyl-beta-D-glucosaminidases and their potential substrates: structure/function relationships. *Res. Microbiol.* 148, 661–671.
- Karimova, G., Dautin, N., Ladant, D., 2005. Interaction network among *Escherichia coli* membrane proteins involved in cell division as revealed by bacterial two-hybrid analysis. *J. Bacteriol.* 187, 2233–2243.
- Karimova, G., Pidoux, J., Ullmann, A., Ladant, D., 1998. A bacterial two-hybrid system based on a reconstituted signal transduction pathway. *Proc. Natl. Acad. Sci. U.S.A.* 95, 5752–5756.
- Kawai, Y., Marles-Wright, J., Cleverley, R.M., Emmins, R., Ishikawa, S., Kuwano, M., Heinz, N., Bui, N.K., Hoyland, C.N., Ogasawara, N., Lewis, R.J., Vollmer, W., Daniel, R.A., Errington, J., 2011. A widespread family of bacterial cell wall assembly proteins. *The EMBO Journal* 30, 4931–4941.
- Kleiner, D.E., Stetlerstevenson, W.G., 1994. Quantitative Zymography: Detection of Picogram Quantities of Gelatinases. *Analytical Biochemistry* 218, 325–329.
- Kloos, W.E., Bannerman, T.L., 1994. Update on clinical significance of coagulase-negative staphylococci. *Clin Microbiol Rev* 7, 117–140.
- Kobayashi, K., Ehrlich, S.D., Albertini, A., Amati, G., Andersen, K.K., et al., 2003. Essential *Bacillus subtilis* genes. *Proc. Natl. Acad. Sci. U.S.A.* 100, 4678–4683.
- Koch, A.L., 1998. Orientation of the peptidoglycan chains in the sacculus of *Escherichia coli*. *Res. Microbiol.* 149, 689–701.
- Komatsuzawa, H., Sugai, M., Nakashima, S., Yamada, S., Matsumoto, A., Oshida, T., Suginaka, H., 1997. Subcellular localization of the major autolysin, ATL and its processed proteins in *Staphylococcus aureus*. *Microbiol. Immunol.* 41, 469–479.
- Koraimann, G., 2003. Lytic transglycosylases in macromolecular transport systems of Gram-negative bacteria. *Cell. Mol. Life Sci.* 60, 2371–2388.
- Kraft, A.R., Prabhu, J., Ursinus, A., Höltje, J.V., 1999. Interference with murein turnover has no effect on growth but reduces beta-lactamase induction in *Escherichia coli*. *J. Bacteriol.* 181, 7192–7198.
- Kreiswirth, B.N., Löfdahl, S., Betley, M.J., O'Reilly, M., Schlievert, P.M., Bergdoll, M.S., Novick, R.P., 1983. The toxic shock syndrome exotoxin structural gene is not detectably transmitted by a prophage. *Nature* 305, 709–712.
- Kristian, S.A., Lauth, X., Nizet, V., Goetz, F., Neumeister, B., Peschel, A., Landmann, R., 2003. Alanylation of teichoic acids protects *Staphylococcus aureus* against Toll-like receptor 2-dependent host defense in a mouse tissue cage infection model. *J. Infect. Dis.* 188, 414–423.
- Kuroda, M., Ohta, T., Uchiyama, I., Baba, T., Yuzawa, H., Kobayashi, I., Cui, L., Oguchi, A., Aoki, K., Nagai, Y., Lian, J., Ito, T., Kanamori, M., Matsumaru, H., Maruyama, A., Murakami, H.,

- Hosoyama, A., Mizutani-Ui, Y., Takahashi, N.K., Sawano, T., Inoue, R., Kaito, C., Sekimizu, K., Hirakawa, H., Kuhara, S., Goto, S., Yabuzaki, J., Kanehisa, M., Yamashita, A., Oshima, K., Furuya, K., Yoshino, C., Shiba, T., Hattori, M., Ogasawara, N., Hayashi, H., Hiramatsu, K., 2001. Whole genome sequencing of meticillin-resistant *Staphylococcus aureus*. *Lancet* 357, 1225–1240.
- Lambert, P.A., Hancock, I.C., Baddiley, J., 1977. Occurrence and function of membrane teichoic acids. *Biochim. Biophys. Acta* 472, 1–12.
- Lara, B., Ayala, J.A., 2002. Topological characterization of the essential *Escherichia coli* cell division protein FtsW. *FEMS Microbiol. Lett.* 216, 23–32.
- Lazarevic, V., Margot, P., Soldo, B., Karamata, D., 1992. Sequencing and analysis of the *Bacillus subtilis* lytRABC divergon: a regulatory unit encompassing the structural genes of the N-acetylmuramoyl-L-alanine amidase and its modifier. *J. Gen. Microbiol.* 138, 1949–1961.
- Le Gouëllec, A., Roux, L., Fadda, D., Massidda, O., Vernet, T., Zapun, A., 2008. Roles of pneumococcal DivIB in cell division. *J. Bacteriol.* 190, 4501–4511.
- Lefman, J., Scott, K., Stranick, S., 2011. Live, video-rate super-resolution microscopy using structured illumination and rapid GPU-based parallel processing. *Microsc. Microanal.* 17, 191–196.
- Leung, B.O., Chou, K.C., 2011. Review of super-resolution fluorescence microscopy for biology. *Appl Spectrosc* 65, 967–980.
- Levin, P.A., Kurtser, I.G., Grossman, A.D., 1999. Identification and characterization of a negative regulator of FtsZ ring formation in *Bacillus subtilis*. *Proc. Natl. Acad. Sci. U.S.A.* 96, 9642–9647.
- Liang, X., Yu, C., Sun, J., Liu, H., Landwehr, C., Holmes, D., Ji, Y., 2006. Inactivation of a two-component signal transduction system, SaeRS, eliminates adherence and attenuates virulence of *Staphylococcus aureus*. *Infect. Immun.* 74, 4655–4665.
- Lorenz, U., Lorenz, B., Schmitter, T., Streker, K., Erck, C., Wehland, J., Nickel, J., Zimmermann, B., Ohlsen, K., 2011. Functional antibodies targeting IsaA of *Staphylococcus aureus* augment host immune response and open new perspectives for antibacterial therapy. *Antimicrob. Agents Chemother.* 55, 165–173.
- Lowy, F.D., 1998. Staphylococcus aureus infections. *N. Engl. J. Med.* 339, 520–532.
- Lowy, F.D., 2003. Antimicrobial resistance: the example of *Staphylococcus aureus*. *J Clin Invest* 111, 1265–1273.
- Lu, C., Reedy, M., Erickson, H.P., 2000. Straight and curved conformations of FtsZ are regulated by GTP hydrolysis. *J. Bacteriol.* 182, 164–170.
- Lu, M., Kleckner, N., 1994. Molecular cloning and characterization of the pgm gene encoding phosphoglucomutase of *Escherichia coli*. *J. Bacteriol.* 176, 5847–5851.
- Lugtenberg, B., Van Alphen, L., 1983. Molecular architecture and functioning of the outer membrane of *Escherichia coli* and other gram-negative bacteria. *Biochim. Biophys. Acta* 737, 51–115.
- Lützner, N., Pätzold, B., Zoll, S., Stehle, T., Kalbacher, H., 2009. Development of a novel fluorescent substrate for Autolysin E, a bacterial type II amidase. *Biochem. Biophys. Res. Commun.* 380, 554–558.
- Ma, X., Ehrhardt, D.W., Margolin, W., 1996. Colocalization of cell division proteins FtsZ and FtsA to cytoskeletal structures in living *Escherichia coli* cells by using green fluorescent protein. *Proc. Natl. Acad. Sci. U.S.A.* 93, 12998–13003.
- Ma, X., Margolin, W., 1999. Genetic and functional analyses of the conserved C-terminal core domain of *Escherichia coli* FtsZ. *J. Bacteriol.* 181, 7531–7544.
- McAulay, 2011. Glycosylation of *Staphylococcus aureus* surface proteins. University of Sheffield.
- Madigan M.T, Martiko J.M, Parker J., 2002. Brock biology of microorganisms. Prentice Hall/Pearson Education, UpperSaddle River, NJ.

- Maggi, S., Massidda, O., Luzi, G., Fadda, D., Paolozzi, L., Ghelardini, P., 2008.** Division protein interaction web: identification of a phylogenetically conserved common interactome between *Streptococcus pneumoniae* and *Escherichia coli*. *Microbiology (Reading, Engl.)* 154, 3042–3052.
- Mandal, D.K., Brewer, C.F., 1993.** Differences in the binding affinities of dimeric concanavalin A (including acetyl and succinyl derivatives) and tetrameric concanavalin A with large oligomannose-type glycopeptides. *Biochemistry* 32, 5116–5120.
- Marbouty, M., Mazouni, K., Saguez, C., Cassier-Chauvat, C., Chauvat, F., 2009a.** Characterization of the *Synechocystis* strain PCC 6803 penicillin-binding proteins and cytokinetic proteins FtsQ and FtsW and their network of interactions with ZipN. *J. Bacteriol.* 191, 5123–5133.
- Marbouty, M., Saguez, C., Cassier-Chauvat, C., Chauvat, F., 2009b.** Characterization of the FtsZ-interacting septal proteins SepF and Ftn6 in the spherical-celled cyanobacterium *Synechocystis* strain PCC 6803. *J. Bacteriol.* 191, 6178–6185.
- Margolin, W., 2000.** Themes and variations in prokaryotic cell division. *FEMS Microbiol. Rev.* 24, 531–548.
- Margolin, W., 2001.** Spatial regulation of cytokinesis in bacteria. *Current Opinion in Microbiology* 4, 647–652.
- Margot, P., Mauël, C., Karamata, D., 1994.** The gene of the N-acetylglucosaminidase, a *Bacillus subtilis* 168 cell wall hydrolase not involved in vegetative cell autolysis. *Mol. Microbiol.* 12, 535–545.
- Marino, M., Banerjee, M., Jonquières, R., Cossart, P., Ghosh, P., 2002.** GW domains of the *Listeria monocytogenes* invasion protein InlB are SH3-like and mediate binding to host ligands. *EMBO J.* 21, 5623–5634.
- Markiewicz, Z., Glauner, B., Schwarz, U., 1983.** Murein structure and lack of DD- and LD-carboxypeptidase activities in *Caulobacter crescentus*. *J. Bacteriol.* 156, 649–655.
- Marquis, R.E., Mayzel, K., Carstensen, E.L., 1976.** Cation exchange in cell walls of gram-positive bacteria. *Can. J. Microbiol.* 22, 975–982.
- Marshall, J.H., Wilmoth, G.J., 1981.** Pigments of *Staphylococcus aureus*, a series of triterpenoid carotenoids. *J. Bacteriol.* 147, 900–913.
- Marston, A.L., Thomaidis, H.B., Edwards, D.H., Sharpe, M.E., Errington, J., 1998.** Polar localization of the MinD protein of *Bacillus subtilis* and its role in selection of the mid-cell division site. *Genes Dev* 12, 3419–3430.
- Martin, P.K., Li, T., Sun, D., Biek, D.P., Schmid, M.B., 1999.** Role in cell permeability of an essential two-component system in *Staphylococcus aureus*. *J. Bacteriol.* 181, 3666–3673.
- Mateos-Gil, P., Paez, A., Hörger, I., Rivas, G., Vicente, M., Tarazona, P., Vélez, M., 2012.** Depolymerization dynamics of individual filaments of bacterial cytoskeletal protein FtsZ. *Proc. Natl. Acad. Sci. U.S.A.* 109, 8133–8138.
- Matias, V.R.F., Beveridge, T.J., 2005.** Cryo-electron microscopy reveals native polymeric cell wall structure in *Bacillus subtilis* 168 and the existence of a periplasmic space. *Mol. Microbiol.* 56, 240–251.
- Matias, V.R.F., Beveridge, T.J., 2006.** Native cell wall organization shown by cryo-electron microscopy confirms the existence of a periplasmic space in *Staphylococcus aureus*. *J. Bacteriol.* 188, 1011–1021.
- Matias, V.R.F., Beveridge, T.J., 2007.** Cryo-electron microscopy of cell division in *Staphylococcus aureus* reveals a mid-zone between nascent cross walls. *Mol. Microbiol.* 64, 195–206.
- Matias, V.R.F., Beveridge, T.J., 2008.** Lipoteichoic acid is a major component of the *Bacillus subtilis* periplasm. *J. Bacteriol.* 190, 7414–7418.
- May, J.J., Finking, R., Wiegeshoff, F., Weber, T.T., Bandur, N., Koert, U., Marahiel, M.A., 2005.** Inhibition of the D-alanine:D-alanyl carrier protein ligase from *Bacillus subtilis* increases the bacterium's susceptibility to antibiotics that target the cell wall. *FEBS J.* 272, 2993–3003.

- Mazmanian, S.K., Ton-That, H., Su, K., Schneewind, O.,** 2002. An iron-regulated sortase anchors a class of surface protein during *Staphylococcus aureus* pathogenesis. *Proc. Natl. Acad. Sci. U.S.A.* 99, 2293–2298.
- Mazouni, K., Domain, F., Cassier-Chauvat, C., Chauvat, F.,** 2004. Molecular analysis of the key cytokinetic components of cyanobacteria: FtsZ, ZipN and MinCDE. *Mol. Microbiol.* 52, 1145–1158.
- McDevitt, D., Francois, P., Vaudaux, P., Foster, T.J.,** 1994. Molecular characterization of the clumping factor (fibrinogen receptor) of *Staphylococcus aureus*. *Mol. Microbiol.* 11, 237–248.
- Memmi, G., Filipe, S.R., Pinho, M.G., Fu, Z., Cheung, A.,** 2008. *Staphylococcus aureus* PBP4 is essential for beta-lactam resistance in community-acquired methicillin-resistant strains. *Antimicrob. Agents Chemother.* 52, 3955–3966.
- Mercer, K.L.N., Weiss, D.S.,** 2002. The *Escherichia coli* cell division protein FtsW is required to recruit its cognate transpeptidase, FtsI (PBP3), to the division site. *J. Bacteriol.* 184, 904–912.
- Mirelman, D., Beck, B.D., Shaw, D.R.,** 1970. The location of the D-alanyl ester in the ribitol teichoic acid of *Staphylococcus aureus*. *Biochem. Biophys. Res. Commun.* 39, 712–717.
- Mohamed S,** 2007. Analysis of N-acetylglucosaminidase family of *Staphylococcus aureus*. The University of Sheffield.
- Möll, A., Thanbichler, M.,** 2009. FtsN-like proteins are conserved components of the cell division machinery in proteobacteria. *Mol. Microbiol.* 72, 1037–1053.
- Monahan, L.G., Robinson, A., Harry, E.J.,** 2009. Lateral FtsZ association and the assembly of the cytokinetic Z ring in bacteria. *Mol. Microbiol.* 74, 1004–1017.
- Mongkolrattanothai, K., Boyle, S., Murphy, T.V., Daum, R.S.,** 2004. Novel Non-mecA-Containing *Staphylococcal* Chromosomal Cassette Composite Island Containing *pbp4* and *tagF* Genes in a Commensal *Staphylococcal* Species: a Possible Reservoir for Antibiotic Resistance Islands in *Staphylococcus aureus*. *Antimicrob Agents Chemother* 48, 1823–1836.
- Moscoso, M., Claverys, J.-P.,** 2004. Release of DNA into the medium by competent *Streptococcus pneumoniae*: kinetics, mechanism and stability of the liberated DNA. *Mol. Microbiol.* 54, 783–794.
- Müller, P., Ewers, C., Bertsche, U., Anstett, M., Kallis, T., Breukink, E., Fraipont, C., Terrak, M., Nguyen-Distèche, M., Vollmer, W.,** 2007. The essential cell division protein FtsN interacts with the murein (peptidoglycan) synthase PBP1B in *Escherichia coli*. *J. Biol. Chem.* 282, 36394–36402.
- Murray, B.E.,** 2000. Vancomycin-resistant *enterococcal* infections. *N. Engl. J. Med.* 342, 710–721.
- Murray J,** 2001. Molecular analysis of the role and regulation of the autolysins of *Staphylococcus aureus*. The University of Sheffield.
- Navarre, W.W., Schneewind, O.,** 1999. Surface Proteins of Gram-Positive Bacteria and Mechanisms of Their Targeting to the Cell Wall Envelope. *Microbiol. Mol. Biol. Rev.* 63, 174–229.
- Navratna, V., Nadig, S., Sood, V., Prasad, K., Arakere, G., Gopal, B.,** 2010. Molecular Basis for the Role of *Staphylococcus aureus* Penicillin Binding Protein 4 in Antimicrobial Resistance. *J Bacteriol* 192, 134–144.
- Nelson, D.E., Young, K.D.,** 2001. Contributions of PBP 5 and DD-carboxypeptidase penicillin binding proteins to maintenance of cell shape in *Escherichia coli*. *J. Bacteriol.* 183, 3055–3064.
- Neuhaus, F.C., Baddiley, J.,** 2003. A Continuum of Anionic Charge: Structures and Functions of d-Alanyl-Teichoic Acids in Gram-Positive Bacteria. *Microbiol Mol Biol Rev* 67, 686–723.
- Ng, W.-L., Robertson, G.T., Kazmierczak, K.M., Zhao, J., Gilmour, R., Winkler, M.E.,** 2003. Constitutive expression of PcsB suppresses the requirement for the essential VicR (YycF) response regulator in *Streptococcus pneumoniae* R6. *Mol. Microbiol.* 50, 1647–1663.

- Ní Eidhin, D., Perkins, S., Francois, P., Vaudaux, P., Höök, M., Foster, T.J., 1998. Clumping factor B (ClfB), a new surface-located fibrinogen-binding adhesin of *Staphylococcus aureus*. *Mol. Microbiol.* 30, 245–257.
- Noble, W.C., Virani, Z., Cree, R.G.A., 1992. Co-transfer of vancomycin and other resistance genes from *Enterococcus faecalis* NCTC 12201 to *Staphylococcus aureus*. *FEMS Microbiology Letters* 93, 195–198.
- Noirclerc-Savoie, M., Le Gouëllec, A., Morlot, C., Dideberg, O., Vernet, T., Zapun, A., 2005. In vitro reconstitution of a trimeric complex of DivIB, DivIC and FtsL, and their transient co-localization at the division site in *Streptococcus pneumoniae*. *Mol. Microbiol.* 55, 413–424.
- Novick R. P., 2000. Pathogenicity factors and their regulation. In Gram-positive pathogens. ASM Press, Washington D.C.
- Novick, R.P., Ross, H.F., Projan, S.J., Kornblum, J., Kreiswirth, B., Moghazeh, S., 1993. Synthesis of *staphylococcal* virulence factors is controlled by a regulatory RNA molecule. *EMBO J.* 12, 3967–3975.
- Odintsov, S.G., Sabala, I., Marcyjaniak, M., Bochtler, M., 2004. Latent LytM at 1.3Å resolution. *J. Mol. Biol.* 335, 775–785.
- Oku, Y., Kurokawa, K., Matsuo, M., Yamada, S., Lee, B.-L., Sekimizu, K., 2009. Pleiotropic roles of polyglycerolphosphate synthase of lipoteichoic acid in growth of *Staphylococcus aureus* cells. *J. Bacteriol.* 191, 141–151.
- Okuno, T., Ogoh, M., Tanina, H., Funasaki, N., Kogure, K., 2009. Direct monitoring of interaction between *Escherichia coli* proteins, MinC and monomeric FtsZ, in solution. *Biol. Pharm. Bull.* 32, 1473–1475.
- Osborn, M.J., Rothfield, L., 2007. Cell shape determination in *Escherichia coli*. *Curr. Opin. Microbiol.* 10, 606–610.
- Oshida, T., Sugai, M., Komatsuzawa, H., Hong, Y.M., Suginaka, H., Tomasz, A., 1995. A *Staphylococcus aureus* autolysin that has an N-acetylmuramoyl-L-alanine amidase domain and an endo-beta-N-acetylglucosaminidase domain: cloning, sequence analysis, and characterization. *Proc. Natl. Acad. Sci. U.S.A.* 92, 285–289.
- Osteryoung, K.W., Stokes, K.D., Rutherford, S.M., Percival, A.L., Lee, W.Y., 1998. Chloroplast division in higher plants requires members of two functionally divergent gene families with homology to bacterial ftsZ. *Plant Cell* 10, 1991–2004.
- Over, B., Heusser, R., McCallum, N., Schulthess, B., Kupferschmid, P., Gaiani, J.M., Sifri, C.D., Berger-Bächi, B., Stutzmann Meier, P., 2011. LytR-CpsA-Psr proteins in *Staphylococcus aureus* display partial functional redundancy and the deletion of all three severely impairs septum placement and cell separation. *FEMS Microbiol. Lett.* 320, 142–151.
- Park, J.T., Strominger, J.L., 1957. Mode of action of penicillin. *Science* 125, 99–101.
- Patrick, J.E., Kearns, D.B., 2008. MinJ (YvjD) is a topological determinant of cell division in *Bacillus subtilis*. *Mol. Microbiol.* 70, 1166–1179.
- Peacock, S.J., de Silva, I., Lowy, F.D., 2001. What determines nasal carriage of *Staphylococcus aureus*? *Trends Microbiol.* 9, 605–610.
- Pearce, M.J., Mintseris, J., Ferreyra, J., Gygi, S.P., Darwin, K.H., 2008. Ubiquitin-like protein involved in the proteasome pathway of *Mycobacterium tuberculosis*. *Science* 322, 1104–1107.
- Pease, P.J., Levy, O., Cost, G.J., Gore, J., Ptacin, J.L., Sherratt, D., Bustamante, C., Cozzarelli, N.R., 2005. Sequence-directed DNA translocation by purified FtsK. *Science* 307, 586–590.
- Pereira, S.F.F., Henriques, A.O., Pinho, M.G., de Lencastre, H., Tomasz, A., 2007. Role of PBP1 in cell division of *Staphylococcus aureus*. *J. Bacteriol.* 189, 3525–3531.
- Peschel, A., Otto, M., Jack, R.W., Kalbacher, H., Jung, G., Götz, F., 1999. Inactivation of the *dlt* operon in *Staphylococcus aureus* confers sensitivity to defensins, protegrins, and other antimicrobial peptides. *J. Biol. Chem.* 274, 8405–8410.

- Peschel, A., Vuong, C., Otto, M., Götz, F.,** 2000. The D-alanine residues of *Staphylococcus aureus* teichoic acids alter the susceptibility to vancomycin and the activity of autolytic enzymes. *Antimicrob. Agents Chemother.* 44, 2845–2847.
- Peters, P.C., Migocki, M.D., Thoni, C., Harry, E.J.,** 2007. A new assembly pathway for the cytokinetic Z ring from a dynamic helical structure in vegetatively growing cells of *Bacillus subtilis*. *Mol. Microbiol.* 64, 487–499.
- Petty, H.R.,** 2007. Fluorescence microscopy: established and emerging methods, experimental strategies, and applications in immunology. *Microsc. Res. Tech.* 70, 687–709.
- Pichoff, S., Lutkenhaus, J.,** 2002. Unique and overlapping roles for ZipA and FtsA in septal ring assembly in *Escherichia coli*. *EMBO J.* 21, 685–693.
- Pieper, R., Gatlin-Bunai, C.L., Mongodin, E.F., Parmar, P.P., Huang, S.-T., Clark, D.J., Fleischmann, R.D., Gill, S.R., Peterson, S.N.,** 2006. Comparative proteomic analysis of *Staphylococcus aureus* strains with differences in resistance to the cell wall-targeting antibiotic vancomycin. *Proteomics* 6, 4246–4258.
- Pinho, M.G., Errington, J.,** 2003. Dispersed mode of *Staphylococcus aureus* cell wall synthesis in the absence of the division machinery. *Mol. Microbiol.* 50, 871–881.
- Pinho, M.G., Errington, J.,** 2004. A divIVA null mutant of *Staphylococcus aureus* undergoes normal cell division. *FEMS Microbiol. Lett.* 240, 145–149.
- Pinho, M.G., Errington, J.,** 2005. Recruitment of penicillin-binding protein PBP2 to the division site of *Staphylococcus aureus* is dependent on its transpeptidation substrates. *Mol. Microbiol.* 55, 799–807.
- Pollack, J.H., Neuhaus, F.C.,** 1994. Changes in wall teichoic acid during the rod-sphere transition of *Bacillus subtilis* 168. *J. Bacteriol.* 176, 7252–7259.
- Pooley, H.M., Schlaeppli, J.-M., Karamata, D.,** 1978. Localised insertion of new cell wall in *Bacillus subtilis*. , Published online: 20 July 1978; | doi:10.1038/274264a0 274, 264–266.
- Potluri, L., Karczmarek, A., Verheul, J., Piette, A., Wilkin, J.-M., Werth, N., Banzhaf, M., Vollmer, W., Young, K.D., Nguyen-Distèche, M., den Blaauwen, T.,** 2010. Septal and lateral wall localization of PBP5, the major D,D-carboxypeptidase of *Escherichia coli*, requires substrate recognition and membrane attachment. *Mol. Microbiol.* 77, 300–323.
- Potluri, L.-P., de Pedro, M.A., Young, K.D.,** 2012. *Escherichia coli* low-molecular-weight penicillin-binding proteins help orient septal FtsZ, and their absence leads to asymmetric cell division and branching. *Molecular Microbiology* 84, 203–224.
- Pourmand, M.R., Clarke, S.R., Schuman, R.F., Mond, J.J., Foster, S.J.,** 2006. Identification of antigenic components of *Staphylococcus epidermidis* expressed during human infection. *Infect. Immun.* 74, 4644–4654.
- Pratt, R.F.,** 2008. Substrate specificity of bacterial DD-peptidases (penicillin-binding proteins). *Cell. Mol. Life Sci.* 65, 2138–2155.
- Projan, S. J., Novick, R. P.,** 1997. The molecular basis of pathogenicity., in: *The Staphylococci in Human Disease*. Churchill Livingstone, New York, pp. 55–81.
- Pucci, M.J., Dougherty, T.J.,** 2002. Direct quantitation of the numbers of individual penicillin-binding proteins per cell in *Staphylococcus aureus*. *J. Bacteriol.* 184, 588–591.
- Qamar, A., Golemi-Kotra, D.,** 2012. Dual roles of FmtA in *Staphylococcus aureus* cell wall biosynthesis and autolysis. *Antimicrob. Agents Chemother.* 56, 3797–3805.
- Ramadurai, L., Jayaswal, R.K.,** 1997. Molecular cloning, sequencing, and expression of lytM, a unique autolytic gene of *Staphylococcus aureus*. *J. Bacteriol.* 179, 3625–3631.
- Ramadurai, L., Lockwood, K.J., Nadakavukaren, M.J., Jayaswal, R.K.,** 1999. Characterization of a chromosomally encoded glycylglycine endopeptidase of *Staphylococcus aureus*. *Microbiology (Reading, Engl.)* 145 (Pt 4), 801–808.
- Ramirez-Arcos, S., Szeto, J., Dillon, J.-A.R., Margolin, W.,** 2002. Conservation of dynamic localization among MinD and MinE orthologues: oscillation of *Neisseria gonorrhoeae* proteins in *Escherichia coli*. *Mol. Microbiol.* 46, 493–504.

- Rashid, M.H., Mori, M., Sekiguchi, J.**, 1995. Glucosaminidase of *Bacillus subtilis*: cloning, regulation, primary structure and biochemical characterization. *Microbiology (Reading, Engl.)* 141 (Pt 10), 2391–2404.
- RayChaudhuri, D.**, 1999. ZipA is a MAP-Tau homolog and is essential for structural integrity of the cytokinetic FtsZ ring during bacterial cell division. *EMBO J.* 18, 2372–2383.
- Reed, P., Veiga, H., Jorge, A.M., Terrak, M., Pinho, M.G.**, 2011. Monofunctional transglycosylases are not essential for *Staphylococcus aureus* cell wall synthesis. *J. Bacteriol.* 193, 2549–2556.
- Reichmann, N.T., Gründling, A.**, 2011. Location, synthesis and function of glycolipids and polyglycerolphosphate lipoteichoic acid in Gram-positive bacteria of the phylum Firmicutes. *FEMS Microbiol. Lett.* 319, 97–105.
- Richmond, M.H.**, 1966. One-step micro-constitutive mutations in the penicillinase region of *Staphylococcus aureus*. *Biochem. Biophys. Res. Commun.* 22, 38–42.
- Rigden, D.J., Jedrzejewski, M.J., Galperin, M.Y.**, 2003. Amidase domains from bacterial and phage autolysins define a family of gamma-D,L-glutamate-specific amidohydrolases. *Trends Biochem. Sci.* 28, 230–234.
- Rossi, J., Bischoff, M., Wada, A., Berger-Bächi, B.**, 2003. MsrR, a Putative Cell Envelope-Associated Element Involved in *Staphylococcus aureus* sarA Attenuation. *Antimicrob Agents Chemother* 47, 2558–2564.
- Roure, S., Bonis, M., Chaput, C., Ecobichon, C., Mattox, A., Barrière, C., Geldmacher, N., Guadagnini, S., Schmitt, C., Prévost, M.-C., Labigne, A., Backert, S., Ferrero, R.L., Boneca, I.G.**, 2012. Peptidoglycan maturation enzymes affect flagellar functionality in bacteria. *Mol. Microbiol.*
- Rupp, M.E., Fey, P.D., Heilmann, C., Götz, F.**, 2001. Characterization of the importance of *Staphylococcus epidermidis* autolysin and polysaccharide intercellular adhesin in the pathogenesis of intravascular catheter-associated infection in a rat model. *J. Infect. Dis.* 183, 1038–1042.
- Russell, A.B., Hood, R.D., Bui, N.K., LeRoux, M., Vollmer, W., Mougous, J.D.**, 2011. Type VI secretion delivers bacteriolytic effectors to target cells. *Nature* 475, 343–347.
- Sabala, I., Jonsson, I.-M., Tarkowski, A., Bochtler, M.**, 2012. Anti-staphylococcal activities of lysostaphin and LytM catalytic domain. *BMC Microbiol* 12, 97.
- Sakata, N., Terakubo, S., Mukai, T.**, 2005. Subcellular location of the soluble lytic transglycosylase homologue in *Staphylococcus aureus*. *Curr. Microbiol.* 50, 47–51.
- Sauvage, E., Kerff, F., Terrak, M., Ayala, J.A., Charlier, P.**, 2008. The penicillin-binding proteins: structure and role in peptidoglycan biosynthesis. *FEMS Microbiology Reviews* 32, 234–258.
- Scheffers, D., Driessen, A.J.**, 2001. The polymerization mechanism of the bacterial cell division protein FtsZ. *FEBS Lett.* 506, 6–10.
- Scheffers, D.-J., de Wit, J.G., den Blaauwen, T., Driessen, A.J.M.**, 2002. GTP hydrolysis of cell division protein FtsZ: evidence that the active site is formed by the association of monomers. *Biochemistry* 41, 521–529.
- Scheffers, D.-J., Pinho, M.G.**, 2005. Bacterial Cell Wall Synthesis: New Insights from Localization Studies. *Microbiol Mol Biol Rev* 69, 585–607.
- Schermelleh, L., Heintzmann, R., Leonhardt, H.**, 2010. A guide to super-resolution fluorescence microscopy. *J Cell Biol* 190, 165–175.
- Schirner, K., Marles-Wright, J., Lewis, R.J., Errington, J.**, 2009. Distinct and essential morphogenic functions for wall- and lipo-teichoic acids in *Bacillus subtilis*. *EMBO J.* 28, 830–842.
- Schito, G.C.**, 2006. The importance of the development of antibiotic resistance in *Staphylococcus aureus*. *Clinical Microbiology and Infection* 12, 3–8.
- Schlaepfli, J.M., Karamata, D.**, 1982. Cosegregation of cell wall and DNA in *Bacillus subtilis*. *J. Bacteriol.* 152, 1231–1240.
- Schlaepfli, J.M., Schaefer, O., Karamata, D.**, 1985. Cell wall and DNA cosegregation in *Bacillus subtilis* studied by electron microscope autoradiography. *J. Bacteriol.* 164, 130–135.

- Schlag, M., Biswas, R., Krismer, B., Kohler, T., Zoll, S., Yu, W., Schwarz, H., Peschel, A., Götz, F.,** 2010. Role of *staphylococcal* wall teichoic acid in targeting the major autolysin Atl. *Molecular Microbiology* 75, 864–873.
- Schmidt, K.L., Peterson, N.D., Kustus, R.J., Wissel, M.C., Graham, B., Phillips, G.J., Weiss, D.S.,** 2004. A predicted ABC transporter, FtsEX, is needed for cell division in *Escherichia coli*. *J. Bacteriol.* 186, 785–793.
- Schneewind, O., Mihaylova-Petkov, D., Model, P.,** 1993. Cell wall sorting signals in surface proteins of gram-positive bacteria. *EMBO J.* 12, 4803–4811.
- Schuster, C., Dobrinski, B., Hakenbeck, R.,** 1990. Unusual septum formation in *Streptococcus pneumoniae* mutants with an alteration in the D,D-carboxypeptidase penicillin-binding protein 3. *J. Bacteriol.* 172, 6499–6505.
- Scott, J.R., Barnett, T.C.,** 2006. Surface proteins of gram-positive bacteria and how they get there. *Annu. Rev. Microbiol.* 60, 397–423.
- Sharpe, M.E., Hauser, P.M., Sharpe, R.G., Errington, J.,** 1998. *Bacillus subtilis* cell cycle as studied by fluorescence microscopy: constancy of cell length at initiation of DNA replication and evidence for active nucleoid partitioning. *J. Bacteriol.* 180, 547–555.
- Shockman G. D., Holtje J.-V.,** 1994. Microbial peptidoglycan (Murein) hydrolases. New comprehensive biochemistry, in: *Bacterial Cell Wall* Ed. Elsevier Science, London, pp. 131–166.
- Shtengel, G., Galbraith, J.A., Galbraith, C.G., Lippincott-Schwartz, J., Gillette, J.M., Manley, S., Sougrat, R., Waterman, C.M., Kanchanawong, P., Davidson, M.W., Fetter, R.D., Hess, H.F.,** 2009. Interferometric fluorescent super-resolution microscopy resolves 3D cellular ultrastructure. *Proc. Natl. Acad. Sci. U.S.A.* 106, 3125–3130.
- Sieradzki, K., Tomasz, A.,** 2003. Alterations of cell wall structure and metabolism accompany reduced susceptibility to vancomycin in an isogenic series of clinical isolates of *Staphylococcus aureus*. *J. Bacteriol.* 185, 7103–7110.
- Sieradzki, K., Tomasz, A.,** 2006. Inhibition of the autolytic system by vancomycin causes mimicry of vancomycin-intermediate *Staphylococcus aureus*-type resistance, cell concentration dependence of the MIC, and antibiotic tolerance in vancomycin-susceptible *S. aureus*. *Antimicrob. Agents Chemother.* 50, 527–533.
- Sievers, J., Errington, J.,** 2000. The *Bacillus subtilis* cell division protein FtsL localizes to sites of septation and interacts with DivIC. *Mol. Microbiol.* 36, 846–855.
- Silhavy, T.J., Kahne, D., Walker, S.,** 2010. The bacterial cell envelope. *Cold Spring Harb Perspect Biol* 2, a000414.
- Singh, B.N.,** 1947. Myxobacteria in soils and composts; their distribution, number and lytic action on bacteria. *J. Gen. Microbiol.* 1, 1–10.
- Singh, J.K., Makde, R.D., Kumar, V., Panda, D.,** 2007. A membrane protein, EzrA, regulates assembly dynamics of FtsZ by interacting with the C-terminal tail of FtsZ. *Biochemistry* 46, 11013–11022.
- Singh, J.K., Makde, R.D., Kumar, V., Panda, D.,** 2008. SepF increases the assembly and bundling of FtsZ polymers and stabilizes FtsZ protofilaments by binding along its length. *J. Biol. Chem.* 283, 31116–31124.
- Singh, S.K., SaiSree, L., Amrutha, R.N., Reddy, M.,** 2012. Three redundant murein endopeptidases catalyse an essential cleavage step in peptidoglycan synthesis of *Escherichia coli* K12. *Mol. Microbiol.* 86, 1036–1051.
- Singh, V.K., Carlos, M.R., Singh, K.,** 2010. Physiological Significance of the Peptidoglycan Hydrolase, LytM, in *Staphylococcus aureus*. *FEMS Microbiol Lett* 311, 167–175.
- Sivaraman, K., Venkataraman, N., Cole, A.M.,** 2009. *Staphylococcus aureus* nasal carriage and its contributing factors. *Future Microbiol* 4, 999–1008.

- Sjodahl, J.**, 1977. Repetitive sequences in protein A from *Staphylococcus aureus*. Arrangement of five regions within the protein, four being highly homologous and Fc-binding. *Eur. J. Biochem.* 73, 343–351.
- Smith, G.P.**, 1985. Filamentous fusion phage: novel expression vectors that display cloned antigens on the virion surface. *Science* 228, 1315–1317.
- Smith, T.J., Blackman, S.A., Foster, S.J.**, 2000. Autolysins of *Bacillus subtilis*: multiple enzymes with multiple functions. *Microbiology (Reading, Engl.)* 146 (Pt 2), 249–262.
- So, L.L., Goldstein, I.J.**, 1969. Protein-carbohydrate interaction. XVII. The effect of polysaccharide molecular weight on the concanavalin A-polysaccharide precipitation reaction. *J. Immunol.* 102, 53–57.
- Soldo, B., Lazarevic, V., Karamata, D.**, 2002. tagO is involved in the synthesis of all anionic cell-wall polymers in *Bacillus subtilis* 168. *Microbiology (Reading, Engl.)* 148, 2079–2087.
- Stapleton, M.R., Horsburgh, M.J., Hayhurst, E.J., Wright, L., Jonsson, I.-M., Tarkowski, A., Kokai-Kun, J.F., Mond, J.J., Foster, S.J.**, 2007. Characterization of IsaA and SceD, two putative lytic transglycosylases of *Staphylococcus aureus*. *J. Bacteriol.* 189, 7316–7325.
- Steele, V.R., Bottomley, A.L., Garcia-Lara, J., Kasturiarachchi, J., Foster, S.J.**, 2011. Multiple essential roles for EzrA in cell division of *Staphylococcus aureus*. *Mol. Microbiol.* 80, 542–555.
- Sudo, S., Dworkin, M.**, 1972. Bacteriolytic enzymes produced by *Myxococcus xanthus*. *J. Bacteriol.* 110, 236–245.
- Sugai, M., Fujiwara, T., Akiyama, T., Ohara, M., Komatsuzawa, H., Inoue, S., Suginaka, H.**, 1997a. Purification and molecular characterization of glycylglycine endopeptidase produced by *Staphylococcus capitis* EPK1. *J. Bacteriol.* 179, 1193–1202.
- Sugai, M., Fujiwara, T., Komatsuzawa, H., Suginaka, H.**, 1998. Identification and molecular characterization of a gene homologous to epr (endopeptidase resistance gene) in *Staphylococcus aureus*. *Gene* 224, 67–75.
- Sugai, M., Fujiwara, T., Ohta, K., Komatsuzawa, H., Ohara, M., Suginaka, H.**, 1997b. epr, which encodes glycylglycine endopeptidase resistance, is homologous to femAB and affects serine content of peptidoglycan cross bridges in *Staphylococcus capitis* and *Staphylococcus aureus*. *J. Bacteriol.* 179, 4311–4318.
- Sugai, M., Komatsuzawa, H., Akiyama, T., Hong, Y.M., Oshida, T., Miyake, Y., Yamaguchi, T., Suginaka, H.**, 1995. Identification of endo-beta-N-acetylglucosaminidase and N-acetylmuramyl-L-alanine amidase as cluster-dispersing enzymes in *Staphylococcus aureus*. *J. Bacteriol.* 177, 1491–1496.
- Sun, Q., Margolin, W.**, 1998. FtsZ dynamics during the division cycle of live *Escherichia coli* cells. *J. Bacteriol.* 180, 2050–2056.
- Swoboda, J.G., Campbell, J., Meredith, T.C., Walker, S.**, 2010. Wall Teichoic Acid Function, Biosynthesis, and Inhibition. *ChemBiochem* 11, 35–45.
- Szurmant, H., Mohan, M.A., Imus, P.M., Hoch, J.A.**, 2007. YchH and YclI interact to regulate the essential YycFG two-component system in *Bacillus subtilis*. *J. Bacteriol.* 189, 3280–3289.
- Takahashi, J., Komatsuzawa, H., Yamada, S., Nishida, T., Labischinski, H., Fujiwara, T., Ohara, M., Yamagishi, J., Sugai, M.**, 2002. Molecular characterization of an atl null mutant of *Staphylococcus aureus*. *Microbiol. Immunol.* 46, 601–612.
- Takamatsu, D., Bensing, B.A., Sullam, P.M.**, 2004. Four proteins encoded in the gspB-secY2A2 operon of *Streptococcus gordonii* mediate the intracellular glycosylation of the platelet-binding protein GspB. *J. Bacteriol.* 186, 7100–7111.
- Takano, M., Oshida, T., Yasojima, A., Yamada, M., Okagaki, C., Sugai, M., Suginaka, H., Matsushita, T.**, 2000. Modification of autolysis by synthetic peptides derived from the presumptive binding domain of *Staphylococcus aureus* autolysin. *Microbiol. Immunol.* 44, 463–472.

- Tavares, J.R., de Souza, R.F., Meira, G.L.S., Gueiros-Filho, F.J.,** 2008. Cytological characterization of YpsB, a novel component of the *Bacillus subtilis* divisome. *J. Bacteriol.* 190, 7096–7107.
- Thanedar, S., Margolin, W.,** 2004. FtsZ exhibits rapid movement and oscillation waves in helix-like patterns in *Escherichia coli*. *Curr. Biol.* 14, 1167–1173.
- Thompson, L.S., Beech, P.L., Real, G., Henriques, A.O., Harry, E.J.,** 2006. Requirement for the cell division protein DivIB in polar cell division and engulfment during sporulation in *Bacillus subtilis*. *J. Bacteriol.* 188, 7677–7685.
- Ton-That, H., Marraffini, L.A., Schneewind, O.,** 2004. Protein sorting to the cell wall envelope of Gram-positive bacteria. *Biochimica et Biophysica Acta (BBA) - Molecular Cell Research* 1694, 269–278.
- Tortora, P.J., Funke, B. R., Case, C. L.,** 1997. Microbiology: an introduction, sixth. ed. Benjamin Cummings Publishing Company, California.
- Touhami, A., Jericho, M.H., Beveridge, T.J.,** 2004. Atomic force microscopy of cell growth and division in *Staphylococcus aureus*. *J. Bacteriol.* 186, 3286–3295.
- Tseng, C.-L., Chen, J.-T., Lin, J.-H., Huang, W.-Z., Shaw, G.-C.,** 2011. Genetic evidence for involvement of the alternative sigma factor SigI in controlling expression of the cell wall hydrolase gene *lytE* and contribution of *LytE* to heat survival of *Bacillus subtilis*. *Arch. Microbiol.* 193, 677–685.
- Tsui, H.-C.T., Keen, S.K., Sham, L.-T., Wayne, K.J., Winkler, M.E.,** 2011. Dynamic distribution of the SecA and SecY translocase subunits and septal localization of the HtrA surface chaperone/protease during *Streptococcus pneumoniae* D39 cell division. *MBio* 2.
- Turner, R.D., Hurd, A.F., Cadby, A., Hobbs, J.K., Foster, S.J.,** 2013. Cell wall elongation mode in Gram-negative bacteria is determined by peptidoglycan architecture. *Nat Commun* 4, 1496.
- Turner, R.D., Ratcliffe, E.C., Wheeler, R., Golestanian, R., Hobbs, J.K., Foster, S.J.,** 2010. Peptidoglycan architecture can specify division planes in *Staphylococcus aureus*. *Nat Commun* 1, 26.
- Tzagoloff, H., Novick, R.,** 1977. Geometry of cell division in *Staphylococcus aureus*. *J. Bacteriol.* 129, 343–350.
- Umeda, A., Ueki, Y., Amako, K.,** 1987. Structure of the *Staphylococcus aureus* cell wall determined by the freeze-substitution method. *J Bacteriol* 169, 2482–2487.
- Umeda, A., Yokoyama, S., Arizono, T., Amako, K.,** 1992. Location of peptidoglycan and teichoic acid on the cell wall surface of *Staphylococcus aureus* as determined by immunoelectron microscopy. *J Electron Microsc (Tokyo)* 41, 46–52.
- Ursinus, A., van den Ent, F., Brechtel, S., de Pedro, M., Höltje, J.-V., Löwe, J., Vollmer, W.,** 2004. Murein (peptidoglycan) binding property of the essential cell division protein FtsN from *Escherichia coli*. *J. Bacteriol.* 186, 6728–6737.
- Valisena, S., Varaldo, P.E., Satta, G.,** 1991. *Staphylococcal* endo-beta-N-acetylglucosaminidase inhibits response of human lymphocytes to mitogens and interferes with production of antibodies in mice. *J. Clin. Invest.* 87, 1969–1976.
- Varrone, J.J., Li, D., Daiss, J.L., Schwarz, E.M.,** 2011. Anti-Glucosaminidase Monoclonal Antibodies as a Passive Immunization for Methicillin-Resistant *Staphylococcus aureus* (MRSA) Orthopaedic Infections. *Bonekey Osteovision* 8, 187–194.
- Veiga, H., Jorge, A.M., Pinho, M.G.,** 2011. Absence of nucleoid occlusion effector *Noc* impairs formation of orthogonal FtsZ rings during *Staphylococcus aureus* cell division. *Mol. Microbiol.* 80, 1366–1380.
- Vergara-Irigaray, M., Maira-Litrán, T., Merino, N., Pier, G.B., Penadés, J.R., Lasa, I.,** 2008. Wall teichoic acids are dispensable for anchoring the PNAG exopolysaccharide to the *Staphylococcus aureus* cell surface. *Microbiology (Reading, Engl.)* 154, 865–877.
- Viollier, P.H., Shapiro, L.,** 2003. A lytic transglycosylase homologue, *PleA*, is required for the assembly of pili and the flagellum at the *Caulobacter crescentus* cell pole. *Mol. Microbiol.* 49, 331–345.

- Voet D., Voet J.G.**, 1995. Biochemistry, 3rd edition. ed. John Wiley and Sons, Inc., New York.
- Vollmer, W.**, 2008. Structural variation in the glycan strands of bacterial peptidoglycan. *FEMS Microbiol. Rev.* 32, 287–306.
- Vollmer, W., Höltje, J.-V.**, 2004. The Architecture of the Murein (Peptidoglycan) in Gram-Negative Bacteria: Vertical Scaffold or Horizontal Layer(s)? *J Bacteriol* 186, 5978–5987.
- Vollmer, W., Joris, B., Charlier, P., Foster, S.**, 2008. Bacterial peptidoglycan (murein) hydrolases. *FEMS Microbiology Reviews* 32, 259–286.
- Vollmer, W., Seligman, S.J.**, 2010. Architecture of peptidoglycan: more data and more models. *Trends Microbiol.* 18, 59–66.
- Vollmer, W., von Rechenberg, M., Höltje, J.V.**, 1999. Demonstration of molecular interactions between the murein polymerase PBP1B, the lytic transglycosylase MltA, and the scaffolding protein MipA of *Escherichia coli*. *J. Biol. Chem.* 274, 6726–6734.
- Wallace, W., Schaefer, L.H., Swedlow, J.R.**, 2001. A workingperson's guide to deconvolution in light microscopy. *BioTechniques* 31, 1076–1078, 1080, 1082 passim.
- Wang, S., Furchtgott, L., Huang, K.C., Shaevitz, J.W.**, 2012. Helical insertion of peptidoglycan produces chiral ordering of the bacterial cell wall. *Proc. Natl. Acad. Sci. U.S.A.* 109, E595–604.
- Wang, X., Huang, J., Mukherjee, A., Cao, C., Lutkenhaus, J.**, 1997. Analysis of the interaction of FtsZ with itself, GTP, and FtsA. *J. Bacteriol.* 179, 5551–5559.
- Weart, R.B., Lee, A.H., Chien, A.-C., Haeusser, D.P., Hill, N.S., Levin, P.A.**, 2007. A metabolic sensor governing cell size in bacteria. *Cell* 130, 335–347.
- Weart, R.B., Levin, P.A.**, 2003. Growth Rate-Dependent Regulation of Medial FtsZ Ring Formation. *J Bacteriol* 185, 2826–2834.
- Weidel, W., Frank, H., Martin, H.H.**, 1960. The rigid layer of the cell wall of *Escherichia coli* strain B. *J. Gen. Microbiol.* 22, 158–166.
- Weidenmaier, C., Kokai-Kun, J.F., Kristian, S.A., Chanturiya, T., Kalbacher, H., Gross, M., Nicholson, G., Neumeister, B., Mond, J.J., Peschel, A.**, 2004. Role of teichoic acids in *Staphylococcus aureus* nasal colonization, a major risk factor in nosocomial infections. *Nat. Med.* 10, 243–245.
- Weidenmaier, C., Peschel, A., Xiong, Y.-Q., Kristian, S.A., Dietz, K., Yeaman, M.R., Bayer, A.S.**, 2005. Lack of wall teichoic acids in *Staphylococcus aureus* leads to reduced interactions with endothelial cells and to attenuated virulence in a rabbit model of endocarditis. *J. Infect. Dis.* 191, 1771–1777.
- Weiss, D.S., Chen, J.C., Ghigo, J.M., Boyd, D., Beckwith, J.**, 1999. Localization of FtsI (PBP3) to the septal ring requires its membrane anchor, the Z ring, FtsA, FtsQ, and FtsL. *J. Bacteriol.* 181, 508–520.
- Wheeler R.**, 2012. Peptidoglycan architecture and dynamics of Gram-positive bacteria. The University of Sheffield.
- Wheeler, R., Mesnage, S., Boneca, I.G., Hobbs, J.K., Foster, S.J.**, 2011. Super-resolution microscopy reveals cell wall dynamics and peptidoglycan architecture in *ovococcal* bacteria. *Mol. Microbiol.* 82, 1096–1109.
- White, C.L., Kitich, A., Gober, J.W.**, 2010. Positioning cell wall synthetic complexes by the bacterial morphogenetic proteins MreB and MreD. *Mol. Microbiol.* 76, 616–633.
- Whitt, Salyers**, 2001. Bacterial Pathogenesis. Amer society for microbiology.
- Wickham, J.R., Halye, J.L., Kashtanov, S., Khandogin, J., Rice, C.V.**, 2009. Revisiting magnesium chelation by teichoic acid with phosphorus solid-state NMR and theoretical calculations. *J Phys Chem B* 113, 2177–2183.
- Willig, K.I., Rizzoli, S.O., Westphal, V., Jahn, R., Hell, S.W.**, 2006. STED microscopy reveals that synaptotagmin remains clustered after synaptic vesicle exocytosis. *Nature* 440, 935–939.
- Woodford, N.**, 2005. Biological counterstrike: antibiotic resistance mechanisms of Gram-positive cocci. *Clin. Microbiol. Infect.* 11 Suppl 3, 2–21.

- Wu, L.J., Ishikawa, S., Kawai, Y., Oshima, T., Ogasawara, N., Errington, J., 2009. Noc protein binds to specific DNA sequences to coordinate cell division with chromosome segregation. *EMBO J* 28, 1940–1952.
- Wyke, A.W., Ward, J.B., Hayes, M.V., Curtis, N.A., 1981. A role in vivo for penicillin-binding protein-4 of *Staphylococcus aureus*. *Eur. J. Biochem.* 119, 389–393.
- Xia, G., Kohler, T., Peschel, A., 2010a. The wall teichoic acid and lipoteichoic acid polymers of *Staphylococcus aureus*. *Int. J. Med. Microbiol.* 300, 148–154.
- Xia, G., Maier, L., Sanchez-Carballo, P., Li, M., Otto, M., Holst, O., Peschel, A., 2010b. Glycosylation of wall teichoic acid in *Staphylococcus aureus* by TarM. *J. Biol. Chem.* 285, 13405–13415.
- Xu, H., Chater, K.F., Deng, Z., Tao, M., 2008. A Cellulose Synthase-Like Protein Involved in Hyphal Tip Growth and Morphological Differentiation in *Streptomyces*. *J. Bacteriol* 190, 4971–4978.
- Yamada, S., Ono, T., Mizuno, A., Nemoto, T.K., 2003. A hydrophobic segment within the C-terminal domain is essential for both client-binding and dimer formation of the HSP90-family molecular chaperone. *Eur. J. Biochem.* 270, 146–154.
- Yamada, S., Sugai, M., Komatsuzawa, H., Nakashima, S., Oshida, T., Matsumoto, A., Suginaka, H., 1996. An autolysin ring associated with cell separation of *Staphylococcus aureus*. *J. Bacteriol.* 178, 1565–1571.
- Yan, K., Pearce, K.H., Payne, D.J., 2000. A conserved residue at the extreme C-terminus of FtsZ is critical for the FtsA-FtsZ interaction in *Staphylococcus aureus*. *Biochem. Biophys. Res. Commun.* 270, 387–392.
- Yang, D.C., Peters, N.T., Parzych, K.R., Uehara, T., Markovski, M., Bernhardt, T.G., 2011. An ATP-binding cassette transporter-like complex governs cell-wall hydrolysis at the bacterial cytokinetic ring. *Proc Natl Acad Sci U S A* 108, E1052–E1060.
- Yao, X., Jericho, M., Pink, D., Beveridge, T., 1999. Thickness and Elasticity of Gram-Negative Murein Sacculi Measured by Atomic Force Microscopy. *J. Bacteriol* 181, 6865–6875.
- Yokoyama, K., Mizuguchi, H., Araki, Y., Kaya, S., Ito, E., 1989. Biosynthesis of linkage units for teichoic acids in gram-positive bacteria: distribution of related enzymes and their specificities for UDP-sugars and lipid-linked intermediates. *J. Bacteriol.* 171, 940–946.
- Young, K.H., 1998. Yeast two-hybrid: so many interactions, (in) so little time... *Biology of Reproduction* 58, 302–311.
- Yu, X.C., Weihe, E.K., Margolin, W., 1998. Role of the C terminus of FtsK in *Escherichia coli* chromosome segregation. *J. Bacteriol.* 180, 6424–6428.
- Zapun, A., Contreras-Martel, C., Vernet, T., 2008a. Penicillin-binding proteins and β -lactam resistance. *FEMS Microbiology Reviews* 32, 361–385.
- Zapun, A., Vernet, T., Pinho, M.G., 2008b. The different shapes of cocci. *FEMS Microbiol. Rev.* 32, 345–360.
- Zlatanova, J., Lindsay, S.M., Leuba, S.H., 2000. Single molecule force spectroscopy in biology using the atomic force microscope. *Progress in Biophysics and Molecular Biology* 74, 37–61.
- Zoll, S., Schlag, M., Shkumatov, A.V., Rautenberg, M., Svergun, D.I., Götz, F., Stehle, T., 2012. Ligand-binding properties and conformational dynamics of autolysin repeat domains in *staphylococcal* cell wall recognition. *J. Bacteriol.* 194, 3789–3802.
- Zou, Y., Hou, C., 2010. Systematic analysis of an amidase domain CHAP in 12 *Staphylococcus aureus* genomes and 44 *staphylococcal* phage genomes. *Comput Biol Chem* 34, 251–257.
- Zuber, U., Drzewiecki, K., Hecker, M., 2001. Putative sigma factor SigI (YkoZ) of *Bacillus subtilis* is induced by heat shock. *J. Bacteriol.* 183, 1472–1475.

BACTH APPENDIX 1

| Gene-T18 | TarO | SA2103 | SA1195 | SA0908 | PBP4 |
|-----------------|-------------|---------------|---------------|---------------|-------------|
| FtsZ | | | | | |
| DivIB | | | | | |
| FtsA | | | | | |
| FtsL | | | | | |
| DivIC | | | | | |
| FtsW | | | | | |
| EzrA | | | | | |
| PBP1 | | | | | |
| ParC | | | | | |
| ParE | | | | | |
| YneS | | | | | |
| PBP2 | | | | | |
| GpsB | | | | | |
| YpsA | | | | | |
| SepF | | | | | |
| Noc | | | | | |
| PBP3 | | | | | |
| ZapA | | | | | |
| MreC | | | | | |
| MreD | | | | | |
| RodA | | | | | |
| PBP4 | | | | | |

| | | | | | |
|-------------------------|--|--|--|--|--|
| LtaA (pKNT25) | | | | | |
| LtaA (pKT25) | | | | | |
| LtaS | | | | | |
| YpfP (pKTN25) | | | | | |
| YpfP (pKT25) | | | | | |
| DivIA | | | | | |
| DnaK | | | | | |
| TagO | | | | | |
| SA2103 | | | | | |
| SA1195 (MsrR) | | | | | |
| SA0908 | | | | | |
| T25 | | | | | |

Figure A.1 BACTH analysis of *S.aureus* cell division proteins against T18-POIs

Pairwise interactions of T18-POIs with T25 fused *S.aureus* cell division proteins. 10µl samples of a 1:100 dilution of overnight culture of co-transformed BTH101 were spotted onto minimal medium containing 150µg ml⁻¹ X-gal and incubated at 30°C for a minimum of 18hrs. +ve, T25-zip~T18-zip; -ve, pKT25~pUT18C.

| Gene-T25 | TarO | SA2103 | SA1195 | SA0908 | PBP4 |
|------------------|------|--------|--------|--------|------|
| FtsZ | | | | | |
| DivIB | | | | | |
| FtsA | | | | | |
| FtsL | | | | | |
| DivIC | | | | | |
| FtsW | | | | | |
| EzrA | | | | | |
| YneS | | | | | |
| PBP2 | | | | | |
| GpsB | | | | | |
| YpsA | | | | | |
| SepF | | | | | |
| Noc | | | | | |
| ZapA | | | | | |
| MreC | | | | | |
| MreD | | | | | |
| RodA | | | | | |
| PBP4 | | | | | |
| LtaA (pKNT25) | | | | | |
| LtaA (pKT25) | | | | | |
| LtaS | | | | | |
| YpfP (pKTN25) | | | | | |

| | | | | | |
|-------------------------|--|--|--|--|--|
| YpfP (pKT25) | | | | | |
| TagO | | | | | |
| SA2103 | | | | | |
| SA1195 (MsrR) | | | | | |
| SA0908 | | | | | |
| T18 | | | | | |

Figure A.1 BACTH analysis of *S.aureus* cell division proteins against T25-POIs

Pairwise interactions of T25-POIs with T18 fused *S.aureus* cell division proteins. 10 μ l samples of a 1:100 dilution of overnight culture of co-transformed BTH101 were spotted onto minimal medium containing 150 μ g ml⁻¹ X-gal and incubated at 30°C for a minimum of 18hrs. +ve, T25-zip~T18-zip; -ve, pKT25~pUT18C.

Appendix II

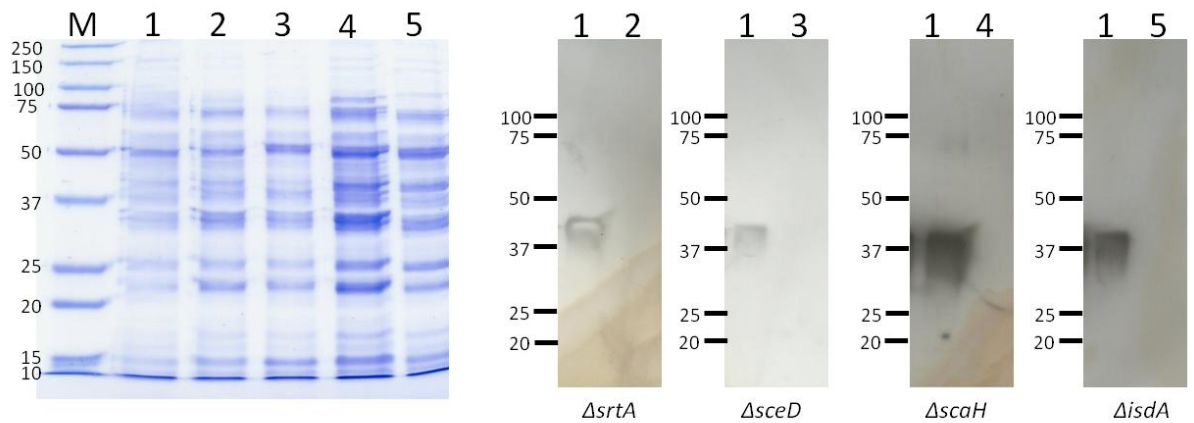


Figure B.1 α -protein A western blots

Strains were transformed with *spa::kan* lysates and tested with α -protein A; 1° antibody 1:5000; 2° antibody 1:20000. Lane 1, SH1000 lysate; Lane 2, Δ *srtA* *spa::kan* lysate; Lane 3 Δ *sceD* *spa::kan* lysate; Lane 4 Δ *scaH* *spa::kan* lysate; Lane 5 Δ *isdA* *spa::kan* lysate.

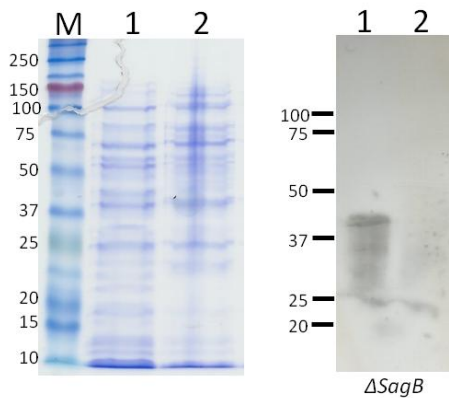


Figure B.2 α -protein A western blots

Strains were transformed with *spa::tet* lysates and tested with α -protein A; 1° antibody 1:5000; 2° antibody 1:20000. Lane 1, SH1000 lysate; Lane 2, Δ *sagB* *spa::tet* lysate.

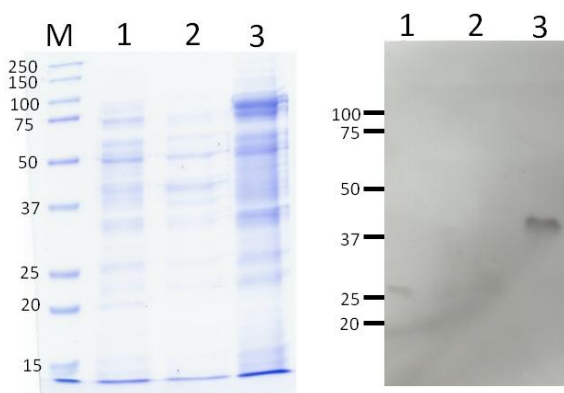


Figure B.3 α -protein A western blots

Strains were transformed with *spa::kan* lysates and tested with α -protein A; 1° antibody 1:5000; 2° antibody 1:20000. Lane 1, Δ *tarO* *spa::kan* lysate (colony 1); Lane 2 Δ *tarO* *spa::kan* lysate (colony 2); Lane 3 Δ *tarO* lysate.